Karlsruhe Institute of Technology

Evaluation of atomic displacement and gas production cross-section for ^{9}Be irradiated with neutrons at energies up to 200 MeV

by A.Yu. Konobeyev[1], U. Fischer[1]

KIT SCIENTIFIC WORKING PAPERS 37

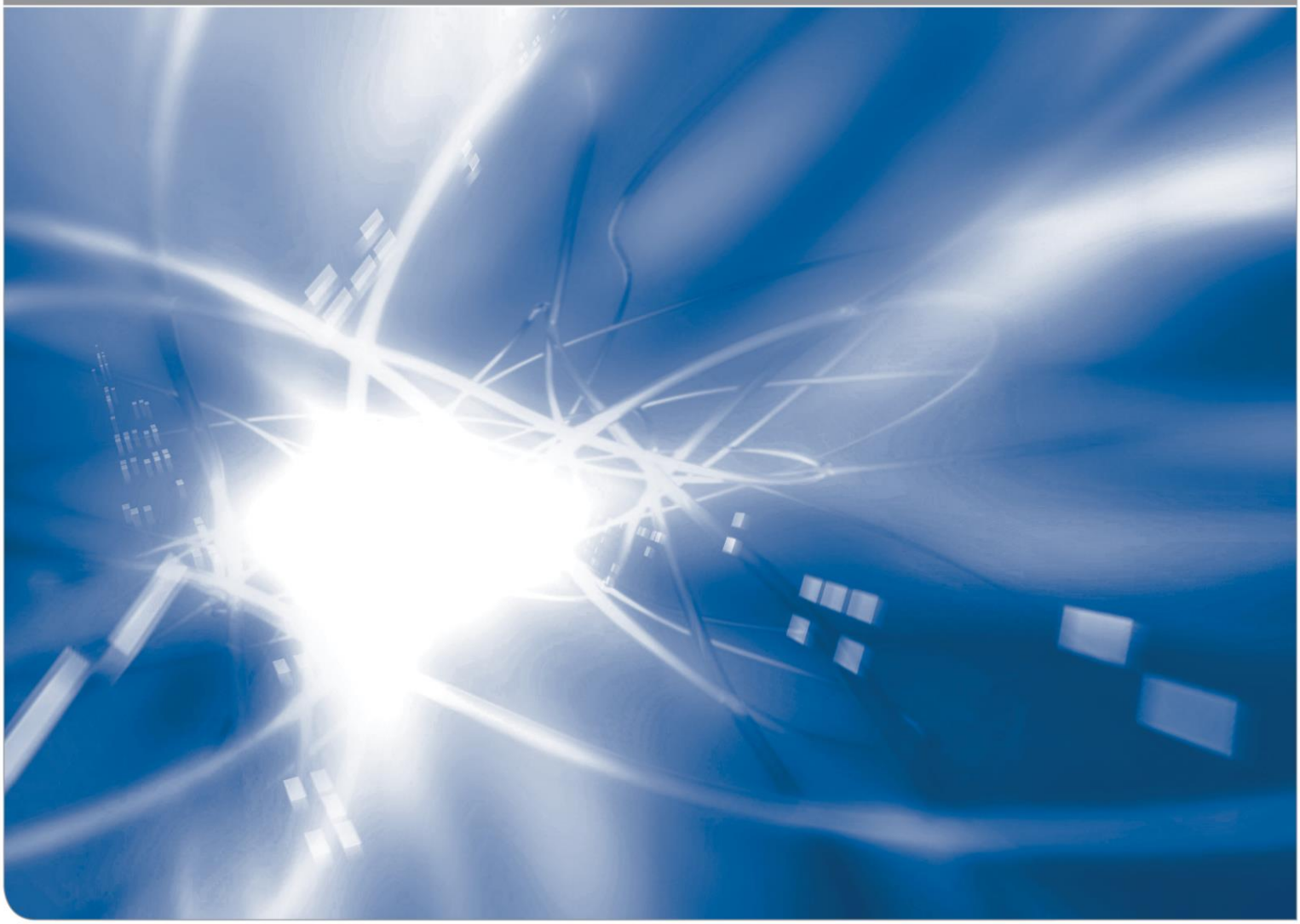

[1] Institut für Neutronenphysik und Reaktortechnik,
Karlsruher Institut für Technologie (KIT)

Impressum

Karlsruher Institut für Technologie (KIT)
www.kit.edu

2015

ISSN: 2194-1629

Abstract

The displacement cross-sections, proton-, deuteron-, triton-, ^{3}He-, and α-particles-production cross-sections were obtained for ^{9}Be at the energies of primary neutrons up to 200 MeV. The evaluation of cross-section was performed using results of model calculations and available experimental data.

CONTENTS

page

1. Introduction

Unique structural, chemical, and nuclear properties [1] make beryllium a promising candidate for application in advanced nuclear units, especially in fusion reactor. An evaluation of nuclear data relevant to the study of radiation damage of beryllium plays an important role for an estimation of efficiency of the use of the material.

In the present work the atomic displacement cross-section and components of gas production cross-section were evaluated for ^{9}Be irradiated with neutrons with the energy up to 200 MeV. The data obtained extend a range of available evaluated data for natural beryllium and supplement existing data from ENDF/B-VI.1, JENDL-4, and JEFF-3.2.

The data evaluation included i) test model calculations of particle distributions in proton induced reactions to estimate the “quality” of model predictions and to quantify the deviation of calculated values and experimental data, ii) calculations of gas production and displacement cross-sections for n+^{9}Be reactions, and iii) an adjustment of calculated values to experimental and existing evaluated cross-sections below 20 MeV providing an agreement with the content of evaluated data files.

Calculations of cross-sections were performed using a number of nuclear models including the pre-equilibrium model, the evaporation model, and the Fermi break-up model implemented in modern computer codes [2,3]. The quality of model predictions was estimated from the comparison with angular and energy distribution of particles in proton induced reactions.

Details of the method of data evaluation are discussed in Section 2. Section 3 describes the calculation and evaluation of cross-sections of gas production components: proton-, deuteron-, triton-, ^{3}He, and α-particle production cross-sections. The evaluation of displacement cross-sections is briefly discussed in Section 4. The information about obtained data files is presented in Section 5.

2. Brief description of method of cross-section evaluation and test calculations

One of the factors complicating the evaluation of gas production and displacement cross-sections for beryllium is the lack of experimental data at neutron energies

above 20 MeV, for tritons above 30 MeV. Another problem [4] is a limited applicability of conventional methods of calculations using pre-equilibrium and evaporation models with approved systematics of model parameters [5].

A promising approach for beryllium is the use of a combination of the intranuclear cascade model, the pre-equilibrium exciton model, and the Fermi break-up model, which applicability for simulation of nuclear reaction for light target nuclei irradiated with nucleons of intermediate energies was demonstrated [6]. Test calculations are done using available experimental data for proton induced reactions, in case of p+^{9}Be reactions, using double differential cross-sections of neutron and light charge particle emission at incident proton energies relevant to the present task [4].

In the present work such calculations were performed using nuclear models Bertini, ISABEL, CEM03, and INCL4 from MCNP6 [2] for a number of angular and energy distributions of particles in p+9Be reactions selected based on available measured data. For comparison, additional calculations were performed using the pre-equilibrium and equilibrium models from the TALYS code [7]. A quantification of deviations of calculated and experimental distributions was made using deviation factors [8].

Experimental data from Refs.[9-11] (Table 1) were approved as relevant to the current task and selected for the test calculations. Figs.1-8 show typical results of calculations. Detailed information is presented in Appendix A.

For neutrons (Fig.1) the calculations using Bertini, ISABEL, INCL4, and CEM03 show similar agreement with experimental data (angles 30^0, 60^0, 150^0) and similar problems (angle 7.5^0). For proton distributions, Bertini and CEM03 models are most successful at the angle 160^0; at other emission angles predictions of various models are similar. CEM03 and INCL4 are the best models for calculation of triton distributions (Fig.3). All models underestimate double differential cross-sections for protons at 60^0 and 90^0. The same is for deuterons (Appendix A) and α-particles (Fig.4); all models underestimate experimental values at lower angles.

The $d^2\sigma/dEd\Omega$ values for discussed reactions (Figs.1-4) calculated using the TALYS code (Figs.5-8) show deviations at different angles and secondary energies; the disagreement can be reduced by a redefinition of model parameters relevant to calculations for light targets, as ^{9}Be.

Table 1. Experimental double differential cross-sections for p+^{9}Be reactions used for test calculations

Incident proton energy, MeV	Ejectiles	Angles, degree	Reference
113	n	7.5, 30, 60, 150	Meier (1989) [9]
190	^{3}He, α-particle	20, 30, 40, 60, 90, 120, 160	Green (1987) [10]
256	n	7.5, 30, 60, 150	Meier (1992) [11]
300	p, d, t, ^{3}He,α-particle	20, 30, 40, 60, 90, 120, 160	Green (1987) [10]

The comparison of angular integrated distributions $d\sigma/d\varepsilon$ calculated using different models for considered reactions (Figs.1-8) is shown in Fig.9. Experimental data for energy particle distributions are absent and the figure demonstrates a general scattering of predictions of discussed nuclear models.

The difference of measured and calculated $d^2\sigma/dEd\Omega$ values was quantified using deviation factors [8]:

$$H = \left(\frac{1}{N} \sum_{i=1}^{N} \left(\frac{\xi_i^{exp} - \xi_i^{calc}}{\Delta\xi_i^{exp}} \right)^2 \right)^{1/2} \quad (1)$$

$$R^{CE} = \frac{1}{N} \sum_{i=1}^{N} \frac{\xi_i^{calc}}{\xi_i^{exp}} \quad (2)$$

$$R^{EC} = \frac{1}{N} \sum_{i=1}^{N} \frac{\xi_i^{exp}}{\xi_i^{calc}} \quad (3)$$

$$< F > = 10^{\left(\frac{1}{N} \sum_{i=1}^{N} \left[\log(\xi_i^{exp}) - \log(\xi_i^{calc}) \right]^2 \right)^{1/2}} \quad (4)$$

$$L = \left[\sum_{i=1}^{N} \left(\frac{\xi_i^{calc}}{\Delta\xi_i^{exp}} \right)^2 \left(\frac{\xi_i^{calc} - \xi_i^{exp}}{\xi_i^{calc}} \right)^2 \Bigg/ \sum_{i=1}^{N} \left(\frac{\xi_i^{calc}}{\Delta\xi_i^{exp}} \right)^2 \right]^{1/2} \quad (5)$$

$$S = 10^{\left\{ \left(\sum_{i=1}^{N} \left[\frac{\lg(\xi_i^{exp}) - \lg(\xi_i^{calc})}{\left(\Delta\xi_i^{exp} / \xi_i^{exp} \right)} \right]^2 \right) \left(\sum_{i=1}^{N} \left[\frac{\xi_i^{exp}}{\left(\Delta\xi_i^{exp} \right)} \right]^2 \right)^{-1} \right\}^{1/2}} \quad (6)$$

$$P_{2.0} = N_{2.0}(0.5 < \xi_i^{calc} / \xi_i^{exp} < 2.0) / N \quad (7)$$

$$P_{10.0} = N_{10.0}(0.1 < \xi_i^{calc} / \xi_i^{exp} < 10) / N \quad (8)$$

where ξ^{exp}_i and $\Delta\xi^{exp}_i$ is the measured value and its uncertainty, ξ^{calc}_i is the calculated value, and N is the total number of experimental points selected for each type of the comparison with the non-zero values of ξ^{calc}_i, $N_{2.0}$ is the number of points with the ratio $0.5 < \xi^{calc}_i/\xi^{exp}_i < 2.0$, and $N_{10.0}$ corresponds to $0.1 < \xi^{calc}_i/\xi^{exp}_i < 10$.

The <F> factor, Eq.(4) is discussed in Ref.[12], the L factor, Eq.(5) in Ref.[13], the S factor, Eq.(6) is an advance form of Eq.(4) with experimental errors taken into account [14]. The meaning of factors is discussed in Ref.[8].

Tables 2 shows deviation factors, Eq.(1)-(8) obtained for all experimental points from Refs.[9-11] and calculated non-zero $d^2\sigma/dEd\Omega$ values. Table 3 presents the factors corresponding to measured and calculated values with the ratio $0.01 < \xi^{calc}_i/\xi^{exp}_i < 100$. The difference in the N values for the models is due to the number of non-zero values of $d^2\sigma/dEd\Omega$ obtained in calculations.

The comparison of the data in Tables 2 and 3 shows that the cases of extreme deviations with the ratio of calculated and measured values less than 0.01 or more than 100 makes a rather small impact on values of all deviation factors except R^{EC}. The R^{EC} factor indicates the basic problem of model calculations, namely, lower calculated values compared with experimental ones (Table 2). It is hoped that the further development of models can solve this problem.

3. Evaluation of gas production cross-sections for n+^{9}Be reactions

The calculation of cross-sections for neutron induced reactions was performed using Bertini, ISABEL, INCL4, CEM03 models, and models implemented in TALYS.

The final calculated values were obtained using the following formula [15]

$$\sigma(E) = \sum_{i=1}^{M} w_i \sigma_i(E) \left(\sum_{i=1}^{M} w_i \right)^{-1}, \quad (9)$$

where σ_i is the cross-section calculated using “i”-th nuclear models, w_i is the statistical weight of the model, M is the total number of different models applied for the calculation of investigated cross-sections.

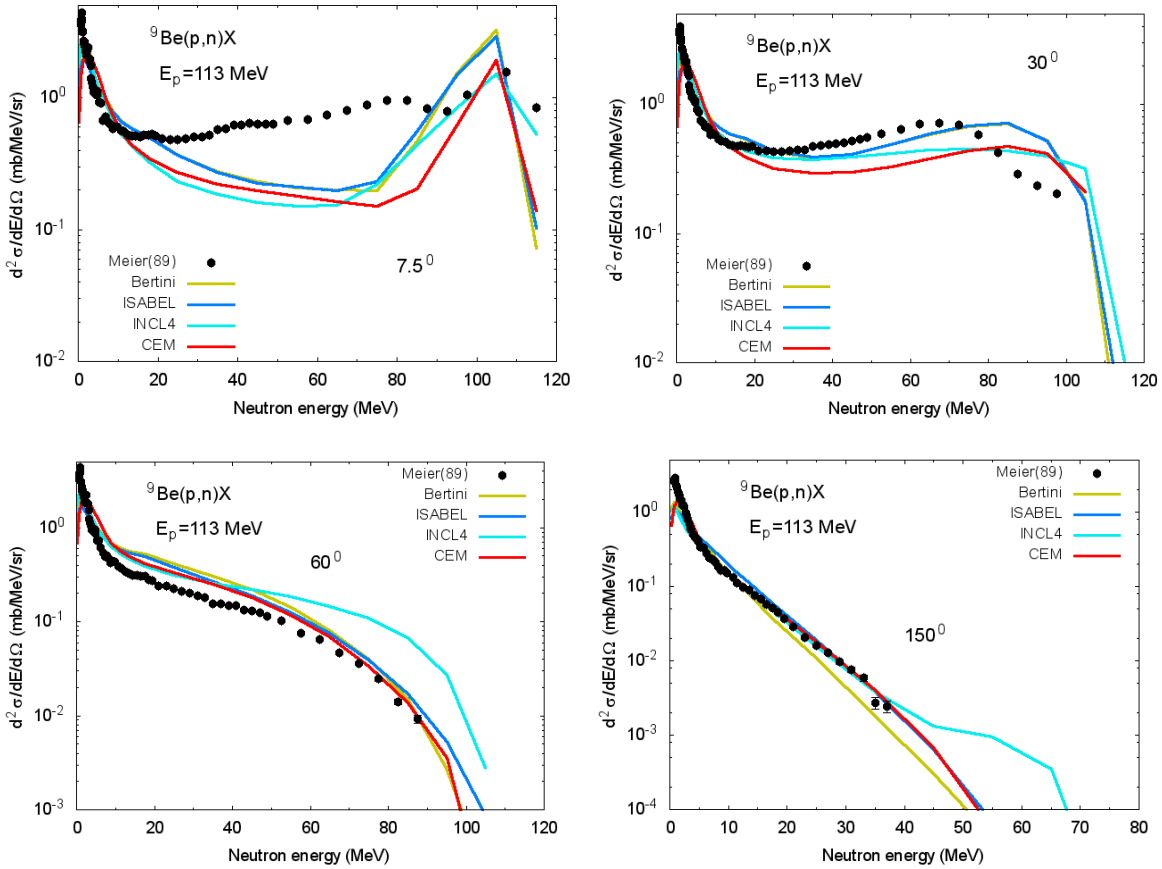

Fig.1 Experimental and calculated neutron distributions for reaction induced by 113 MeV protons

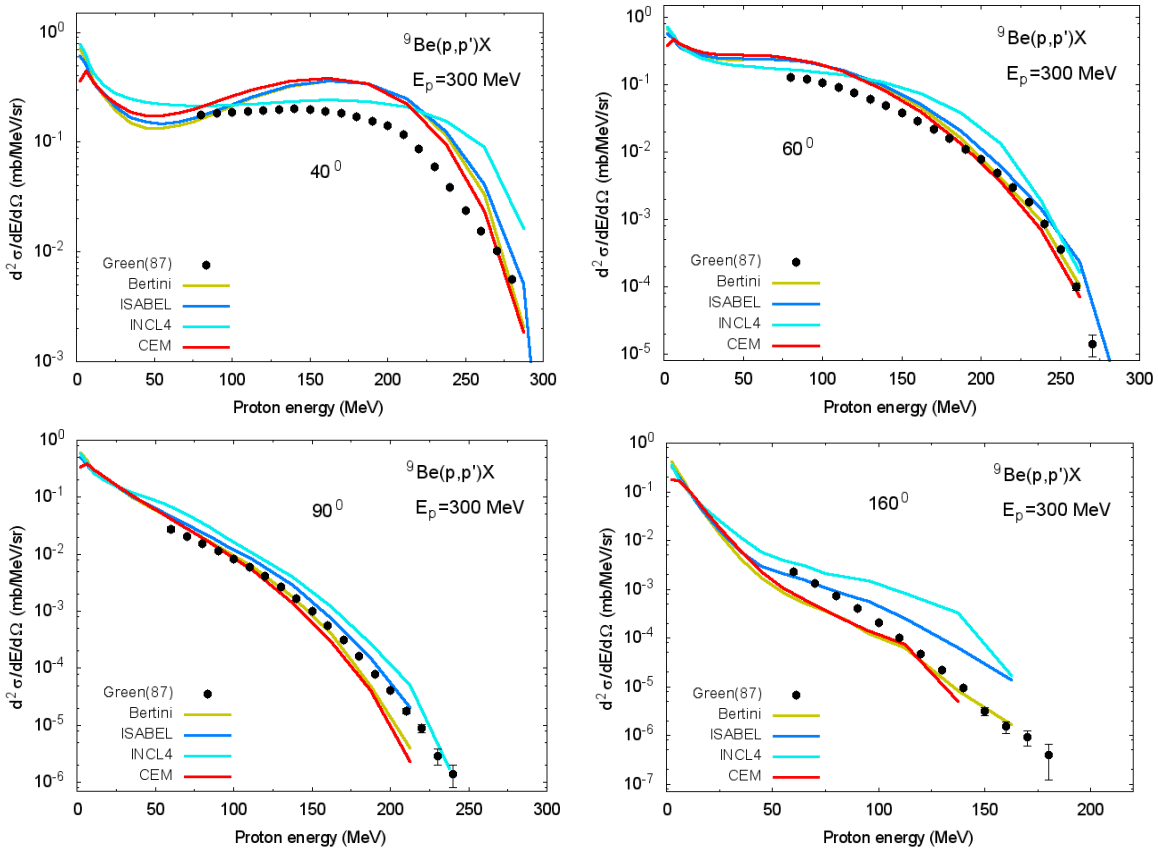

Fig.2 Experimental and calculated proton distributions for reaction induced by 300 MeV protons

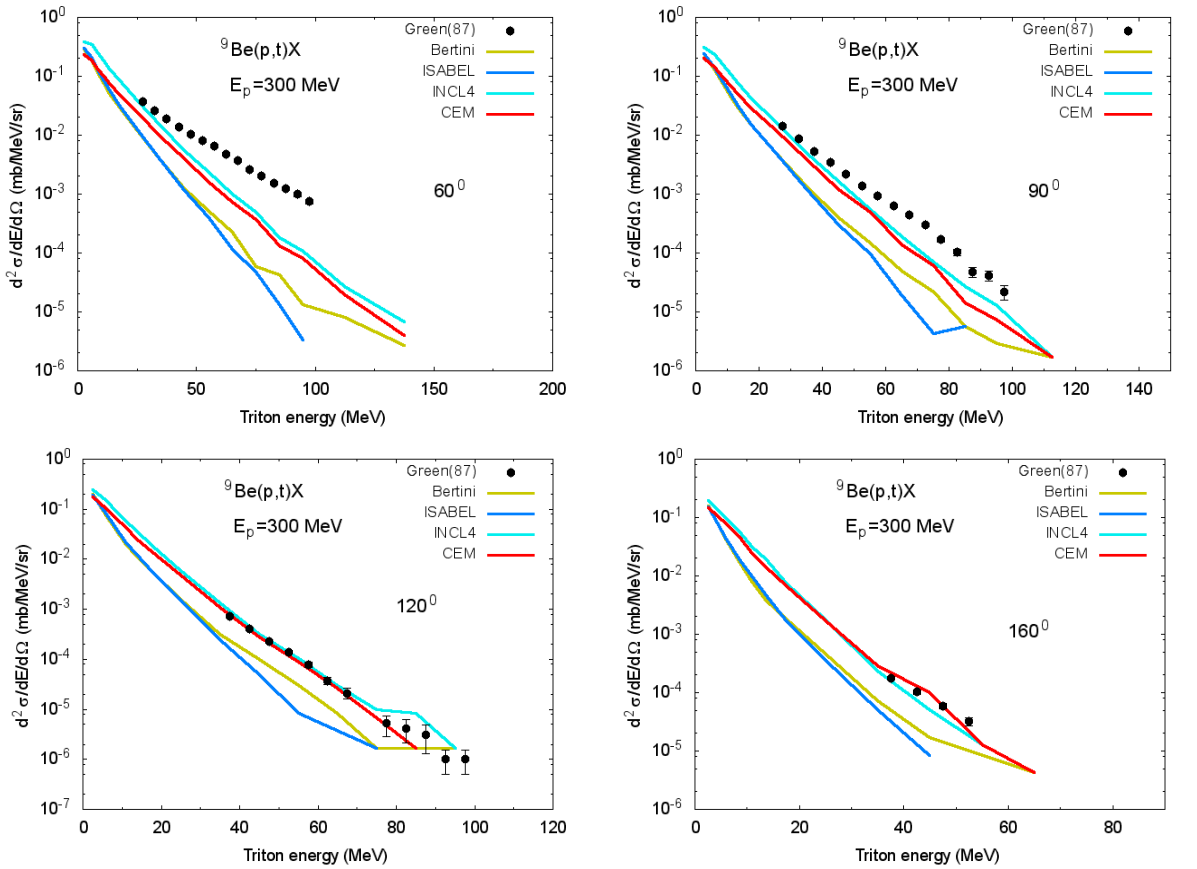

Fig.3 Experimental and calculated triton distributions for reaction induced by 300 MeV protons

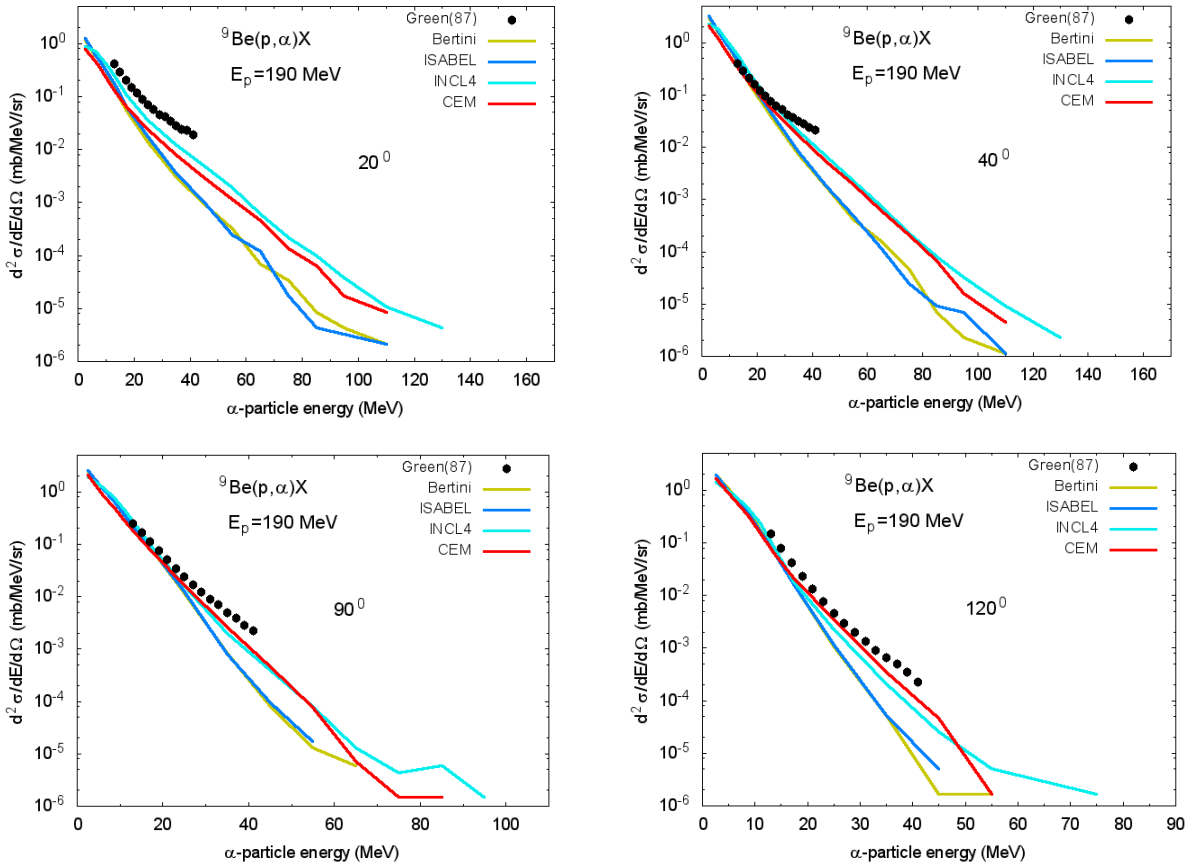

Fig.4 Experimental and calculated α-particle distributions for reaction induced by 190 MeV protons

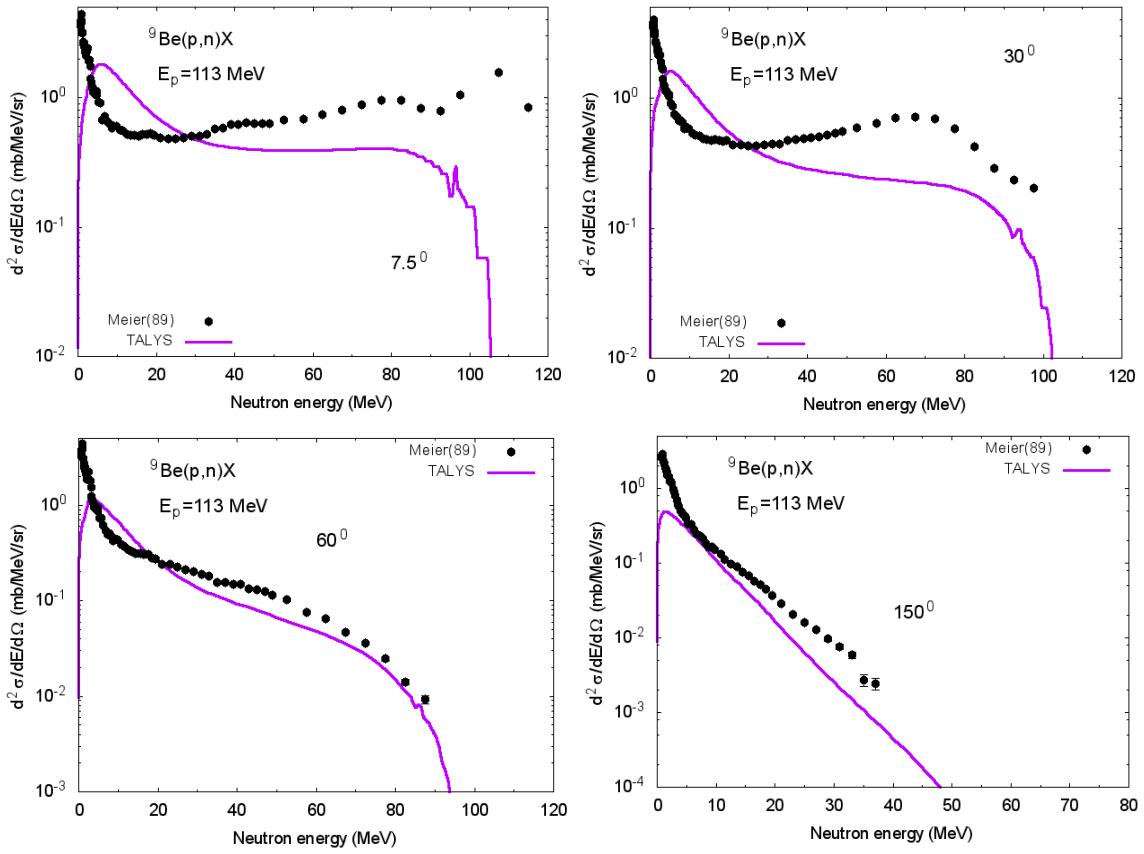

Fig.5 Experimental and calculated neutron distributions for reaction induced by 113 MeV protons

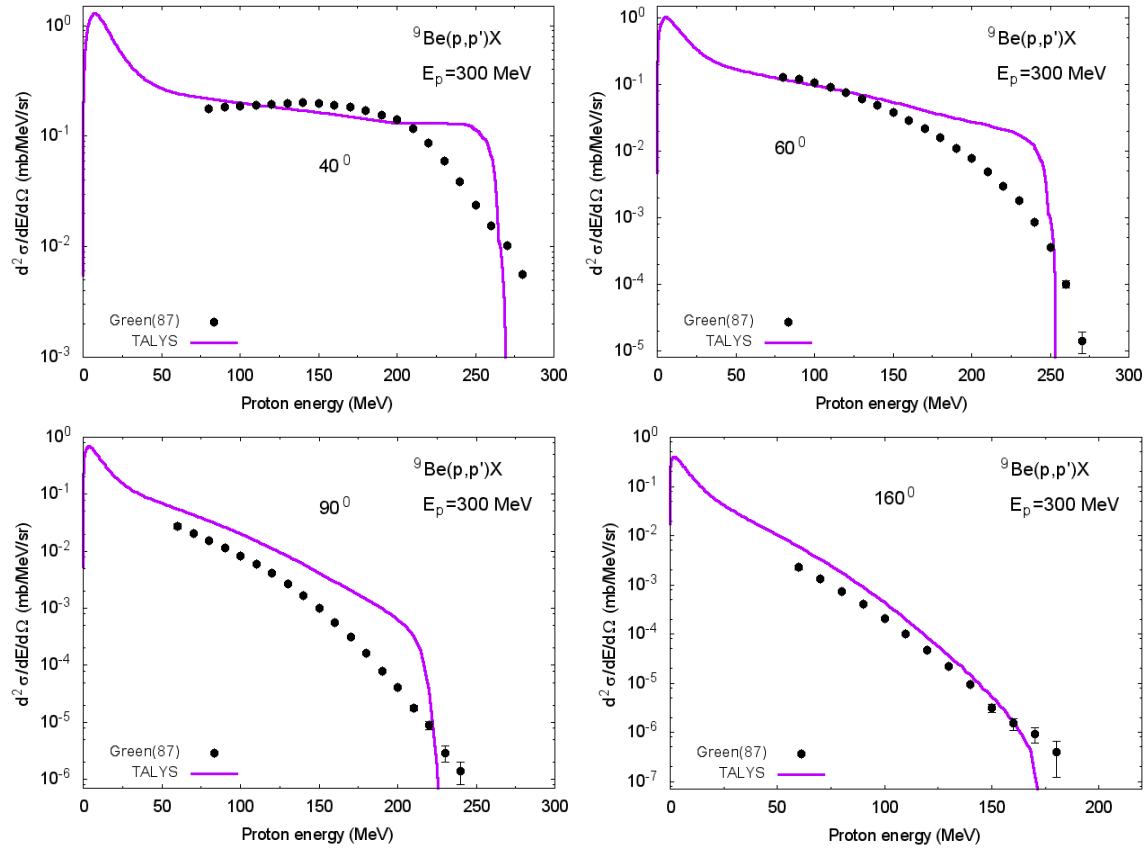

Fig.6 Experimental and calculated proton distributions for reaction induced by 300 MeV protons

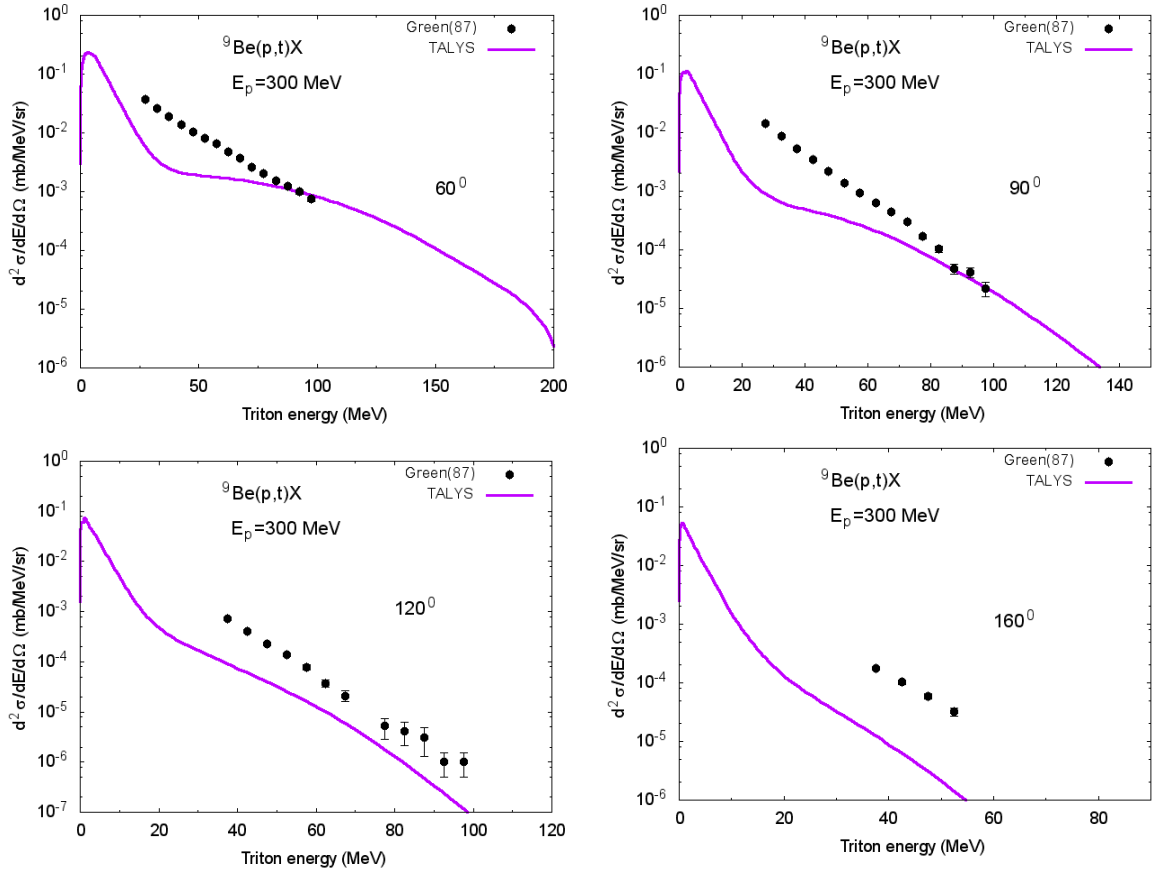

Fig.7 Experimental and calculated triton distributions for reaction induced by 300 MeV protons

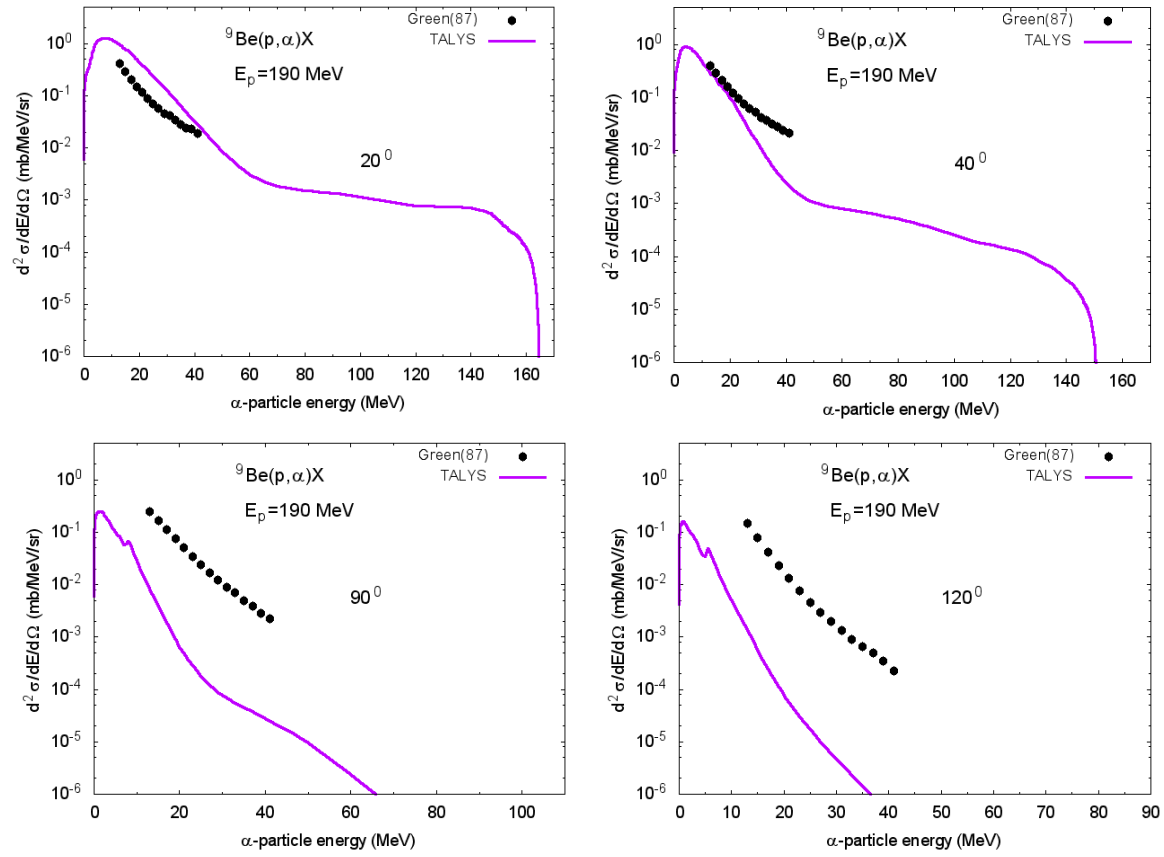

Fig.8 Experimental and calculated α-particle distributions for reaction induced by 190 MeV protons

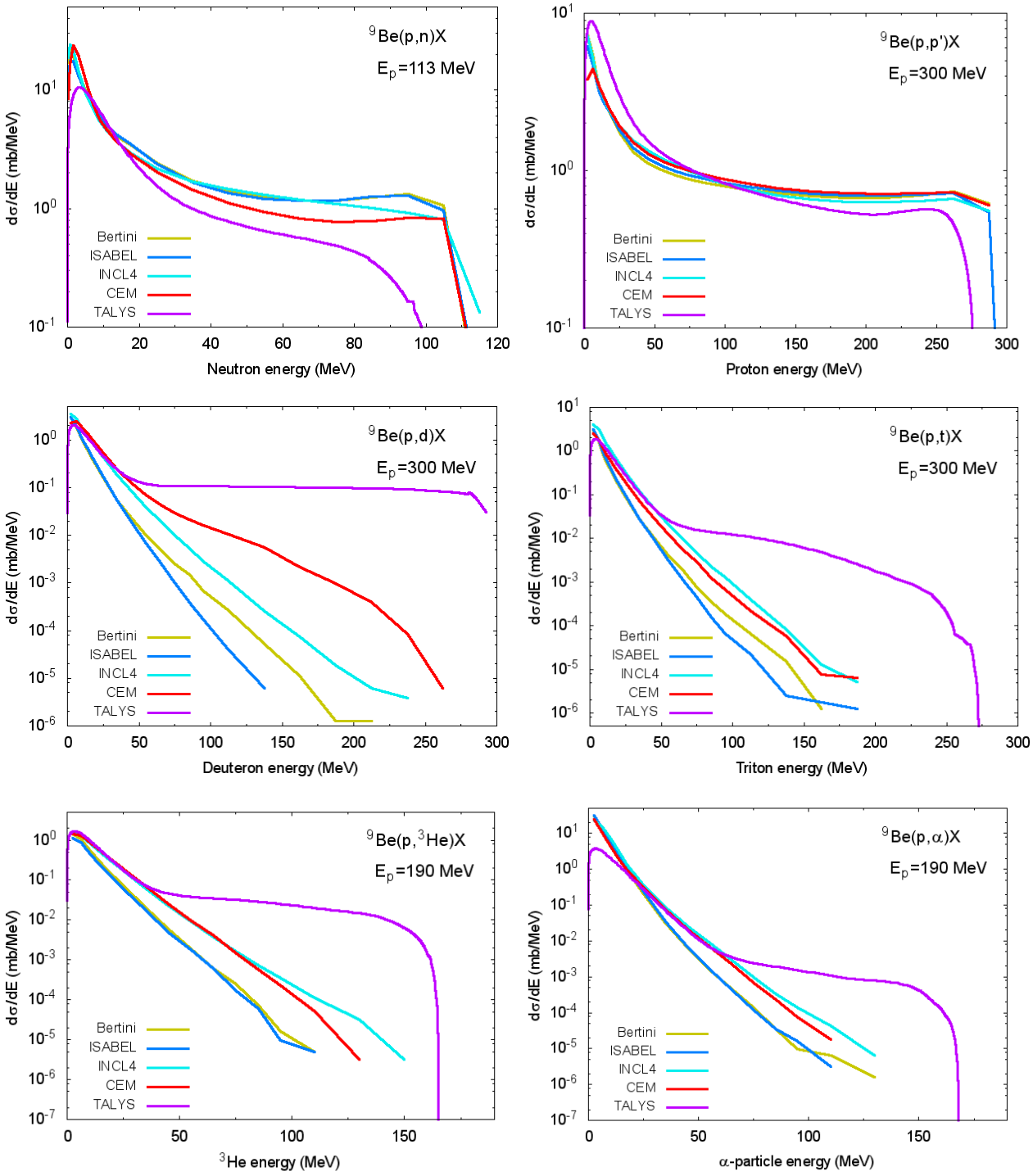

Fig.9 Comparison of particle energy distributions calculated using Bertini, ISABEL, INCL4, and CEM03 models, and nuclear models implemented in the TALYS code for the same reactions as in Figs.1-8.

Inverse values of <F>, Eq.(4) were adopted as weights of the models in Eq.(9). The sum in Eq.(9) includes results of calculations using Bertini, ISABEL, and CEM03; calculations using other models were used for comparative purposes. Some explanations are given below.

3.1 Proton production cross-section

Fig.10 shows the ^{9}Be(n,x)p reaction cross-section (Q=-12,8 MeV) calculated using different models and cross-sections evaluated with Eq.(9). Formally, cross-sections obtained using INCL4 are shown at all considered energies up to 200 MeV corresponding to MCNP calculations. The jump at 100 MeV is not an indication of internal problems of INCL4, because the energy is outside of recommended limit of the model application [16].

Table 2. Values of deviation factors, obtained using $d^2\sigma/dEd\Omega$ distributions calculated with Bertini, ISABEL, INCL4, CEM03, and TALYS for p+^{9}Be interactions and experimental data from Refs.[9-11]. For the P factors holds, the larger the better, for the other factors the opposite holds. See other explanations in the text.

Factor	Bertini	ISABEL	INCL4	CEM	TALYS
H	47.	49.	55.	40.	86.
R^{CE}	0.72	0.83	1.28	0.84	2.01
R^{EC}	74.	81.	39.	43.	45.
<F>	5.7	5.9	4.3	3.3	7.9
L	0.59	0.58	0.57	0.51	0.82
S	3.1	3.3	2.1	2.1	13.0
$P_{2.0}$	0.57	0.56	0.67	0.69	0.37
$P_{10.0}$	0.89	0.88	0.92	0.94	0.83
N	1216	1184	1251	1246	1254

Table 3. Values of deviation factors, obtained using $d^2\sigma/dEd\Omega$ distributions calculated with Bertini, ISABEL, INCL4, CEM03, and TALYS for p+^{9}Be interactions and experimental data from Refs.[9-11]. Only data with the ratio $0.01 < d^2\sigma/dEd\Omega^{(calc)}/ d^2\sigma/dEd\Omega^{(exp)} < 100$ are selected.

Factor	Bertini	ISABEL	INCL4	CEM	TALYS
H	47.	49.	55.	40.	85.
R^{CE}	0.75	0.86	1.3	0.85	2.1
R^{EC}	4.2	4.2	2.9	3.1	4.7
<F>	3.5	3.5	2.8	2.7	4.6
L	0.59	0.58	0.57	0.51	0.79
S	2.8	2.8	1.9	2.0	6.5
$P_{2.0}$	0.59	0.58	0.68	0.69	0.40
$P_{10.0}$	0.92	0.91	0.95	0.95	0.88
N	1173	1141	1217	1234	1177

Fig.11 shows the cross-sections from ENDF/B-VII.1, JENDL-4, and JEFF-3.2 data libraries. Differences are observed as at neutron energies, where experimental data are available, $E_n < 15.5$ MeV [17], as at higher energies.

The final curve was obtained after an adjustment of calculated values, Eq.(9) to cross-sections from JEFF-3.2 at 15.5 MeV. Evaluated proton production cross-sections are shown in Fig.12.

3.2 Deuteron production cross-section

Results of model calculations, values evaluated using Eq.(9), and data of JEFF-3.2 are shown for the reaction ^{9}Be(p,x)d (Q =-14.7 MeV) in Fig.13. There is a large scatter of calculated values compared with proton production cross-section (Fig.10).

Fig.14 illustrates the data from ENDF/B-VII.1, JENDL-4, and JEFF-3.2. The final evaluated curve is shown in Fig.15. Data below 18.8 Me, the maximal neutron energy, where measured data are available [17], are taken from JEFF-3.2.

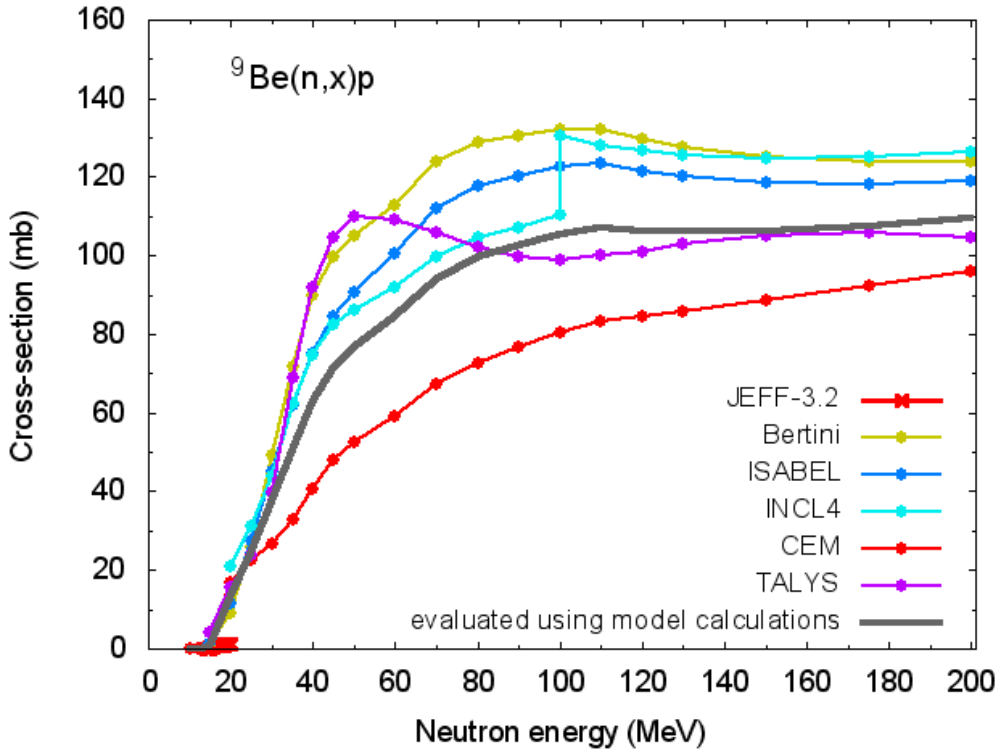

Fig.10 Proton production cross-section for n+^{9}Be interactions calculated using different models, data taken from JEFF-3.2, and cross-section evaluated using model calculations. See explanations in the text.

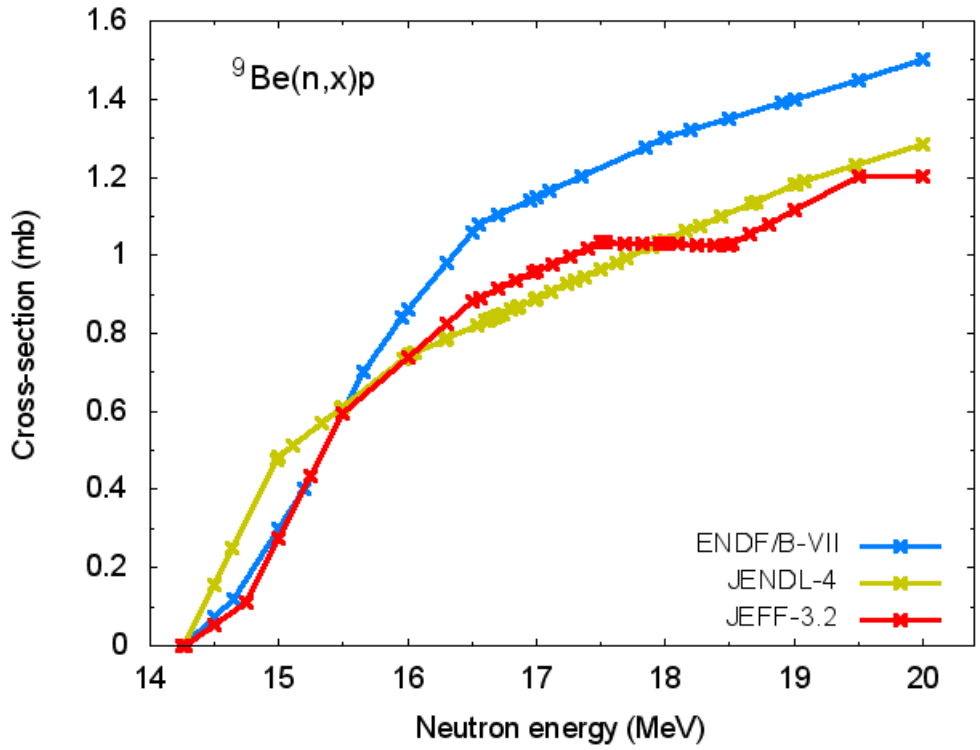

Fig.11 Proton production cross-section for ^{9}Be taken from different data libraries.

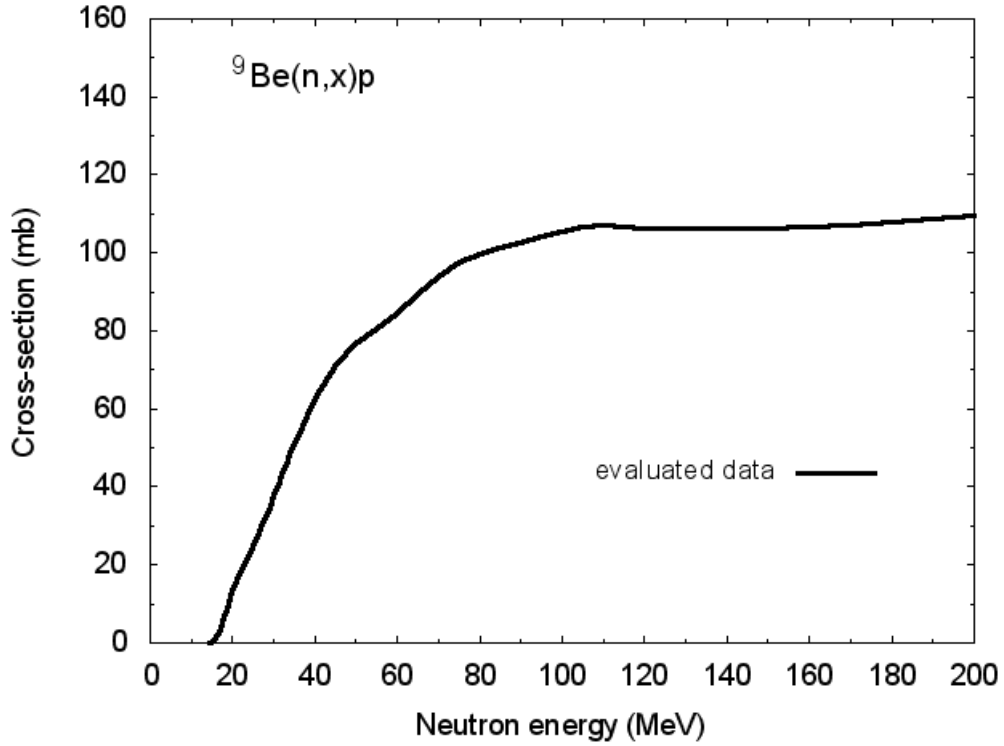

Fig.12 Evaluated proton production cross-section for n+^{9}Be interactions.

3.3 Triton production cross-section

Fig.16 shows calculated values of ^{9}Be(n,x)t reaction cross-section (Q=-10.4 MeV), JEFF-3.2 data, and available experimental data [18-24]. The cross-sections estimated using Eq.(9) are presented in Fig.17.

The difference of experimental data and model predictions (Figs.16,17) is not quite clear. The sharp decrease of ^{9}Be(n,x)t cross-section at 26 – 30 MeV observed in Ref.[24] cannot be justified by present calculations. It seems reasonable to perform new measurements for triton production cross-sections and the further development of models, at least to avoid the discrepancy between calculations and experimental data, discussed in Section 2.

Fig.18 shows data from ENDF/B-VII.1, JENDL-4, and JEFF-3.2 and experimental data [18-24]. The final data obtained after fitting of estimated cross-sections, Eq.(9) to the cross-sections from JEFF-3.2 (Fig.17) are shown in Fig.19. Data below 19,5 MeV are adopted from JEFF-3.2.

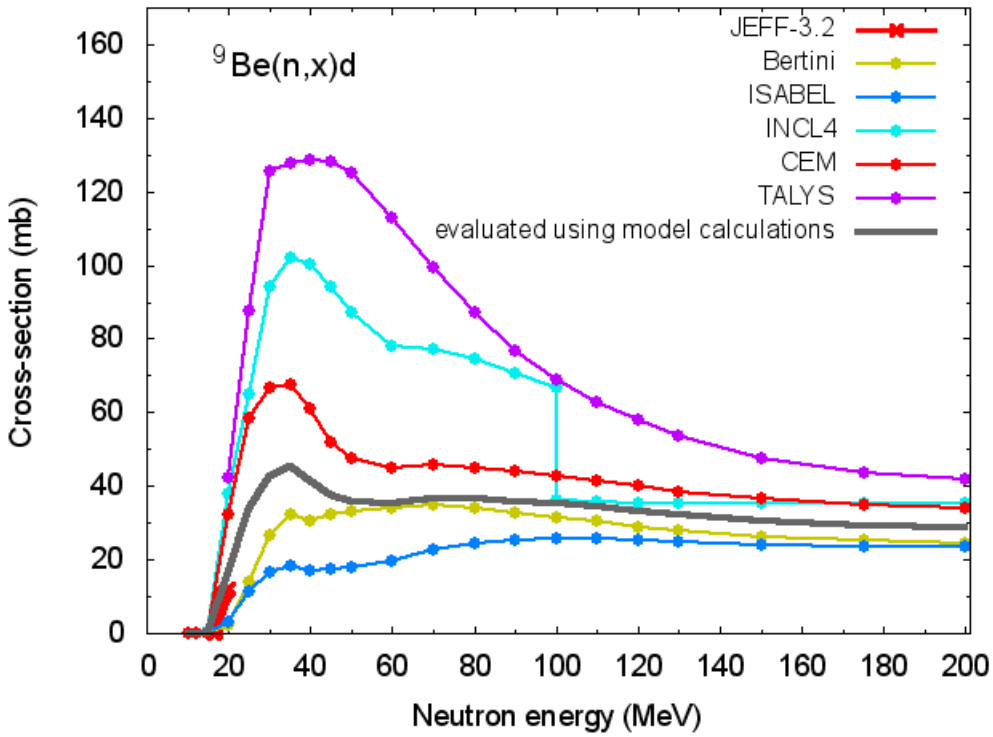

Fig.13 Deuteron production cross-section for n+^{9}Be interactions calculated using different models, data taken from JEFF-3.2, and cross-section evaluated using model calculations.

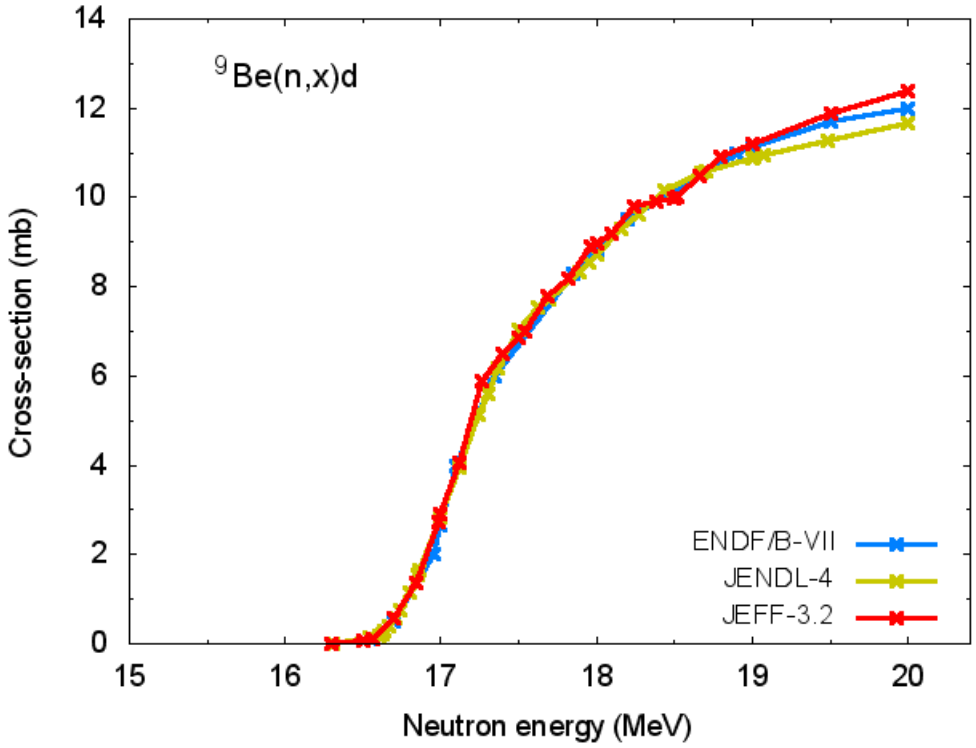

Fig.14 Deuteron production cross-section for ^{9}Be taken from different data libraries.

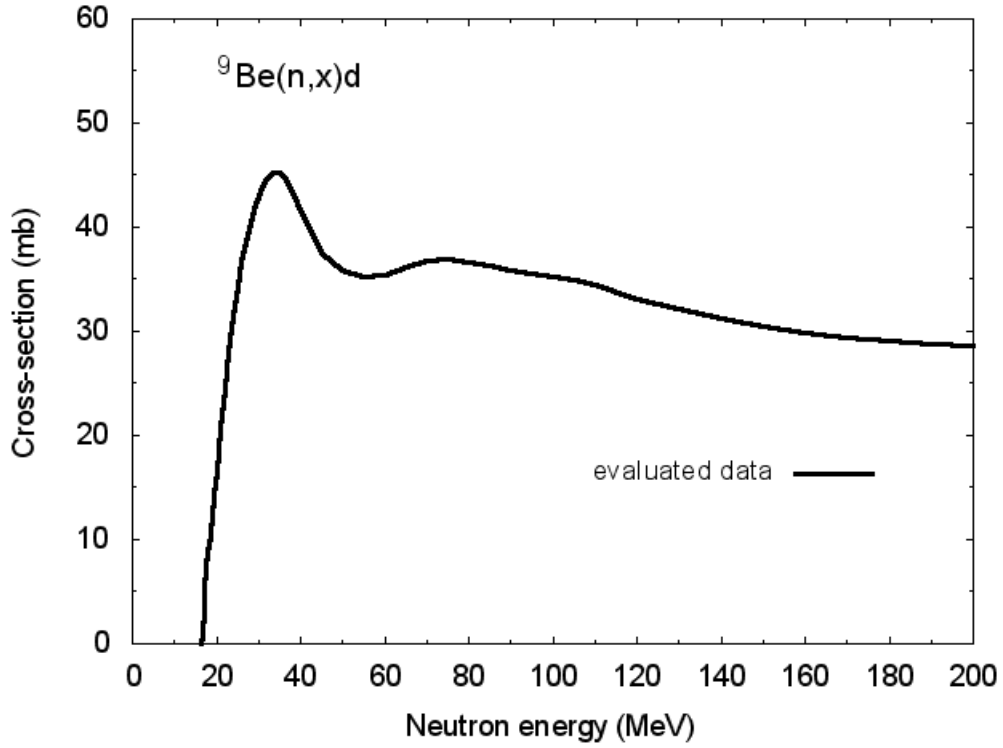

Fig.15 Evaluated deuteron production cross-section for n+^{9}Be interactions

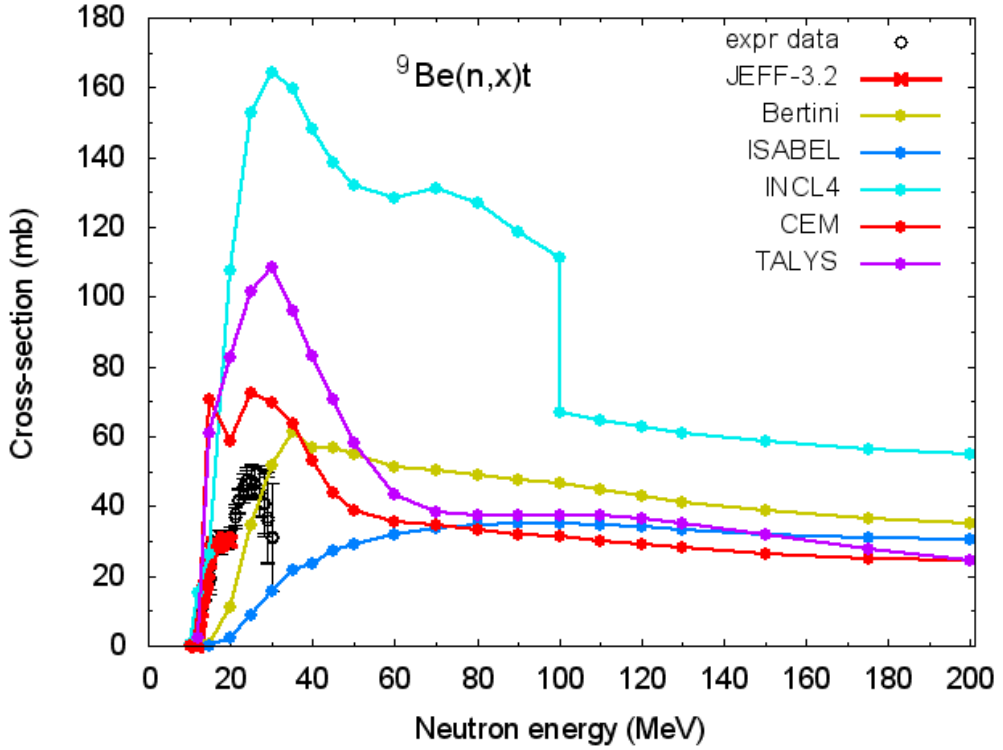

Fig.16 Triton production cross-section for n+^{9}Be interactions calculated using different models, data taken from JEFF-3.2, cross-section evaluated using model calculations, and data measured in Refs.[18-24].

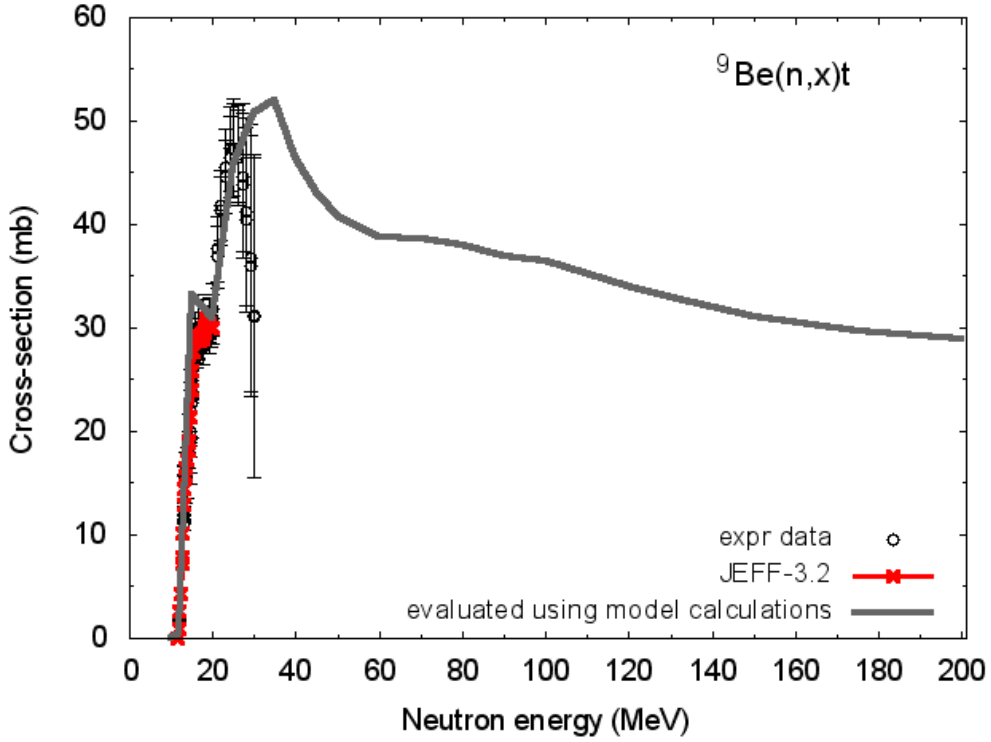

Fig.17 Triton production cross-section for n+^{9}Be interactions taken from JEFF-3.2, cross-section evaluated using model calculations and experimental data [18-24].

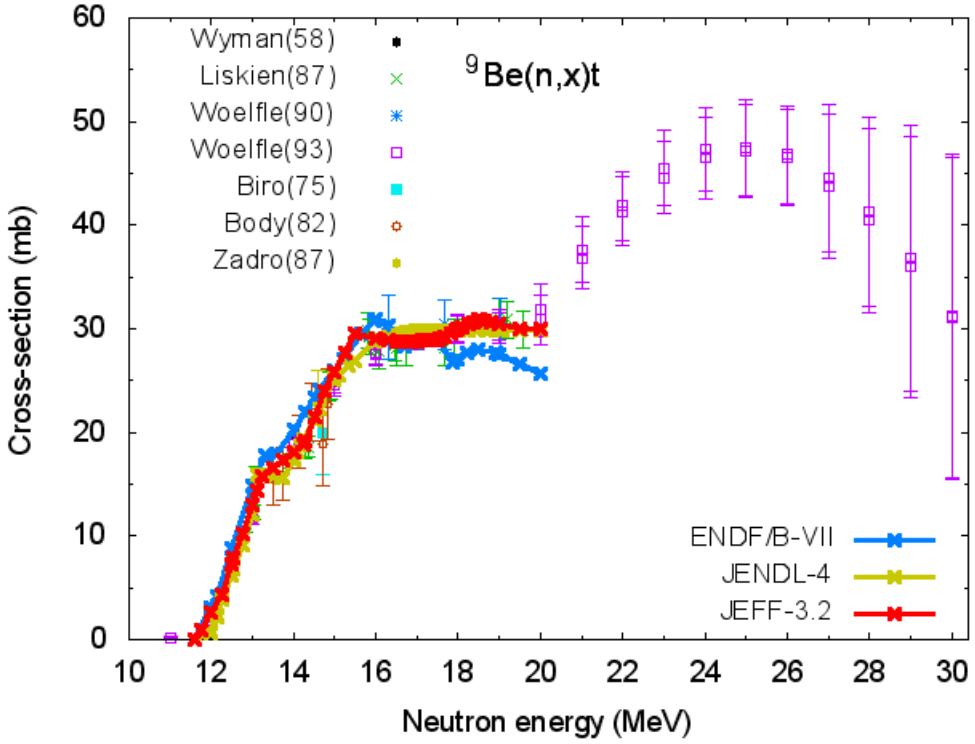

Fig.18 Triton production cross-section for ^{9}Be taken from different data libraries and measured in Refs.[18-24].

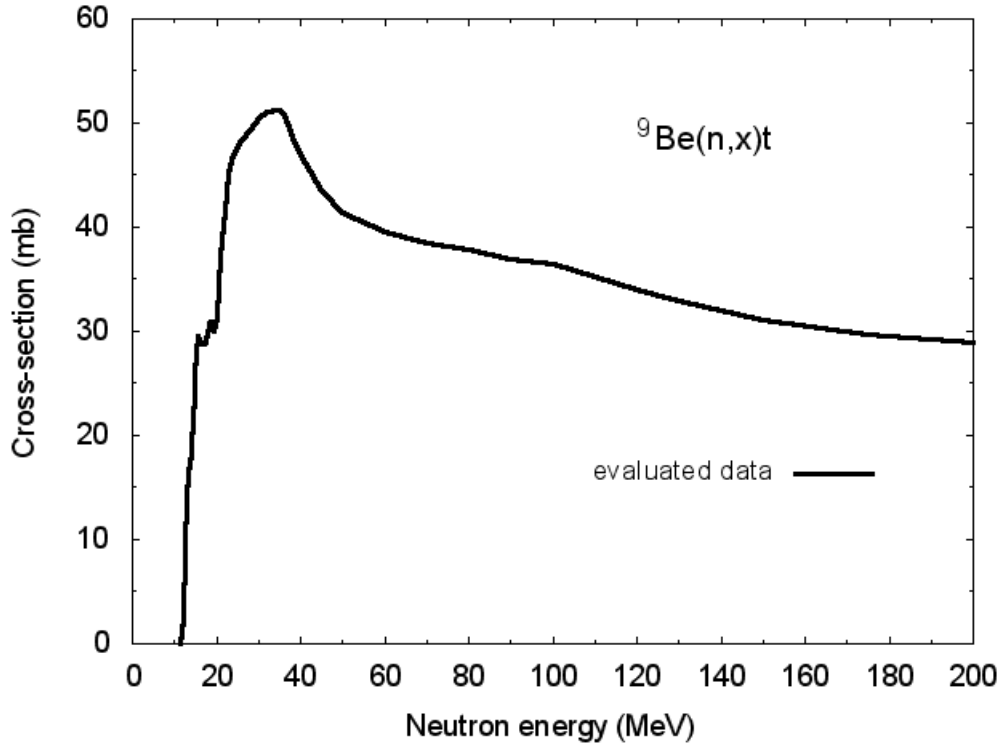

Fig.19. Evaluated triton production cross-section for n+^{9}Be interactions

3.4 ^{3}He production cross-section

Fig.20 shows ^{9}Be(n,x)^{3}He reaction cross-section (Q=-21.6 MeV) calculated using various models and the cross-sections evaluated using Eq.(9).

Final evaluated data are shown in Fig.21.

3.5 α-particle production cross-section

The production of α-particles in neutron irradiation of ^{9}Be occurs in various reactions ^{9}Be(n,a)^{6}He, ^{9}Be(n,2n)^{8}Be, ^{9}Be(n,2nα)α, and others with the maximal Q-value equal to -0.597 MeV. Results of model calculations of α-particle production cross-section and JEFF-3.2 data are shown in Fig.22.

Fig.23 illustrates the cross-sections estimated using Eq.(9) and data from JEFF-3.2. There is a surprisingly good agreement between estimated cross-sections and JEFF-3.2 data at energies around 20 MeV. The good agreement is also observed for the data from different libraries shown in Fig.24.

The α-particle production cross-section evaluated at neutron energies up to 200 MeV is shown in Fig.25. Data below 20 MeV were taken from JEFF-3.2.

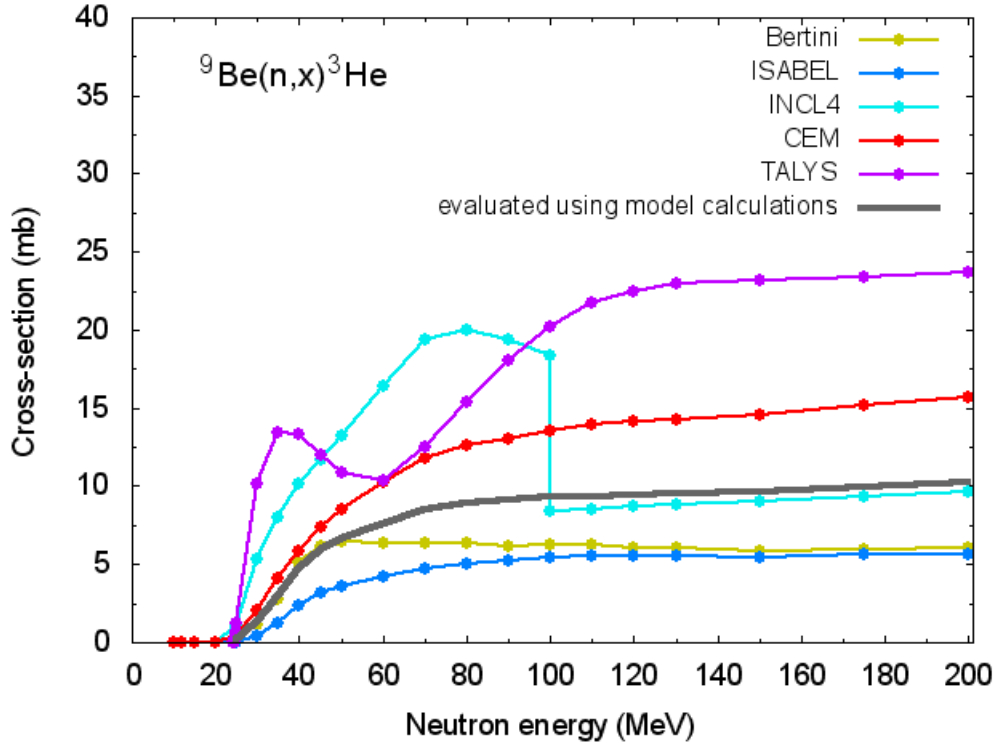

Fig.20 ^{3}He production cross-section for n+^{9}Be interactions calculated using different models and cross-section evaluated using model calculations.

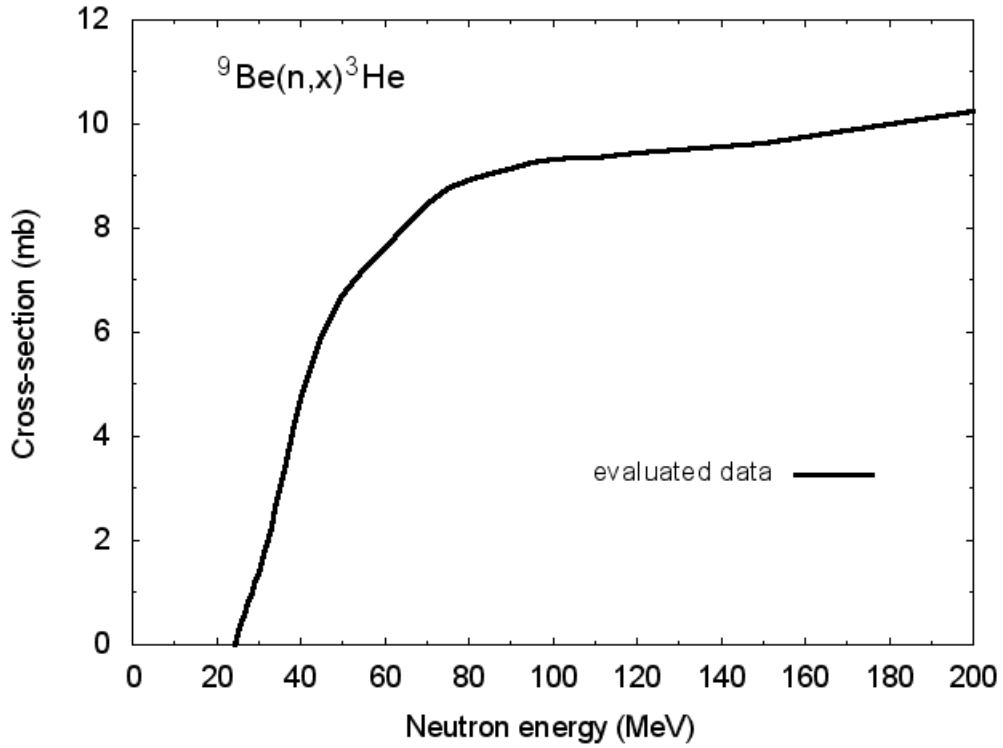

Fig.21 Evaluated ^{3}He production cross-section for n+^{9}Be interactions

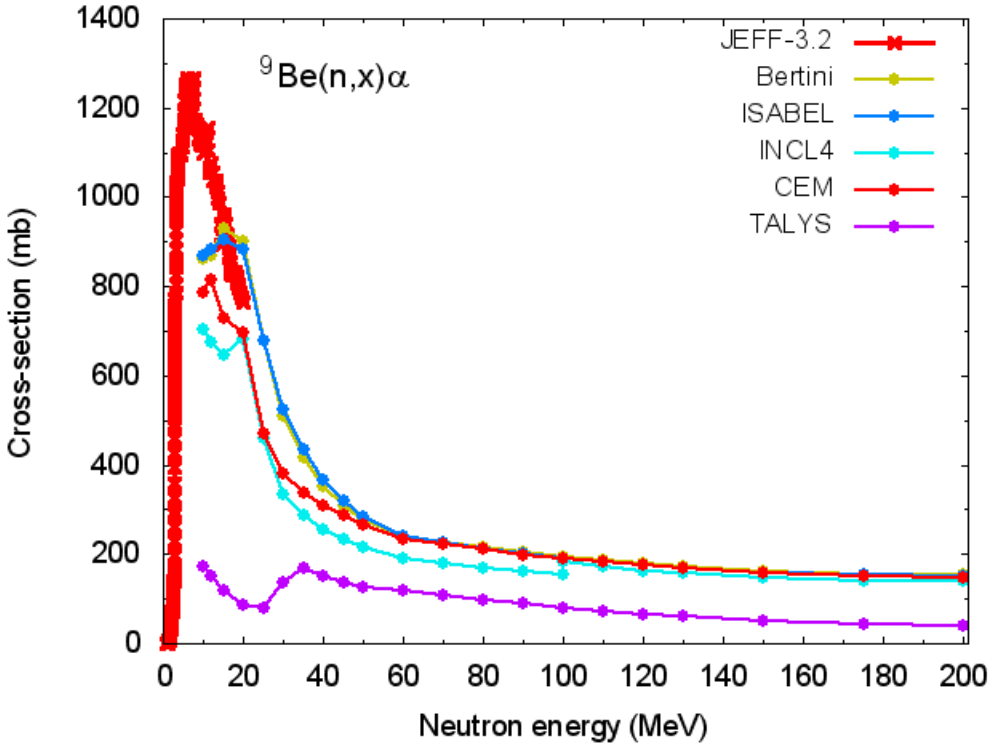

Fig.22 α-particle production cross-section for n+^{9}Be interactions calculated using different models and data taken from JEFF-3.

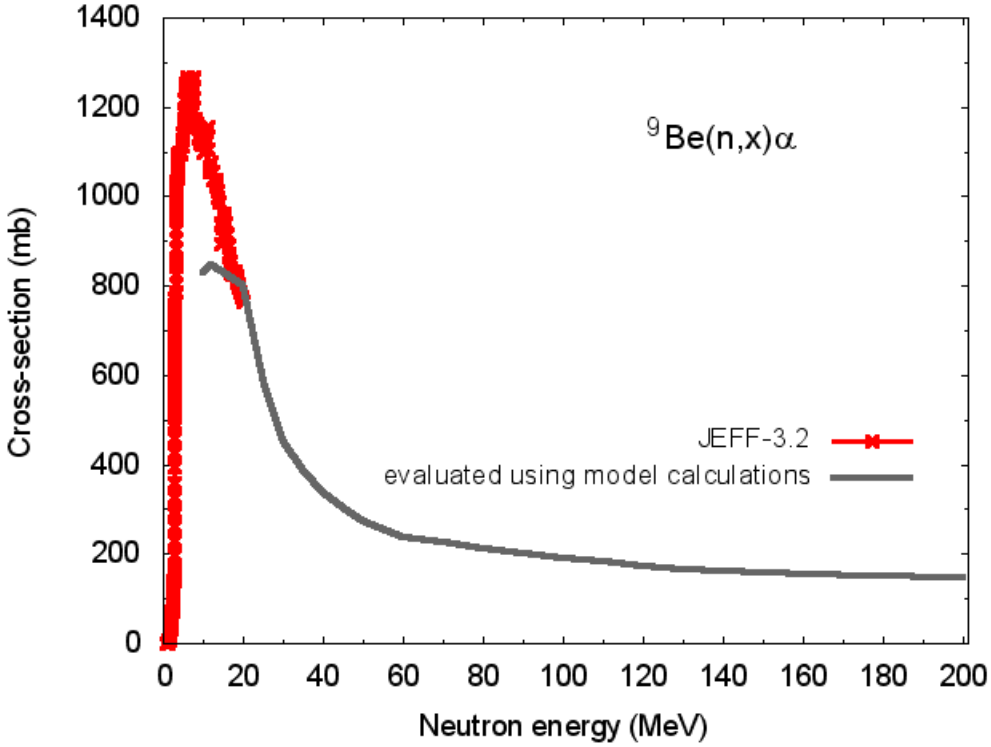

Fig.23 α-particle production cross-section for n+^{9}Be interactions taken from JEFF-3.2 and cross-section evaluated using model calculations.

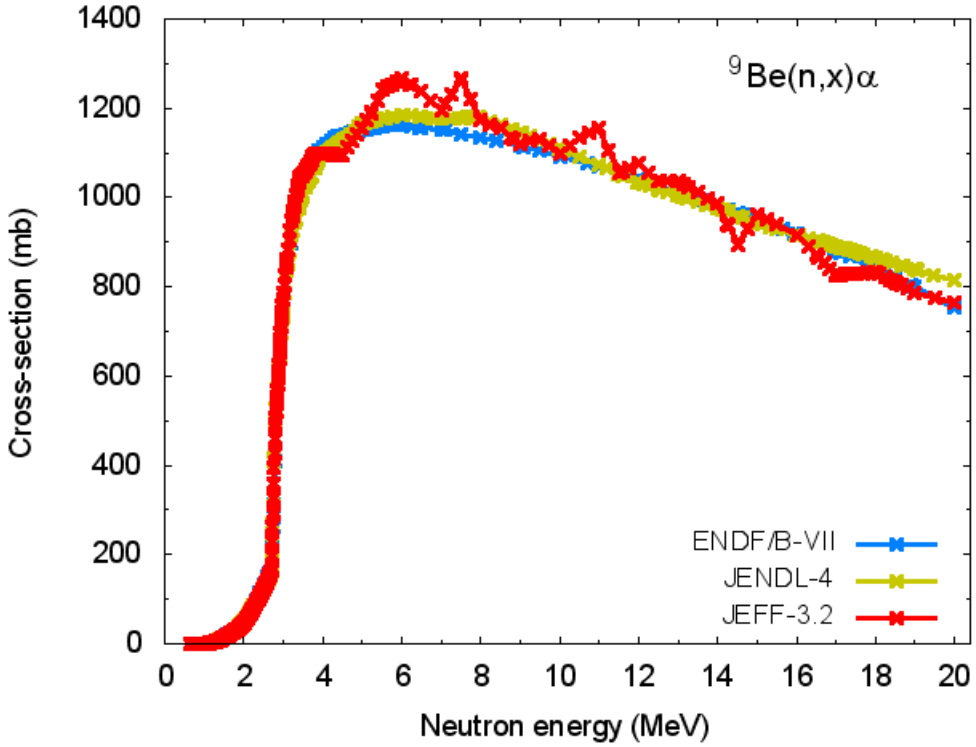

Fig.24 α-particle production cross-section for ^{9}Be taken from different data libraries.

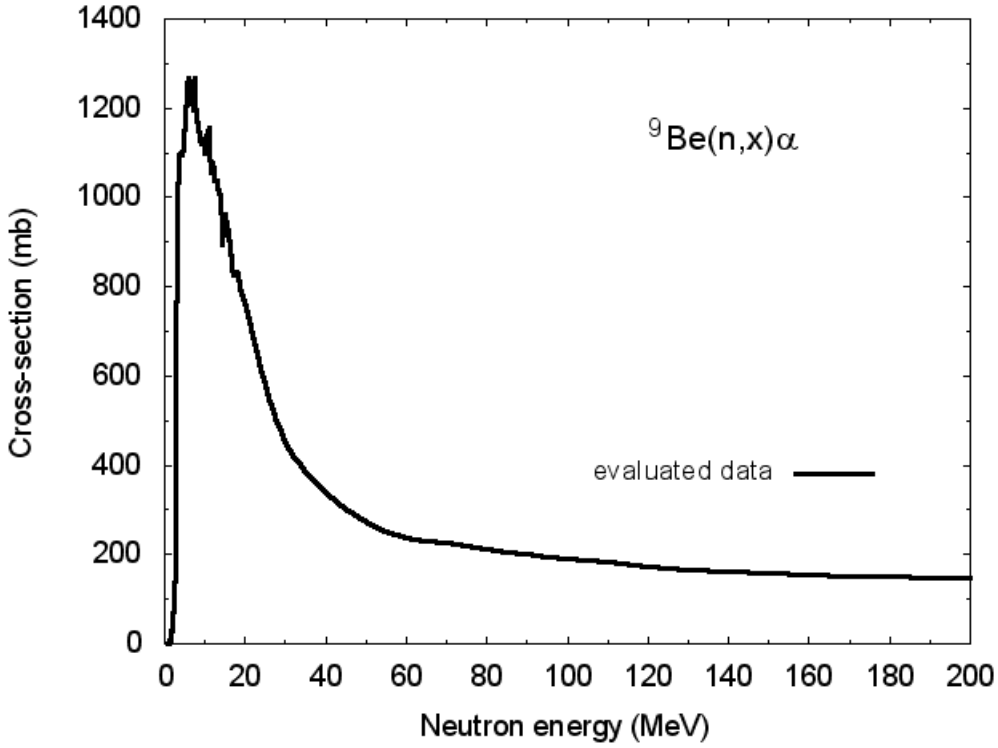

Fig.25 Evaluated α-particle production cross-section for n+^{9}Be interactions

4. Evaluation of atomic displacement cross-sections for n+^{9}Be reactions

There is no reliable data for beryllium to correct or improve the number of stable defects produced under irradiation calculated using standard NRT model [25], as it was made, for example, for iron and tungsten in Refs.[26,27]. For this reason, the calculation of atomic displacement cross-sections for n+^{9}Be reactions was performed applying the NRT model only. The effective threshold displacement energy E_d equal to 31 eV [28] was adopted for calculations.

The displacement cross-section for nonelastic neutron interactions with ^{9}Be $\sigma_d^{(nonel)}$ was calculated using Bertini, ISABEL, INCL4, and CEM03 models and models implemented in the TALYS code.

As in the case of gas production cross-sections, the evaluation of $\sigma_d^{(nonel)}$ was performed using the expression Eq.(9). The sum was made for results of Bertini, ISABEL, and CEM03 with the weights discussed in Section 3. The calculations performed with INCL4 and TALYS are used for comparison with other results, as well as to demonstrate the possible uncertainty of displacement calculations for ^{9}Be applying modern nuclear models.

Fig.26 shows examples of recoil energy distributions obtained using different models; the scatter of the data concerns the typical uncertainty of calculated distributions.

Figs.27 and 28 shows the $\sigma_d^{(nonel)}$ values obtained using data from various data libraries and results of calculations. Evaluated data for nonelastic displacement cross-sections are given in Fig.29. As for gas production cross-sections, the values of $\sigma_d^{(nonel)}$ estimated with Eq.(9) were fitted to the JEFF-3.2 data.

To evaluate the elastic component of displacement cross-section $s_d^{(el)}$ the calculations were performed using the optical model with Koning, Delaroche [29] and Madland [30] potentials.

Figs.30 and 31 show displacement cross-sections for neutron elastic scattering on ^{9}Be obtained using data from ENDF/B-VII.1, JENDL-4, and JEFF-3.2 and calculated cross-sections. There is the good agreement between data form various data libraries (Fig.30).

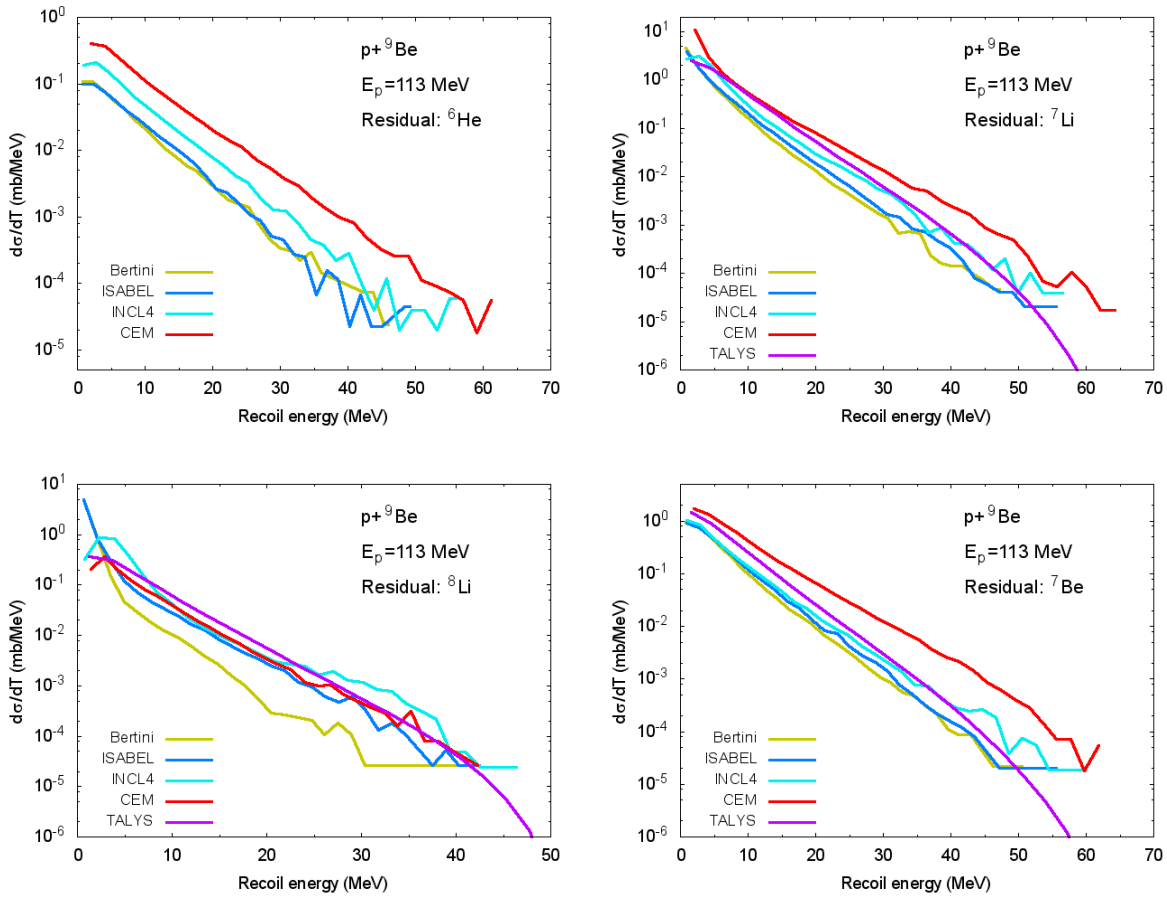

Fig.26 Examples of calculated recoil energy distributions for a number of residual nuclei produced in n+^{9}Be reactions.

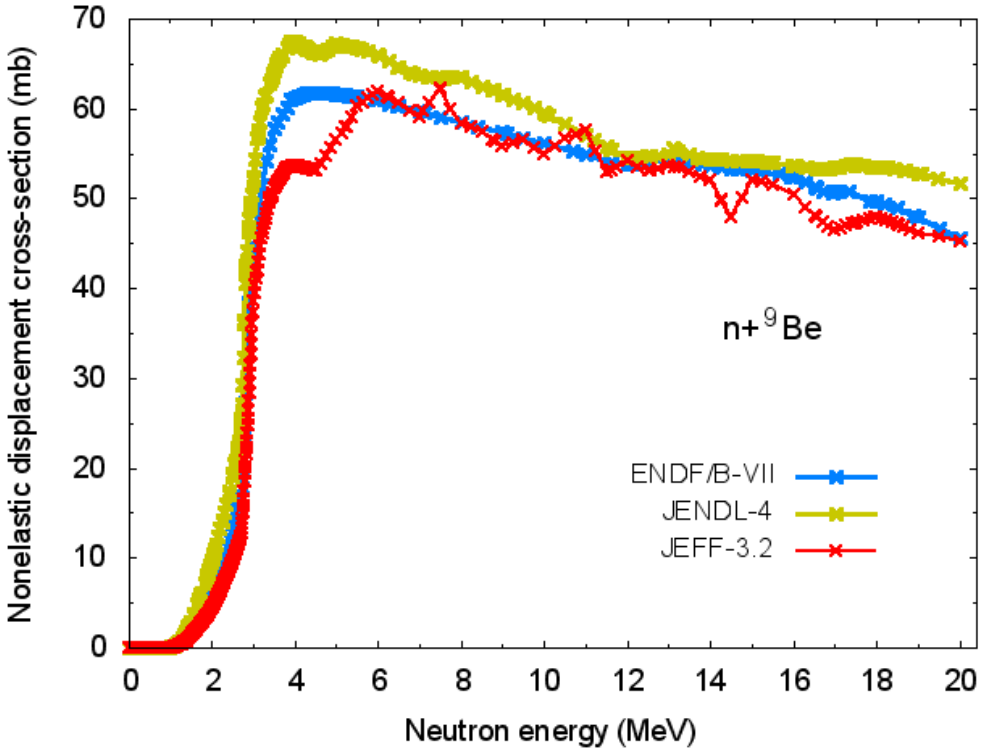

Fig.27 Displacement cross-section for nonelastic neutron interactions with ^{9}Be obtained using data from ENDF/B-VII.1, JENDL-4, and JEFF-3.2.

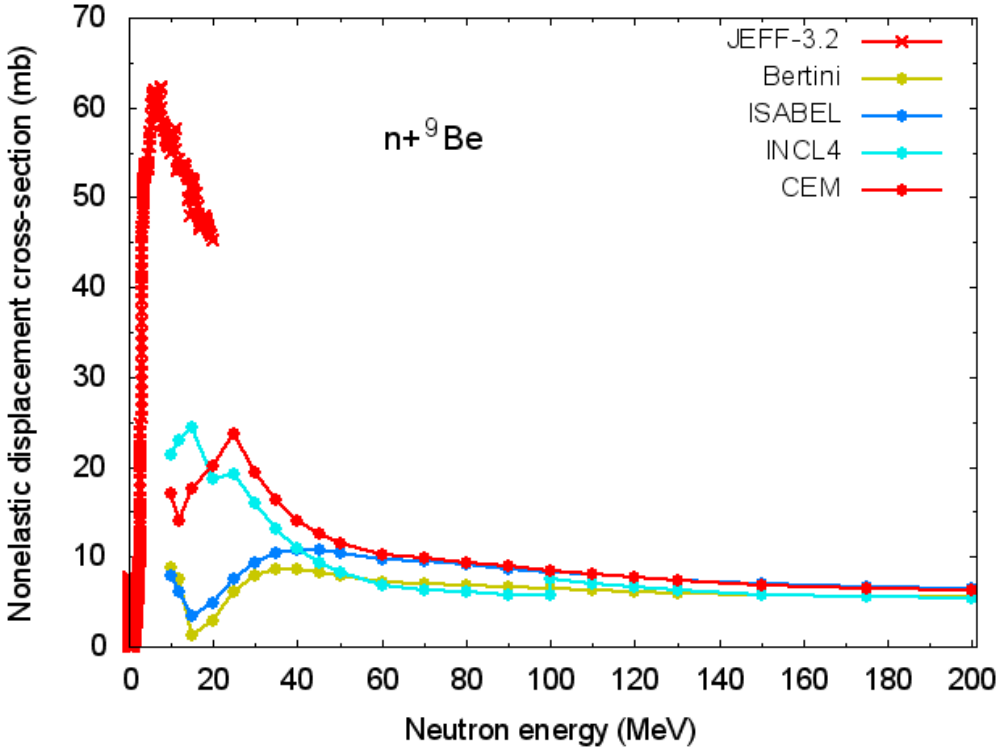

Fig.28 Displacement cross-section for nonelastic neutron interactions with ^{9}Be calculated with the help of different nuclear model and obtained using data from JEFF-3.2.

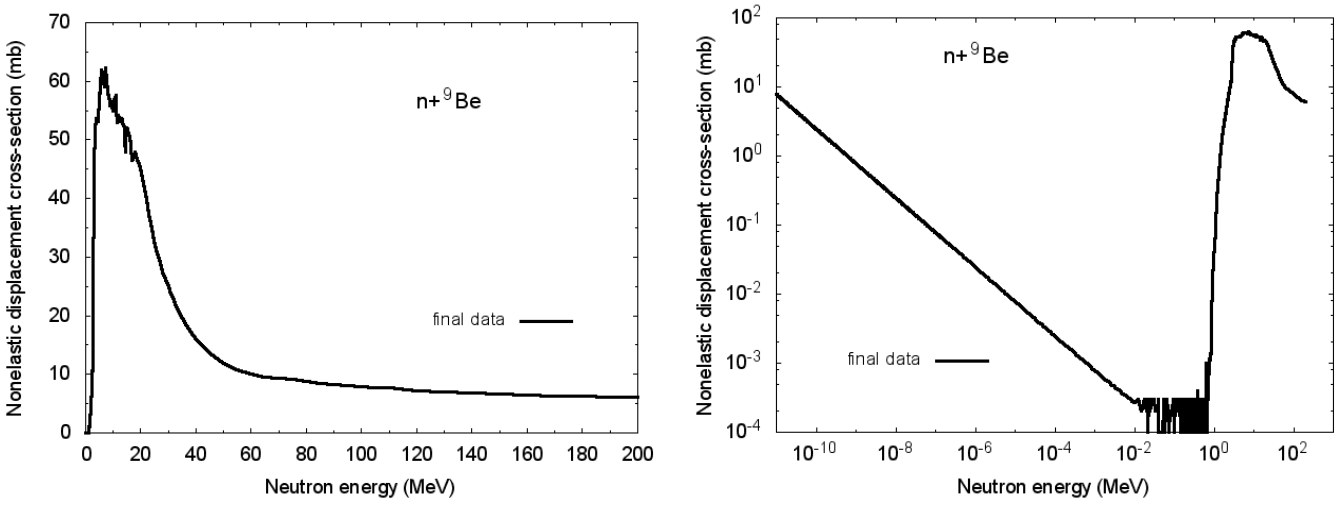

Fig.29 Evaluated displacement cross-section for nonelastic neutron interactions with ^{9}Be in linear and logarithmic scales.

The observed agreement of $\sigma_d^{(el)}$ values calculated using different potentials around 200 MeV and between calculated cross-sections and data from JEFF-3.2 (Fig.31) simplifies the final evaluation of $\sigma_d^{(el)}$. As in the case of gas production cross-sections, the correction was made to fit calculated $\sigma_d^{(el)}$ to JEFF-3.2 data. Fig.32 shows evaluated displacement cross-sections for elastic neutron scattering.

The total evaluated displacement cross-section ($\sigma_d^{(el)}$+ $\sigma_d^{(nonel)}$) is presented in Fig.33.

5. Data in ENDF format

Obtained data were written in the ENDF format. Conventional MT-numbers 203, 204, 205, 206, and 207 were applied for the files with proton-, deuteron-, triton-, ^{3}He-, and α-particle production cross-sections, respectively.

Atomic displacement cross-sections were recorded in barn units. Such data representation is different from the common recording of “damage energy production cross-sections” in eV-barn with MT=444 by the NJOY processing. The calculation of cross-sections assumes the use of the fixed value of threshold displacement energy E_d by the integration of corresponding distributions [26,27] and is not E_d-“independent”. The representation of displacement cross-sections in barns seems rather consistent.

The total displacement cross-section was recorded in the file MF = 3, with MT = 901, as it was made for EUROFER stainless steel in Ref.[31]. The contribution of neutron elastic scattering is given in MT=902.

The file obtained was processed with NJOY to fix possible inconsistencies in the data representation.

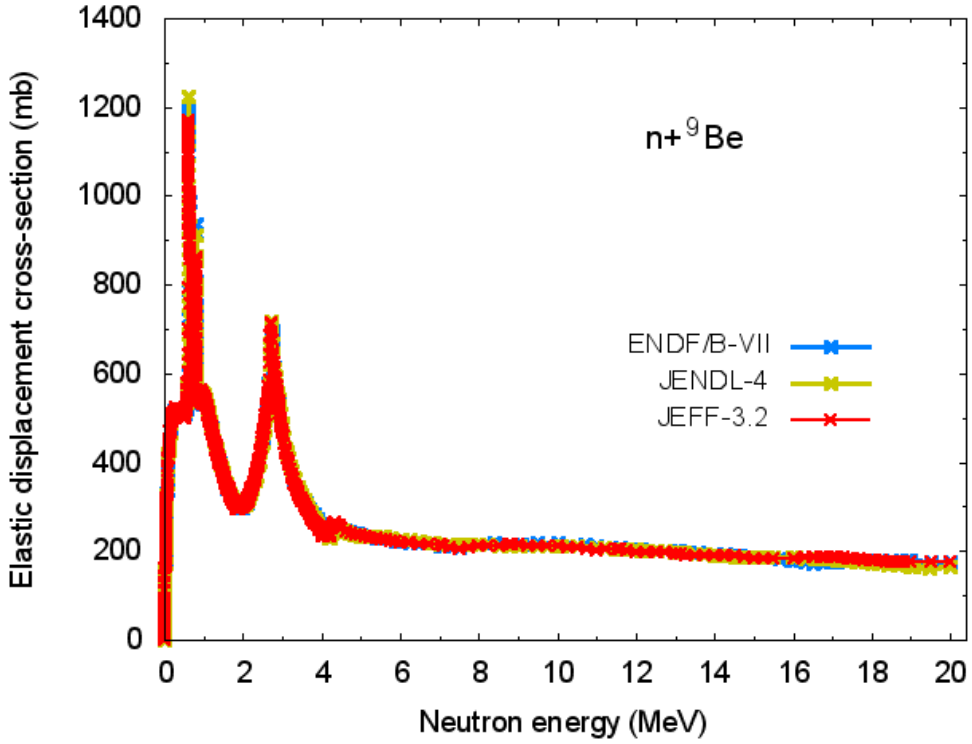

Fig.30 Displacement cross-section for elastic neutron scattering on ^{9}Be obtained using data from ENDF/B-VII.1, JENDL-4, and JEFF-3.2.

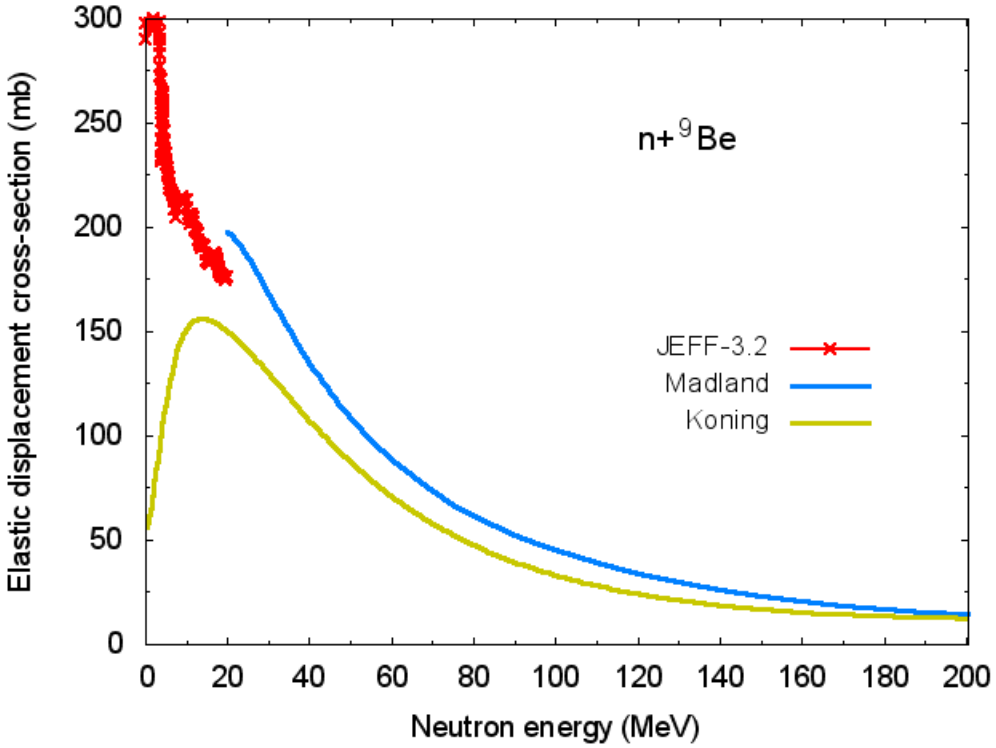

Fig.31 Displacement cross-section for elastic neutron scattering on ^{9}Be obtained using data from JEFF-3.2 and calculated with optical model applying different potentials.

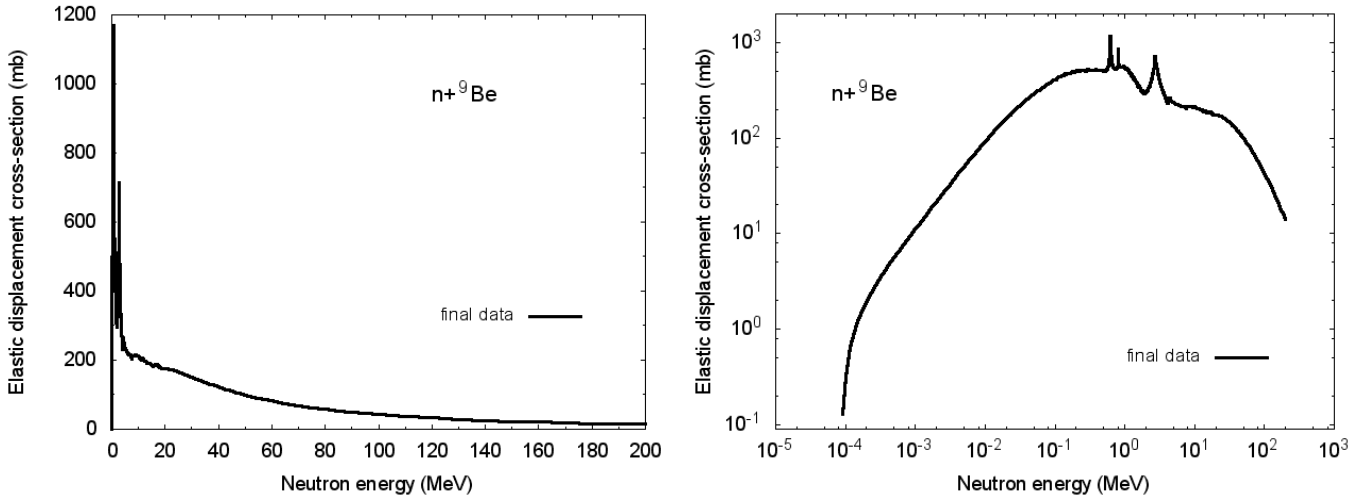

Fig.32 Evaluated displacement cross-section for elastic neutron scattering on ^{9}Be in linear and logarithmic scales.

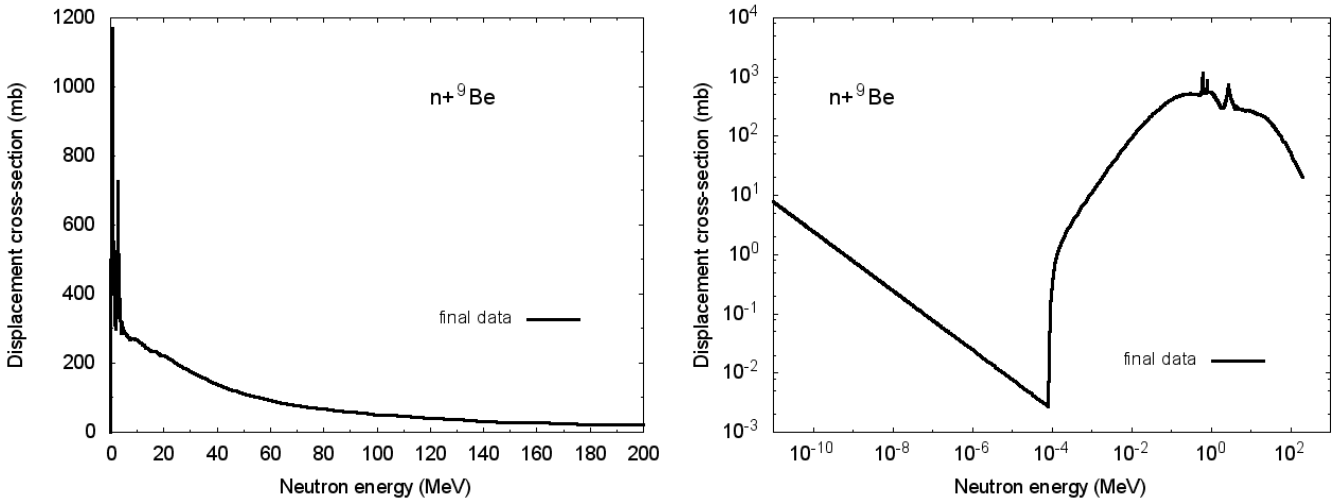

Fig.33 Evaluated total displacement cross-section for n+ ^{9}Be interactions in linear and logarithmic scales.

5. Conclusion

Atomic displacement cross-sections and components of gas production cross-sections: proton-, deuteron-, triton-, ^{3}He, α-particles formation cross-sections were evaluated for ^{9}Be irradiated with neutrons at the energies up to 200 MeV.

Calculations of cross-sections were performed using a number of nuclear models including the pre-equilibrium model, the evaporation model, and the Fermi break-up model implemented in modern computer codes. The quality of model predictions was estimated from the comparison with angular and energy distribution of particles in proton induced reactions. The information obtained was used for the evaluation of investigated cross-sections for neutron induced reactions. Corrections were made to fit evaluated curves to the data from JEFF-3.2.

Final evaluated data were written in ENDF format and processed using the NJOY code.

The data obtained can be applied for the evaluation of radiation damage and gas production rates in natural beryllium irradiated with neutrons in various units including the fusion reactor.

References

[1] T.A. Tomberlin, Beryllium – a unique material in nuclear applications, NEEL/ CON-04-01869, 2004.

[2] J.T. Goorley, M.R. James, T.E. Booth, F.B. Brown, J.S. Bull, L.J. Cox, J.W. Durkee, J.S. Elson, M.L. Fensin, R. A. Forster, J.S. Hendricks, H.G. Hughes, R.C. Johns, B.C. Kiedrowski, R.L. Martz, S.G. Mashnik, G.W. McKinney, D.B. Pelowitz, R.E. Prael, J.E. Sweezy, L.S. Waters, T.A. Wilcox, A. Zukaitis, MCNP6TM User's manual, Ed. D.B. Pelowitz, LA-CP-13-00634, May 2013

[3] A.J. Koning, S. Hilaire, M.C. Duijvestijn, TALYS-1.0, Proc. Int. Conf. on Nuclear Data for Science and Technology (ND2007), April 22-27, 2007, Nice, France, eds. O. Bersillon, F. Gunsing, E. Bauge, R. Jacqmin, S. Leray, EDP Sciences, 2008, p. 211

[4] A.Yu. Konobeyev, U. Fischer, EFFDOC 1236, Nov. 2014, https://www.oecd-nea.org/dbdata/jeff/effdoc.html

[5] Reference Input Parameter Library (RIPL-3), https://www-nds.iaea.org/RIPL-3/

[6] S.G. Mashnik, L.M. Kerby, MCNP6 fragmentation of light nuclei at intermediate energies, *Nucl. Instr. Meth. Phys. Res.* A764 (2014) 59.

[7] A.J. Koning, S. Hilaire, S. Goriely, TALYS-1.6. A nuclear reaction program, http://www.talys.eu/

[8] A.Yu. Konobeyev, U. Fischer, A.J. Koning, H. Leeb, S. Leray, Y. Yariv, What can we expect from the use of nuclear models implemented in MCNPX at projectile energies below 150 MeV? Detailed comparison with experimental data, *J. Korean Phys. Soc.* 59 (2011) 927.

[9] M.M. Meier, D.A. Clark, C.A. Goulding, J.B. McClelland, G.L. Morgan, C.E. Moss, W.B. Amian, Differential neutron production cross sections and neutron yields from stopping-length targets for 113-MeV protons, Nucl. Sci. Eng. 102 (1989) 310

[10] R.E.L. Green, R.G. Korteling, J.M. D'auria, K.P. Jackson, R.L. Helmer, Light fragment spectra to upper kinematic limits for 300 MeV proton reactions with Be and Ag, *Phys. Rev.* C35 (1987) 1341.

[11] M.M. Meier, W.B. Amian, C.A. Goulding, G.L. Morgan, C.E. Moss, Differential neutron production cross sections for 256-MeV protons, *Nucl. Sci. Eng.* 110 (1992) 289.

[12] R. Michel, R. Bodemann, H. Busemann, R. Daunke, M. Gloris, H.-J. Lange, B. Klug, A. Krins, I. Leya, M. Lüpke, S. Neumann, H. Reinhardt, M. Schnatz-Büttgen, U. Herpers, Th. Schiekel, F. Sudbrock, B. Holmqvist, H. Condé, P. Malmborg, M. Suter, B. Dittrich-Hannen, P.-W. Kubik, H.-A. Synal, D. Filges, Cross sections for the production of residual nuclides by low- and medium-energy protons from the target elements C, N, O, Mg, Al, Si, Ca, Ti, V, Mn, Fe,

Co, Ni, Cu, Sr, Y, Zr, Nb, Ba and Au, *Nucl. Instr. Meth. Phys. Res.* B129 (1997) 153.

[13] H. Leeb, M.T. Pigni, I. Raskinyte, Covariances for evaluations based on extensive modelling, Proc. Int. Conf. on Nuclear Data for Science and Technology (ND2004), Santa Fe, USA, Sep. 26 – Oct. 1, 2004, p.161.

[14] D. L. Smith, private talk, ND2007, Nice, (2007).

[15] A.Yu. Konobeyev, U. Fischer, P.E. Pereslavtsev, Computational approach for evaluation of nuclear data including covariance information, *J. Korean Phys. Soc.* 59 (2011) 923.

[16] S. Leray, A. Boudard, J. Cugnon, J.C. David, A. Kelic´-Heil, D. Mancusi, M.V. Ricciardi, Improved modelling of helium and tritium production for spallation targets, *Nucl. Instr. Meth. Phys. Res.* B268 (2010) 581.

[17] Experimental Nuclear Reaction Data (EXFOR), https://www-nds.iaea.org/exfor/exfor.htm

[18] M.E. Wyman, E.M. Fryer, M.Thorpe, (n,t) cross sections for B-10, B-11 and Be-9, *Phys. Rev.* 112 (1958) 1264.

[19] T. Biro, S. Sudar, J.Csikai, Z. Dezso, Cross-sections of (n,t) reactions with 14.7 MeV neutrons determined by direct beta-counting of tritium, *J. Inorganic and Nuclear Chemistry* 37 (1975) 1583.

[20] Z.T. Body, F. Cserpak, J. Csikai, S. Sudar, K. Mihaly, Measurement and evaluation of (n,t) cross sections, EXFOR 30818002 (1982)

[21] H. Liskien, R. Widera, R. Woelfe, R. Widera, Experimentally determined excitation function for the Be-9(n,t) reaction, EXFOR 22035002 (1987)

[22] M. Zadro, S. Blagus, D. Miljanic, D. Rendic, The (n,t) reaction on Be-9 at 14.6 MeV, *Nucl. Sci. Eng.* 95 (1987) 79.

[23] R. Woelfle, S.M. Qaim, H. Liskien, R. Widera, Systematic studies of excitation functions of (n,t) reactions on medium and heavy mass nuclei, *Radiochimica Acta* 50 (1990) 5.

[24] R. Woelfle, A. Suhaimi, S.M. Qaim, Determination of the excitation function of the (n,xt) process on beryllium via activation in diverse neutron fields and unfolding code calculations, *Nucl. Sci. Eng.* 115 (1993) 71.

[25] M.J. Norgett, M.T. Robinson, I.M. Torrens, A proposed method of calculating displacement dose rates, *Nucl. Eng. Des.* 33 (1975) 50.

[26] A.Yu. Konobeyev, C.H.M. Broeders, U. Fischer, Improved displacement cross sections for structural materials irradiated with intermediate and high energy protons, Proc. 8th International Topical Meeting on the Nuclear Applications of Accelerator Technology (AccApp'07), July 30 - August 2, 2007, Pocatello, USA, p.241.

[27] A.Yu. Konobeyev, U. Fischer, L. Zanini, Advanced evaluations of displacement and gas production cross sections for chromium, iron, and nickel up to 3 GeV

incident particle energy, Proc. Tenth International Topical Meeting on Nuclear Applications of Accelerators (AccApp'11), April 3-7, 2011, Knoxville, USA

[28] NJOY: Data processing system of evaluated nuclear data files in ENDF format, https://www.oecd-nea.org/dbprog/njoy-links.html

[29] A.J. Koning, J.P. Delaroche, Local and global nucleon optical models from 1 keV to 200 MeV, *Nucl. Phys.* A713 (2003) 231.

[30] D.G. Madland, Progress in the development of global medium-energy nucleon-nucleus optical model potentials, Proc. Spec. Meeting on the Nucleon Nucleus Optical Model up to 200 MeV, Bruyères-le-Chatel, November 13-15, 1996 p.129

[31] A.Yu. Konobeyev, U. Fischer, P.E. Pereslavtsev, Evaluation of advanced displacement cross-sections for the major EUROFER constituents based on an atomistic modelling approach, KIT (2013).

Appendix

Comparison of double differential cross-sections of neutron emission in p+^{9}Be reactions calculated using Bertini, ISABEL, CEM03, and INCL4 models and models implemented in the TALYS code with available measured data

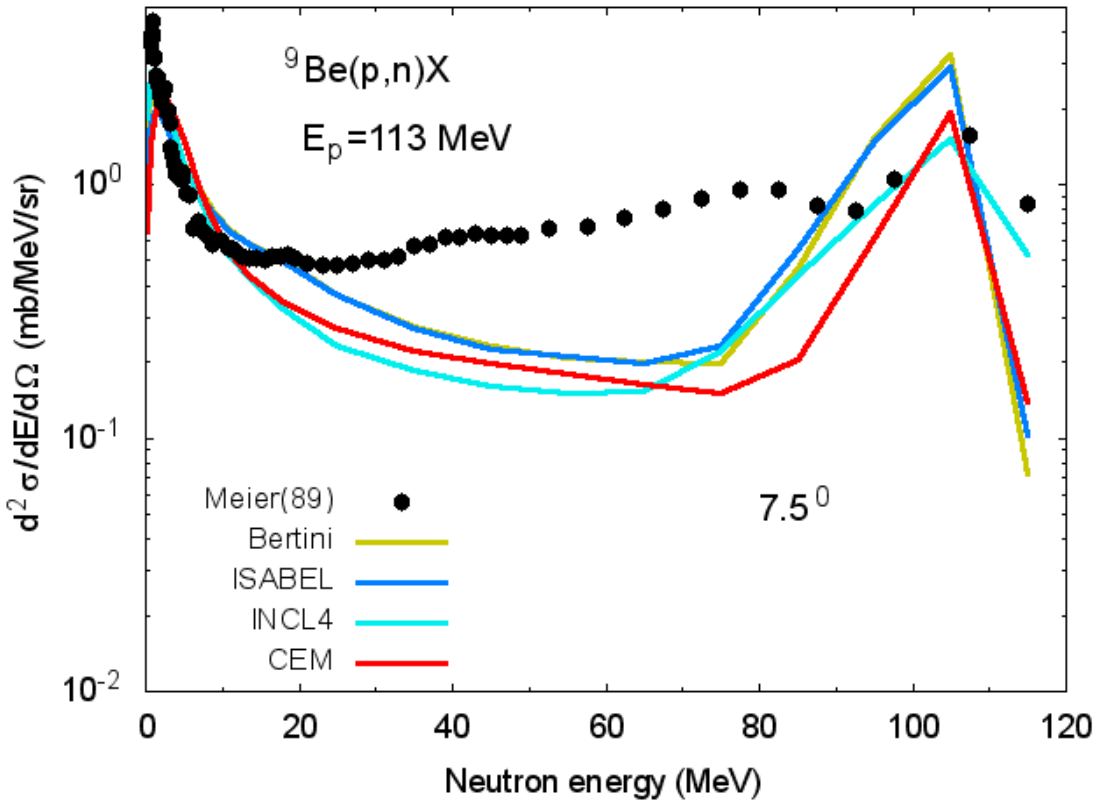
^{9}Be(p,n)X
E_p=113 MeV
7.5^0
Meier(89)
Bertini
ISABEL
INCL4
CEM
$d^2\sigma/dE/d\Omega$ (mb/MeV/sr)
Neutron energy (MeV)

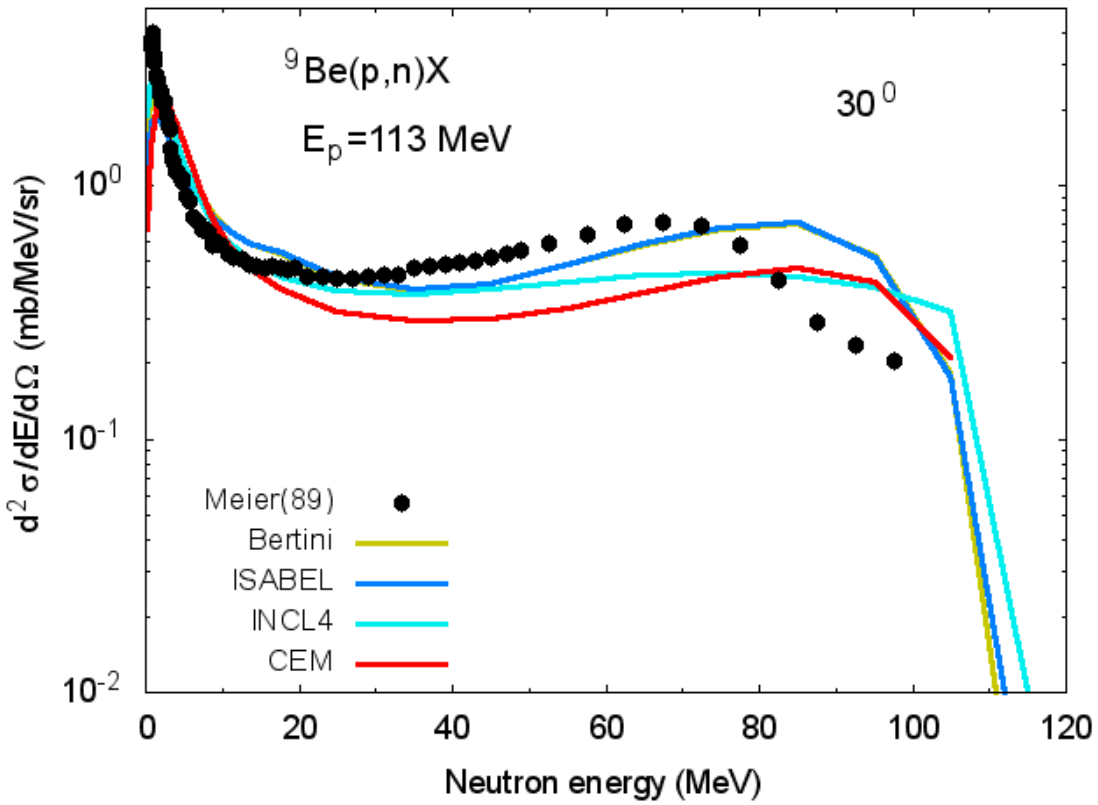
^{9}Be(p,n)X
E_p=113 MeV
30^0
Meier(89)
Bertini
ISABEL
INCL4
CEM
$d^2\sigma/dE/d\Omega$ (mb/MeV/sr)
Neutron energy (MeV)

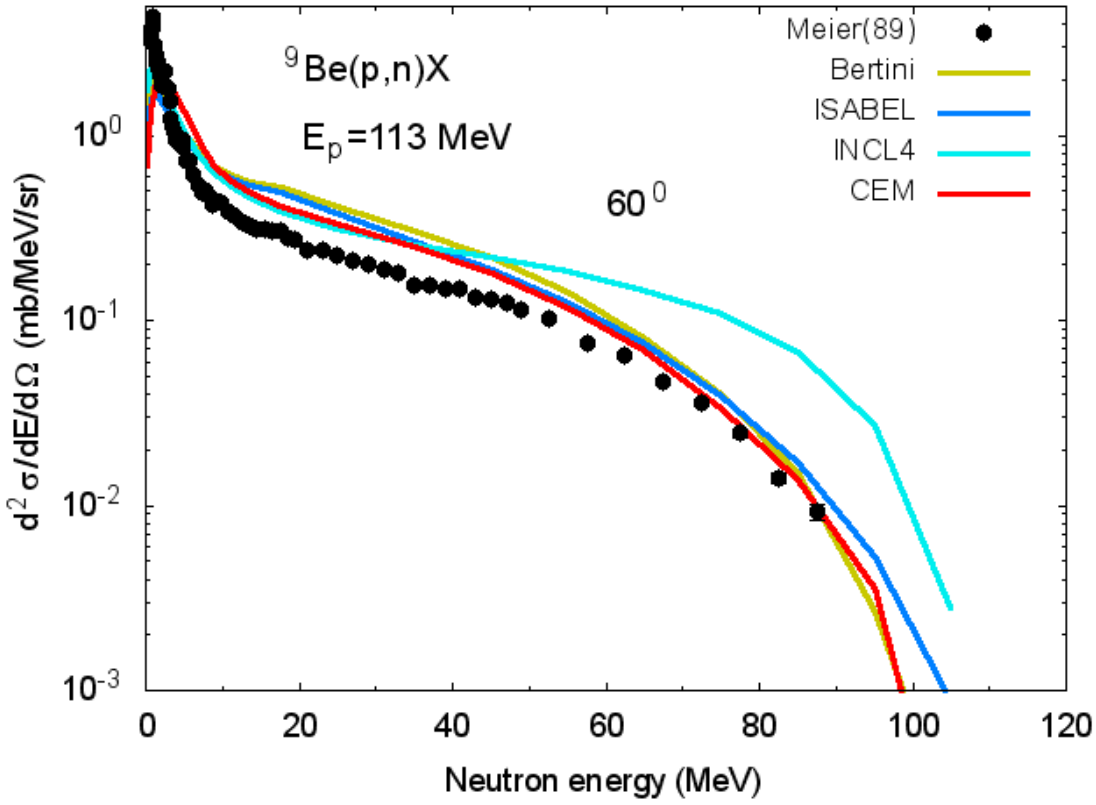
^{9}Be(p,n)X
E_p=113 MeV
60^0
Meier(89)
Bertini
ISABEL
INCL4
CEM
$d^2\sigma/dE/d\Omega$ (mb/MeV/sr)
Neutron energy (MeV)

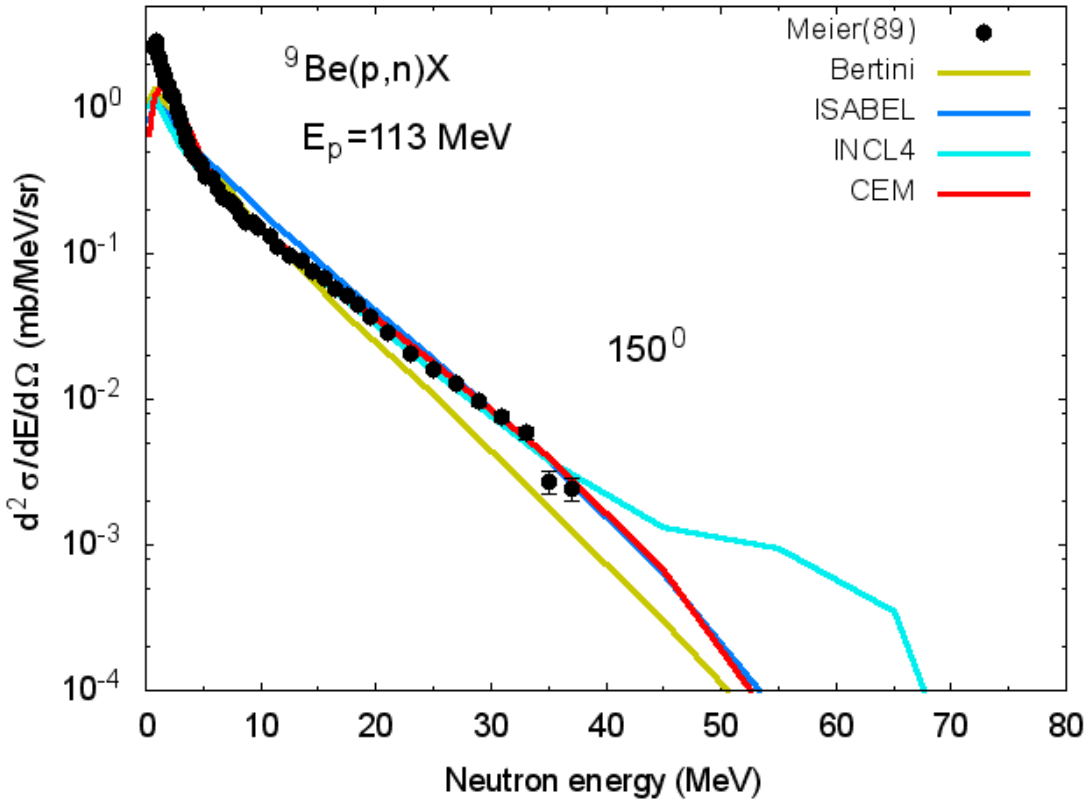
^{9}Be(p,n)X
E_p=113 MeV
150^0
Meier(89)
Bertini
ISABEL
INCL4
CEM
$d^2\sigma/dE/d\Omega$ (mb/MeV/sr)
Neutron energy (MeV)

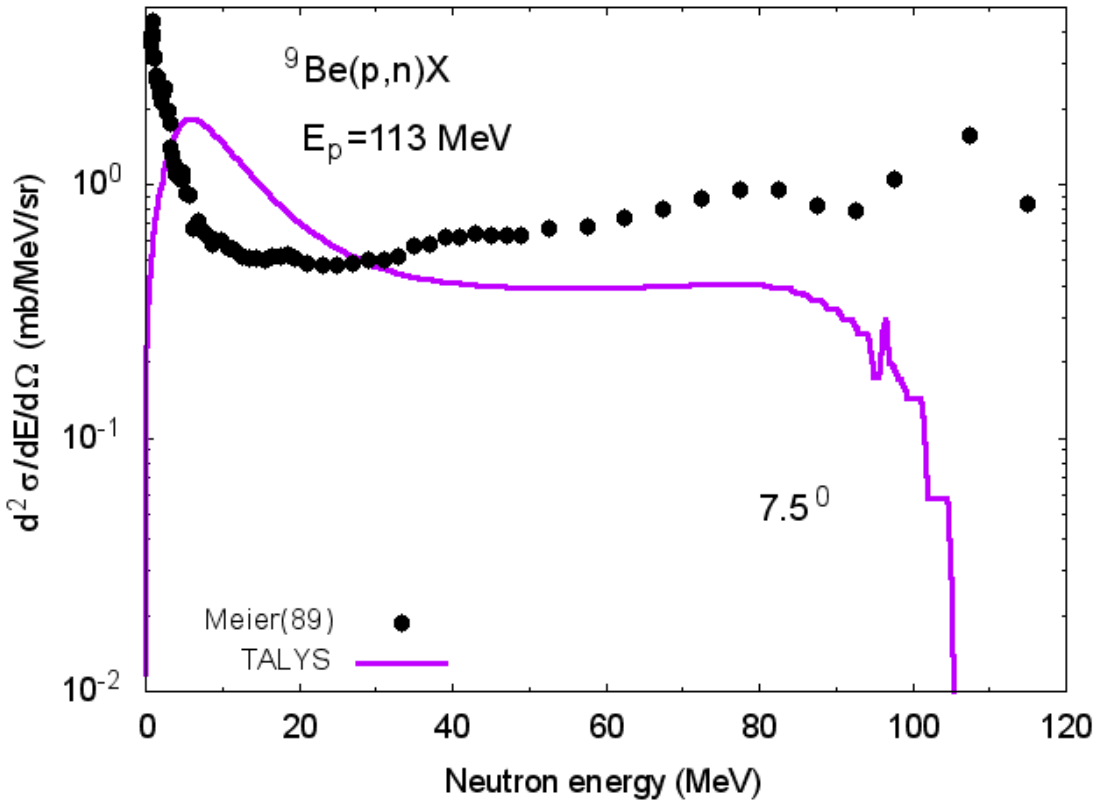
^{9}Be(p,n)X
E_p=113 MeV
7.5^0
Meier(89)
TALYS
10^0
10^{-1}
10^{-2}
0
20
40
60
80
100
120
$d^2\sigma/dE/d\Omega$ (mb/MeV/sr)
Neutron energy (MeV)

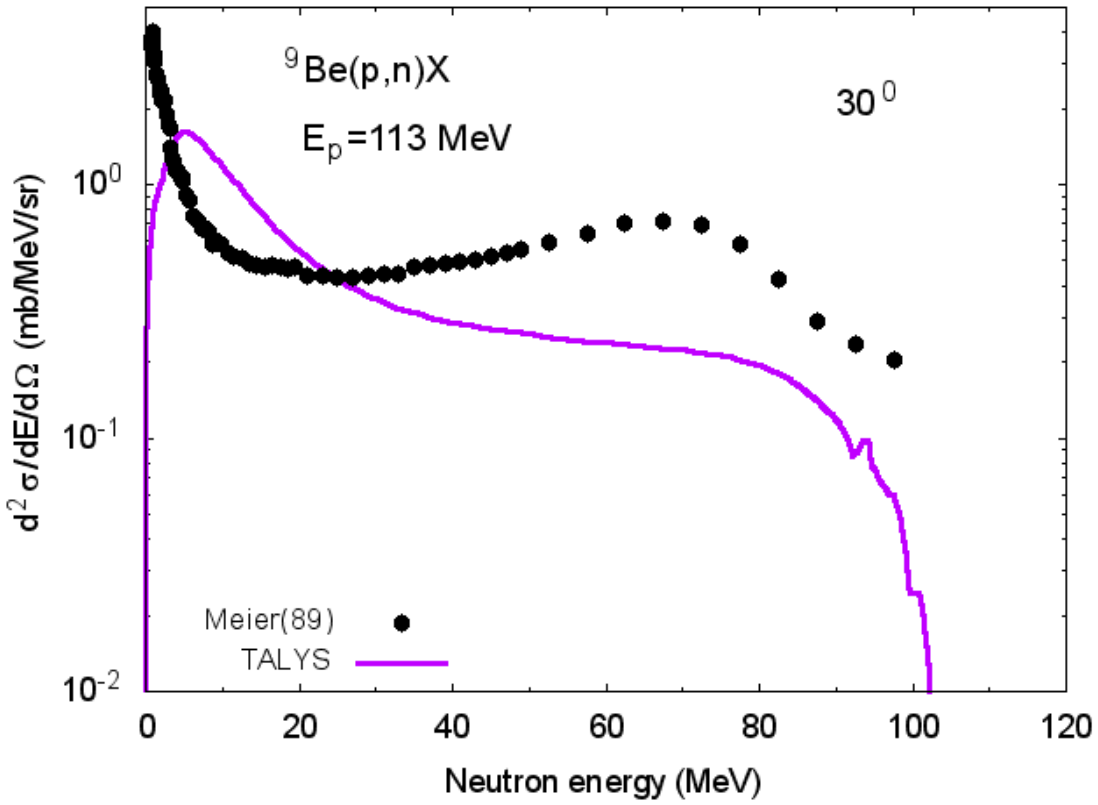
^{9}Be(p,n)X
E_p=113 MeV
30^0
Meier(89)
TALYS
10^0
10^{-1}
10^{-2}
0
20
40
60
80
100
120
$d^2\sigma/dE/d\Omega$ (mb/MeV/sr)
Neutron energy (MeV)

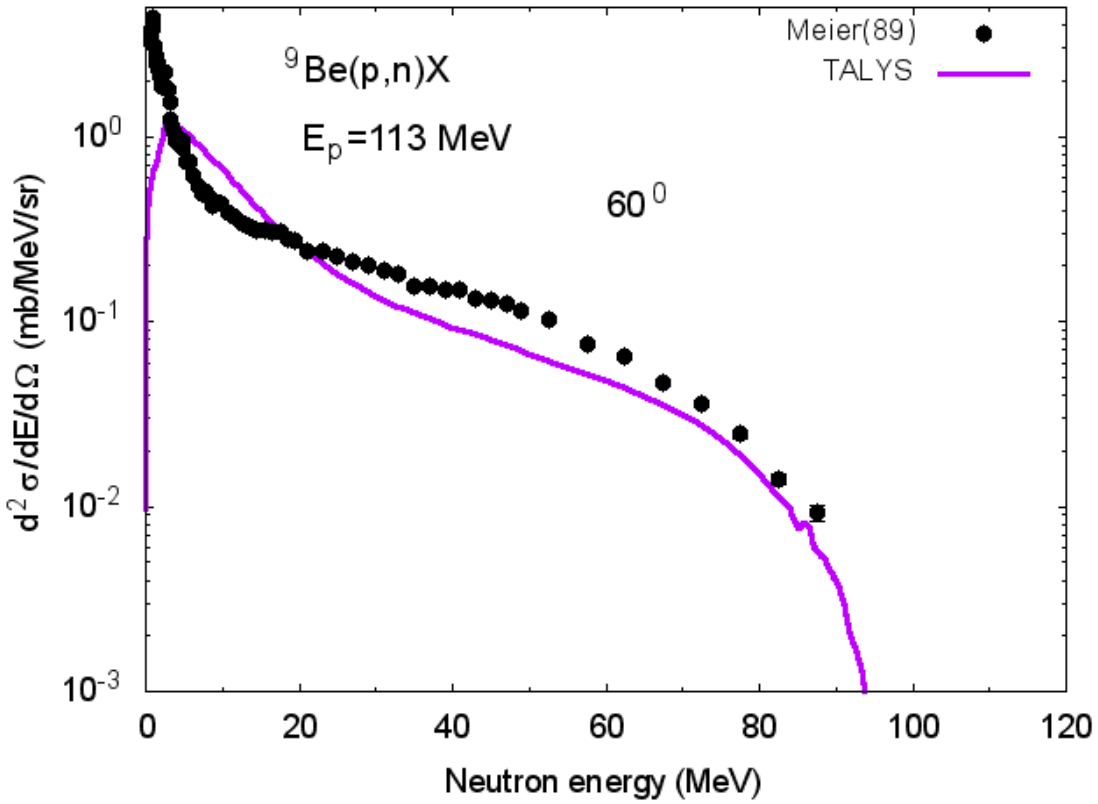
Meier(89)
TALYS
^{9}Be(p,n)X
E_p=113 MeV
60^0
$d^2\sigma/dE/d\Omega$ (mb/MeV/sr)
10^0
10^{-1}
10^{-2}
10^{-3}
0
20
40
60
80
100
120
Neutron energy (MeV)

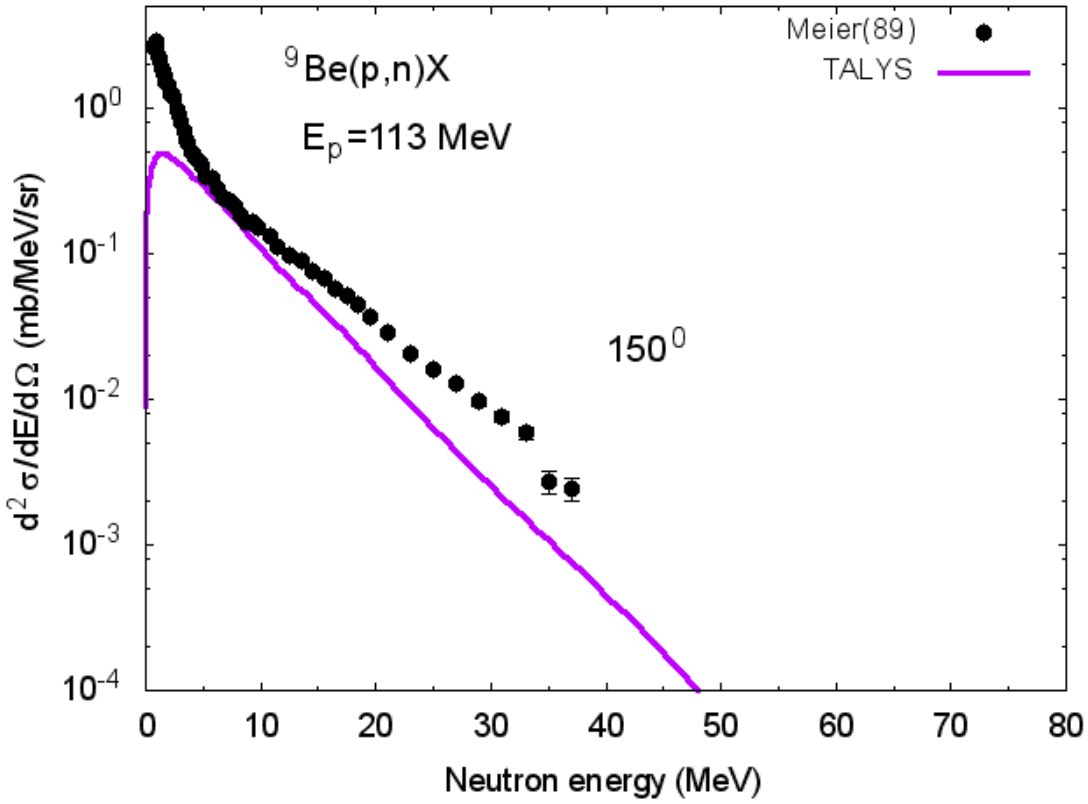
Meier(89)
TALYS
^{9}Be(p,n)X
E_p=113 MeV
150^0
$d^2\sigma/dE/d\Omega$ (mb/MeV/sr)
Neutron energy (MeV)

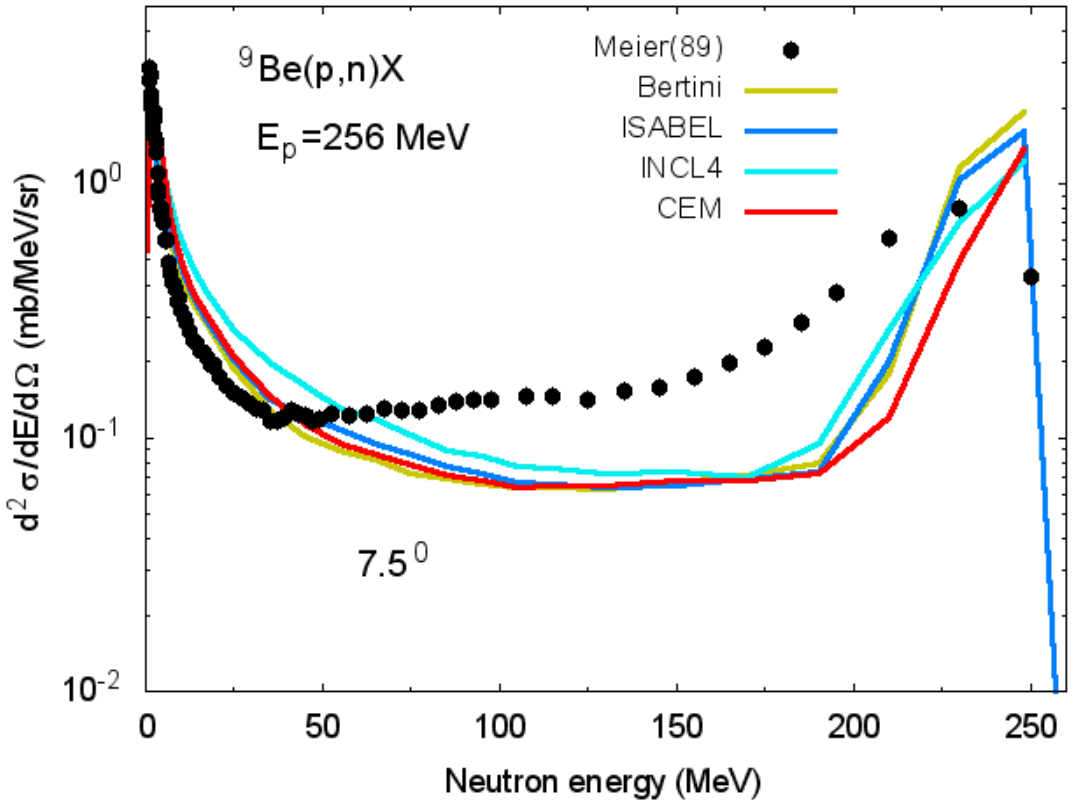
Meier(89)
Bertini
ISABEL
INCL4
CEM
^{9}Be(p,n)X
E_p=256 MeV
7.5^0
$d^2\sigma/dE/d\Omega$ (mb/MeV/sr)
Neutron energy (MeV)

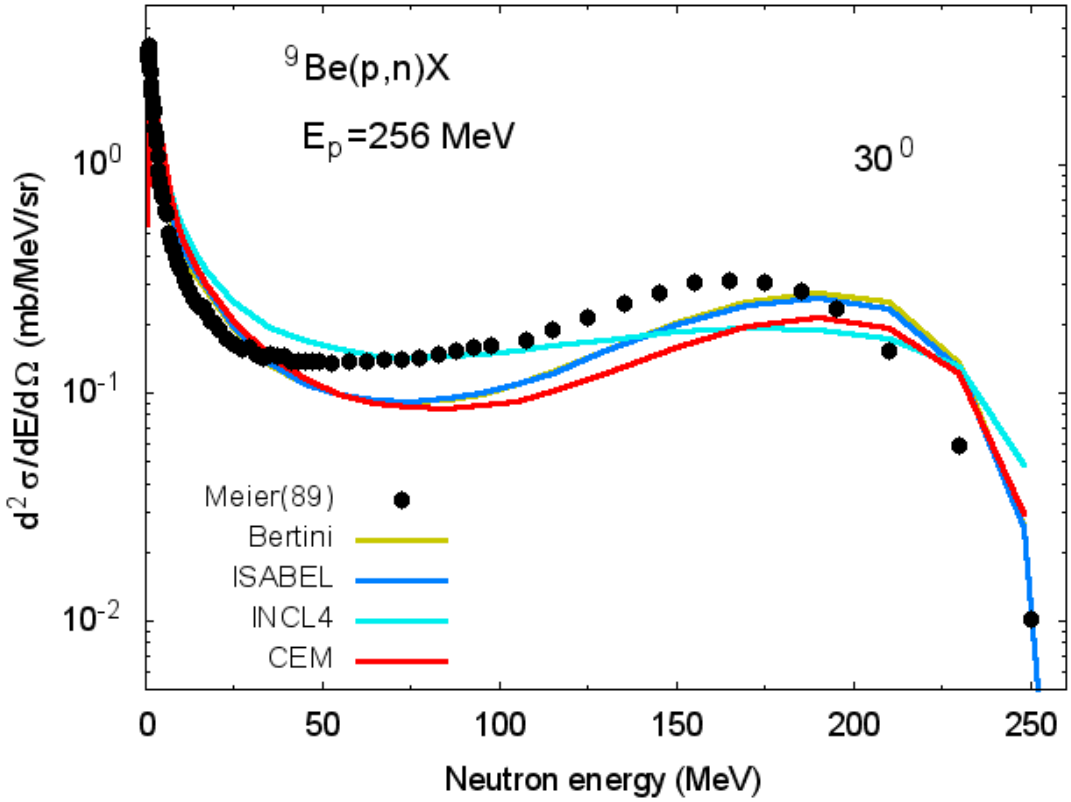
^{9}Be(p,n)X
E_p=256 MeV
30^0
Meier(89)
Bertini
ISABEL
INCL4
CEM
$d^2\sigma/dE/d\Omega$ (mb/MeV/sr)
Neutron energy (MeV)

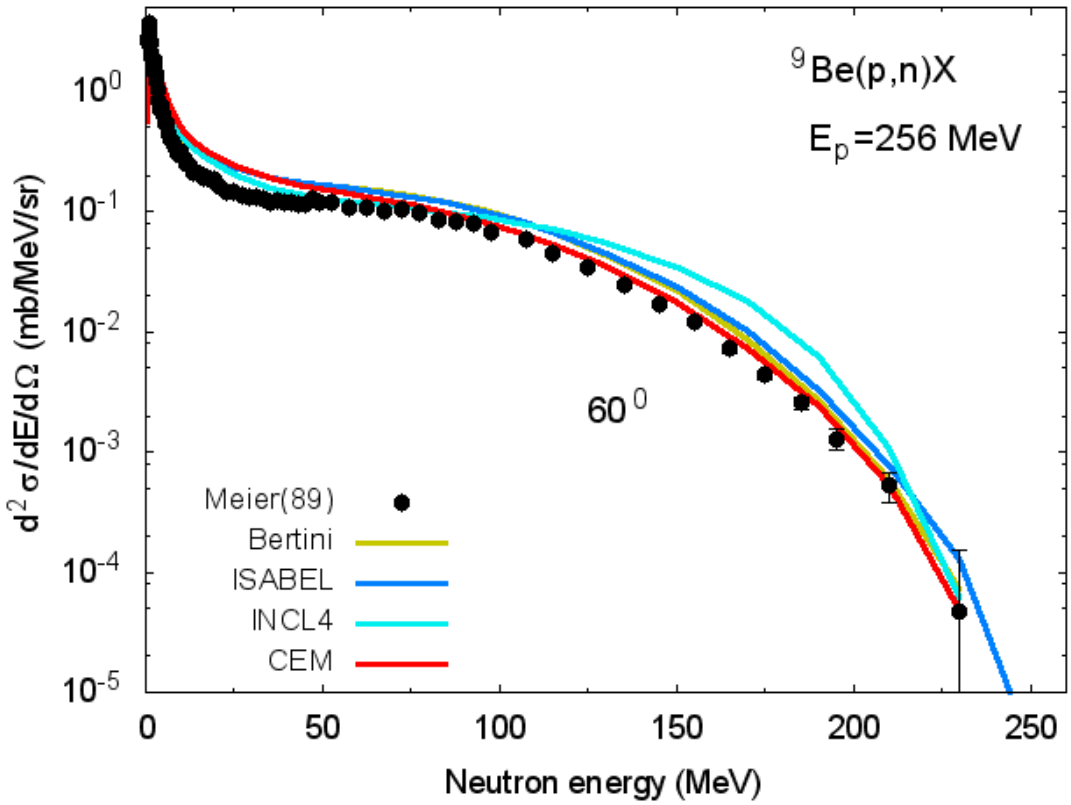
^{9}Be(p,n)X
E_p=256 MeV
60^0
Meier(89)
Bertini
ISABEL
INCL4
CEM
$d^2\sigma/dE/d\Omega$ (mb/MeV/sr)
Neutron energy (MeV)

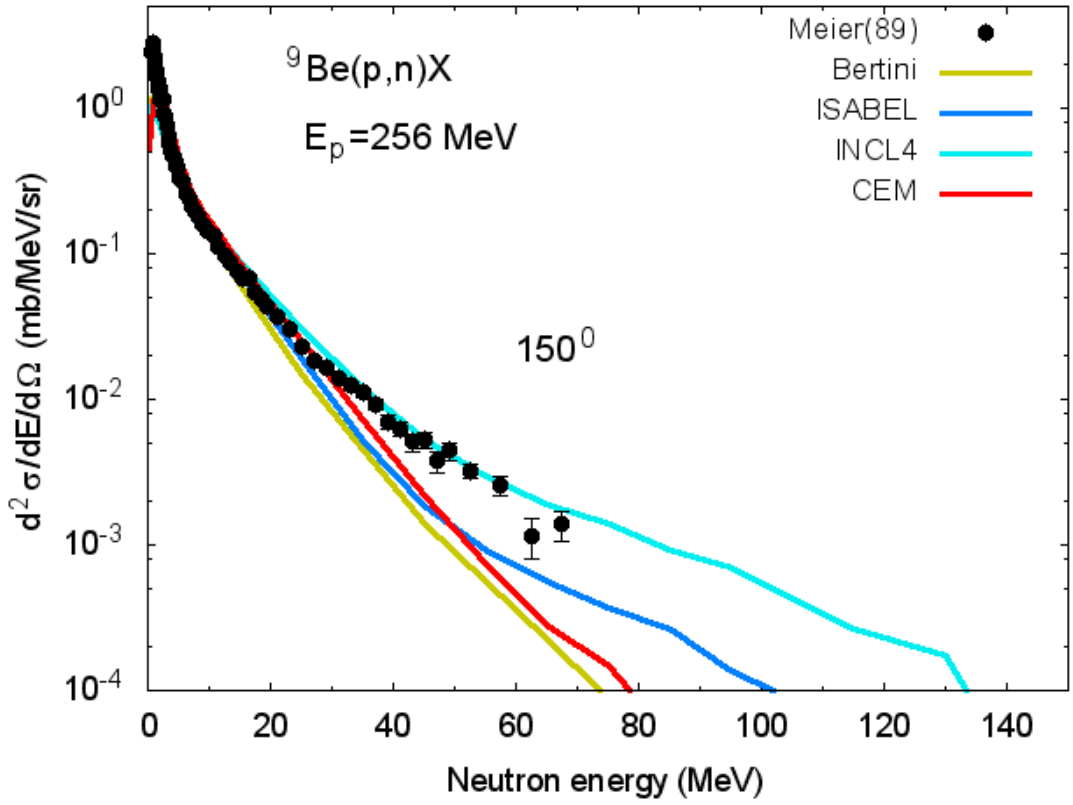
Meier(89)
Bertini
ISABEL
INCL4
CEM
^{9}Be(p,n)X
E_p=256 MeV
150^{0}
$d^2\sigma/dE/d\Omega$ (mb/MeV/sr)
Neutron energy (MeV)
10^{0}
10^{-1}
10^{-2}
10^{-3}
10^{-4}
0
20
40
60
80
100
120
140

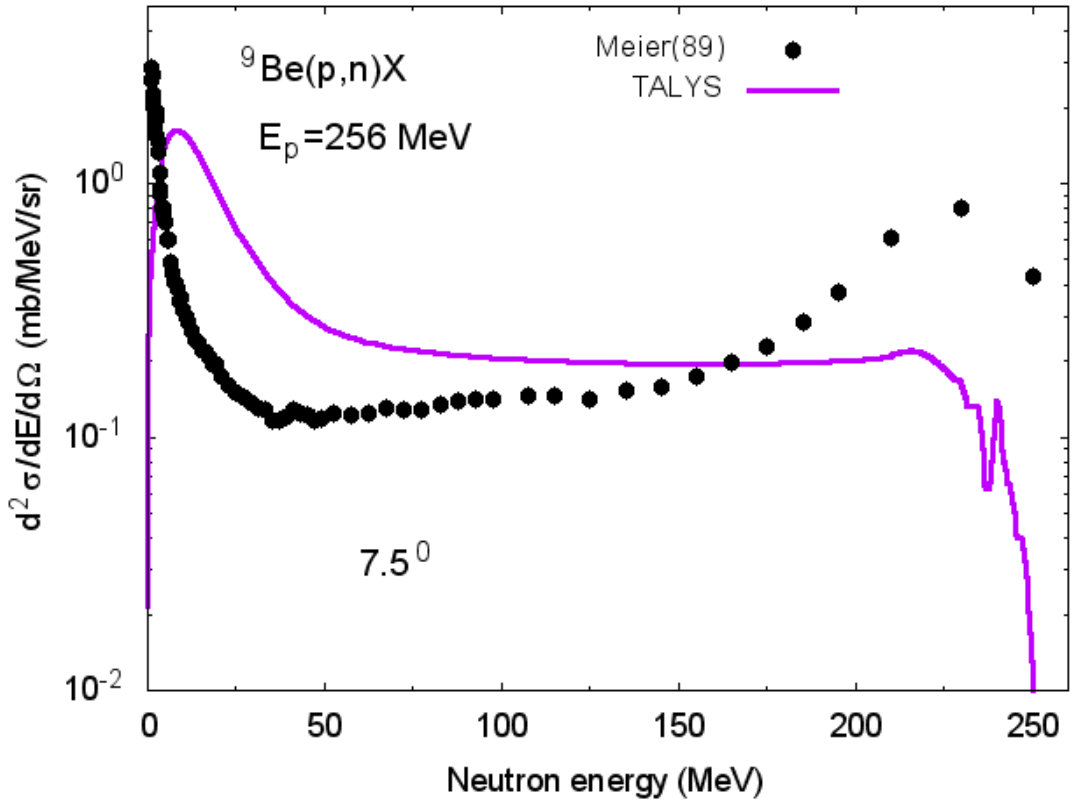
^{9}Be(p,n)X
E_p=256 MeV
Meier(89)
TALYS
7.5^0
$d^2\sigma/dE/d\Omega$ (mb/MeV/sr)
Neutron energy (MeV)

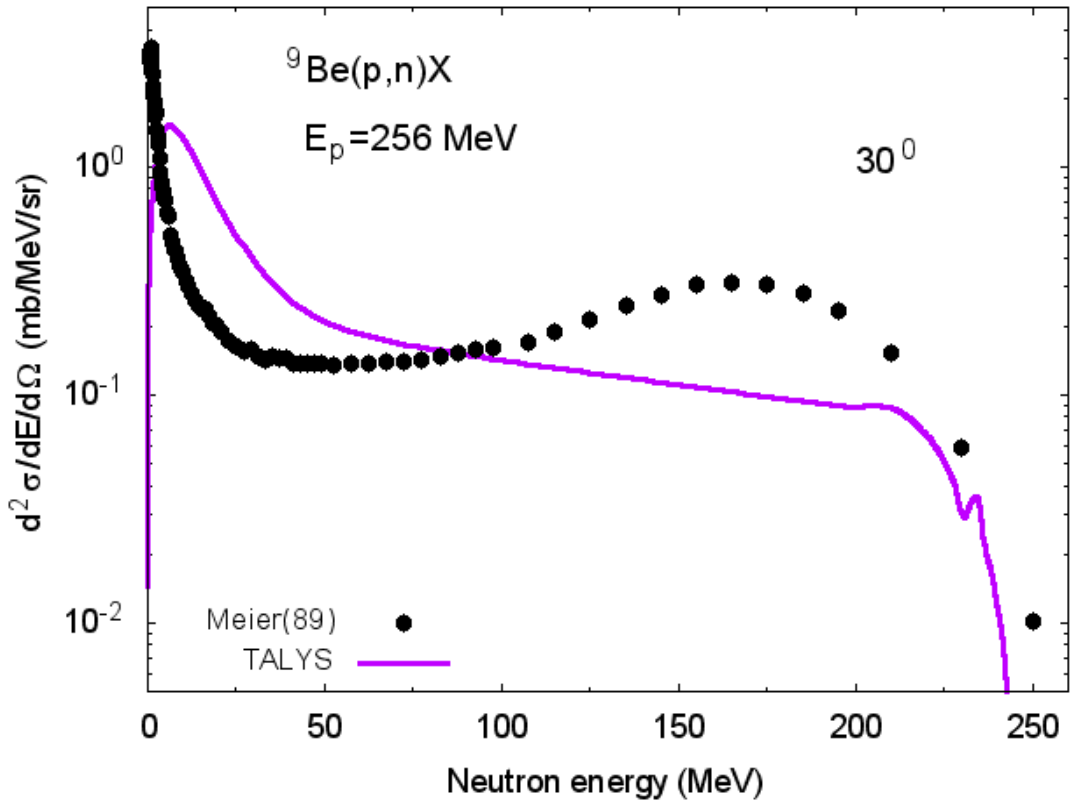
^{9}Be(p,n)X
E_p=256 MeV
30^0
Meier(89)
TALYS
$d^2\sigma/dE/d\Omega$ (mb/MeV/sr)
Neutron energy (MeV)

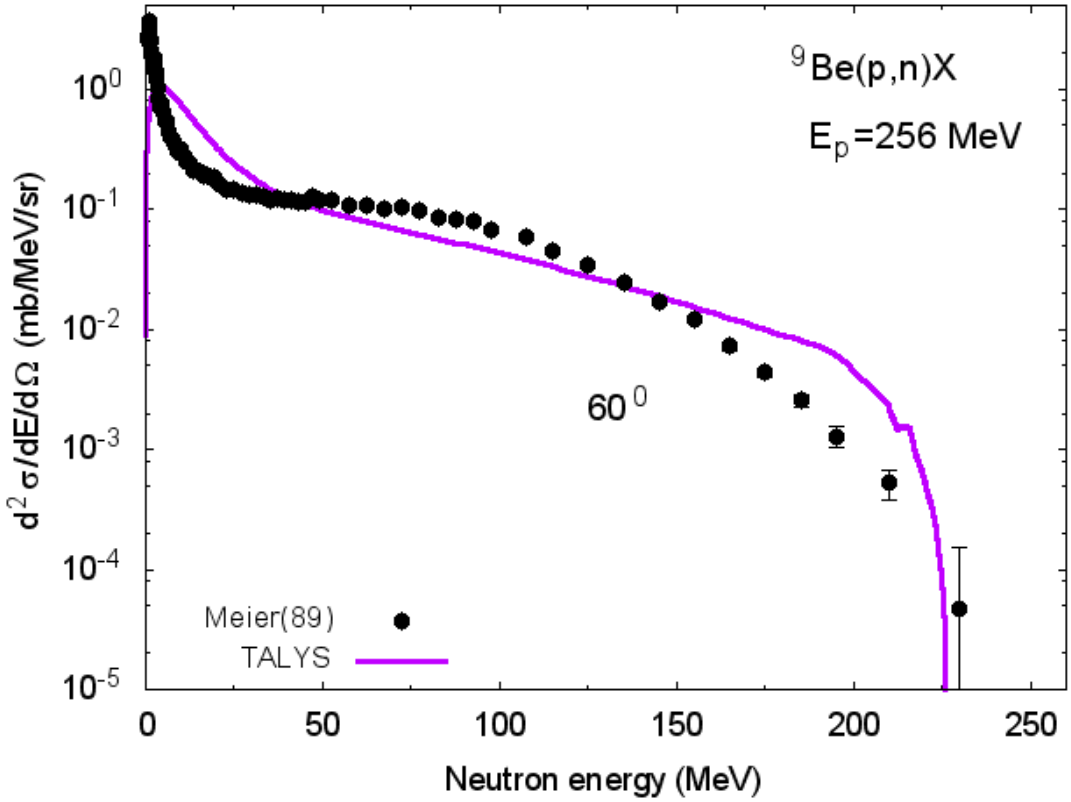
^{9}Be(p,n)X
E_p=256 MeV
60^0
Meier(89)
TALYS
$d^2\sigma/dE/d\Omega$ (mb/MeV/sr)
Neutron energy (MeV)

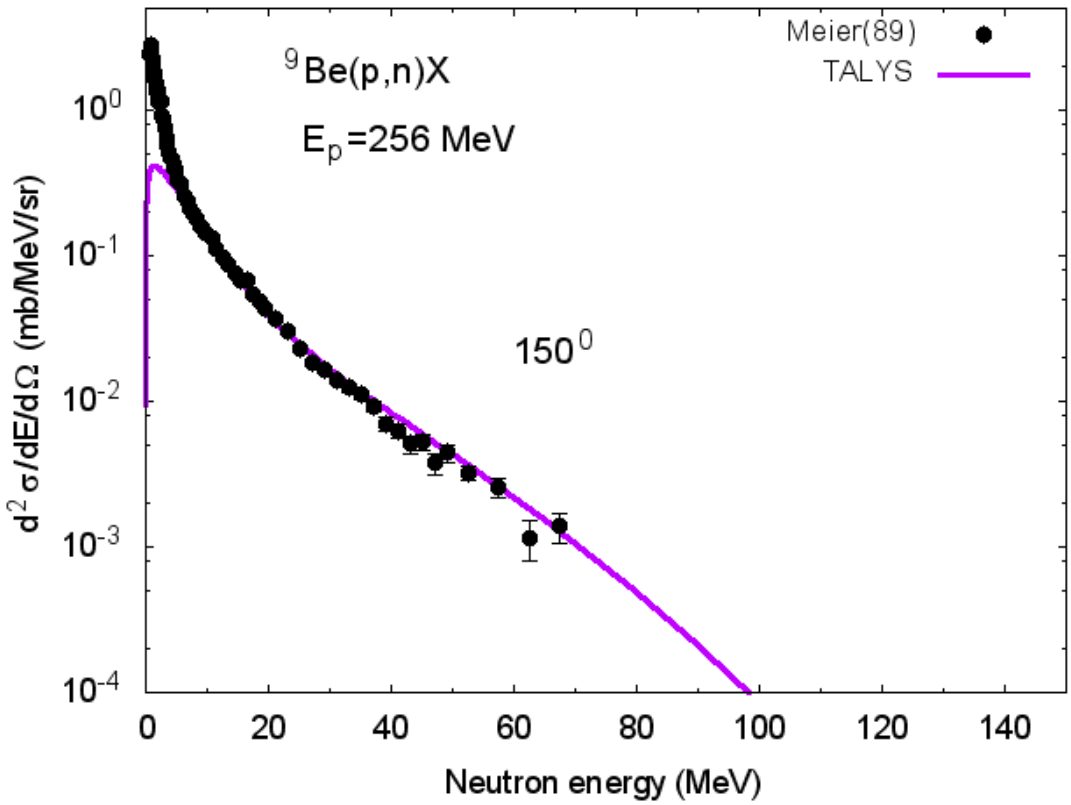
^{9}Be(p,n)X
E_p=256 MeV
150^0
Meier(89)
TALYS
$d^2\sigma/dE/d\Omega$ (mb/MeV/sr)
Neutron energy (MeV)

Comparison of double differential cross-sections of proton emission in p+^{9}Be reactions calculated using Bertini, ISABEL, CEM03, and INCL4 models and models implemented in the TALYS code with available measured data

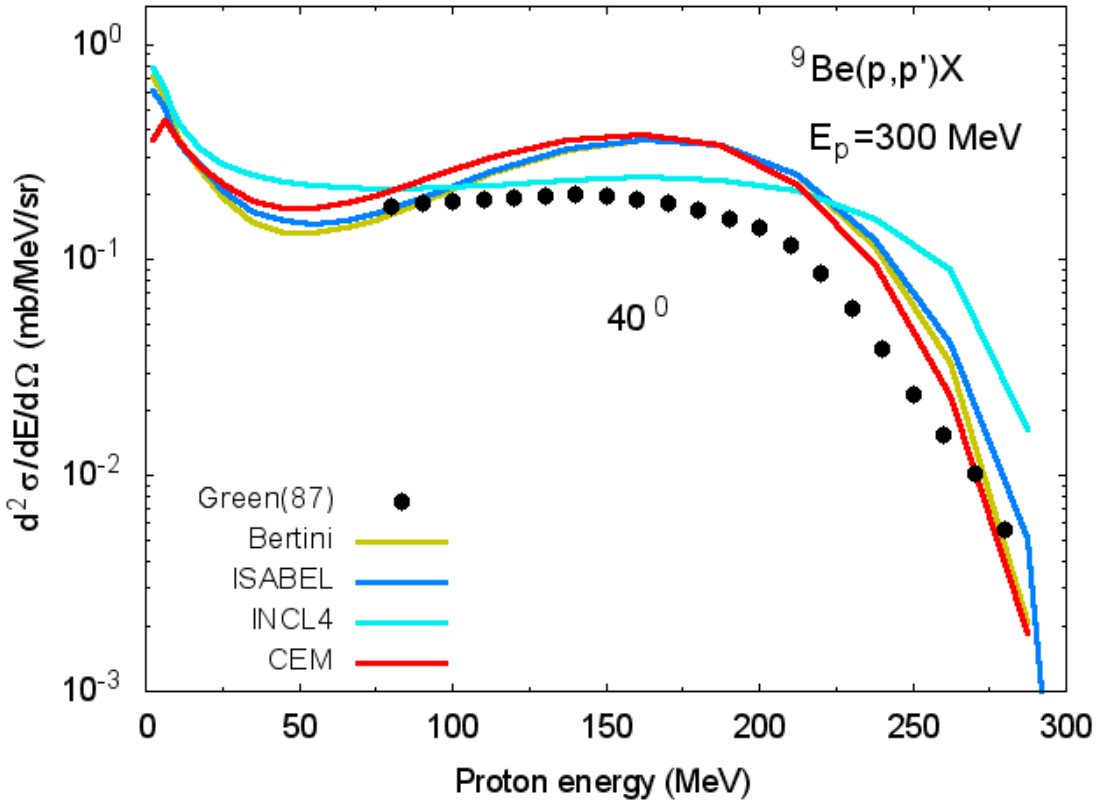
^{9}Be(p,p')X
E_p=300 MeV
40 ^{0}
Green(87)
Bertini
ISABEL
INCL4
CEM
$d^2\sigma/dE/d\Omega$ (mb/MeV/sr)
Proton energy (MeV)

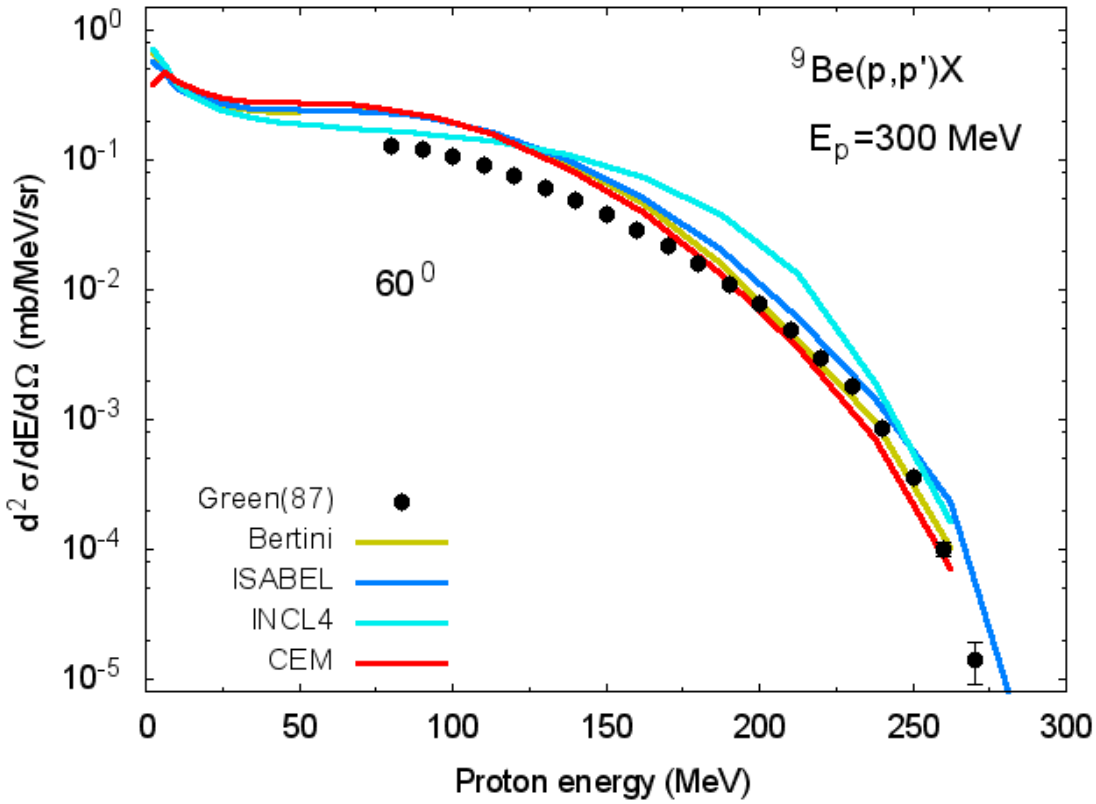
^{9}Be(p,p')X
E_p=300 MeV
60 ^{0}
Green(87)
Bertini
ISABEL
INCL4
CEM
$d^2\sigma/dE/d\Omega$ (mb/MeV/sr)
Proton energy (MeV)

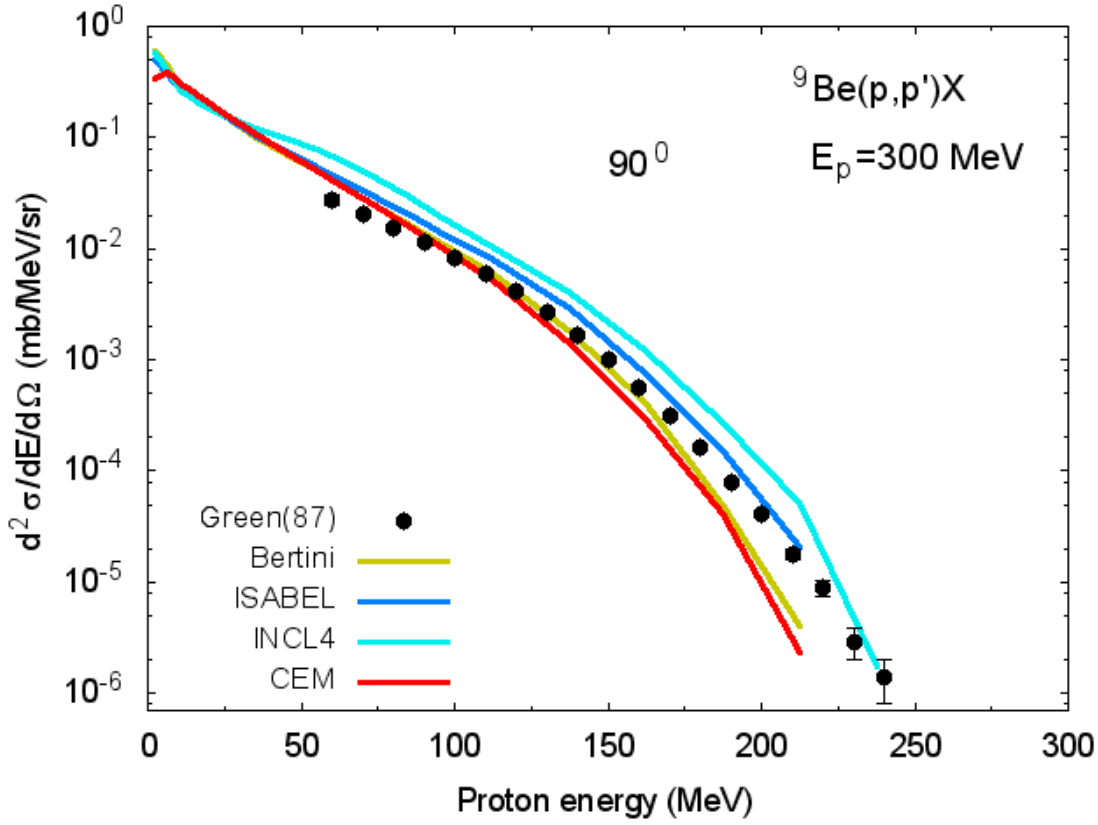
^{9}Be(p,p')X
90^0
E_p=300 MeV
Green(87)
Bertini
ISABEL
INCL4
CEM
$d^2\sigma/dE/d\Omega$ (mb/MeV/sr)
Proton energy (MeV)

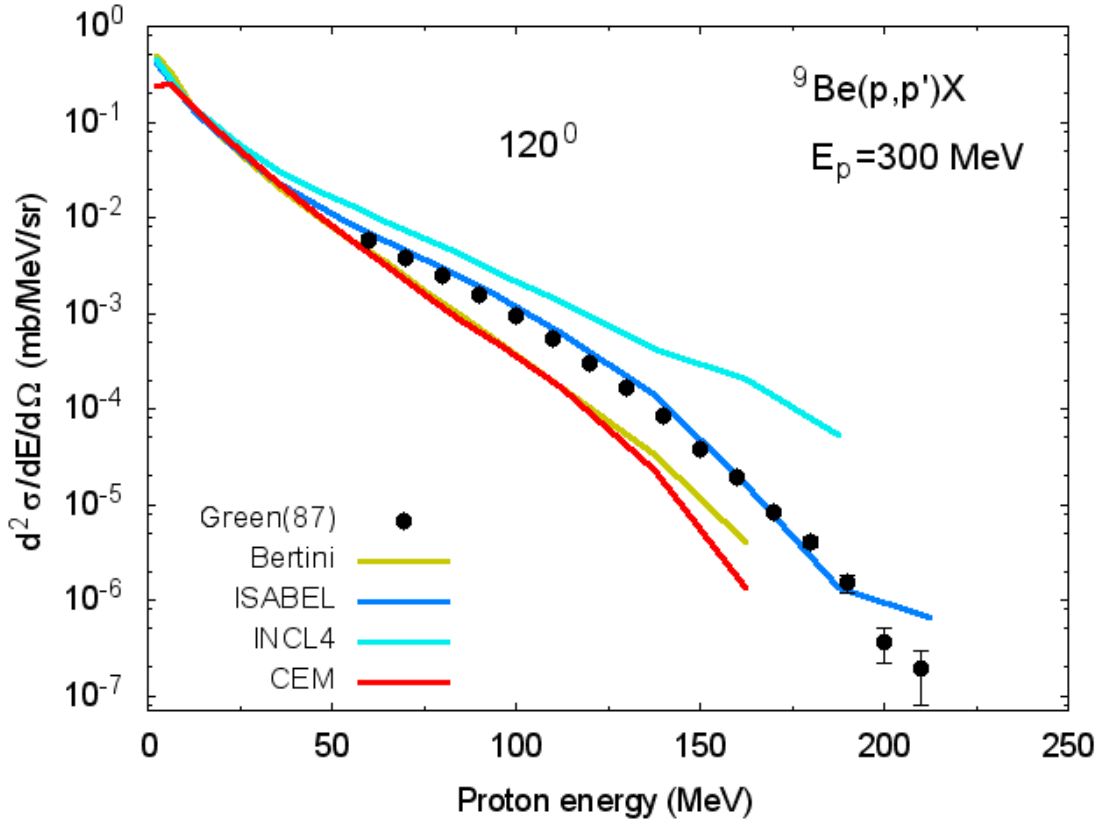
^{9}Be(p,p')X
120^0
E_p=300 MeV
Green(87)
Bertini
ISABEL
INCL4
CEM
$d^2\sigma/dE/d\Omega$ (mb/MeV/sr)
Proton energy (MeV)

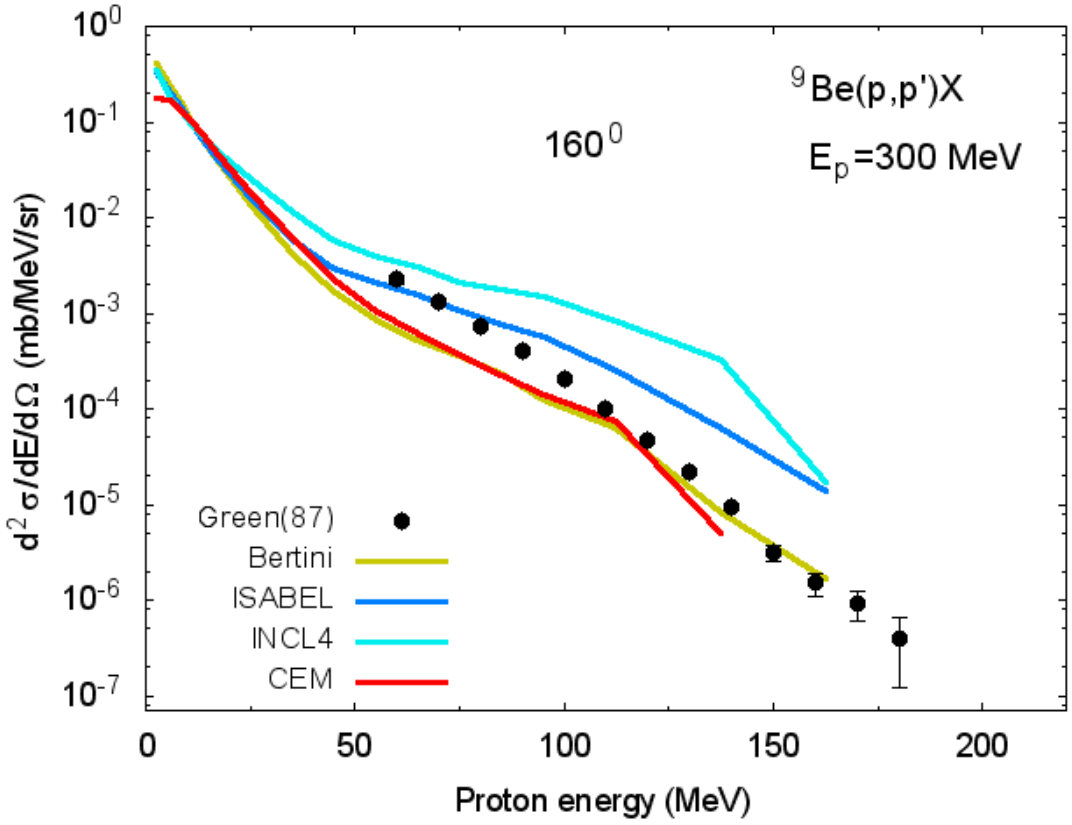
^{9}Be(p,p')X
E_p=300 MeV
160^0
Green(87)
Bertini
ISABEL
INCL4
CEM
$d^2\sigma/dE/d\Omega$ (mb/MeV/sr)
Proton energy (MeV)

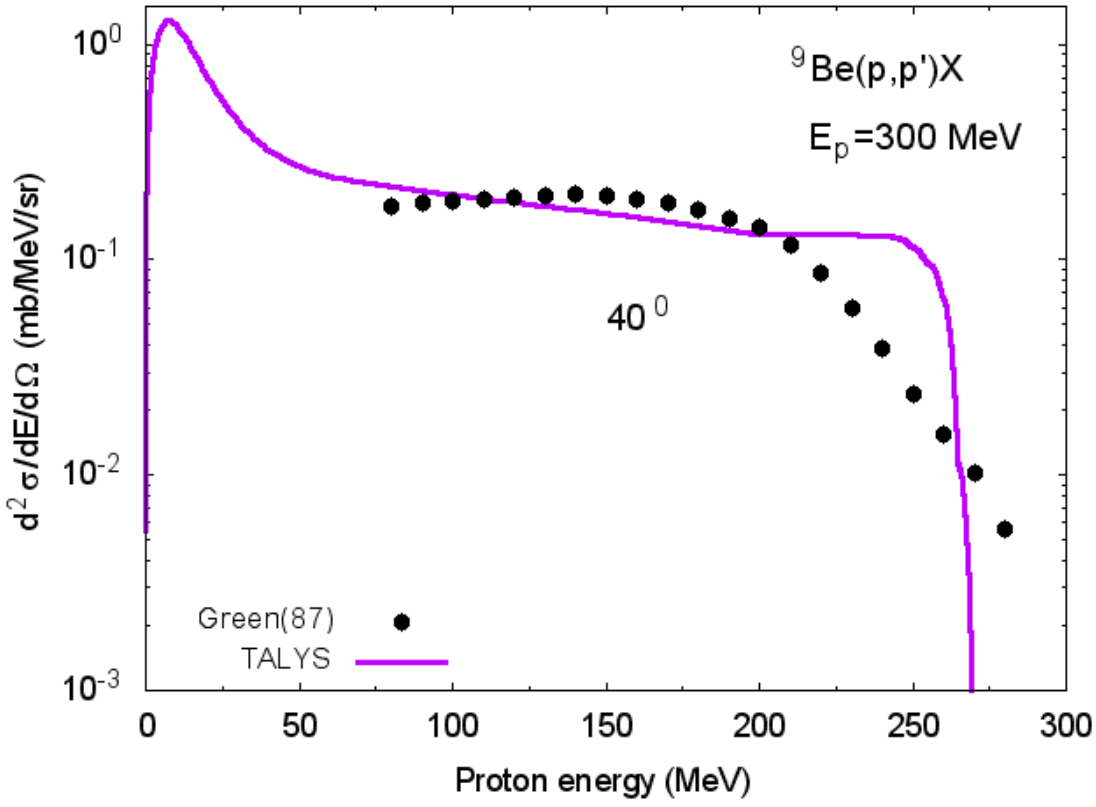
^{9}Be(p,p')X
E_p=300 MeV
40^0
Green(87)
TALYS
$d^2\sigma/dE/d\Omega$ (mb/MeV/sr)
Proton energy (MeV)

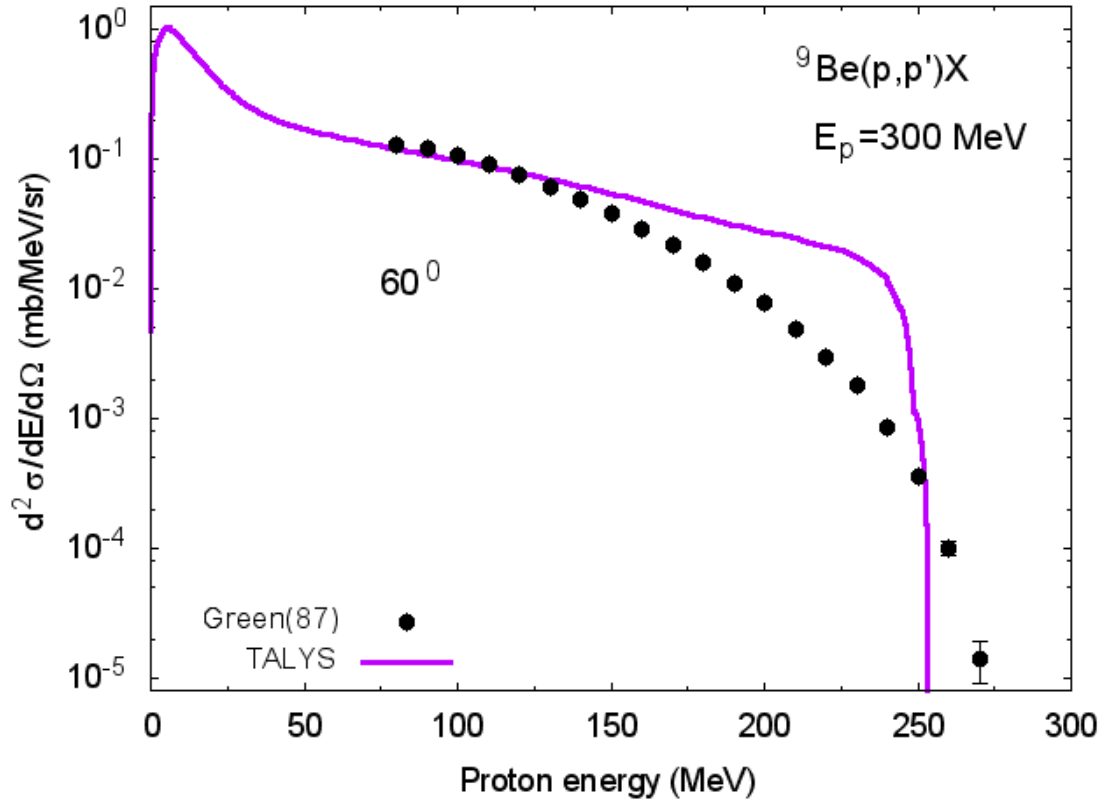
^{9}Be(p,p')X
E_p=300 MeV
60^0
Green(87)
TALYS
d$^2\sigma$/dE/dΩ (mb/MeV/sr)
Proton energy (MeV)

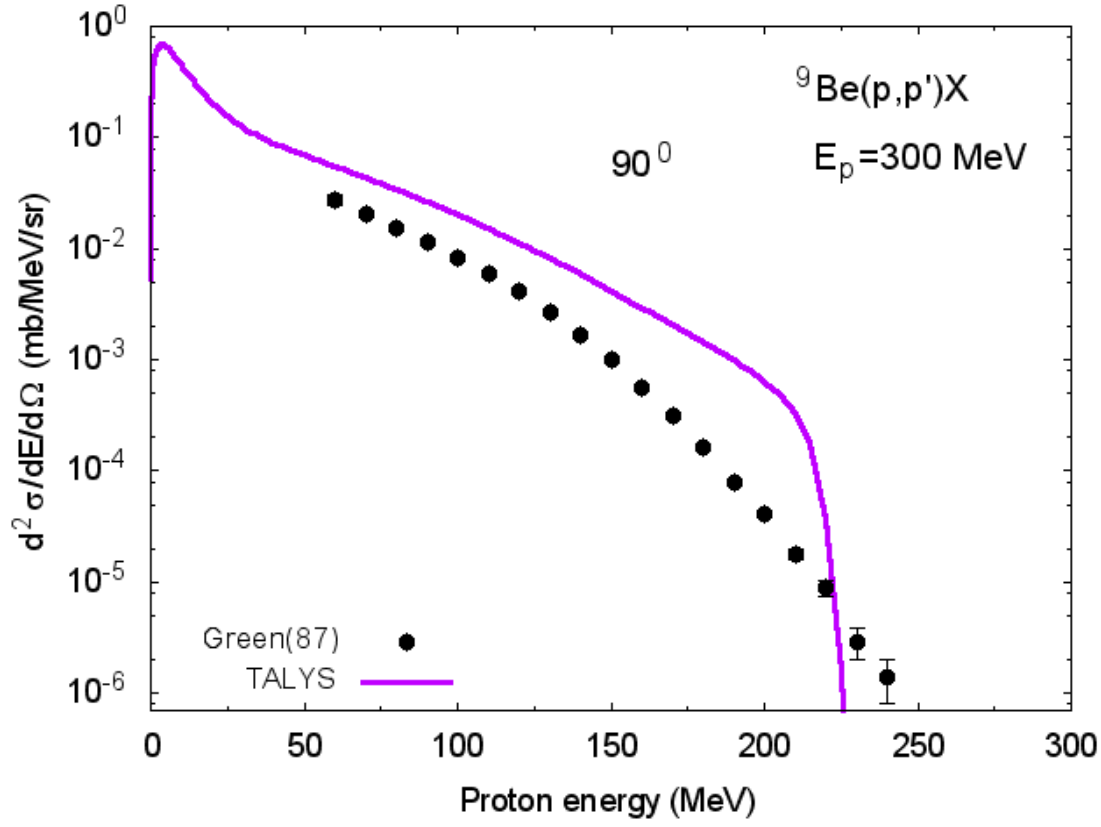
^{9}Be(p,p')X
E_p=300 MeV
90^0
Green(87)
TALYS
d$^2\sigma$/dE/dΩ (mb/MeV/sr)
Proton energy (MeV)

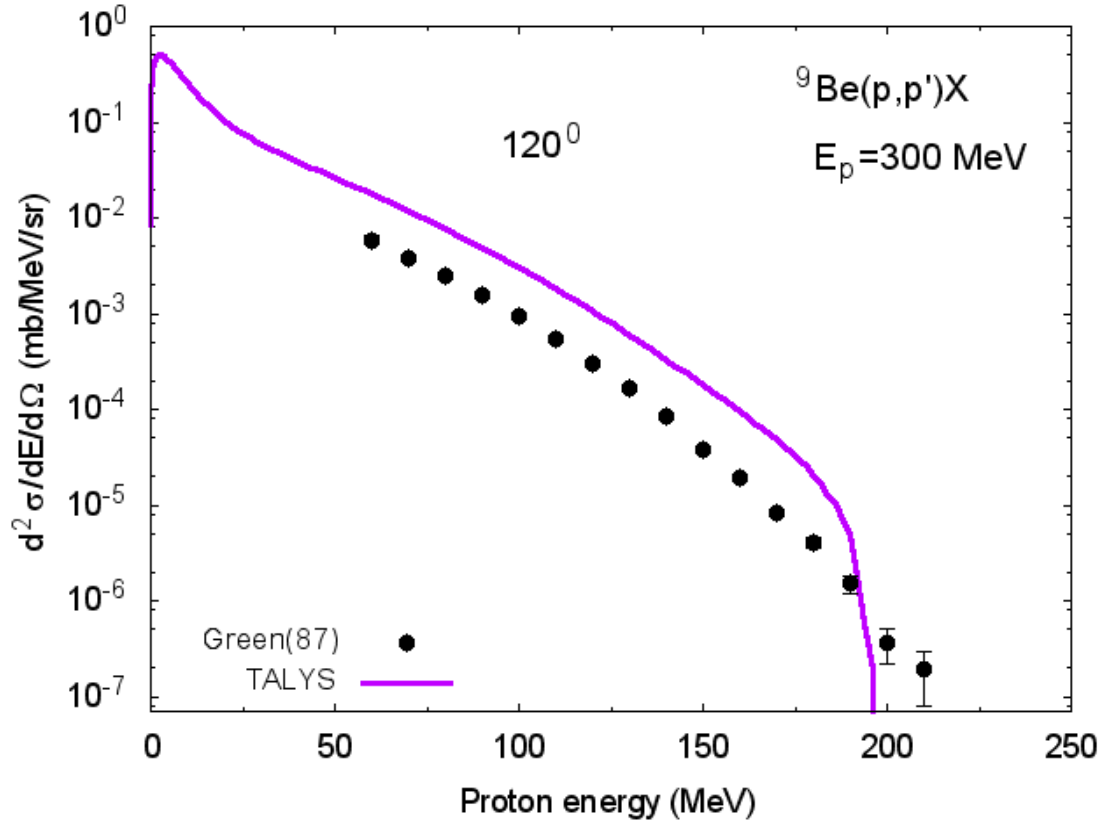
^{9}Be(p,p')X
120^0
E_p=300 MeV
Green(87)
TALYS
d$^2\sigma$/dE/dΩ (mb/MeV/sr)
Proton energy (MeV)

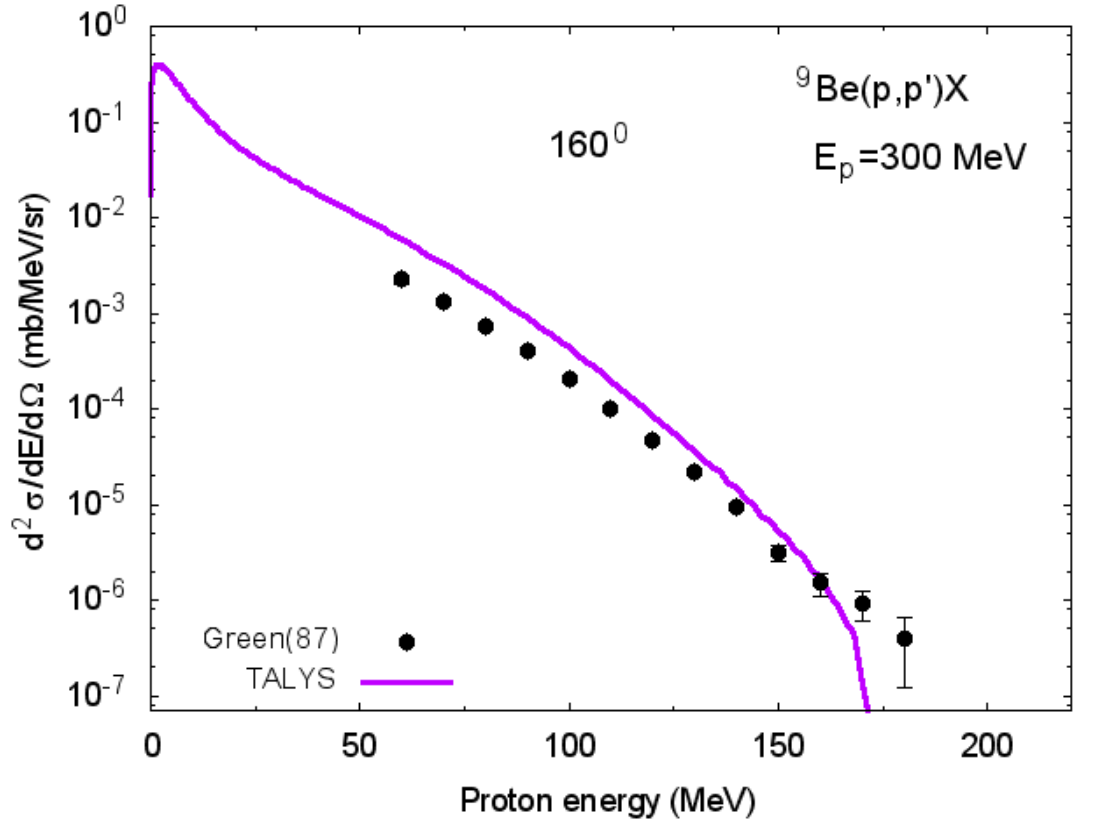
^{9}Be(p,p')X
160^0
E_p=300 MeV
Green(87)
TALYS
d$^2\sigma$/dE/dΩ (mb/MeV/sr)
Proton energy (MeV)

Comparison of double differential cross-sections of deuteron emission in p+^{9}Be reactions calculated using Bertini, ISABEL, CEM03, and INCL4 models and models implemented in the TALYS code with available measured data

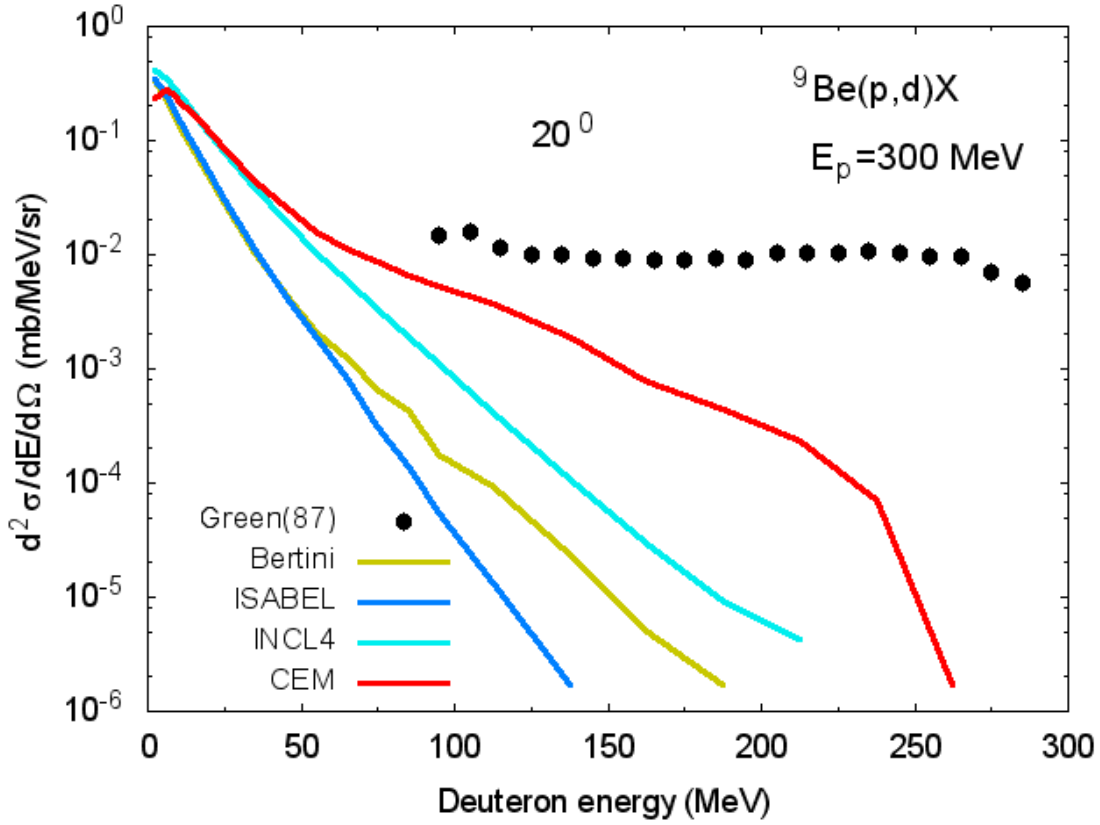
^{9}Be(p,d)X
20 ^{0}
E_p=300 MeV
Green(87)
Bertini
ISABEL
INCL4
CEM
$d^2\sigma/dE/d\Omega$ (mb/MeV/sr)
Deuteron energy (MeV)

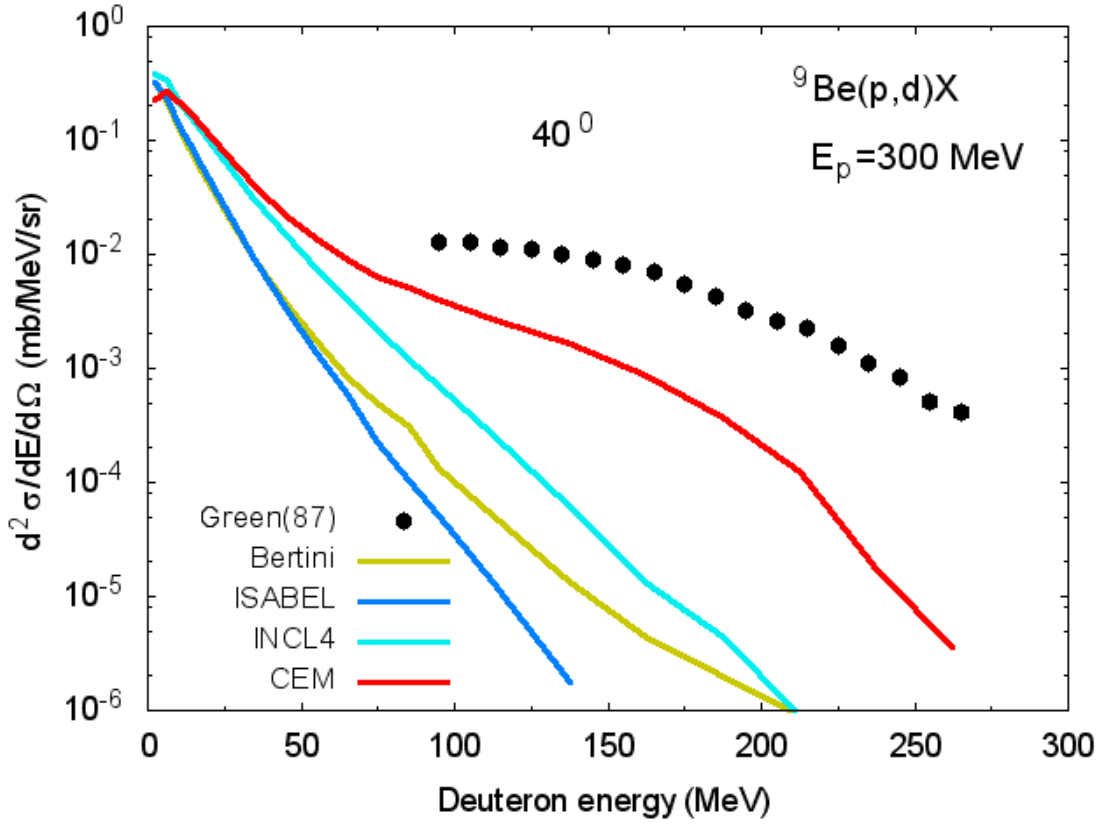
^{9}Be(p,d)X
40 ^{0}
E_p=300 MeV
Green(87)
Bertini
ISABEL
INCL4
CEM
$d^2\sigma/dE/d\Omega$ (mb/MeV/sr)
Deuteron energy (MeV)

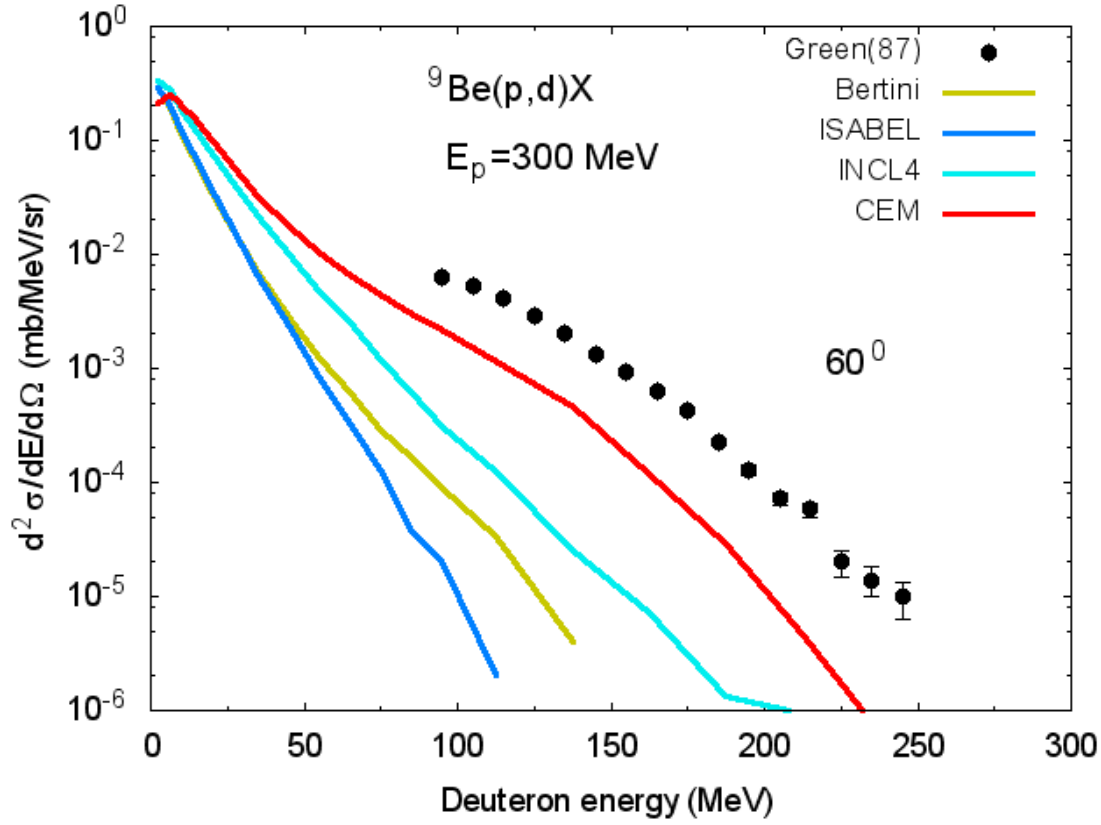
^{9}Be(p,d)X
E_p=300 MeV
60^0
Green(87)
Bertini
ISABEL
INCL4
CEM
$d^2\sigma/dE/d\Omega$ (mb/MeV/sr)
Deuteron energy (MeV)

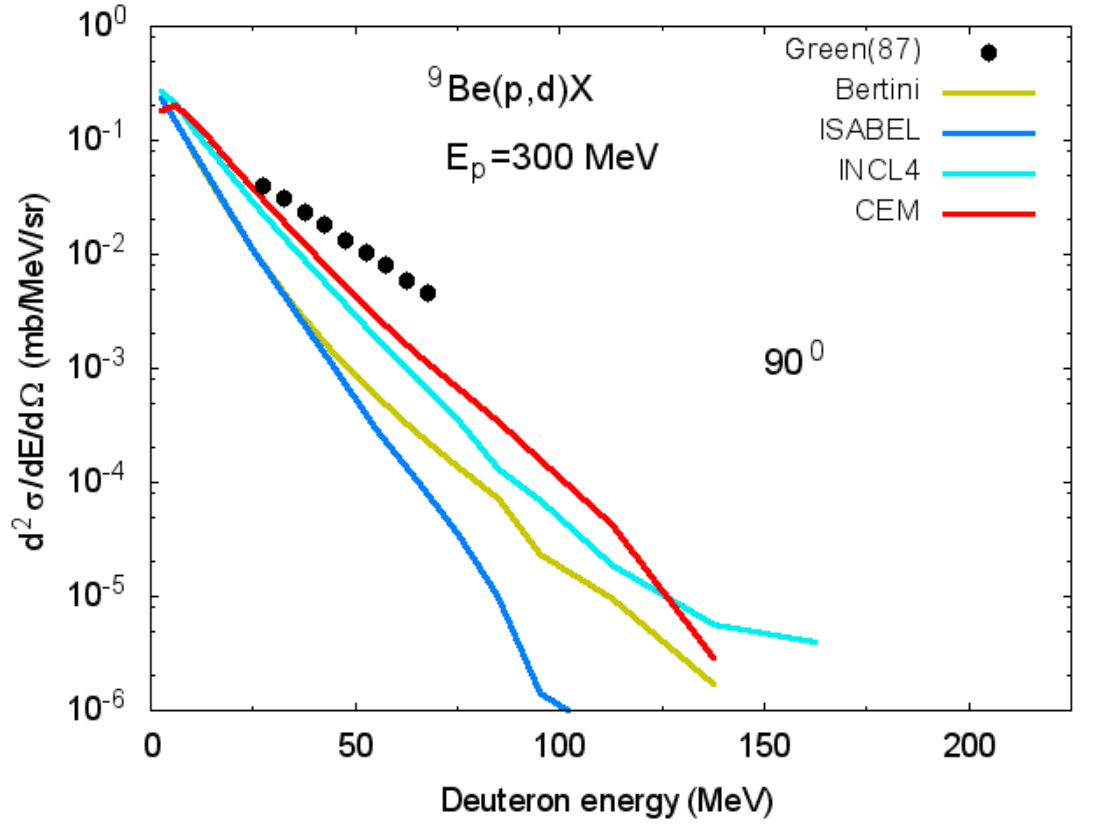
^{9}Be(p,d)X
E_p=300 MeV
90^0
Green(87)
Bertini
ISABEL
INCL4
CEM
$d^2\sigma/dE/d\Omega$ (mb/MeV/sr)
Deuteron energy (MeV)

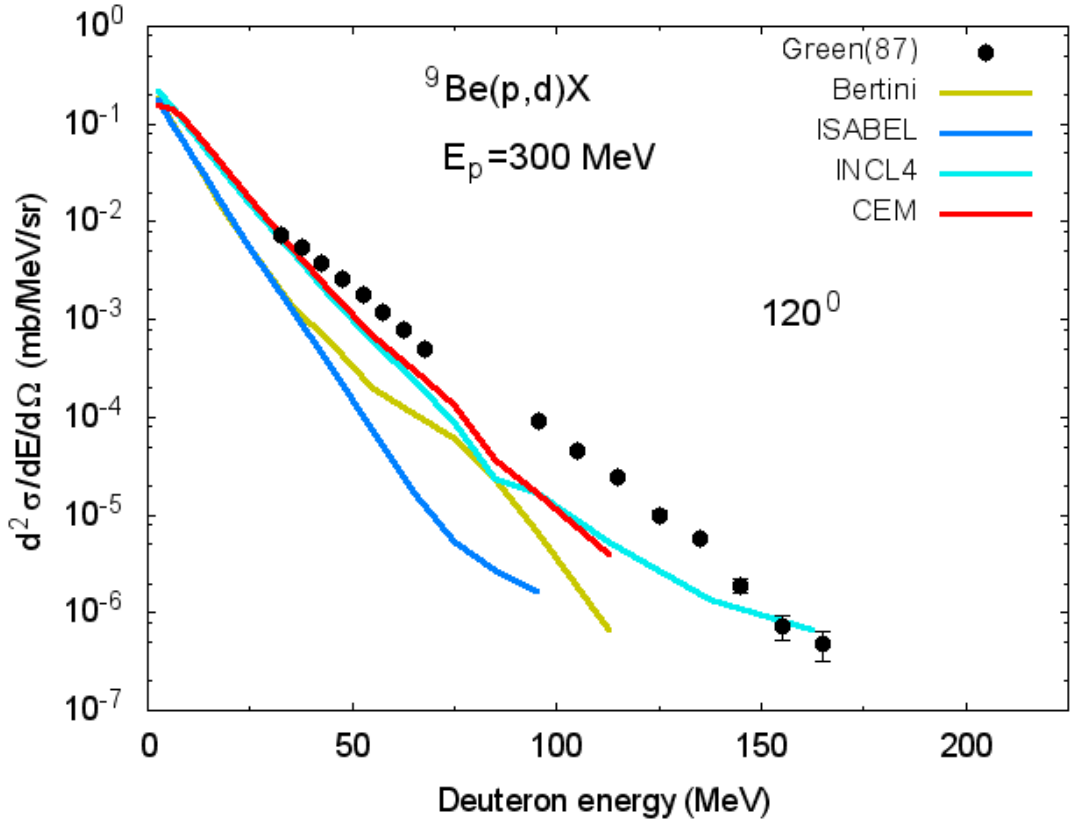
^{9}Be(p,d)X
E_p=300 MeV
120^0
Green(87)
Bertini
ISABEL
INCL4
CEM
$d^2\sigma/dE/d\Omega$ (mb/MeV/sr)
Deuteron energy (MeV)

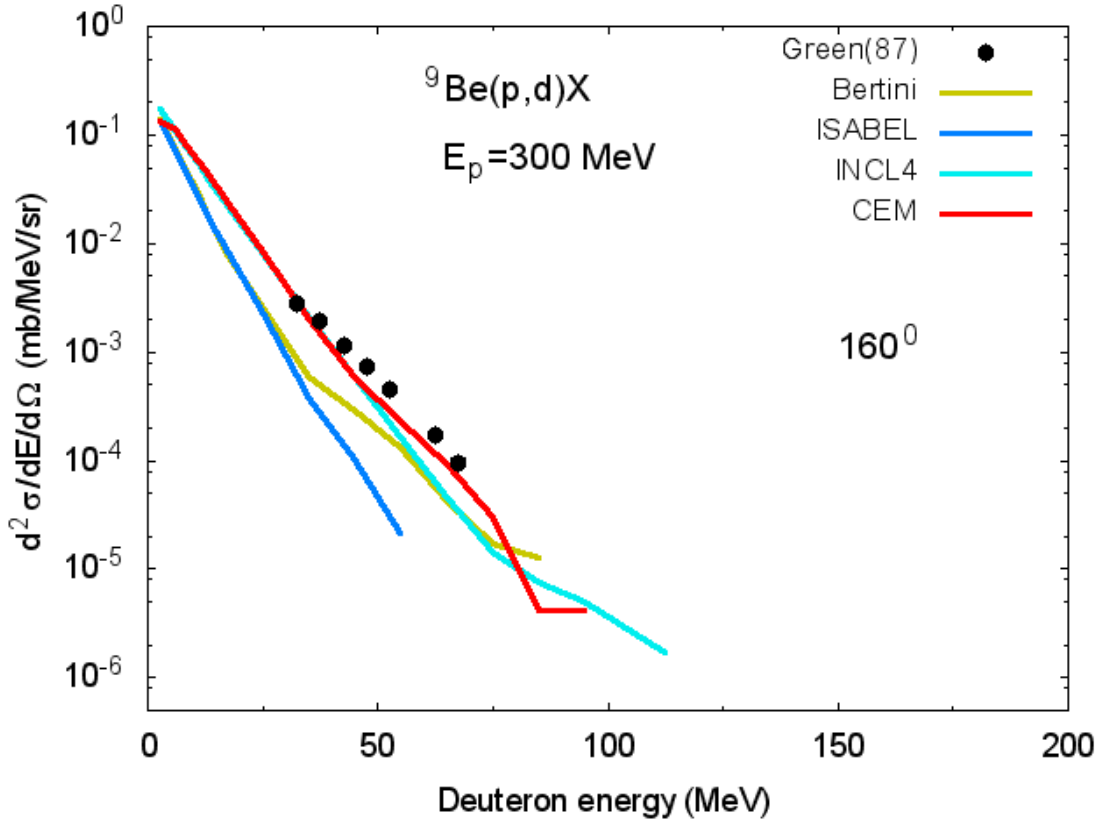
^{9}Be(p,d)X
E_p=300 MeV
160^0
Green(87)
Bertini
ISABEL
INCL4
CEM
$d^2\sigma/dE/d\Omega$ (mb/MeV/sr)
Deuteron energy (MeV)

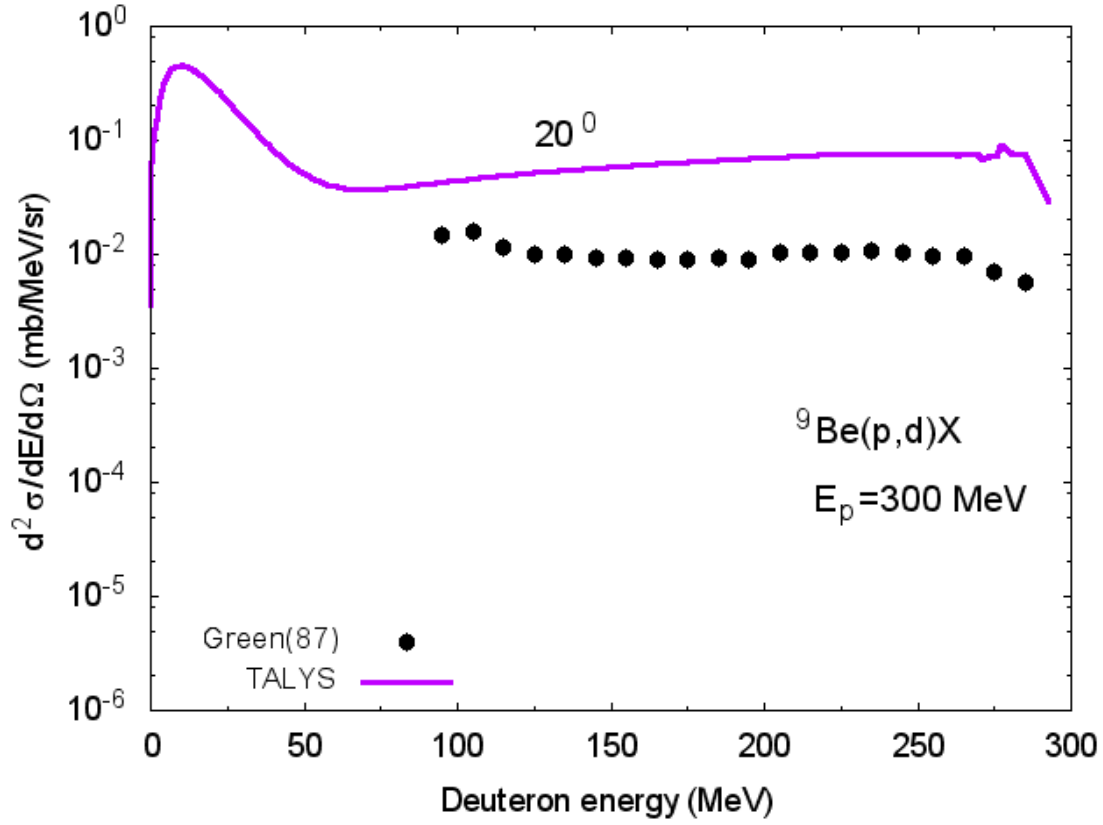
10^0
10^{-1}
10^{-2}
10^{-3}
10^{-4}
10^{-5}
10^{-6}
$d^2\sigma/dE/d\Omega$ (mb/MeV/sr)
20^0
^{9}Be(p,d)X
E_p=300 MeV
Green(87)
TALYS
0
50
100
150
200
250
300
Deuteron energy (MeV)

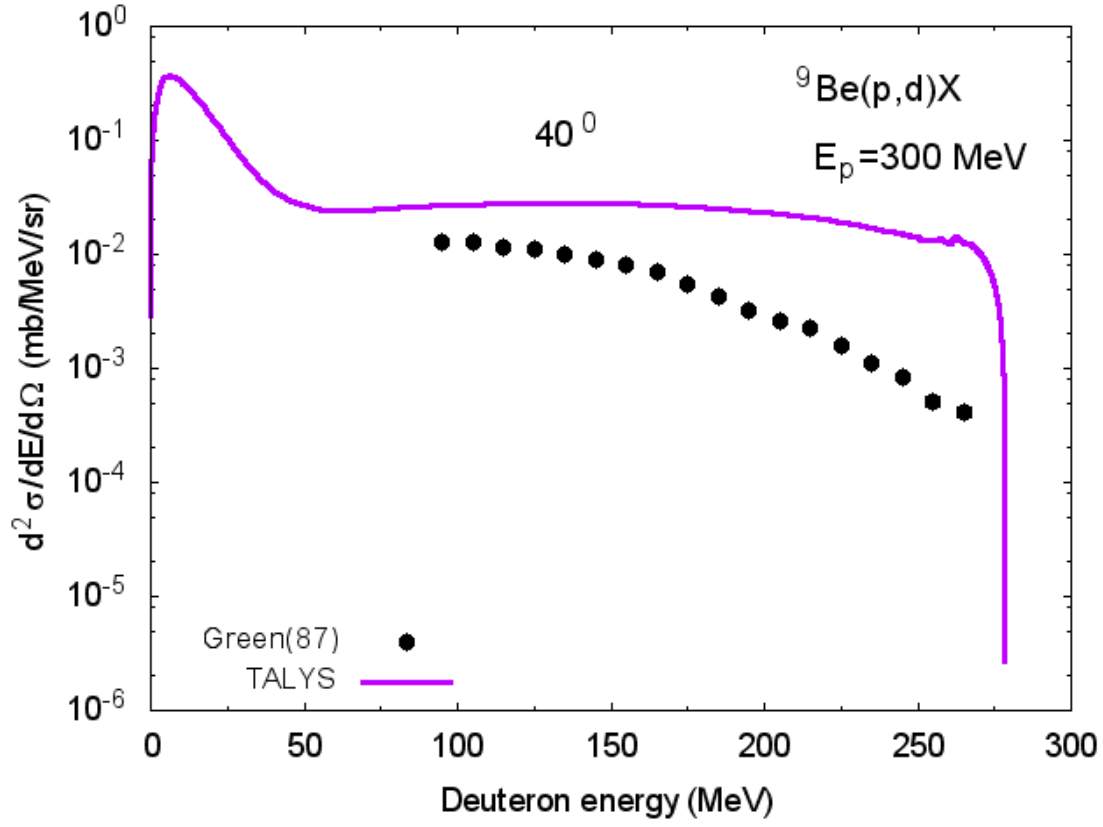
10^0
10^{-1}
10^{-2}
10^{-3}
10^{-4}
10^{-5}
10^{-6}
$d^2\sigma/dE/d\Omega$ (mb/MeV/sr)
40^0
^{9}Be(p,d)X
E_p=300 MeV
Green(87)
TALYS
0
50
100
150
200
250
300
Deuteron energy (MeV)

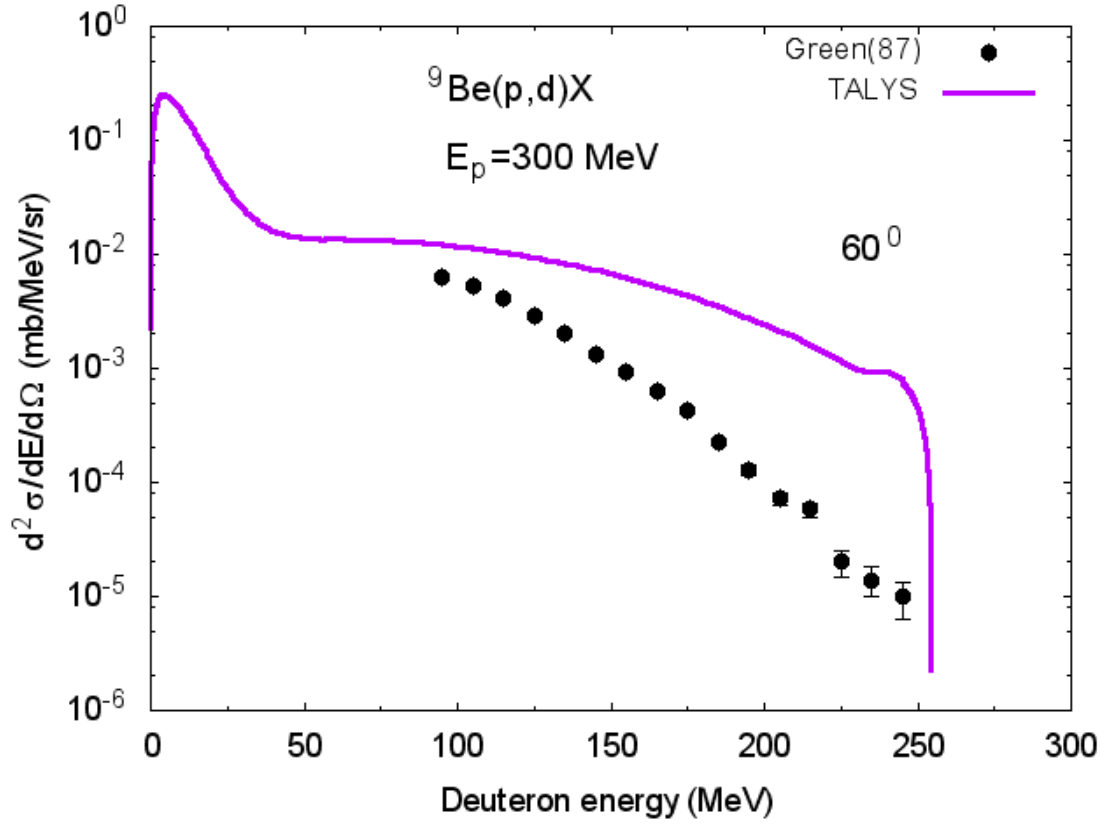
Green(87)
TALYS
^{9}Be(p,d)X
E_p=300 MeV
60^0
$d^2\sigma/dE/d\Omega$ (mb/MeV/sr)
Deuteron energy (MeV)

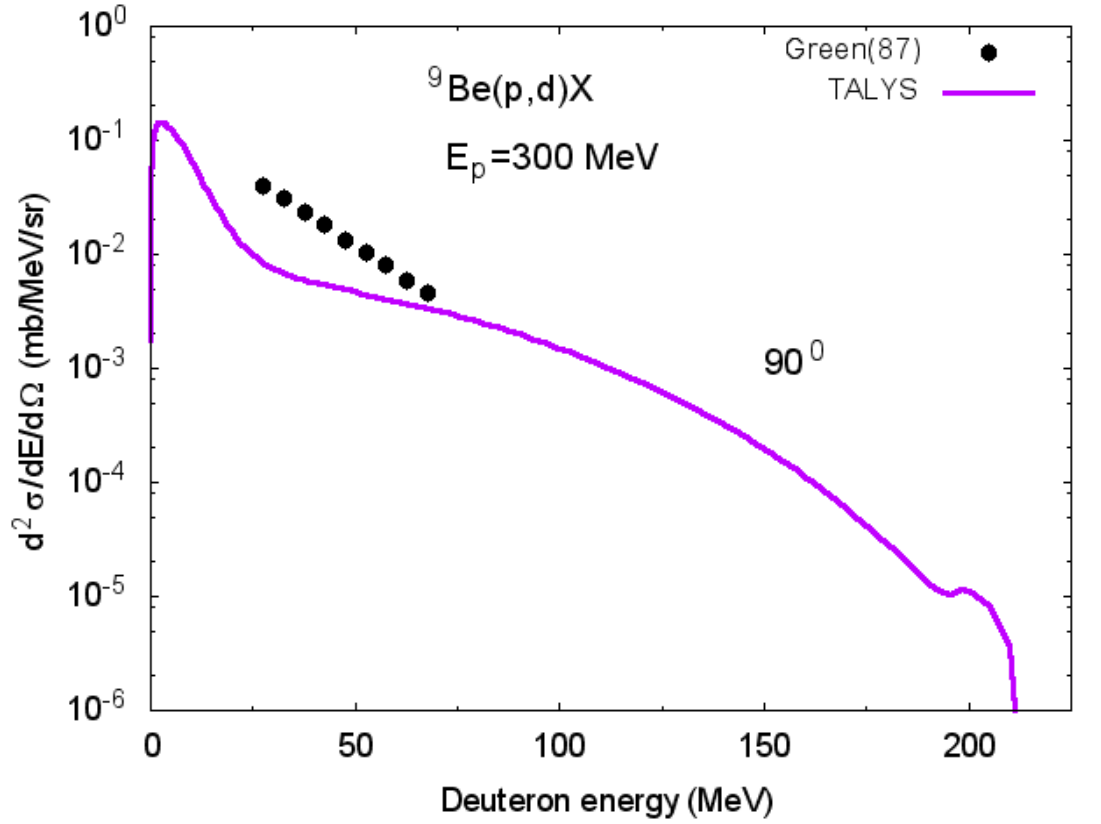
Green(87)
TALYS
^{9}Be(p,d)X
E_p=300 MeV
90^0
$d^2\sigma/dE/d\Omega$ (mb/MeV/sr)
Deuteron energy (MeV)

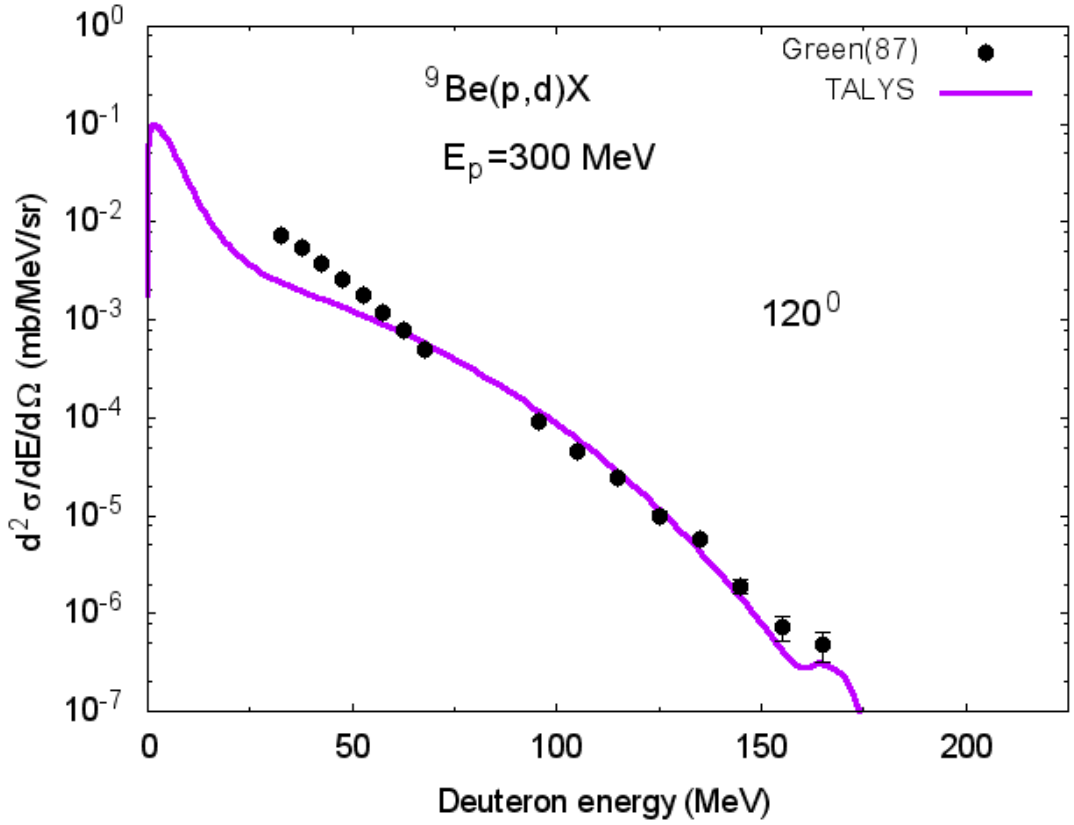
Green(87)
TALYS
^{9}Be(p,d)X
E_p=300 MeV
120^0
$d^2\sigma/dE/d\Omega$ (mb/MeV/sr)
Deuteron energy (MeV)

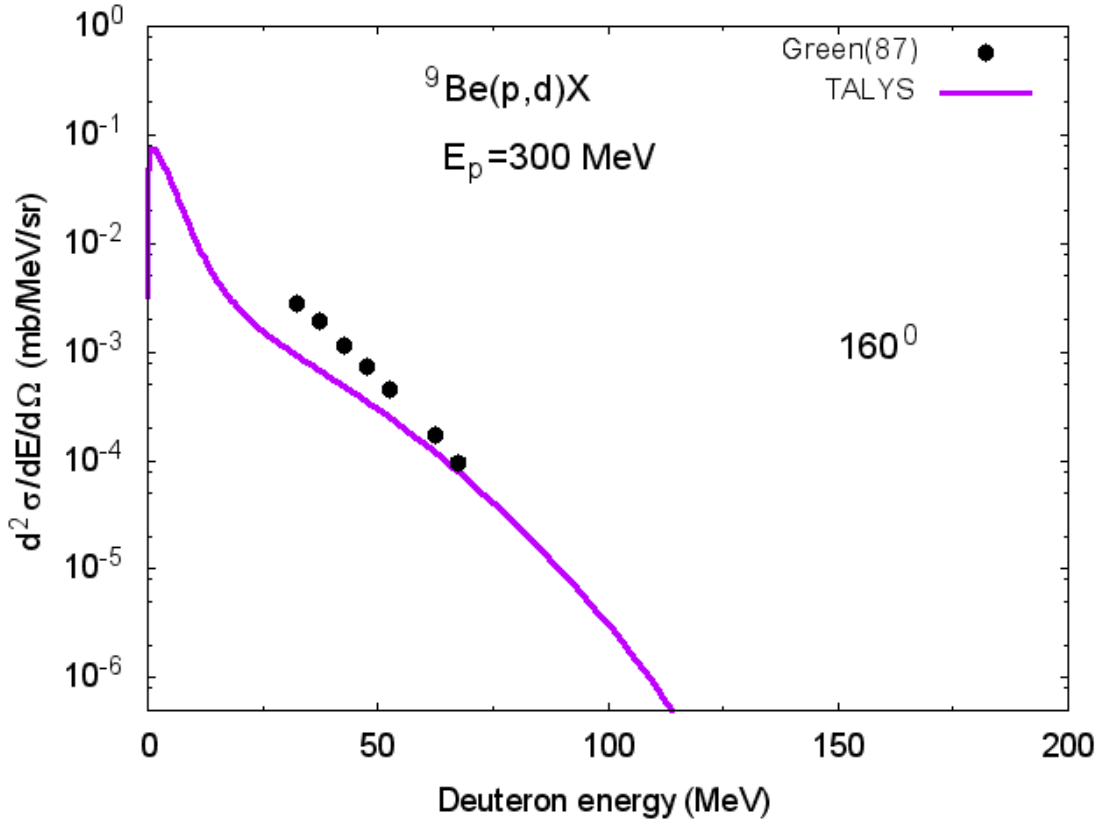
Green(87)
TALYS
^{9}Be(p,d)X
E_p=300 MeV
160^0
$d^2\sigma/dE/d\Omega$ (mb/MeV/sr)
Deuteron energy (MeV)

Comparison of double differential cross-sections of triton emission in p+^{9}Be reactions calculated using Bertini, ISABEL, CEM03, and INCL4 models and models implemented in the TALYS code with available measured data

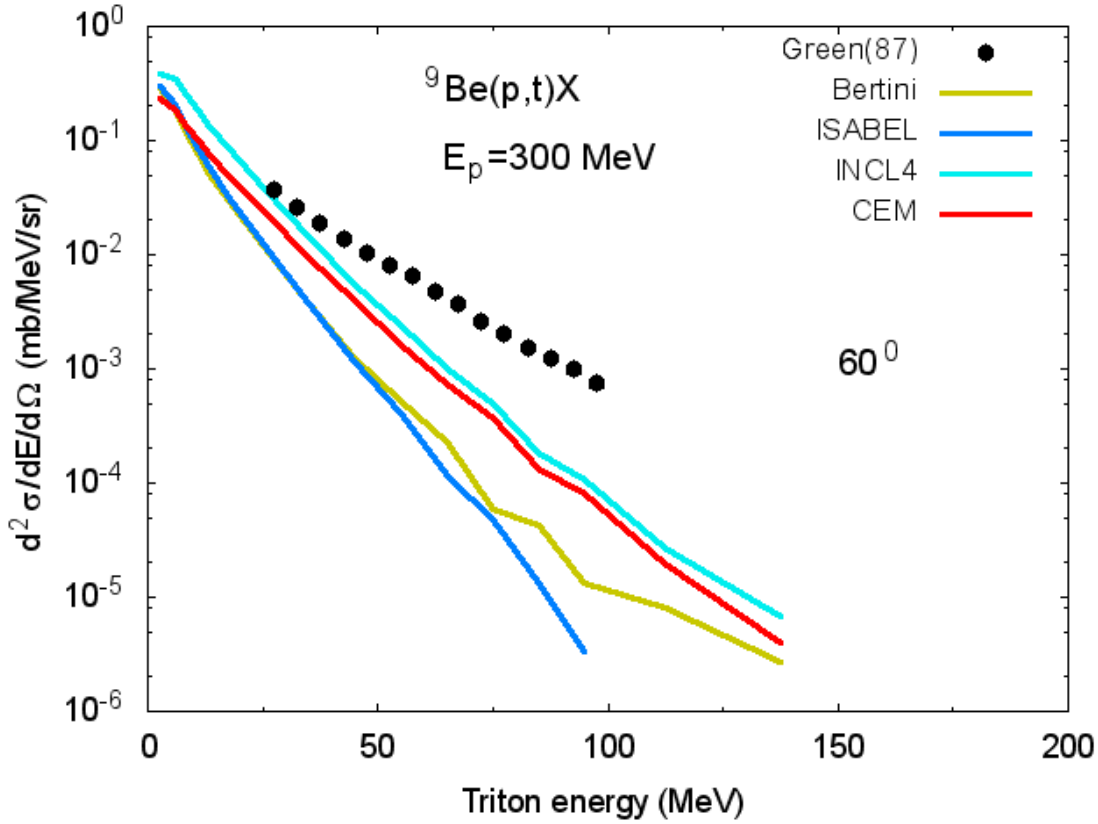
^{9}Be(p,t)X
E_p=300 MeV
60^0
Green(87)
Bertini
ISABEL
INCL4
CEM
$d^2\sigma/dE/d\Omega$ (mb/MeV/sr)
Triton energy (MeV)

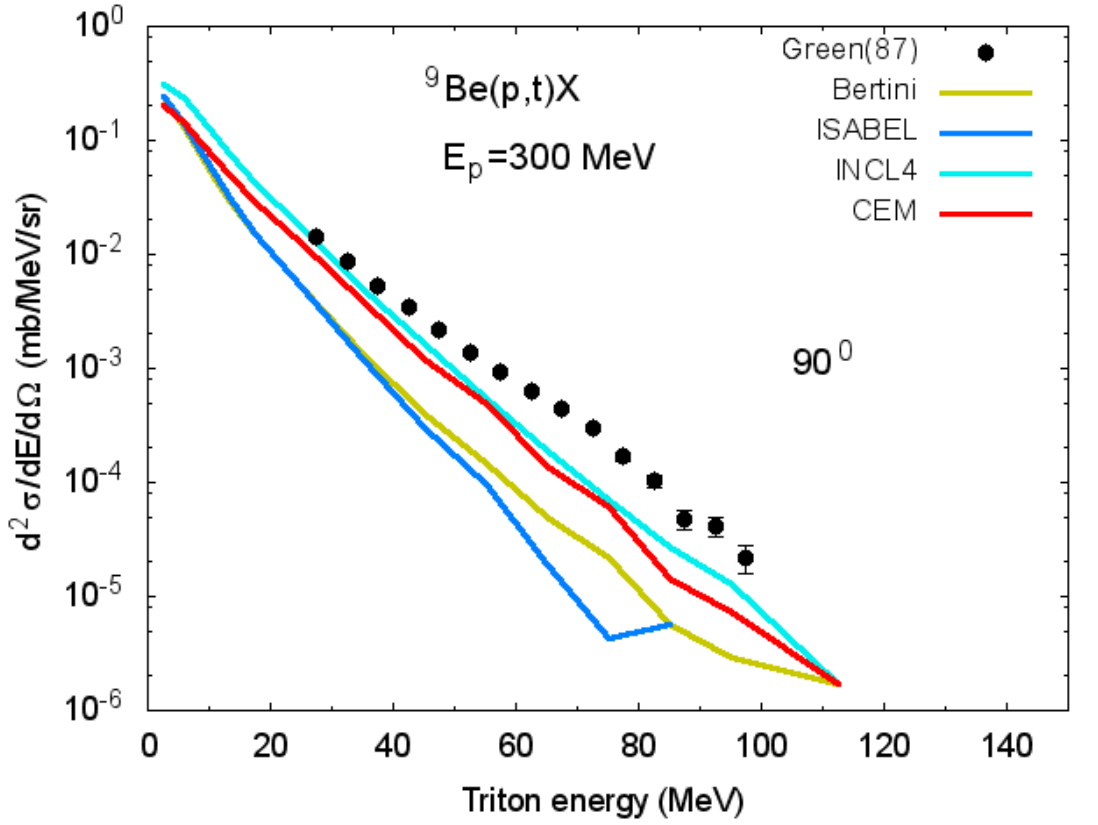
^{9}Be(p,t)X
E_p=300 MeV
90^0
Green(87)
Bertini
ISABEL
INCL4
CEM
$d^2\sigma/dE/d\Omega$ (mb/MeV/sr)
Triton energy (MeV)

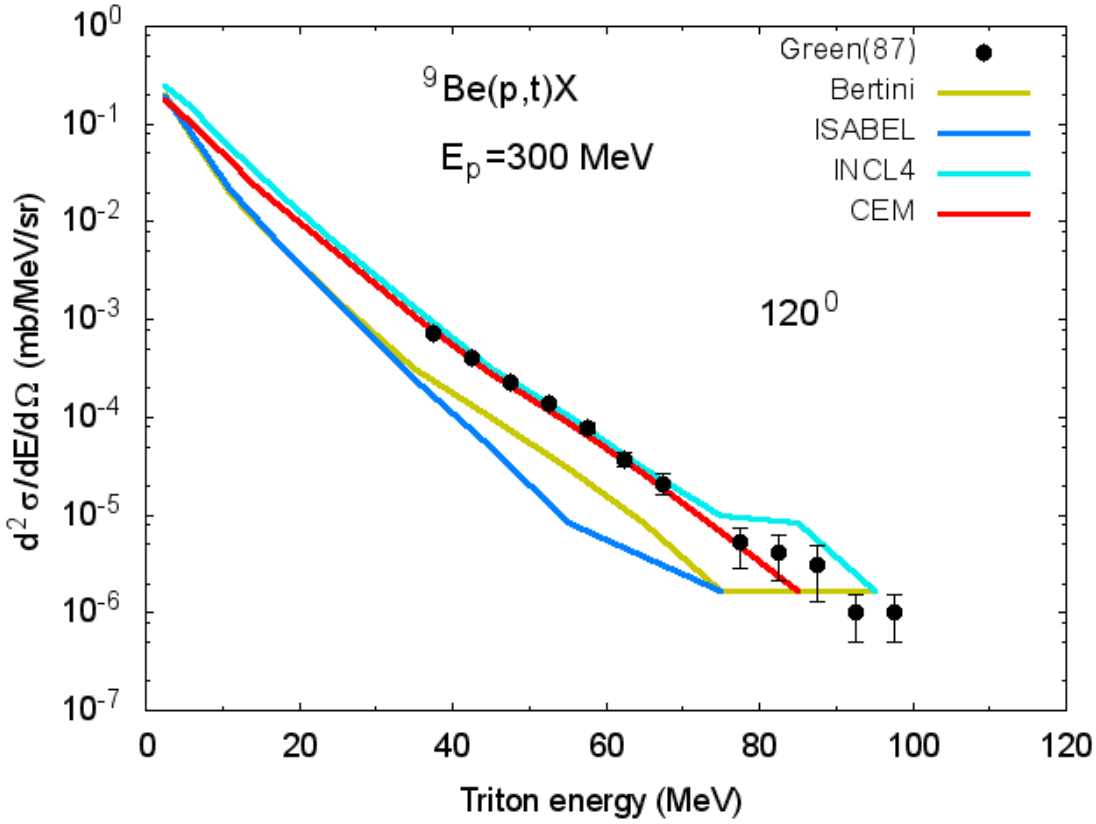
^{9}Be(p,t)X
E_p=300 MeV
120^0
Green(87)
Bertini
ISABEL
INCL4
CEM
$d^2\sigma/dE/d\Omega$ (mb/MeV/sr)
Triton energy (MeV)

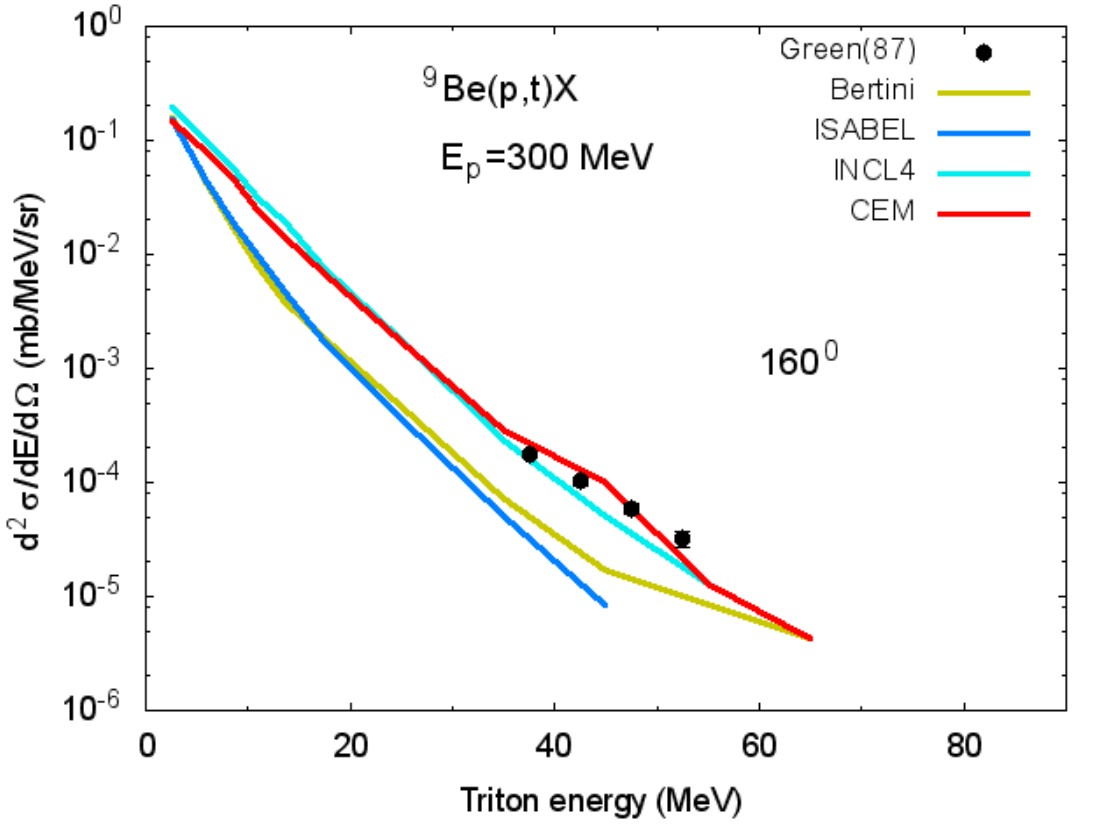
^{9}Be(p,t)X
E_p=300 MeV
160^0
Green(87)
Bertini
ISABEL
INCL4
CEM
$d^2\sigma/dE/d\Omega$ (mb/MeV/sr)
Triton energy (MeV)

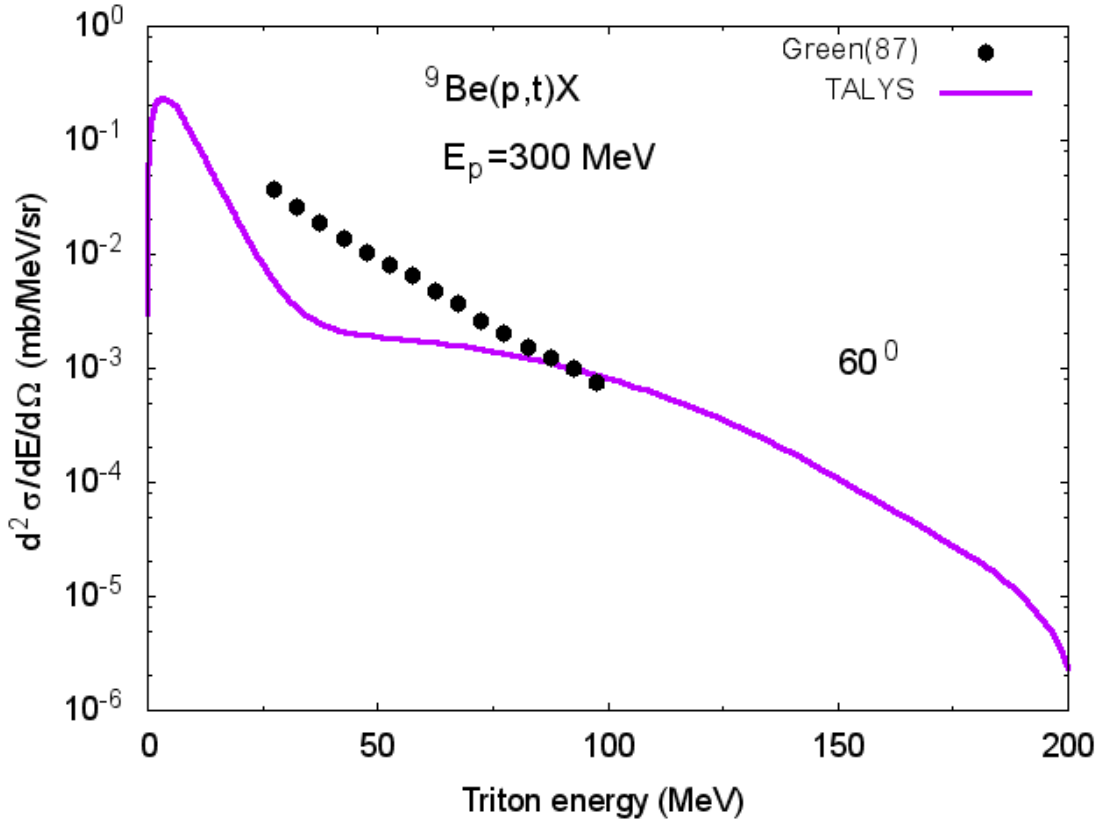
Green(87)
TALYS
^{9}Be(p,t)X
E_p=300 MeV
60^0
$d^2\sigma/dE/d\Omega$ (mb/MeV/sr)
Triton energy (MeV)

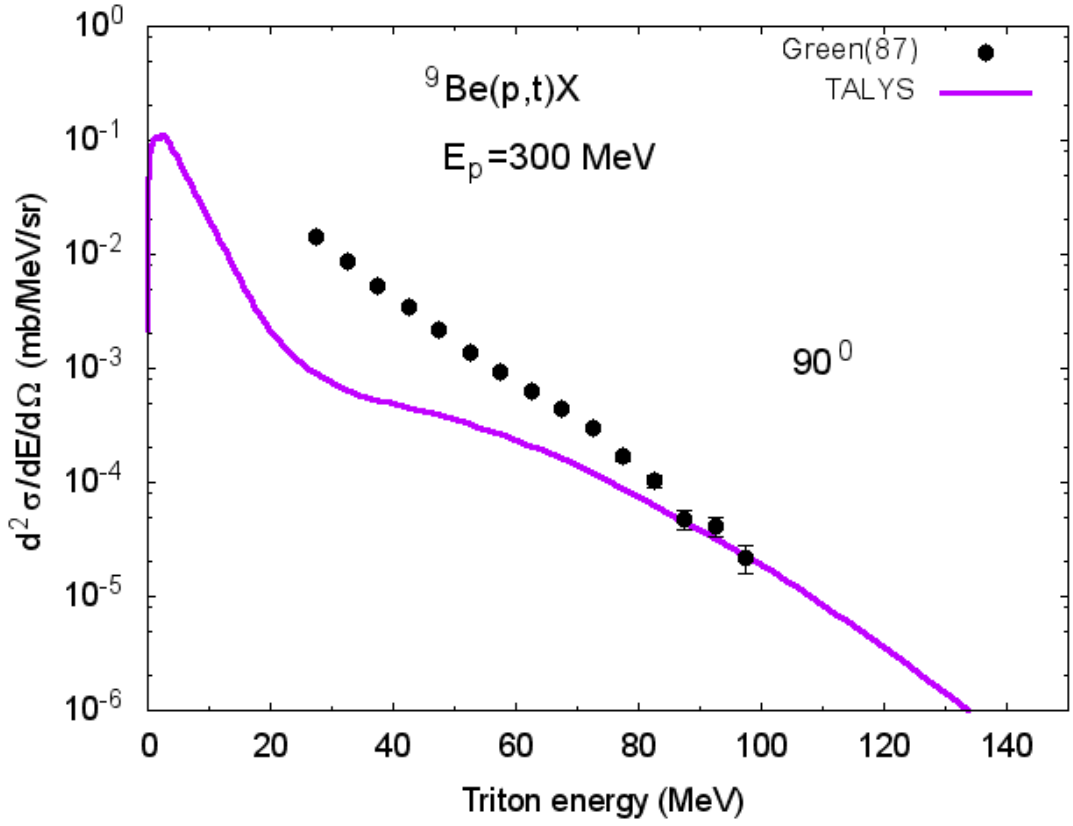
Green(87)
TALYS
^{9}Be(p,t)X
E_p=300 MeV
90^0
$d^2\sigma/dE/d\Omega$ (mb/MeV/sr)
Triton energy (MeV)

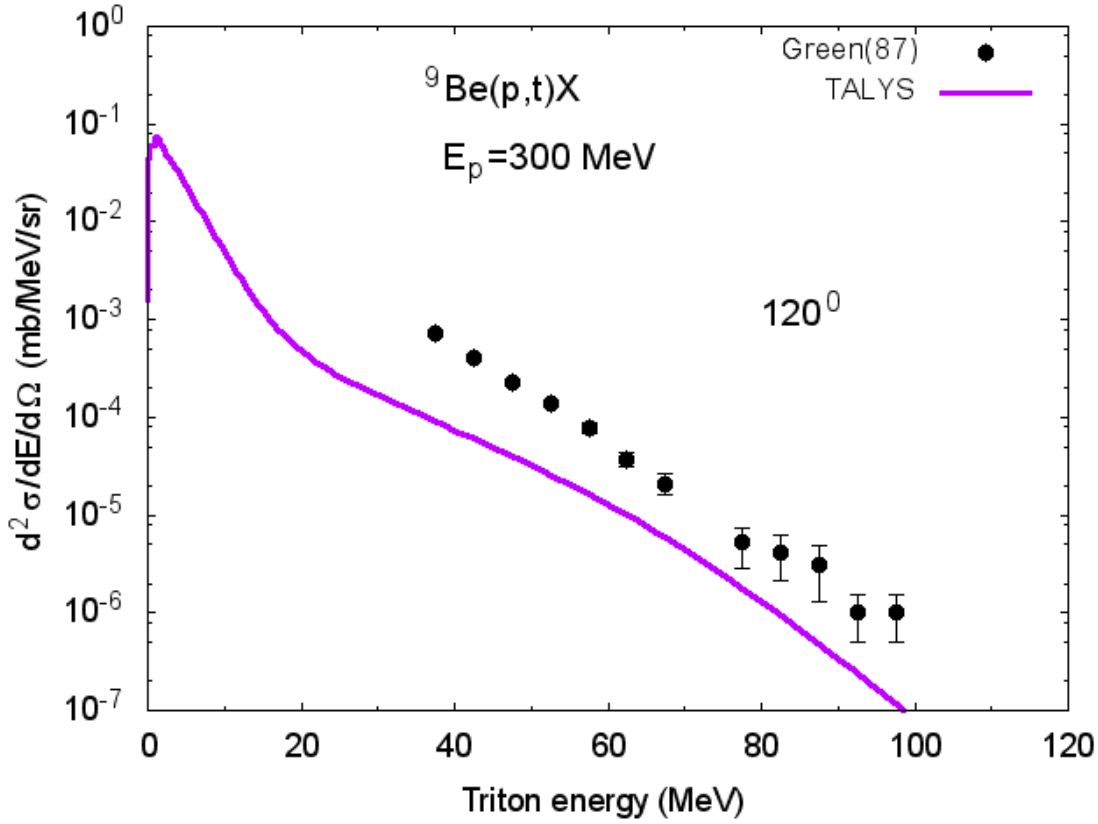
Green(87)
TALYS
^{9}Be(p,t)X
E_p=300 MeV
120^0
$d^2\sigma/dE/d\Omega$ (mb/MeV/sr)
Triton energy (MeV)

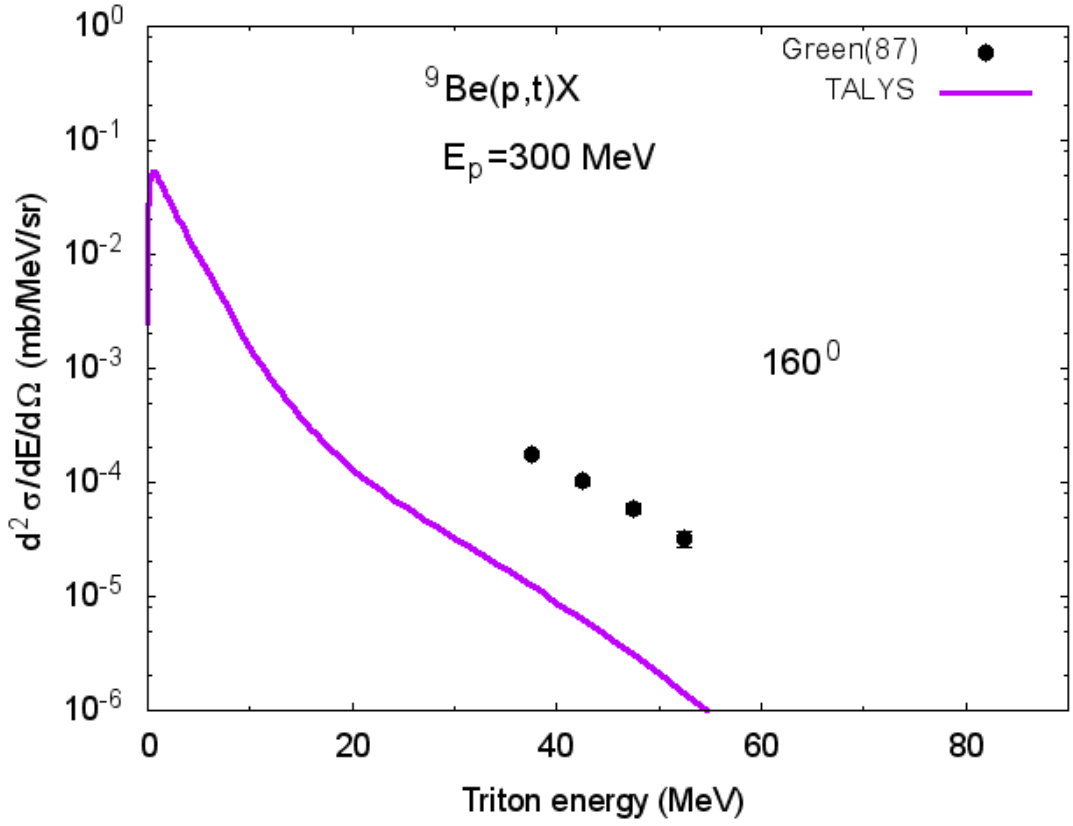
Green(87)
TALYS
^{9}Be(p,t)X
E_p=300 MeV
160^0
$d^2\sigma/dE/d\Omega$ (mb/MeV/sr)
Triton energy (MeV)

Comparison of double differential cross-sections of ^{3}He- emission in p+^{9}Be reactions calculated using Bertini, ISABEL, CEM03, and INCL4 models and models implemented in the TALYS code with available measured data

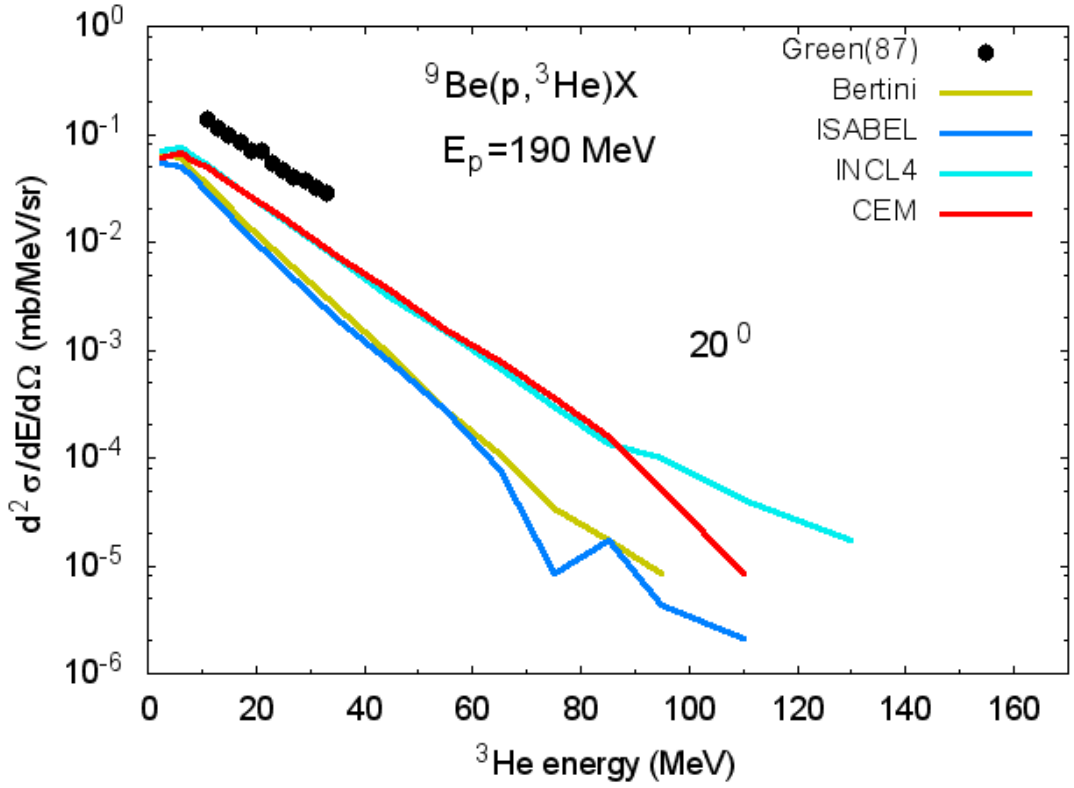
^{9}Be(p,^{3}He)X
E_p=190 MeV
20 ^{0}
Green(87)
Bertini
ISABEL
INCL4
CEM
$d^2\sigma/dE/d\Omega$ (mb/MeV/sr)
^{3}He energy (MeV)

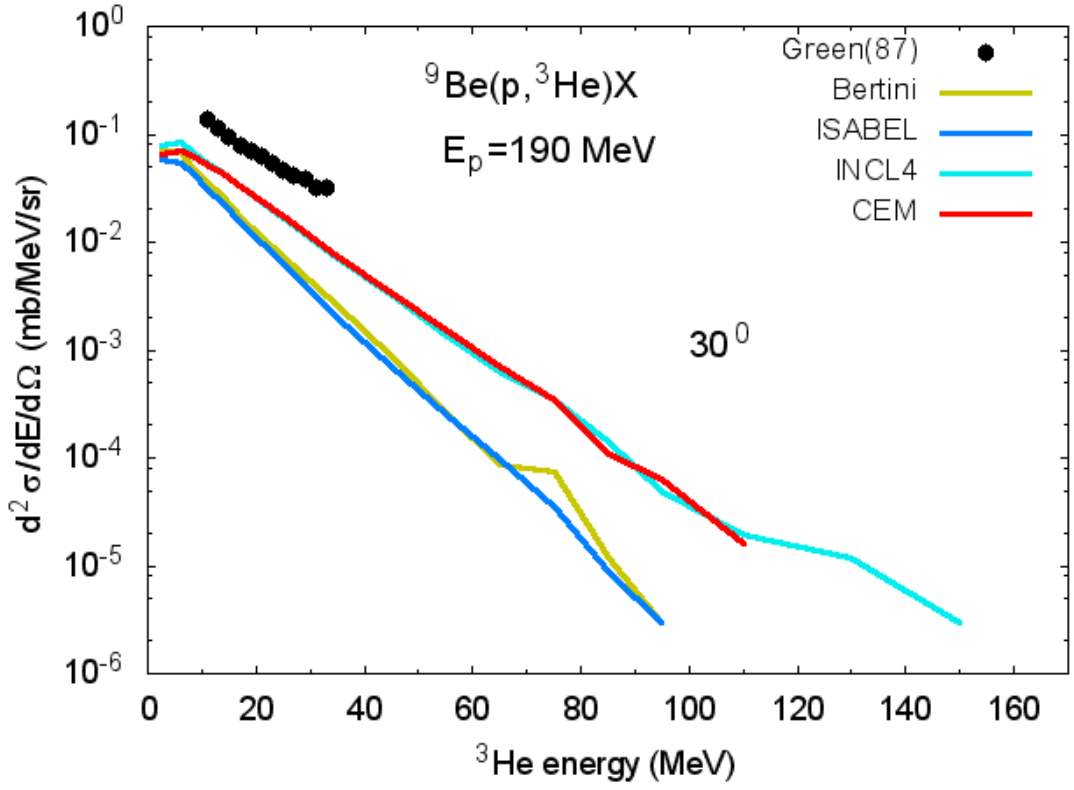
^{9}Be(p,^{3}He)X
E_p=190 MeV
30 ^{0}
Green(87)
Bertini
ISABEL
INCL4
CEM
$d^2\sigma/dE/d\Omega$ (mb/MeV/sr)
^{3}He energy (MeV)

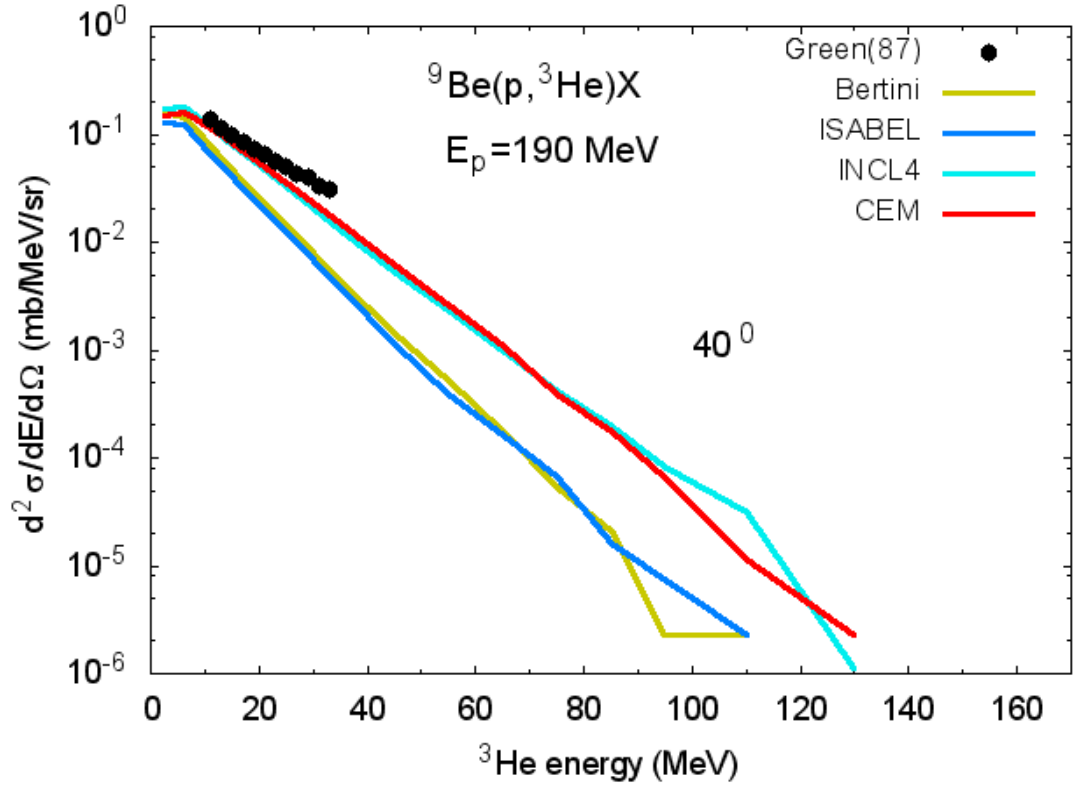
^{9}Be(p,^{3}He)X
E_p=190 MeV
40 ^{0}
Green(87)
Bertini
ISABEL
INCL4
CEM
$d^2\sigma/dE/d\Omega$ (mb/MeV/sr)
^{3}He energy (MeV)

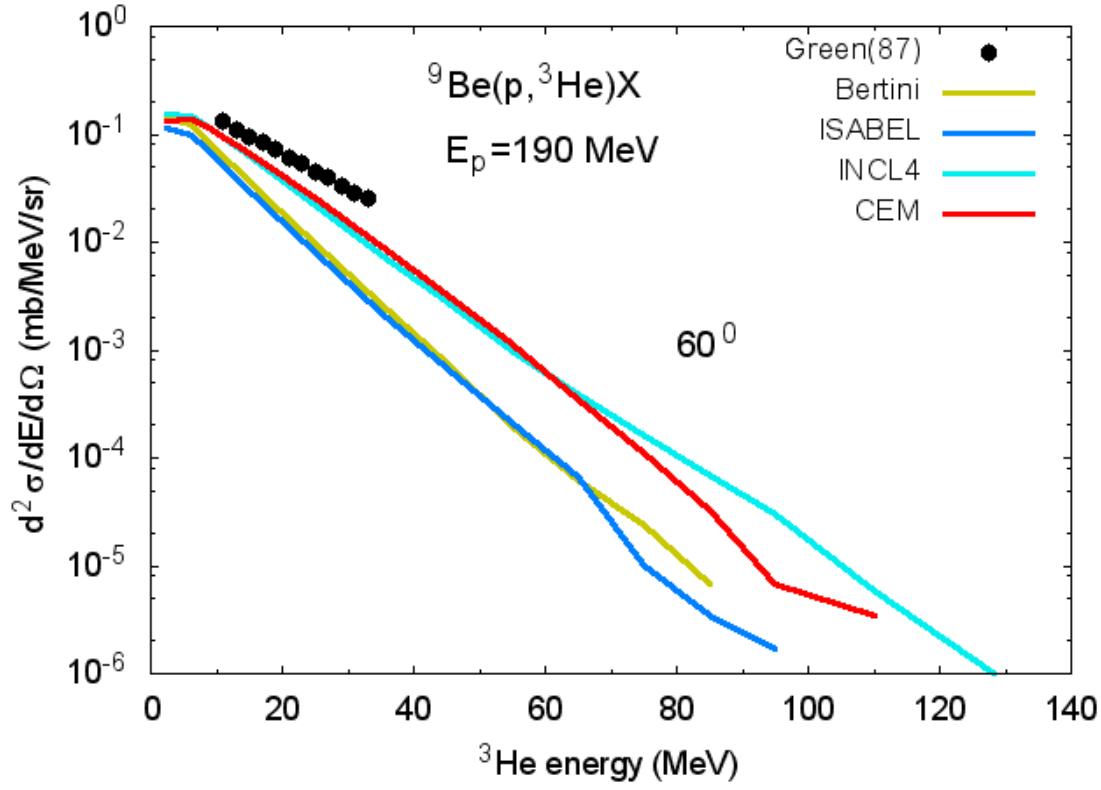
^{9}Be(p,^{3}He)X
E_p=190 MeV
60 ^{0}
Green(87)
Bertini
ISABEL
INCL4
CEM
$d^2\sigma/dE/d\Omega$ (mb/MeV/sr)
^{3}He energy (MeV)

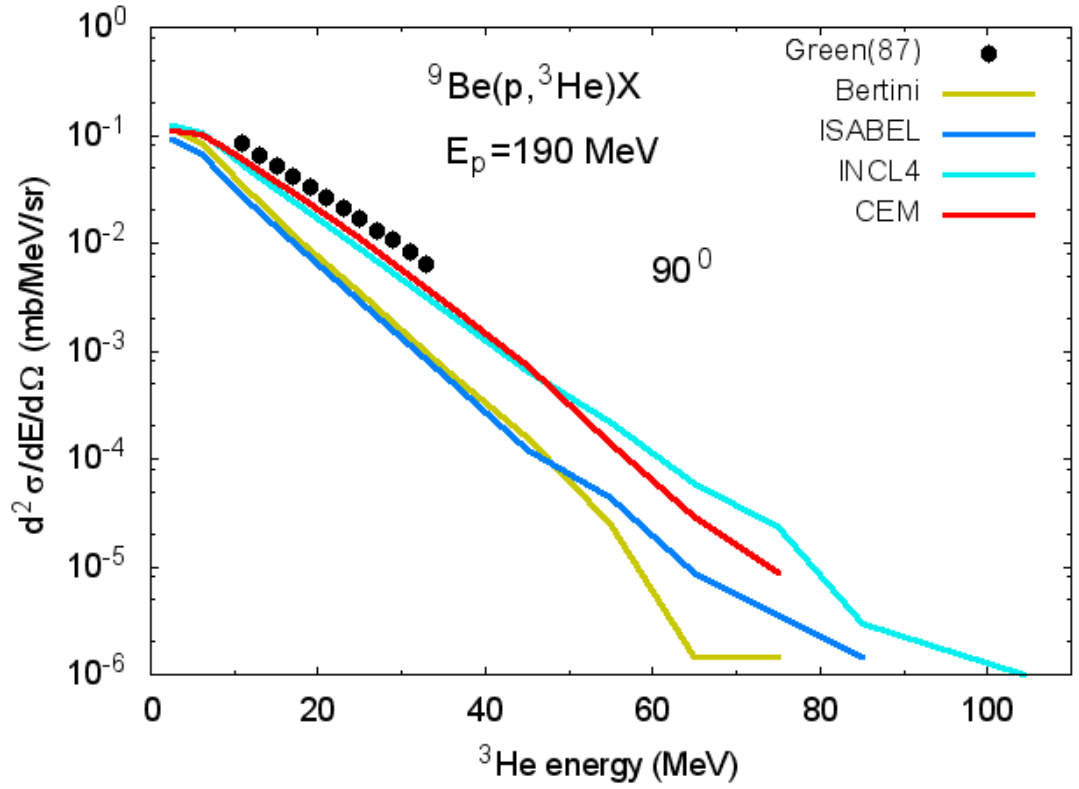
^{9}Be(p,^{3}He)X
E_p=190 MeV
90^0
Green(87)
Bertini
ISABEL
INCL4
CEM
d$^2\sigma$/dE/dΩ (mb/MeV/sr)
^{3}He energy (MeV)

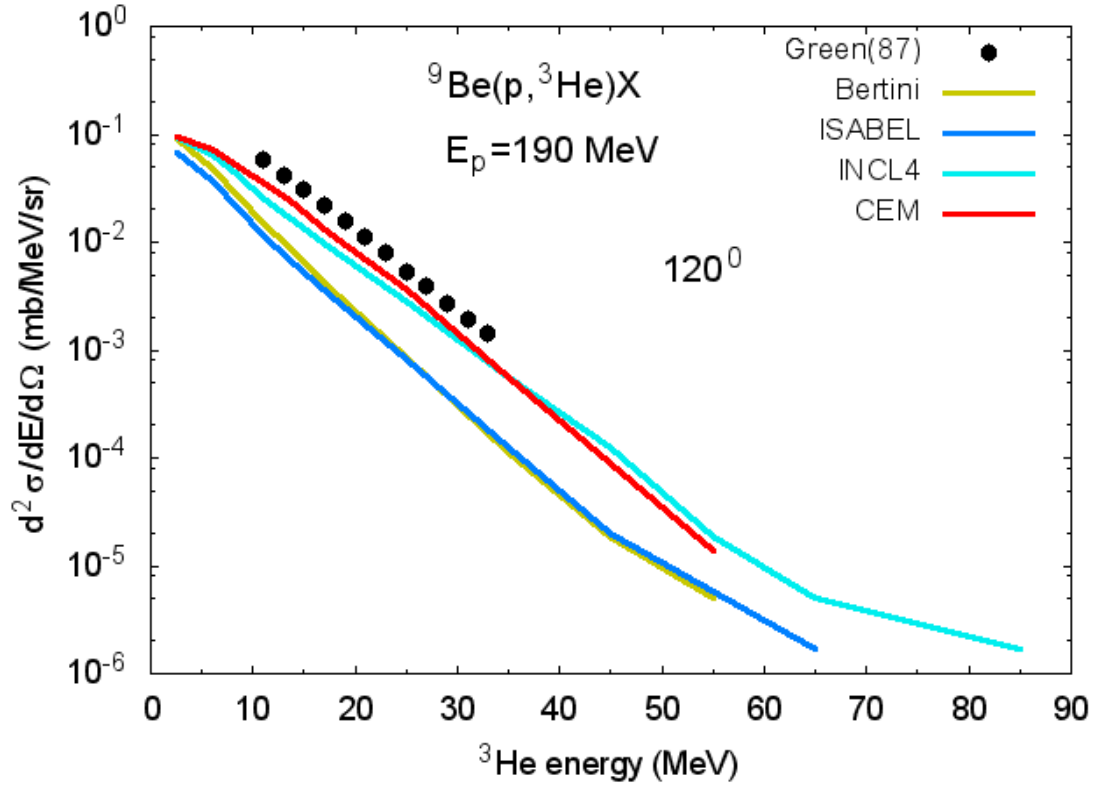
^{9}Be(p,^{3}He)X
E_p=190 MeV
120^0
Green(87)
Bertini
ISABEL
INCL4
CEM
d$^2\sigma$/dE/dΩ (mb/MeV/sr)
^{3}He energy (MeV)

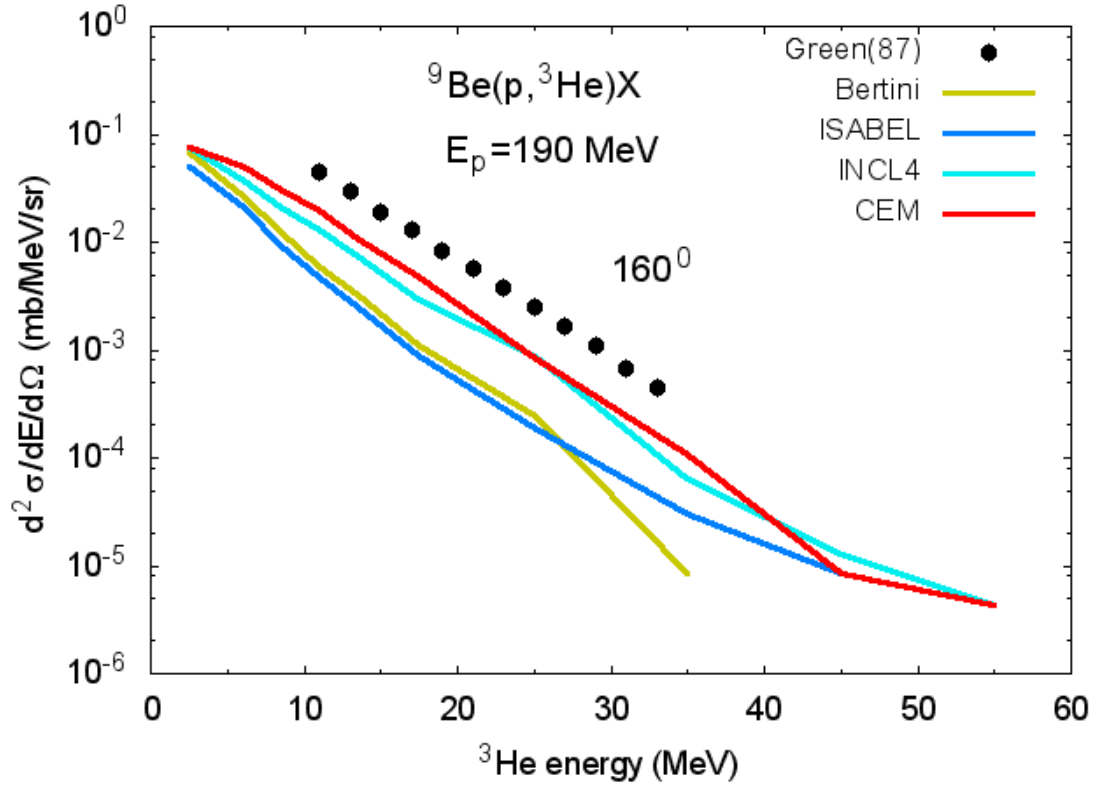
Green(87)
Bertini
ISABEL
INCL4
CEM
^{9}Be(p,^{3}He)X
E_p=190 MeV
160^{0}
d$^{2}\sigma$/dE/dΩ (mb/MeV/sr)
^{3}He energy (MeV)

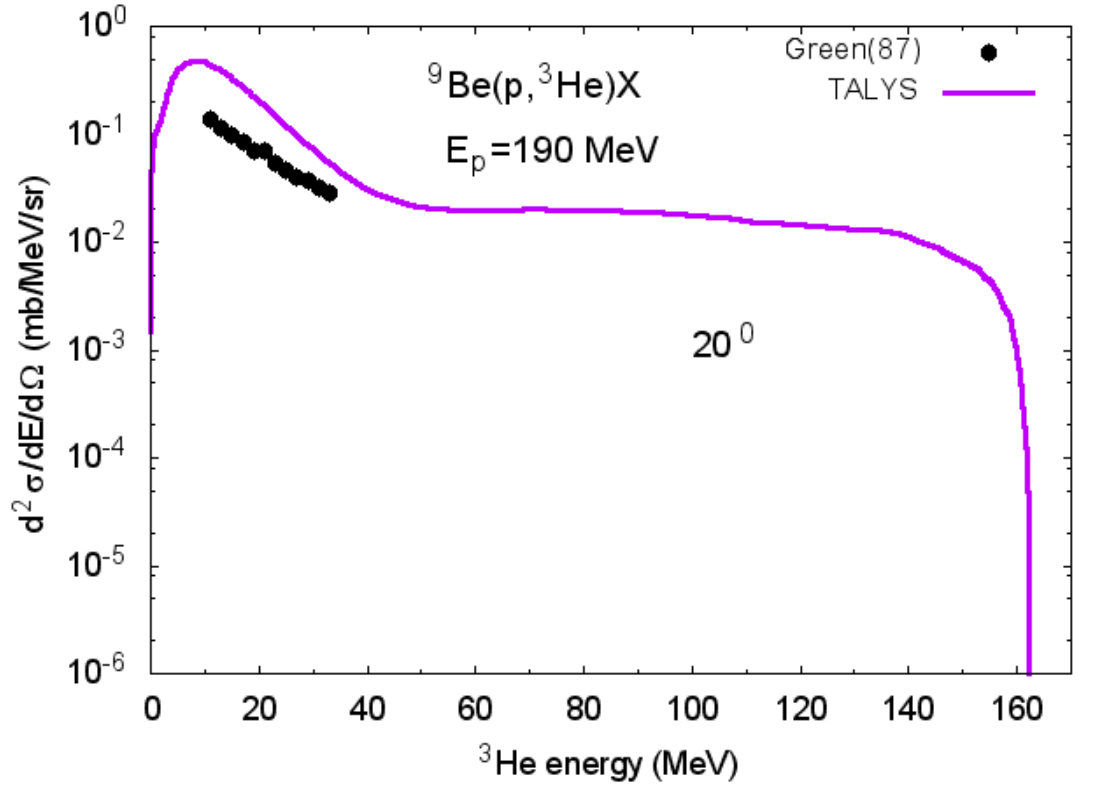
Green(87)
TALYS
^{9}Be(p,^{3}He)X
E_p=190 MeV
20^{0}
d$^{2}\sigma$/dE/dΩ (mb/MeV/sr)
^{3}He energy (MeV)

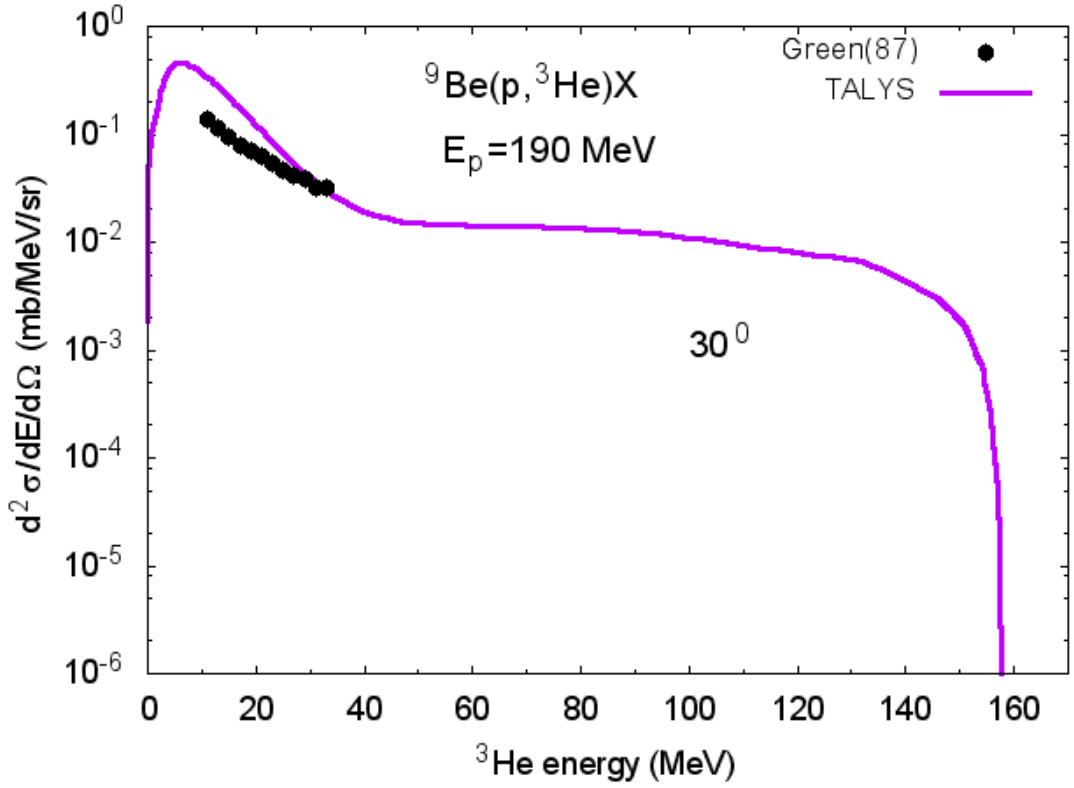
Green(87)
TALYS
^{9}Be(p,^{3}He)X
E_p=190 MeV
30 ^{0}
$d^2\sigma/dE/d\Omega$ (mb/MeV/sr)
^{3}He energy (MeV)

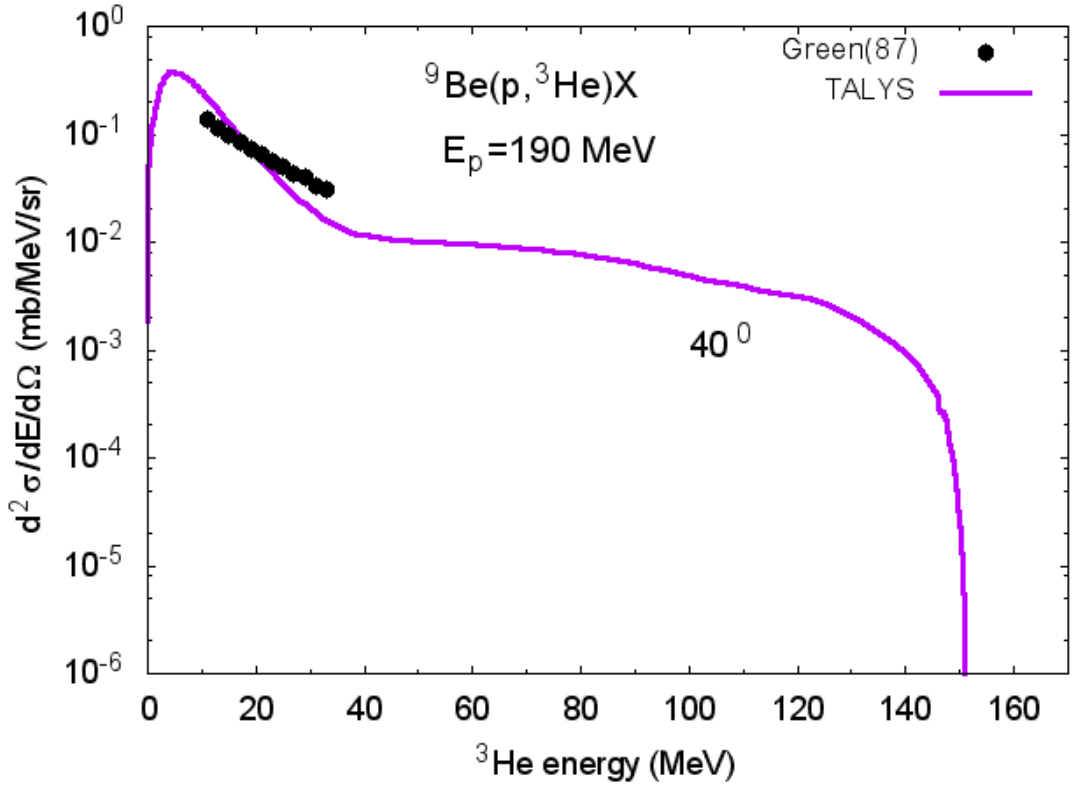
Green(87)
TALYS
^{9}Be(p,^{3}He)X
E_p=190 MeV
40 ^{0}
$d^2\sigma/dE/d\Omega$ (mb/MeV/sr)
^{3}He energy (MeV)

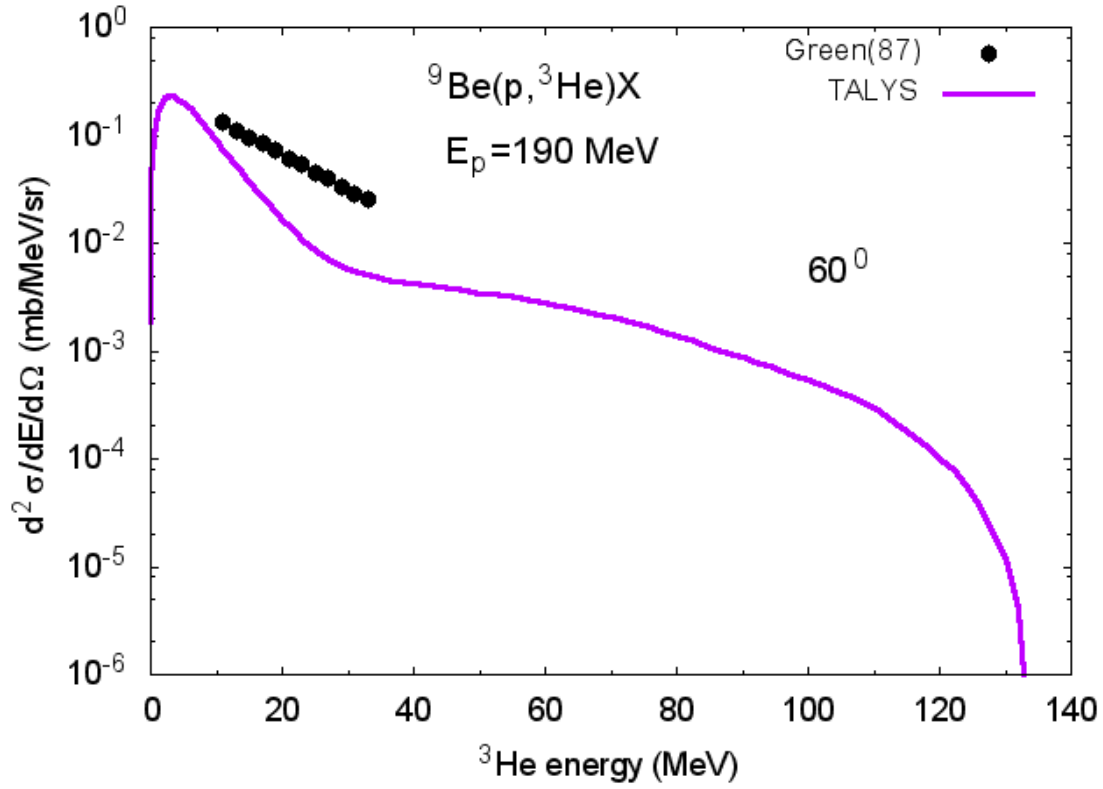
Green(87)
TALYS
^{9}Be(p,^{3}He)X
E_p=190 MeV
60^{0}
d^{2}σ/dEdΩ (mb/MeV/sr)
^{3}He energy (MeV)

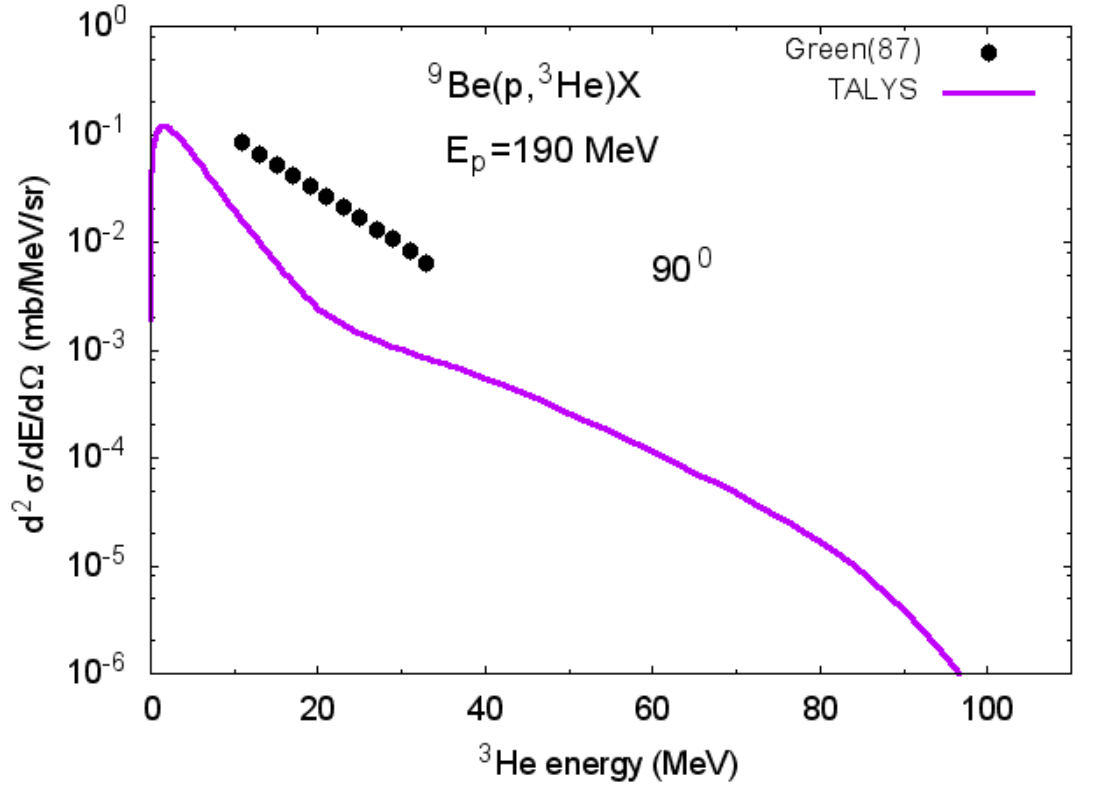
Green(87)
TALYS
^{9}Be(p,^{3}He)X
E_p=190 MeV
90^{0}
d^{2}σ/dEdΩ (mb/MeV/sr)
^{3}He energy (MeV)

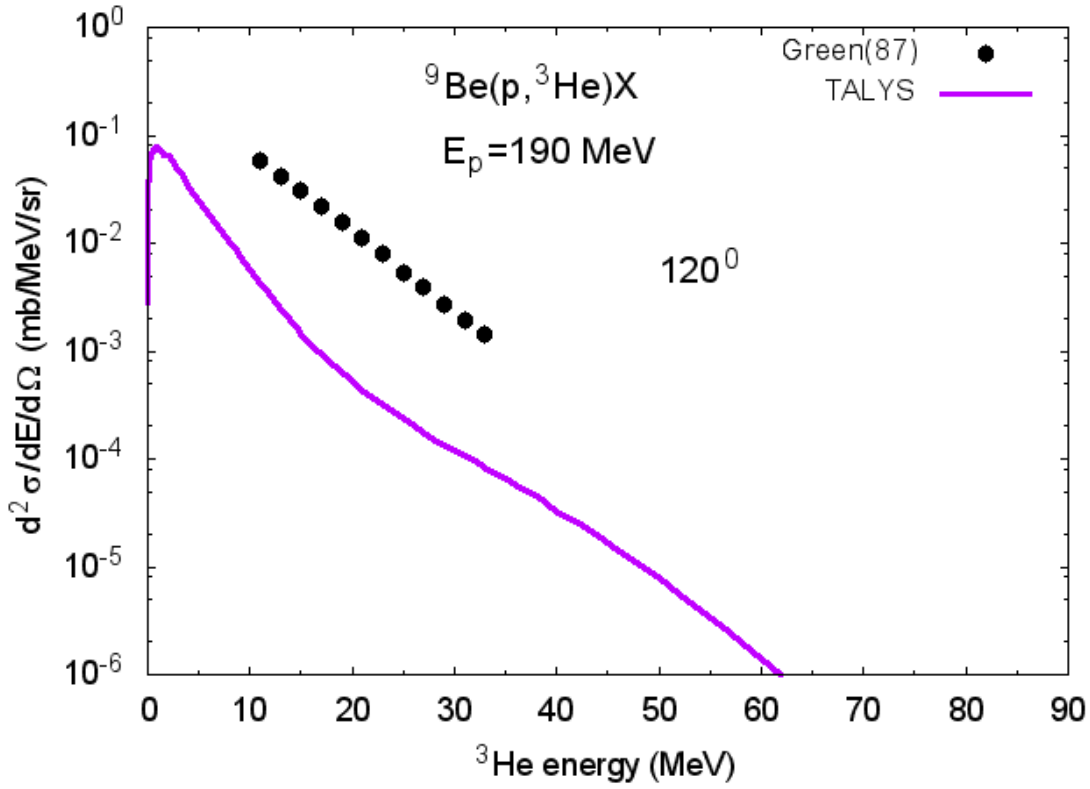
Green(87)
TALYS
^{9}Be(p,^{3}He)X
E_p=190 MeV
120^{0}
d^{2}σ/dEdΩ (mb/MeV/sr)
^{3}He energy (MeV)

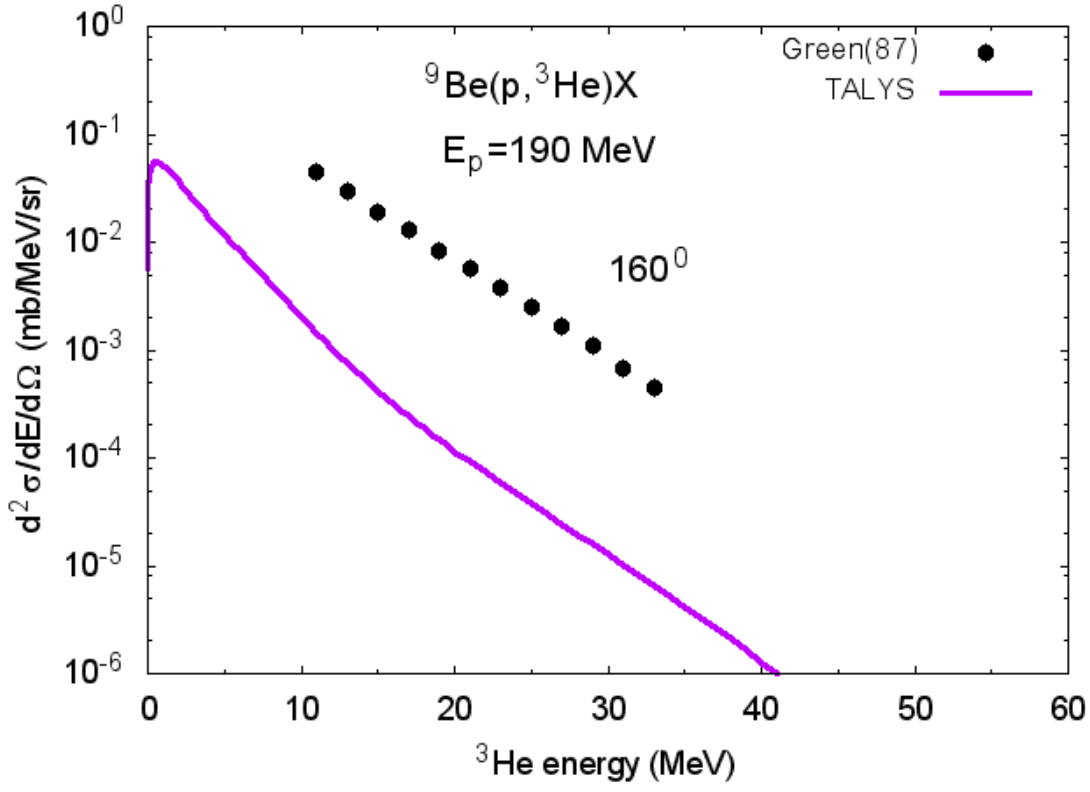
Green(87)
TALYS
^{9}Be(p,^{3}He)X
E_p=190 MeV
160^{0}
d^{2}σ/dEdΩ (mb/MeV/sr)
^{3}He energy (MeV)

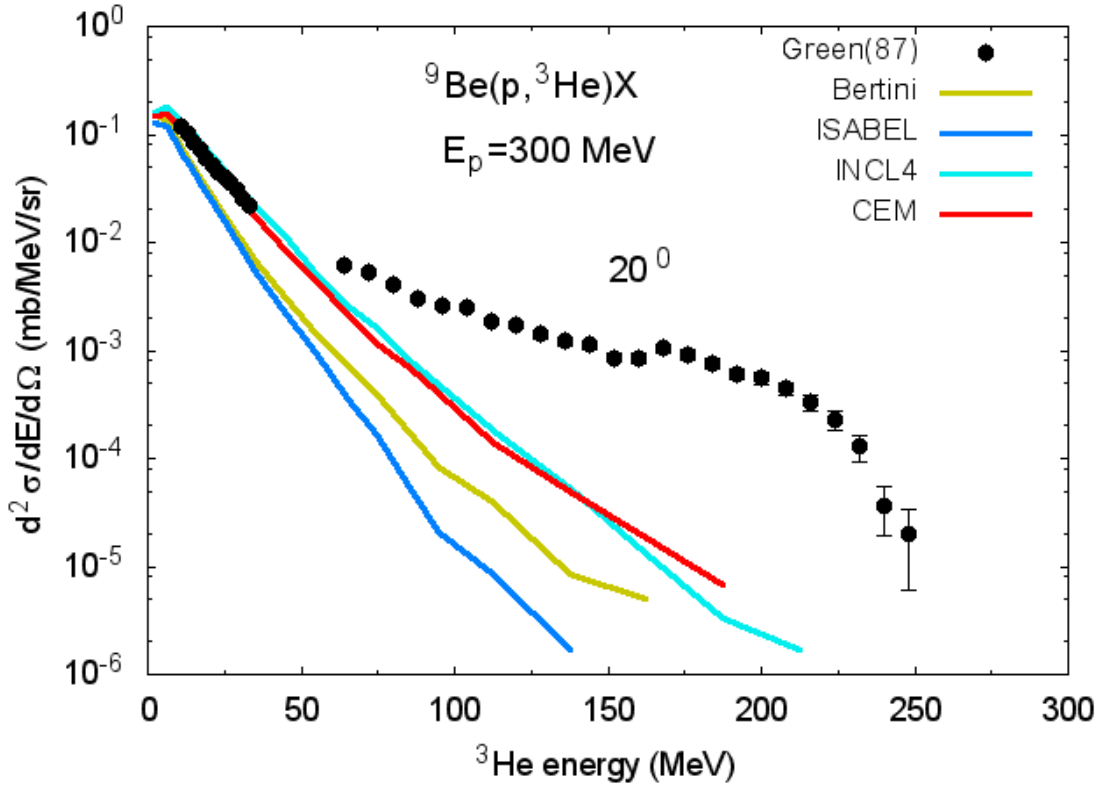
^{9}Be(p,^{3}He)X
E_p=300 MeV
20 ^{0}
Green(87)
Bertini
ISABEL
INCL4
CEM
$d^2\sigma/dE/d\Omega$ (mb/MeV/sr)
^{3}He energy (MeV)

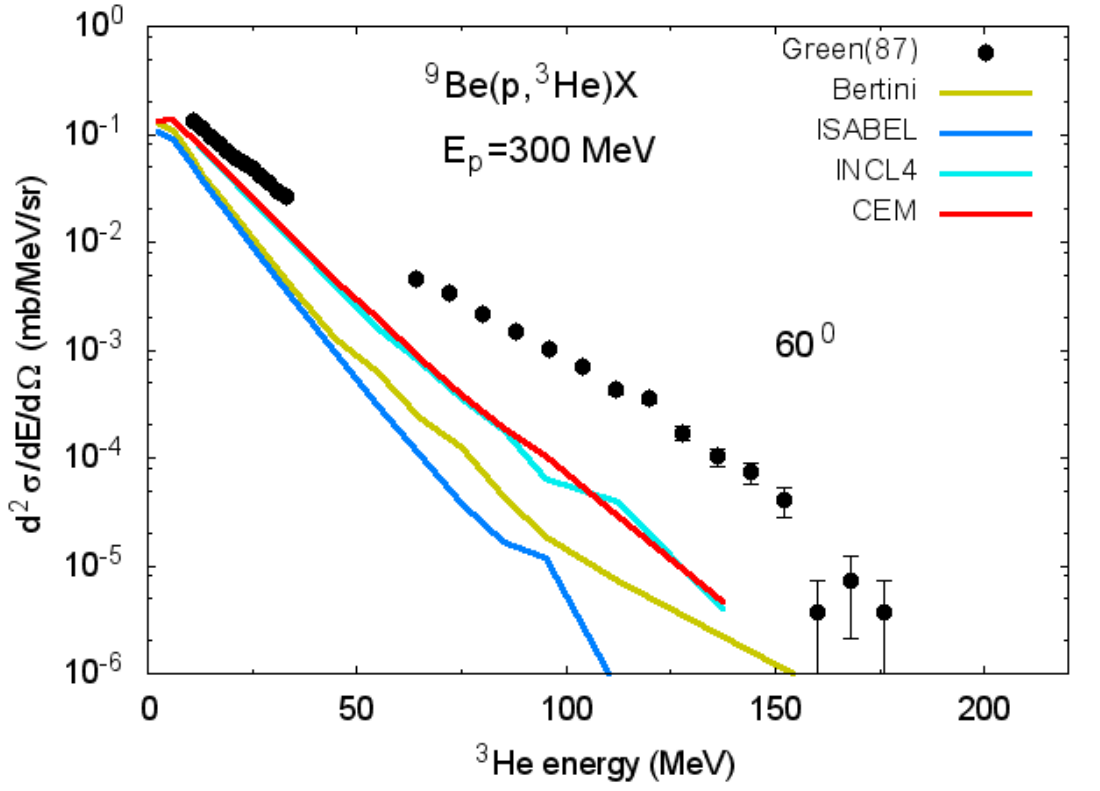
^{9}Be(p,^{3}He)X
E_p=300 MeV
60 ^{0}
Green(87)
Bertini
ISABEL
INCL4
CEM
$d^2\sigma/dE/d\Omega$ (mb/MeV/sr)
^{3}He energy (MeV)

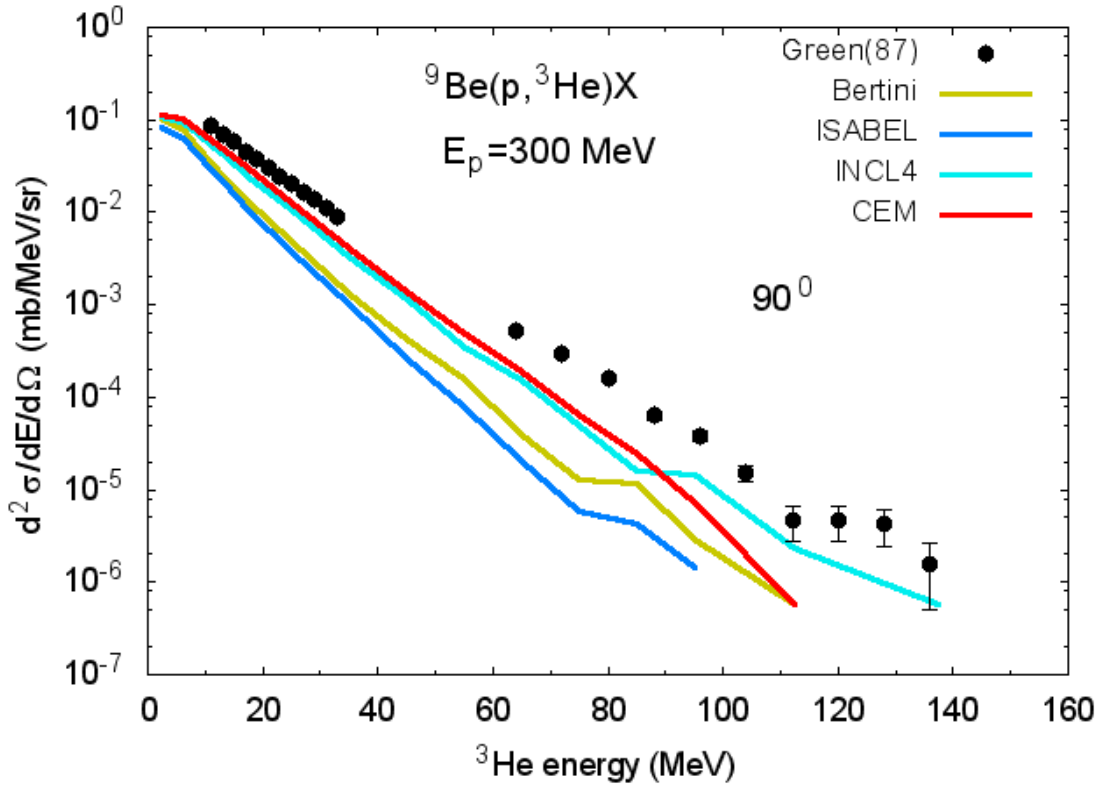
^{9}Be(p,^{3}He)X
E_p=300 MeV
90^0
Green(87)
Bertini
ISABEL
INCL4
CEM
d$^2\sigma$/dE/dΩ (mb/MeV/sr)
^{3}He energy (MeV)

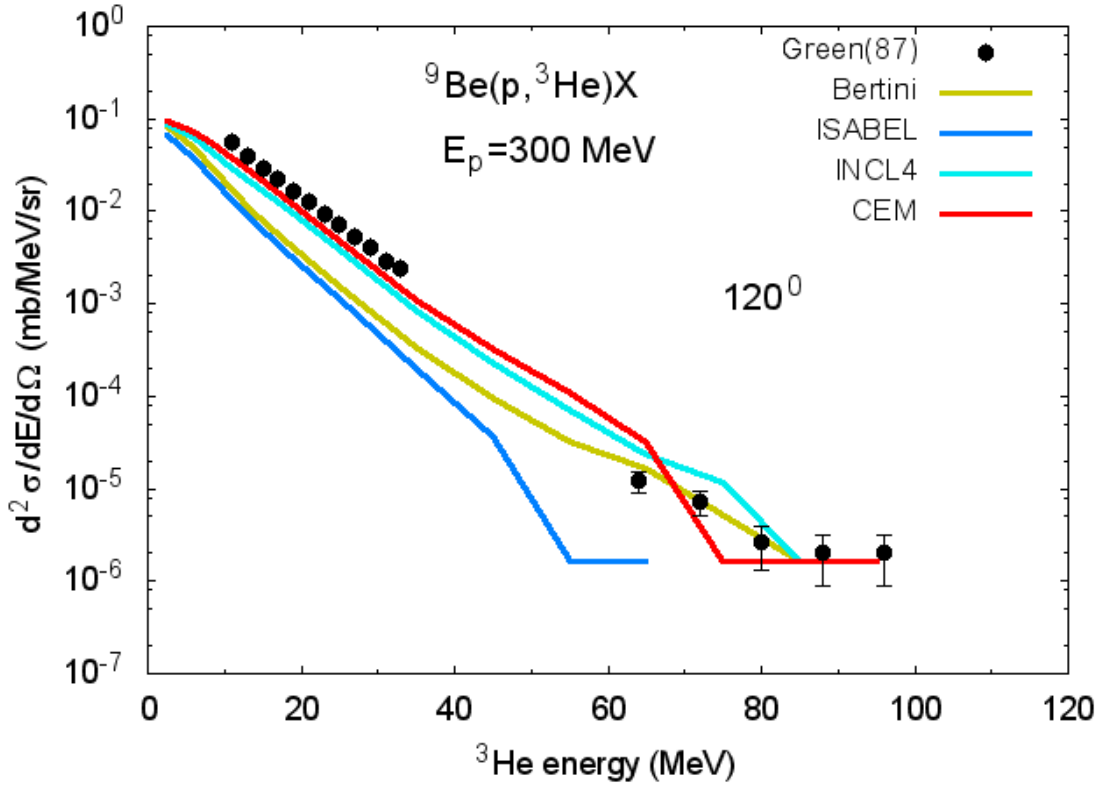
^{9}Be(p,^{3}He)X
E_p=300 MeV
120^0
Green(87)
Bertini
ISABEL
INCL4
CEM
d$^2\sigma$/dE/dΩ (mb/MeV/sr)
^{3}He energy (MeV)

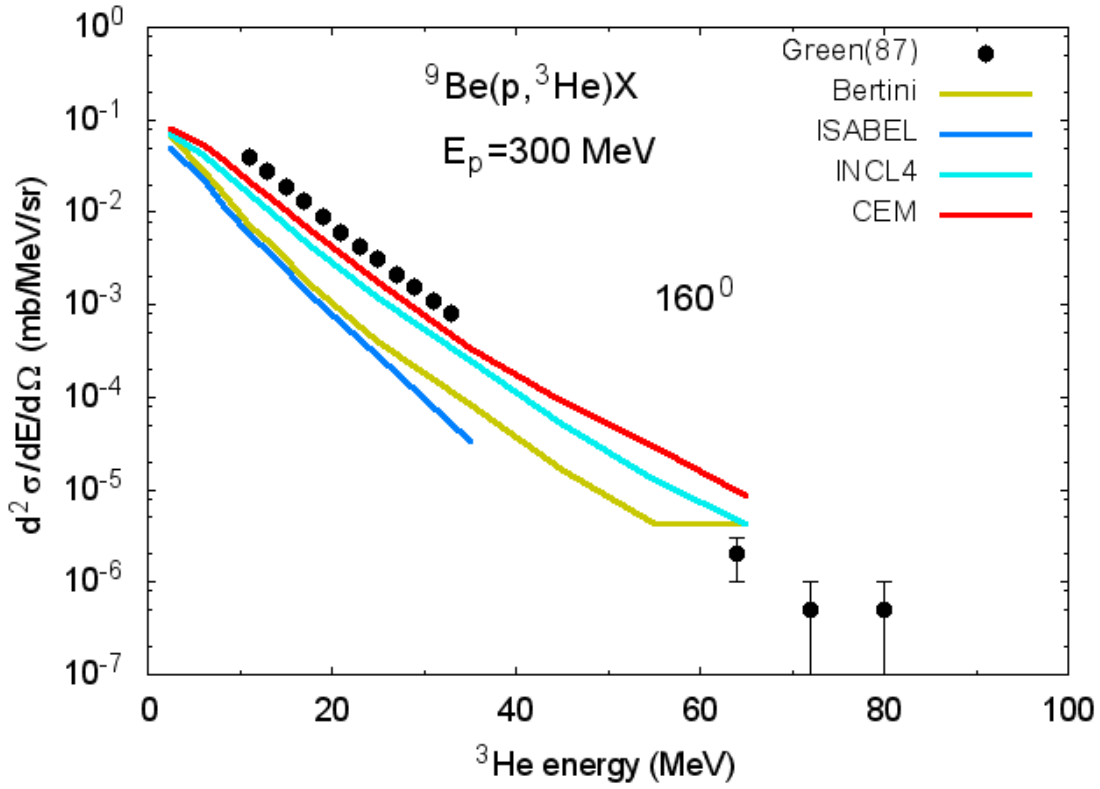
^{9}Be(p,^{3}He)X
E_p=300 MeV
160^0
Green(87)
Bertini
ISABEL
INCL4
CEM
d$^2\sigma$/dE/dΩ (mb/MeV/sr)
^{3}He energy (MeV)

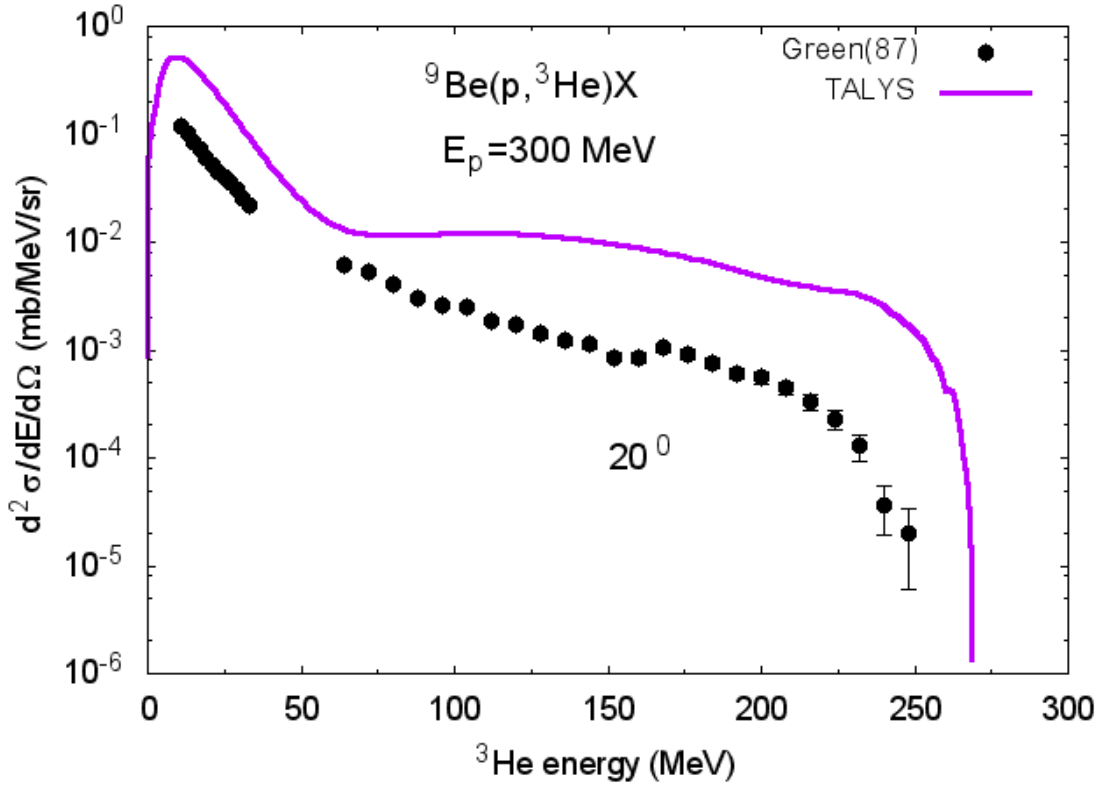
^{9}Be(p,^{3}He)X
E_p=300 MeV
20^0
Green(87)
TALYS
d$^2\sigma$/dE/dΩ (mb/MeV/sr)
^{3}He energy (MeV)

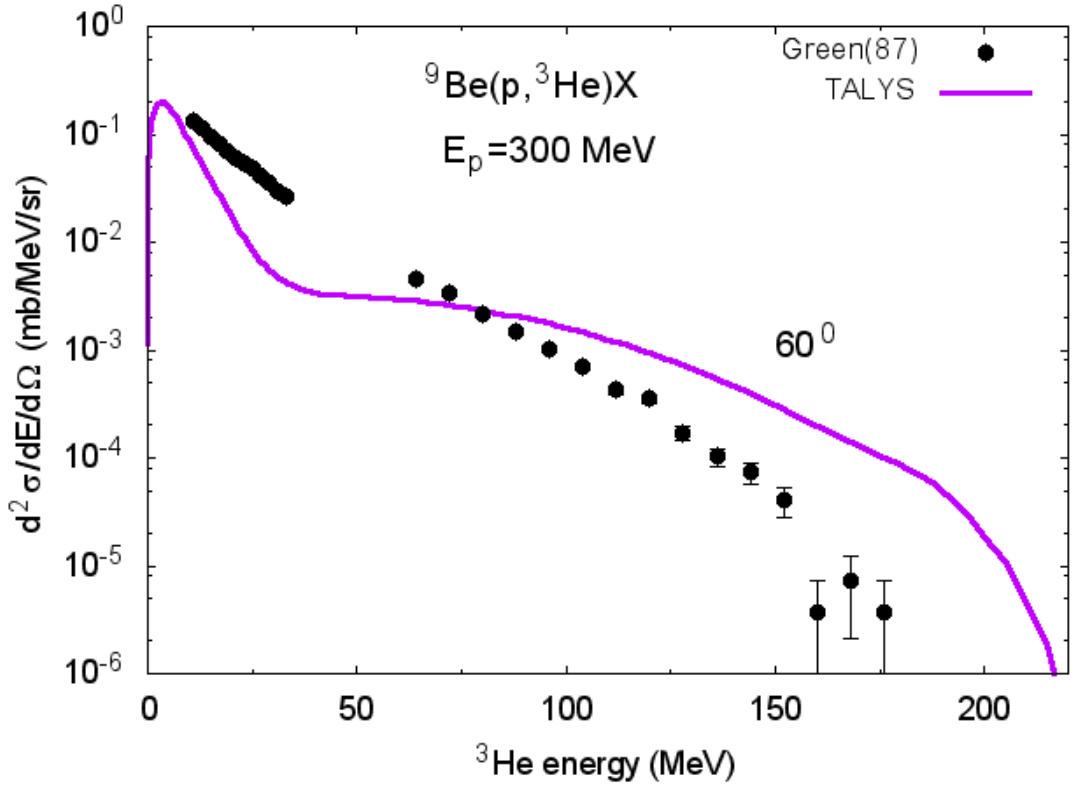
Green(87)
TALYS
^{9}Be(p,^{3}He)X
E_p=300 MeV
60^{0}
d$^{2}\sigma$/dE/dΩ (mb/MeV/sr)
^{3}He energy (MeV)

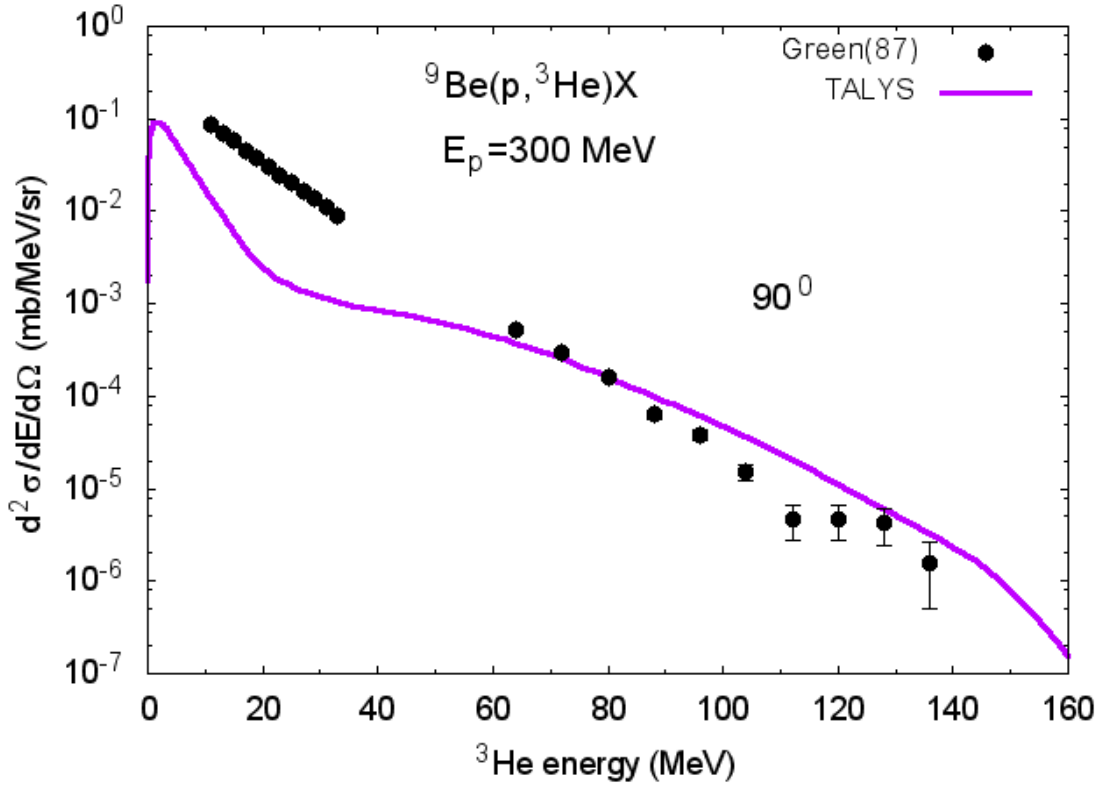
Green(87)
TALYS
^{9}Be(p,^{3}He)X
E_p=300 MeV
90^{0}
d$^{2}\sigma$/dE/dΩ (mb/MeV/sr)
^{3}He energy (MeV)

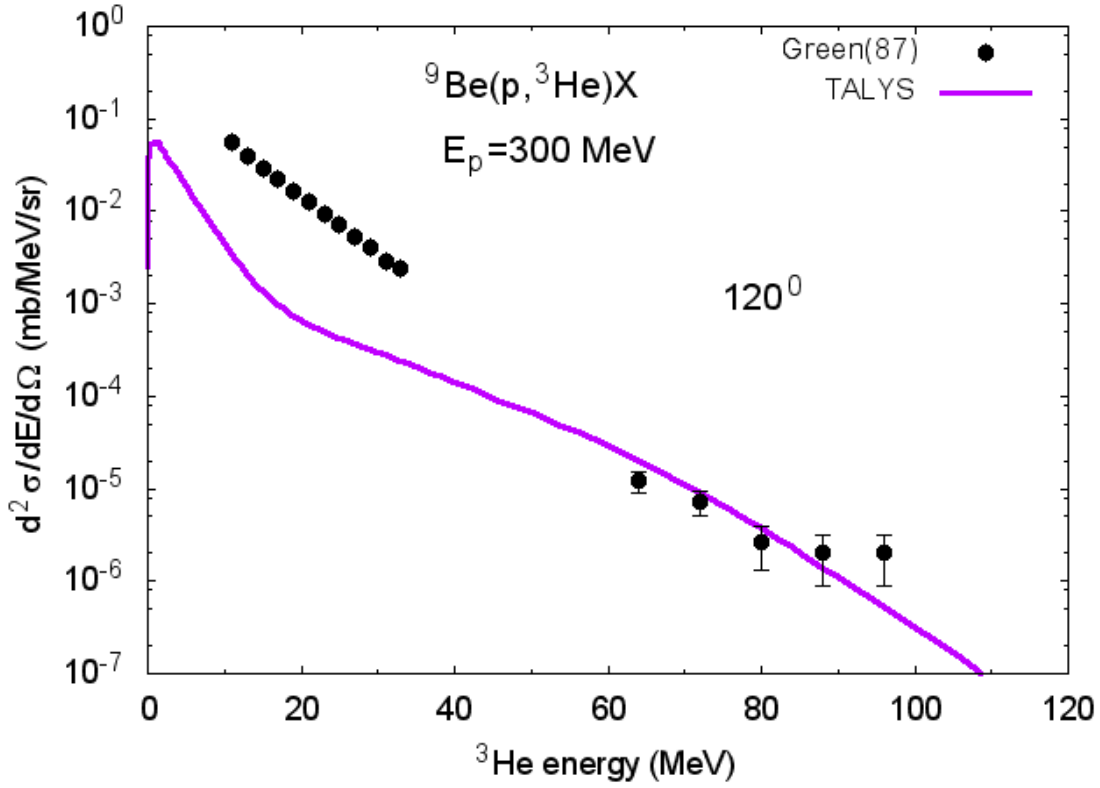
Green(87)
TALYS
^{9}Be(p,^{3}He)X
E_p=300 MeV
120^0
$d^2\sigma/dE/d\Omega$ (mb/MeV/sr)
^{3}He energy (MeV)

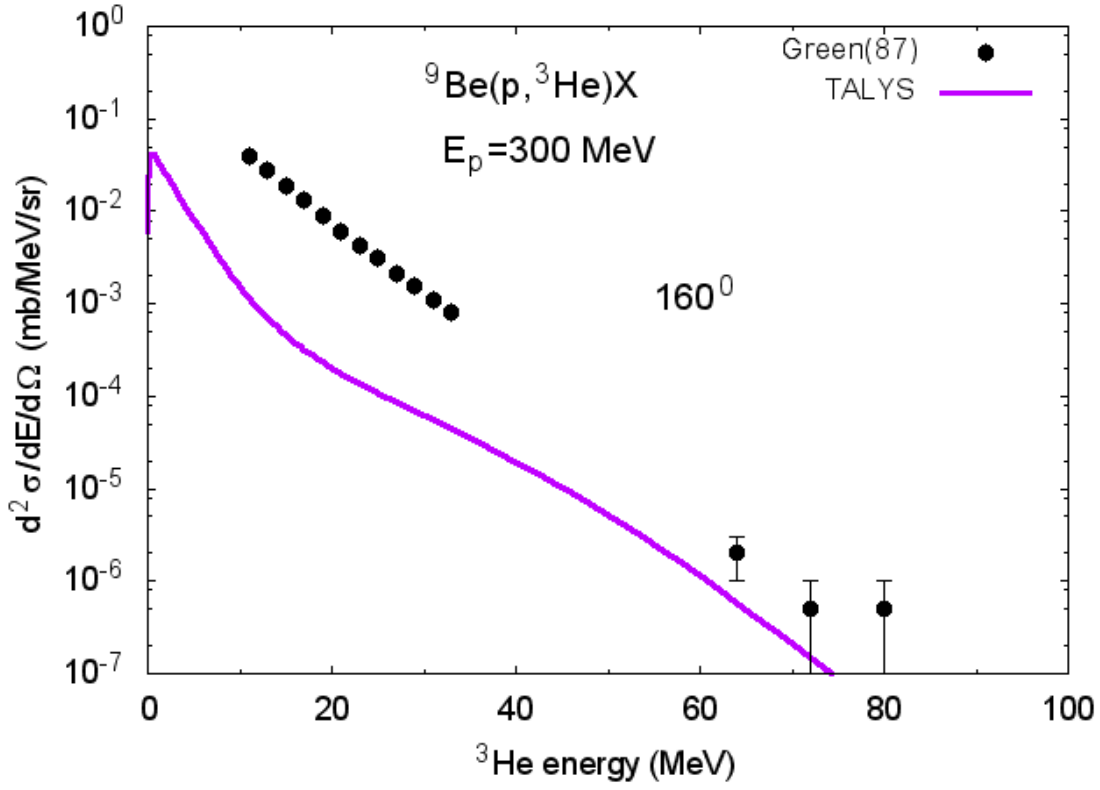
Green(87)
TALYS
^{9}Be(p,^{3}He)X
E_p=300 MeV
160^0
$d^2\sigma/dE/d\Omega$ (mb/MeV/sr)
^{3}He energy (MeV)

Comparison of double differential cross-sections of α-particle emission in p+^{9}Be reactions calculated using Bertini, ISABEL, CEM03, and INCL4 models and models implemented in the TALYS code with available measured data

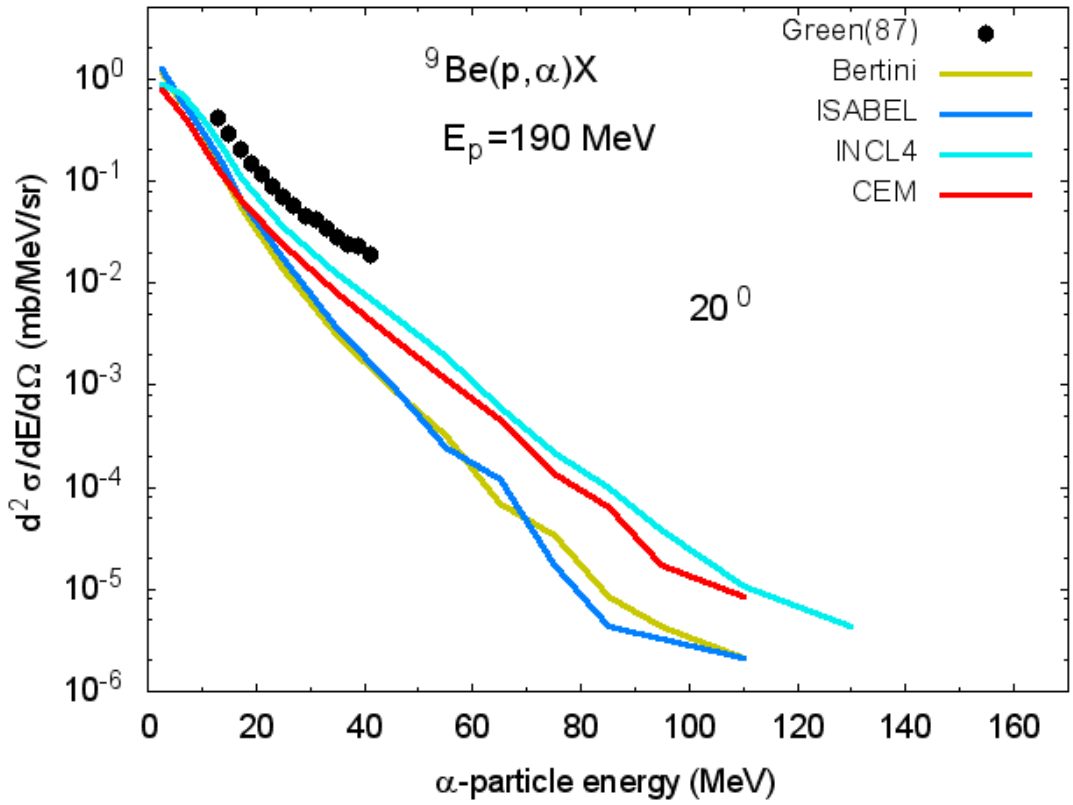
Green(87)
Bertini
ISABEL
INCL4
CEM
^{9}Be(p,α)X
E_p=190 MeV
20 ^{0}
$d^2\sigma/dE/d\Omega$ (mb/MeV/sr)
α-particle energy (MeV)

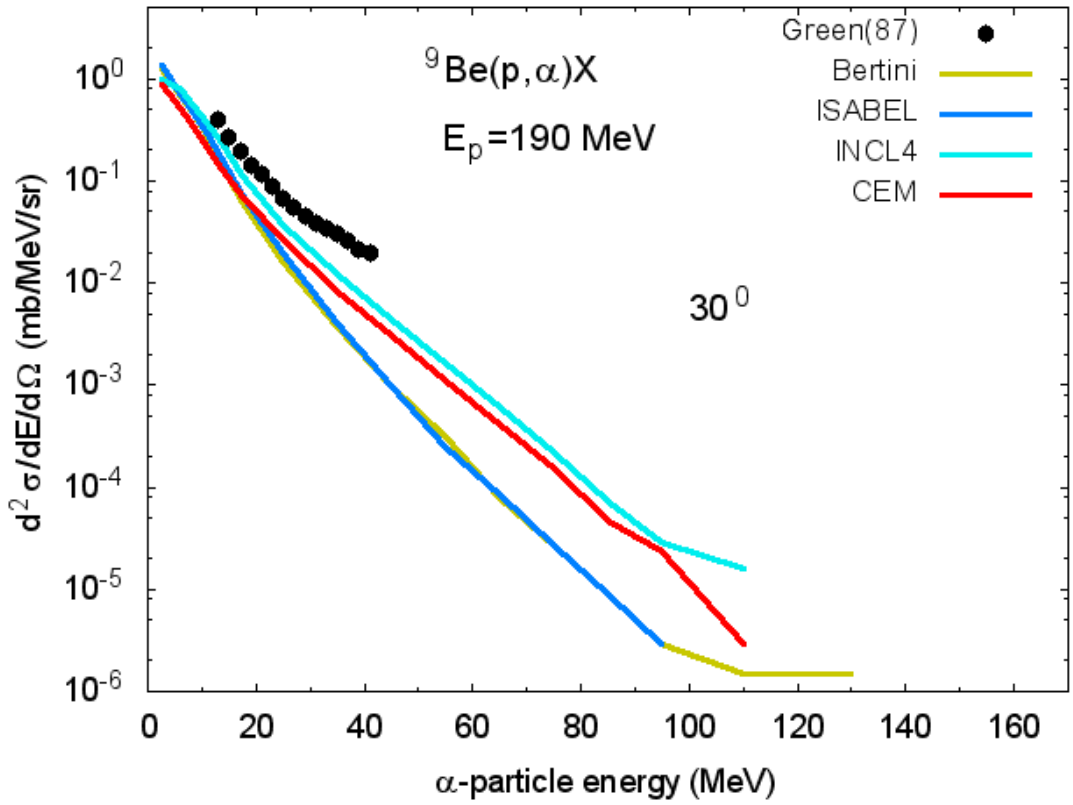
Green(87)
Bertini
ISABEL
INCL4
CEM
^{9}Be(p,α)X
E_p=190 MeV
30 ^{0}
$d^2\sigma/dE/d\Omega$ (mb/MeV/sr)
α-particle energy (MeV)

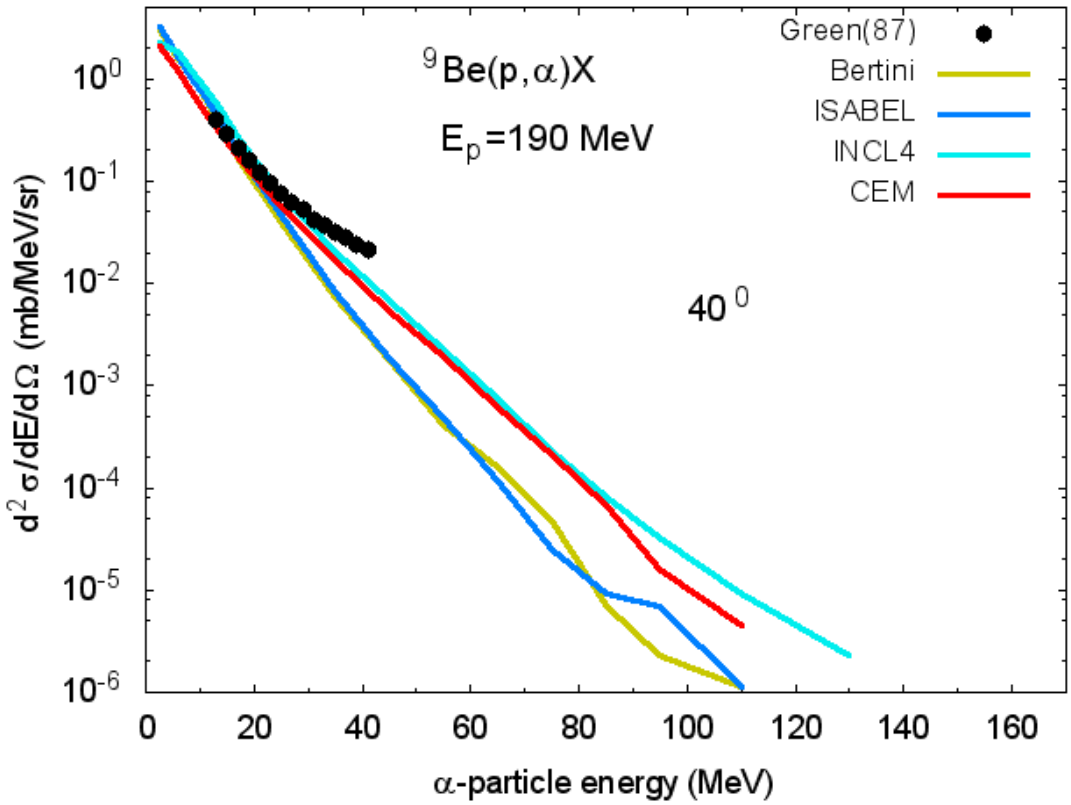
Green(87)
Bertini
ISABEL
INCL4
CEM
^{9}Be(p,α)X
E_p=190 MeV
40 ^{0}
$d^2\sigma/dE/d\Omega$ (mb/MeV/sr)
α-particle energy (MeV)

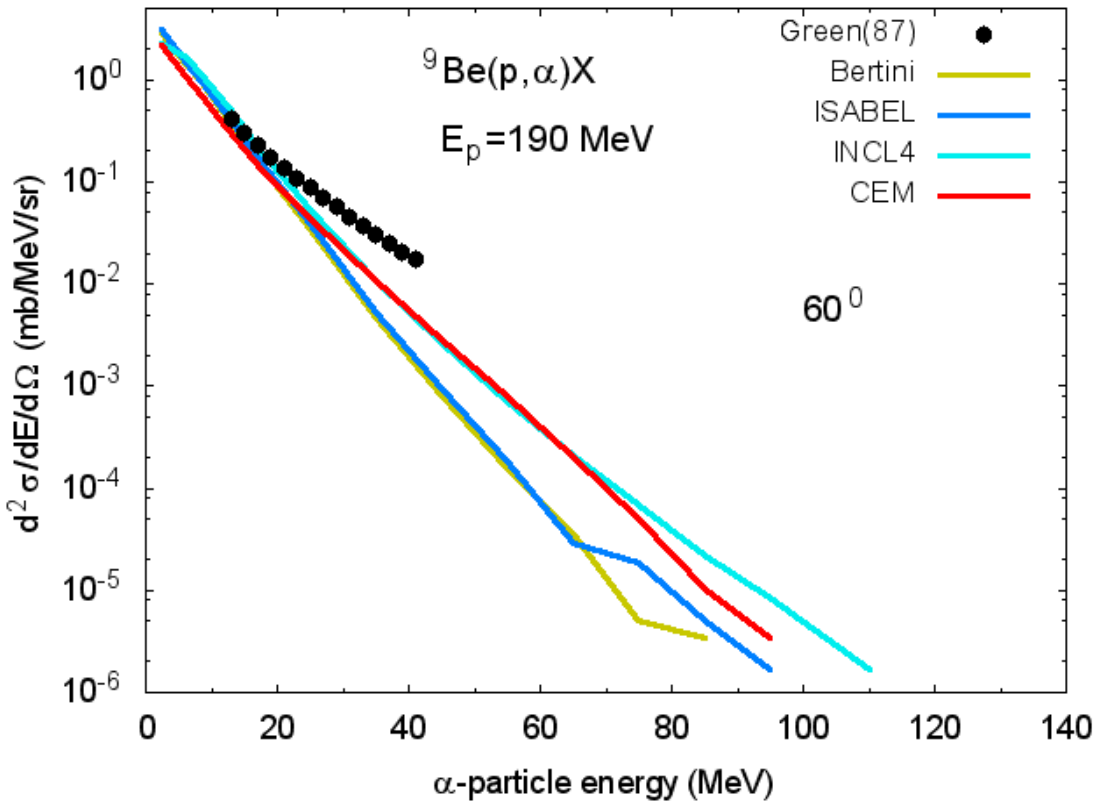
Green(87)
Bertini
ISABEL
INCL4
CEM
^{9}Be(p,α)X
E_p=190 MeV
60 ^{0}
$d^2\sigma/dE/d\Omega$ (mb/MeV/sr)
α-particle energy (MeV)

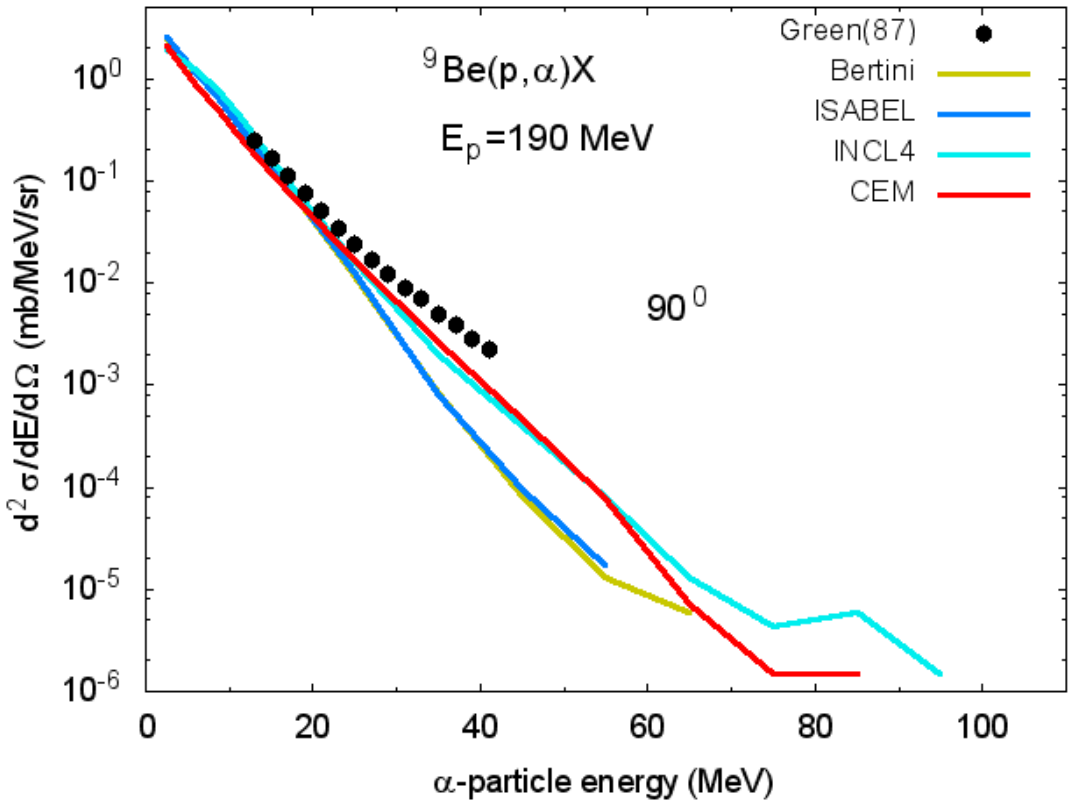
Green(87)
Bertini
ISABEL
INCL4
CEM
^{9}Be(p,α)X
E_p=190 MeV
90^0
$d^2\sigma/dE/d\Omega$ (mb/MeV/sr)
α-particle energy (MeV)

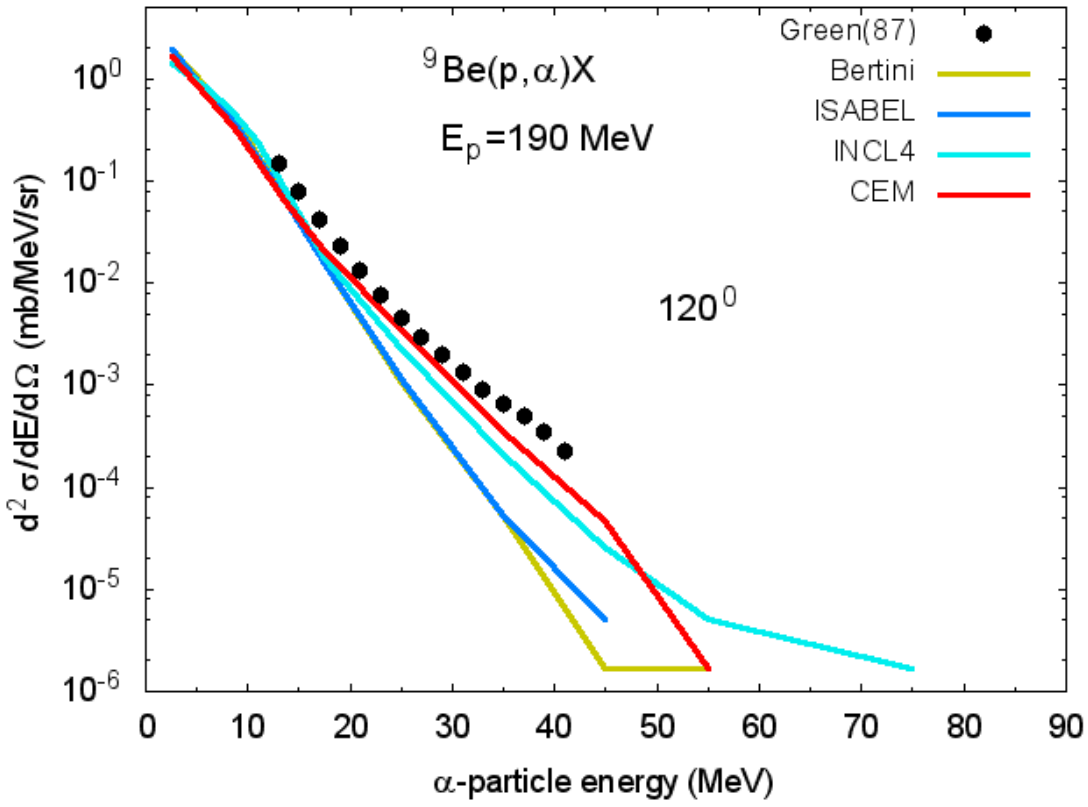
Green(87)
Bertini
ISABEL
INCL4
CEM
^{9}Be(p,α)X
E_p=190 MeV
120^0
$d^2\sigma/dE/d\Omega$ (mb/MeV/sr)
α-particle energy (MeV)

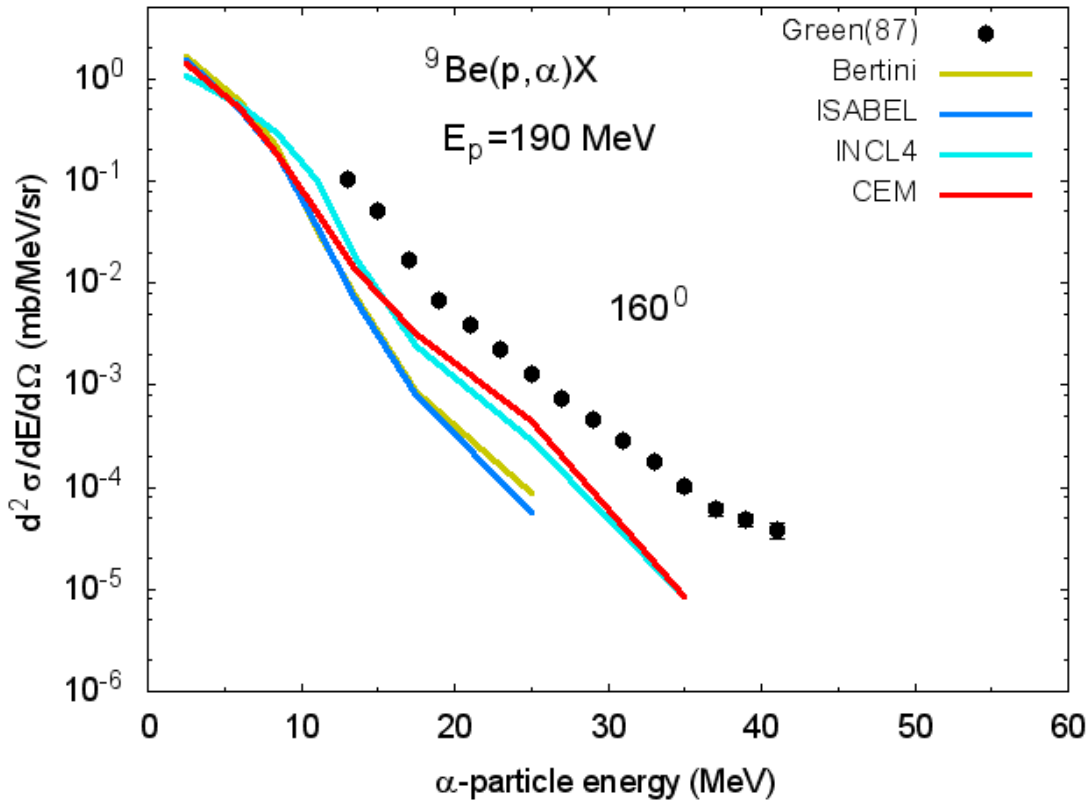
Green(87)
Bertini
ISABEL
INCL4
CEM
^{9}Be(p,α)X
E_p=190 MeV
160^{0}
$d^2\sigma/dE/d\Omega$ (mb/MeV/sr)
α-particle energy (MeV)

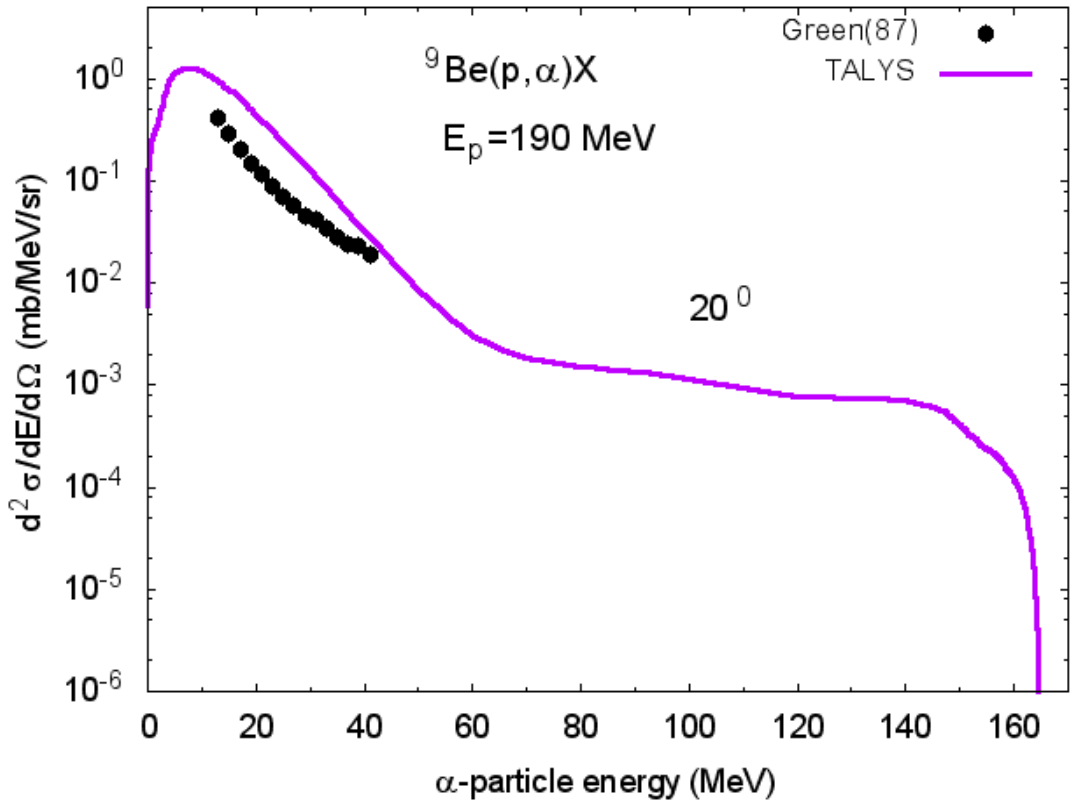
Green(87)
TALYS
^{9}Be(p,α)X
E_p=190 MeV
20^{0}
$d^2\sigma/dE/d\Omega$ (mb/MeV/sr)
α-particle energy (MeV)

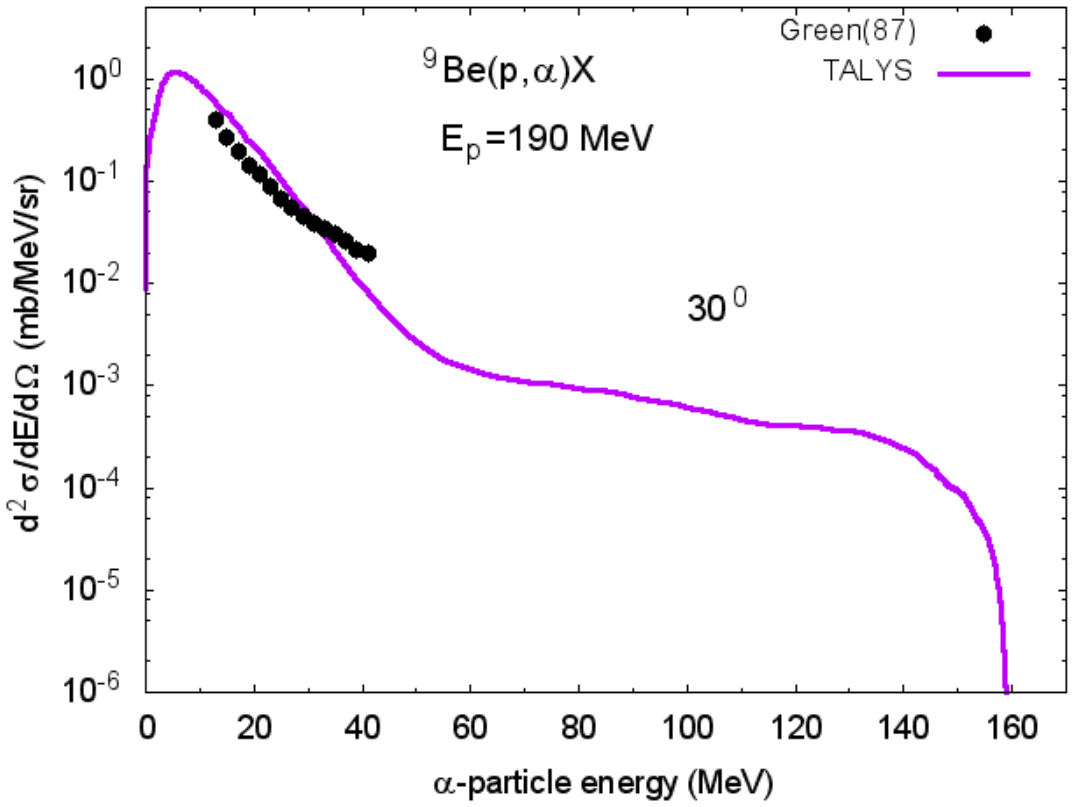
Green(87)
TALYS
^{9}Be(p,α)X
E_p=190 MeV
30 ^{0}
d^{2}σ/dE/dΩ (mb/MeV/sr)
α-particle energy (MeV)

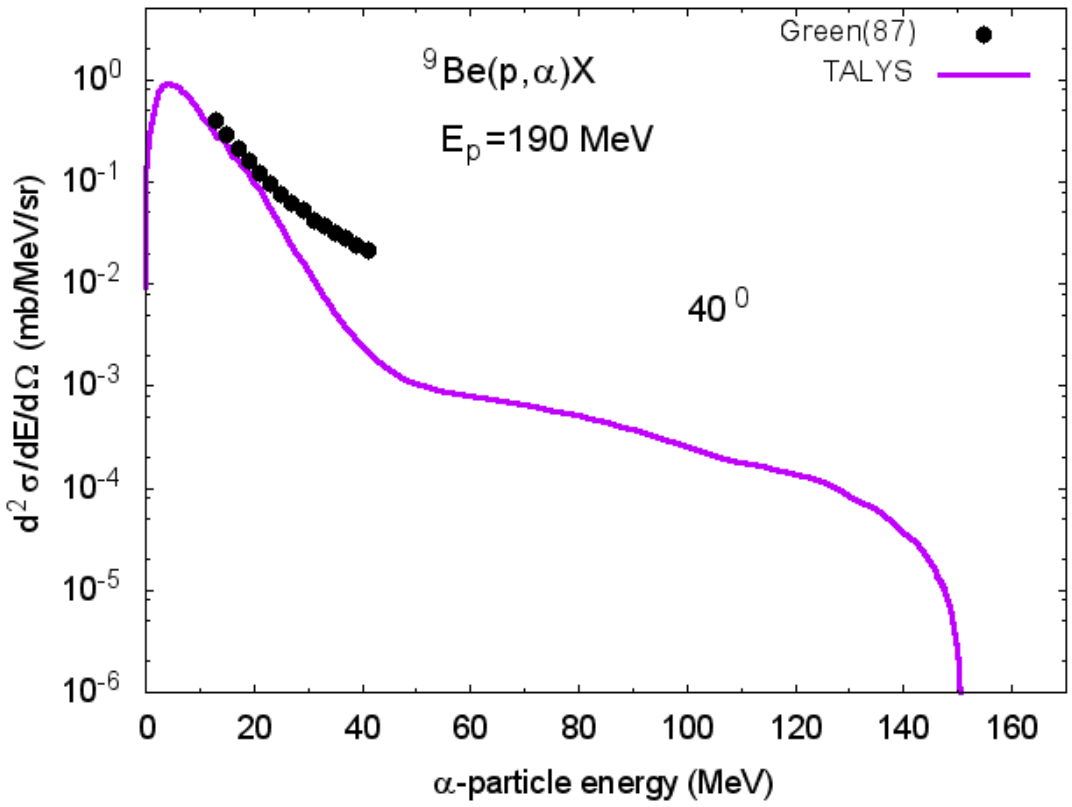
Green(87)
TALYS
^{9}Be(p,α)X
E_p=190 MeV
40 ^{0}
d^{2}σ/dE/dΩ (mb/MeV/sr)
α-particle energy (MeV)

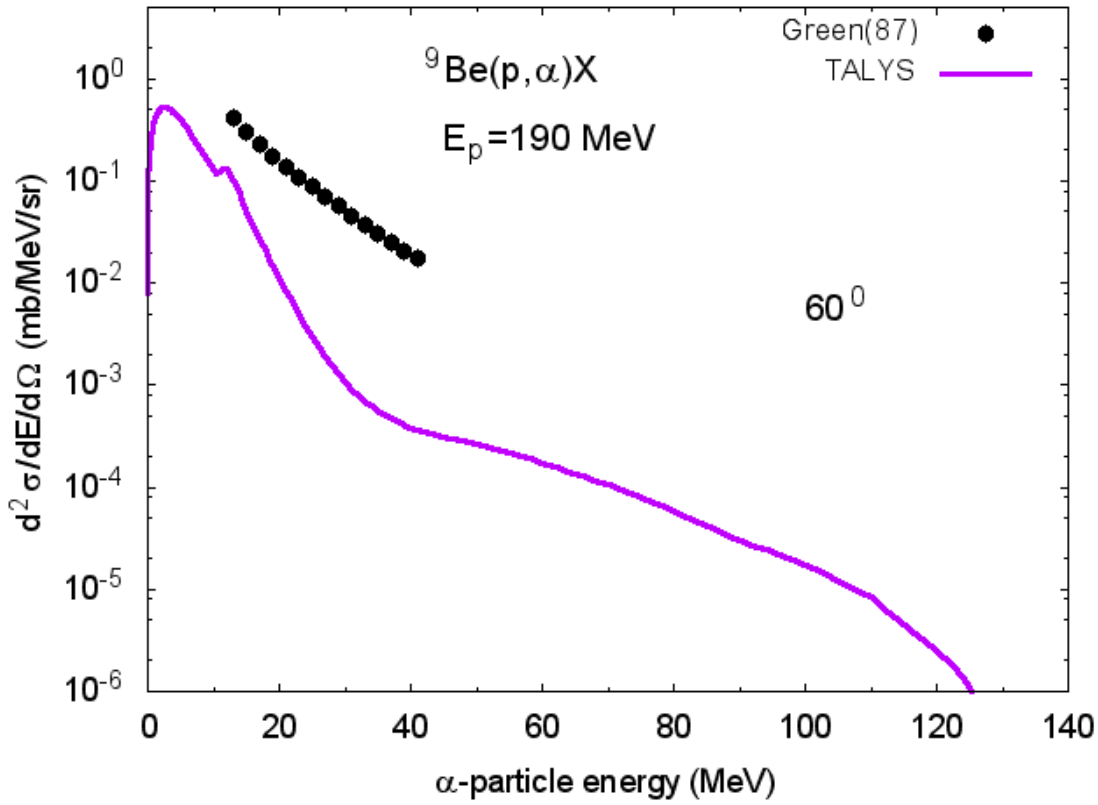
Green(87)
TALYS
^{9}Be(p,α)X
E_p=190 MeV
60^0
d^{2}σ/dE/dΩ (mb/MeV/sr)
α-particle energy (MeV)

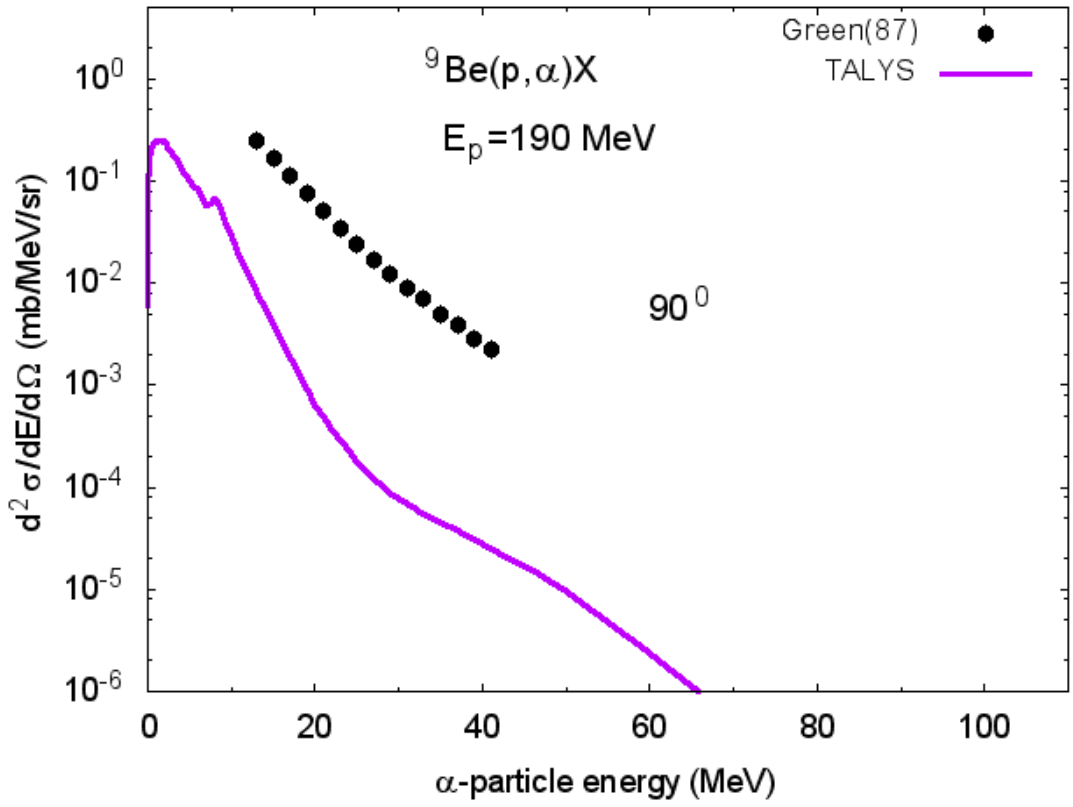
Green(87)
TALYS
^{9}Be(p,α)X
E_p=190 MeV
90^0
d^{2}σ/dE/dΩ (mb/MeV/sr)
α-particle energy (MeV)

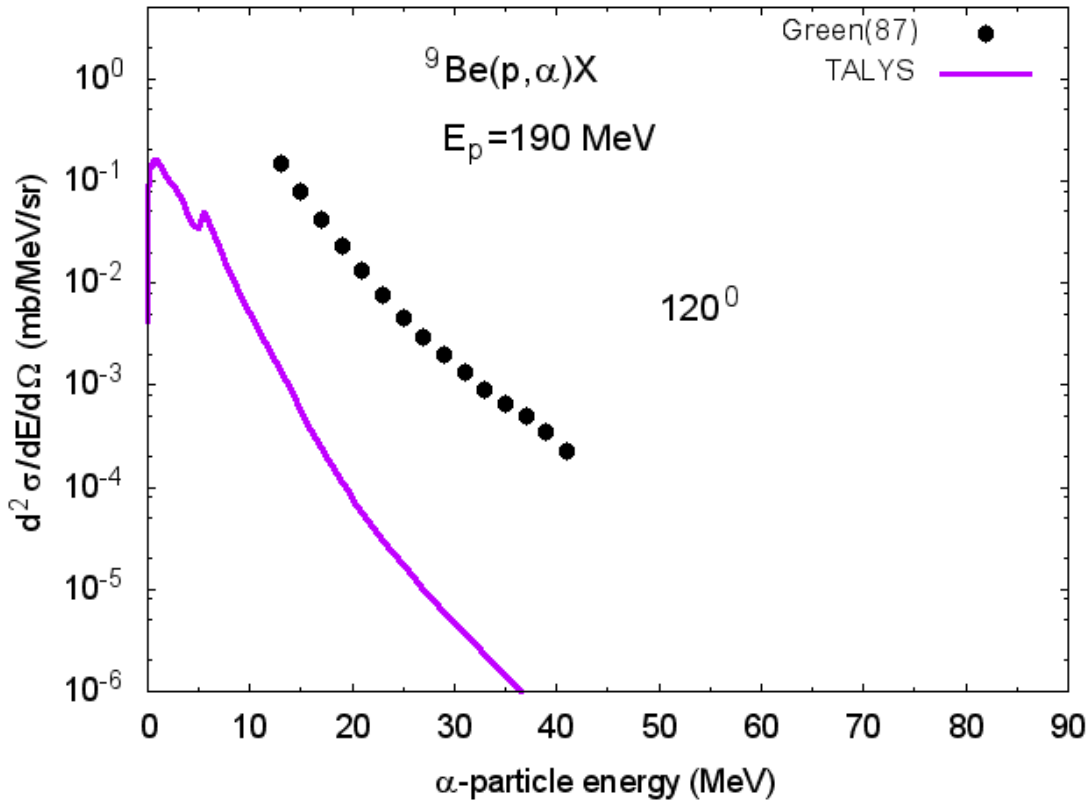
Green(87)
TALYS
^{9}Be(p,α)X
E_p=190 MeV
120^0
$d^2\sigma/dE/d\Omega$ (mb/MeV/sr)
α-particle energy (MeV)

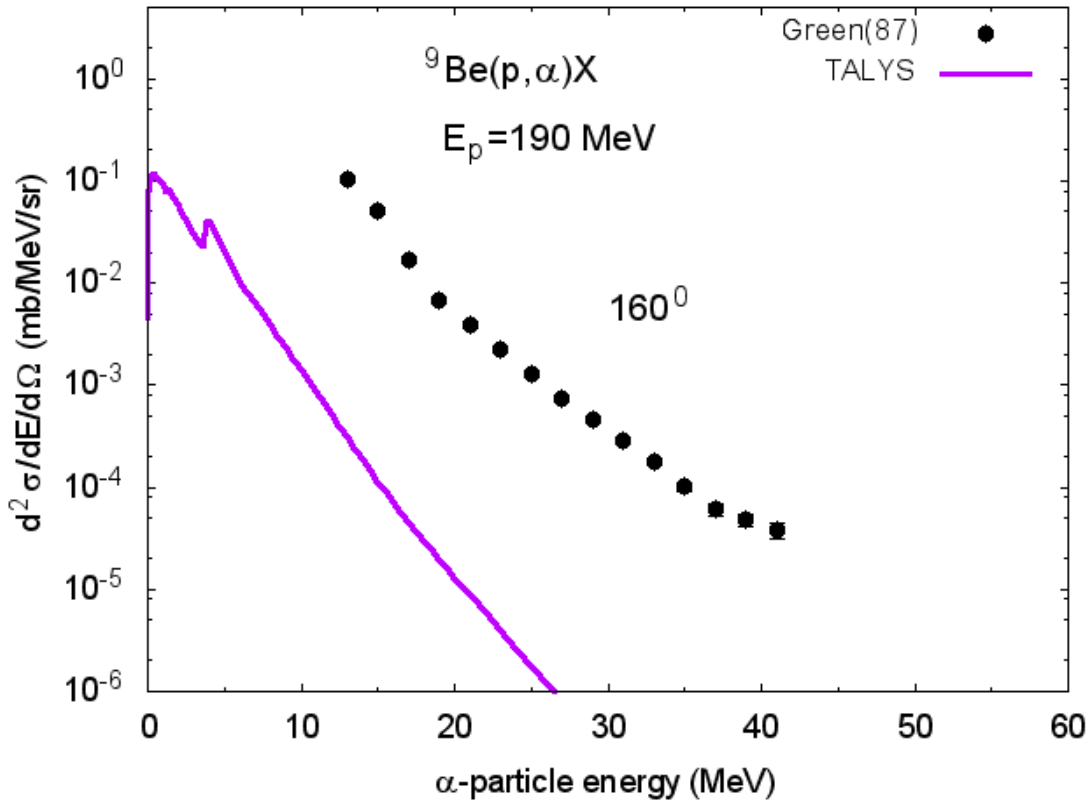
Green(87)
TALYS
^{9}Be(p,α)X
E_p=190 MeV
160^0
$d^2\sigma/dE/d\Omega$ (mb/MeV/sr)
α-particle energy (MeV)

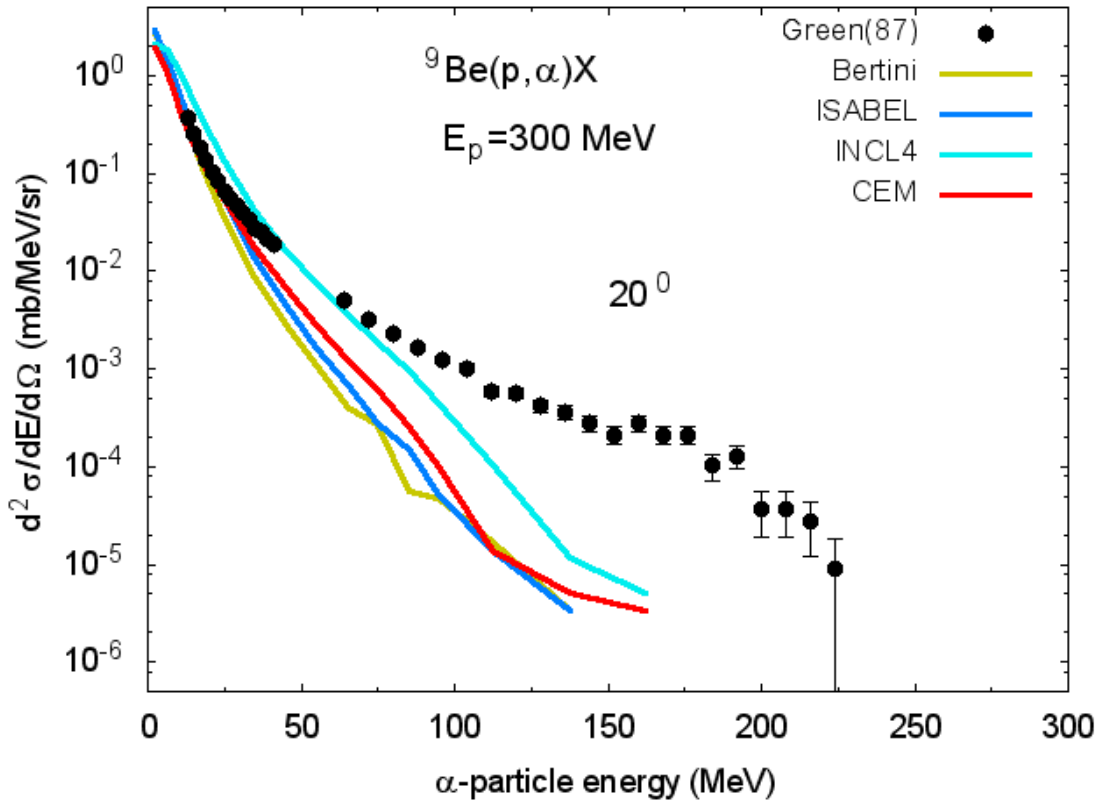
Green(87)
Bertini
ISABEL
INCL4
CEM
^{9}Be(p,α)X
E_p=300 MeV
20 ^{0}
$d^2\sigma/dE/d\Omega$ (mb/MeV/sr)
α-particle energy (MeV)

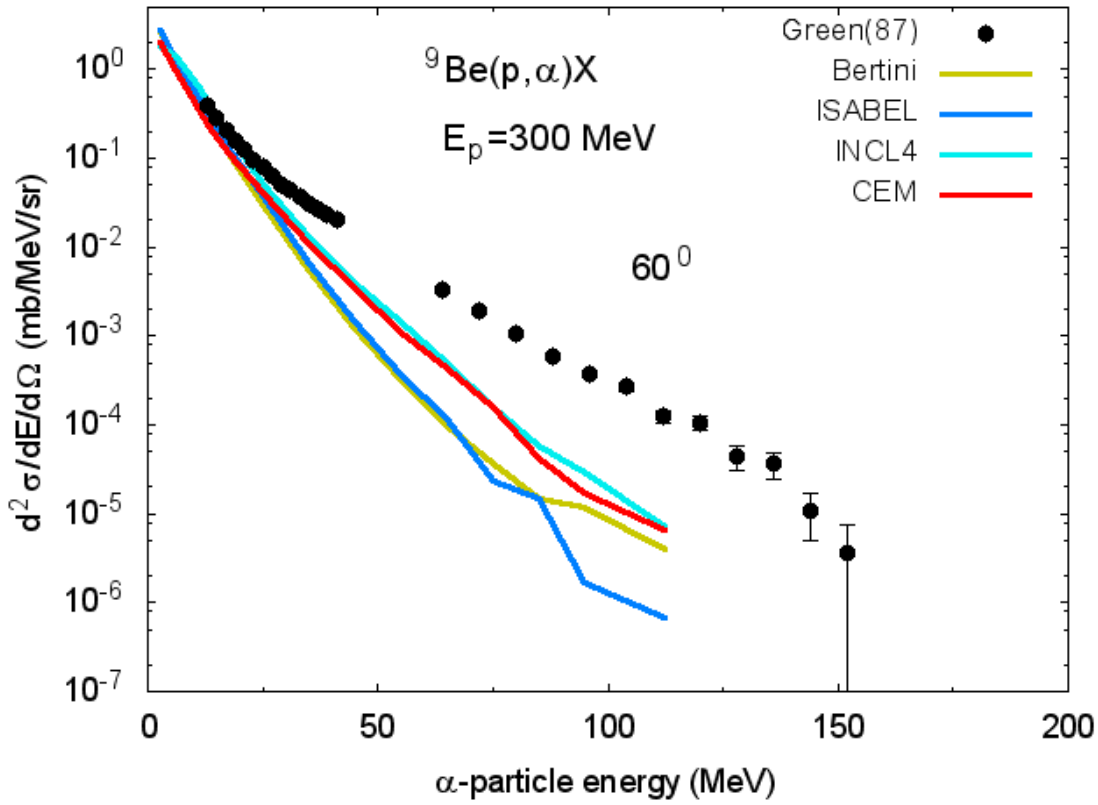
Green(87)
Bertini
ISABEL
INCL4
CEM
^{9}Be(p,α)X
E_p=300 MeV
60 ^{0}
$d^2\sigma/dE/d\Omega$ (mb/MeV/sr)
α-particle energy (MeV)

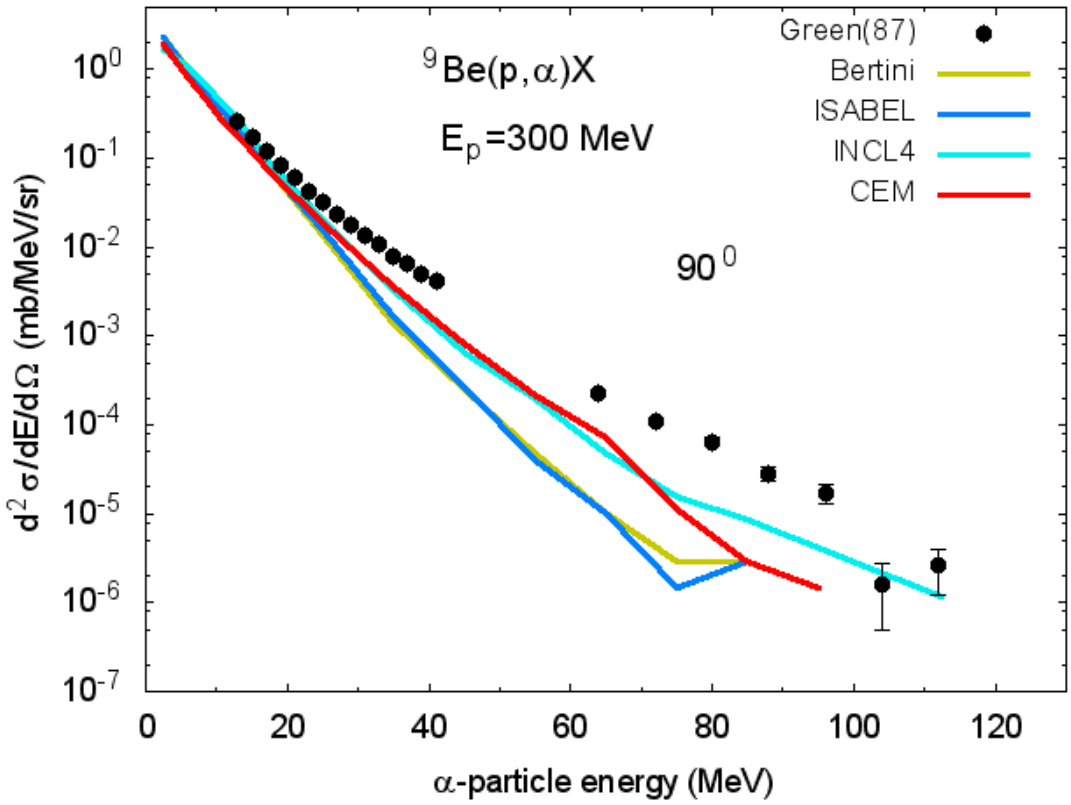
Green(87)
Bertini
ISABEL
INCL4
CEM
^{9}Be(p,α)X
E_p=300 MeV
90^0
$d^2\sigma/dE/d\Omega$ (mb/MeV/sr)
α-particle energy (MeV)

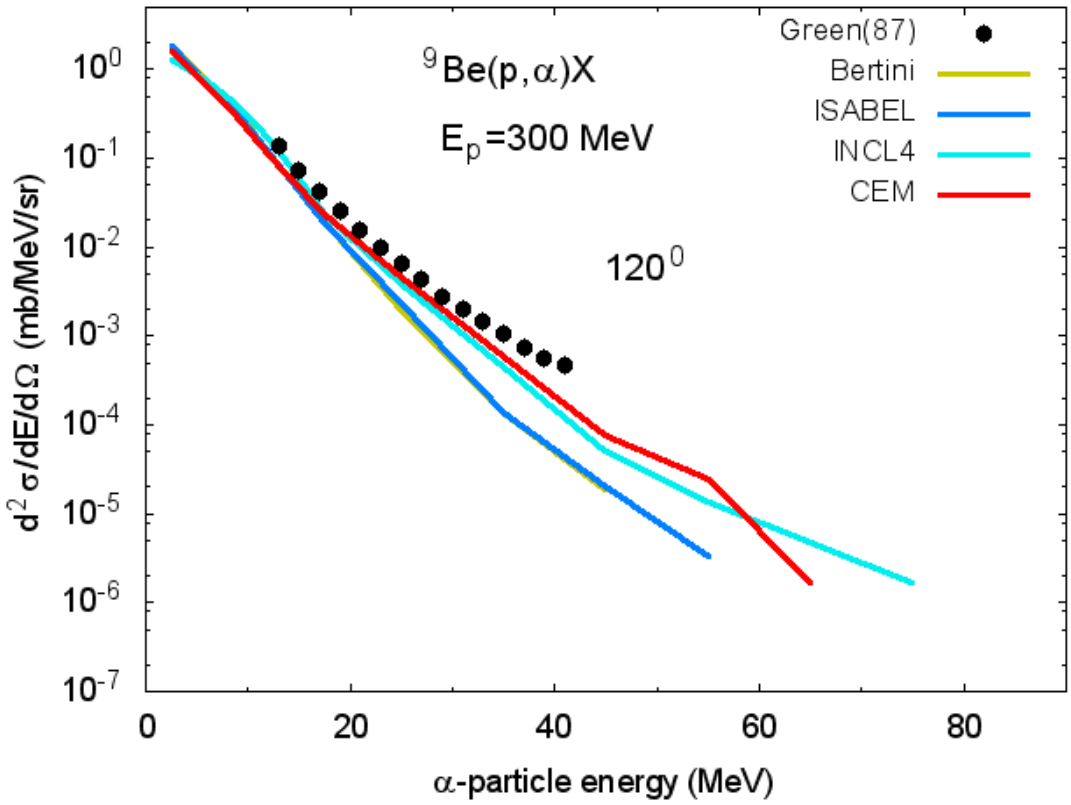
Green(87)
Bertini
ISABEL
INCL4
CEM
^{9}Be(p,α)X
E_p=300 MeV
120^0
$d^2\sigma/dE/d\Omega$ (mb/MeV/sr)
α-particle energy (MeV)

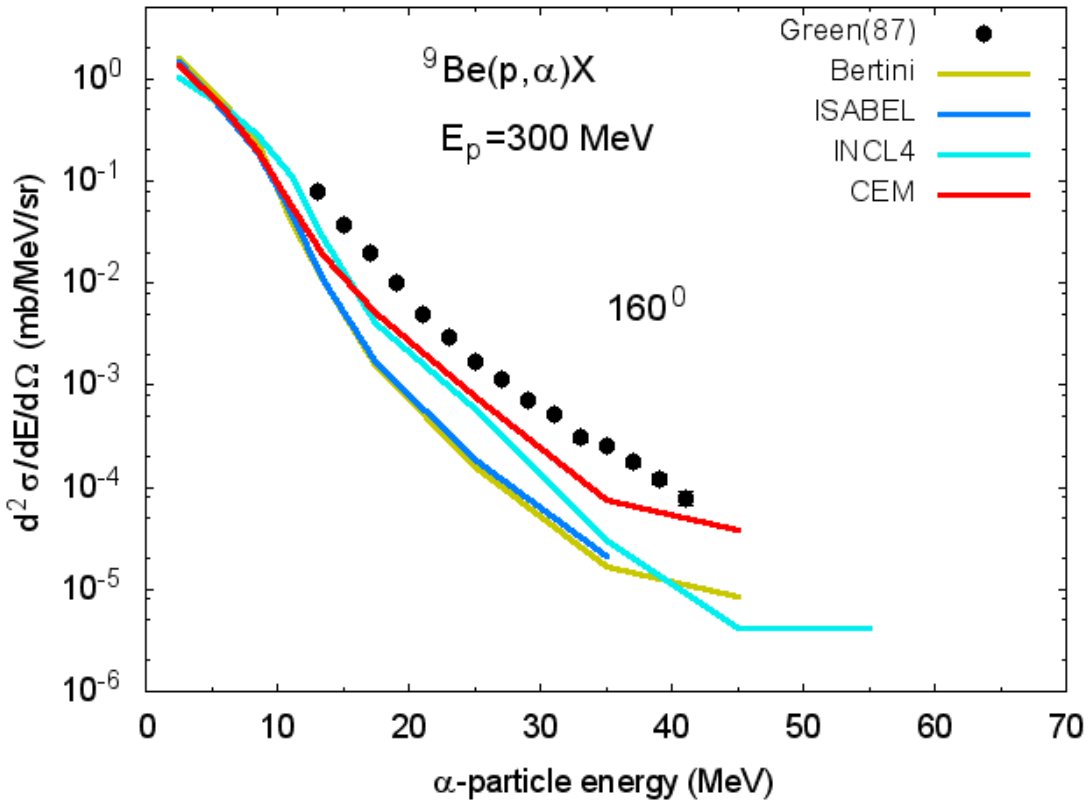
Green(87)
Bertini
ISABEL
INCL4
CEM
^{9}Be(p,α)X
E_p=300 MeV
160^{0}
$d^2\sigma/dE/d\Omega$ (mb/MeV/sr)
α-particle energy (MeV)

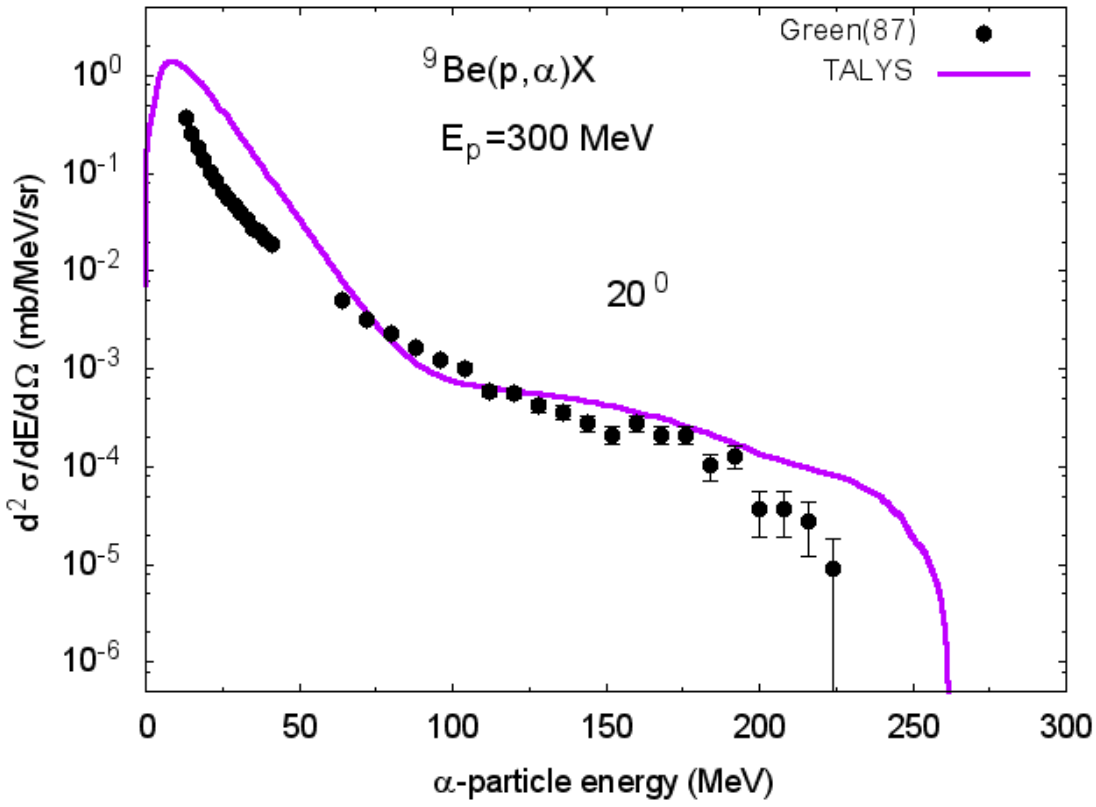
Green(87)
TALYS
^{9}Be(p,α)X
E_p=300 MeV
20^{0}
$d^2\sigma/dE/d\Omega$ (mb/MeV/sr)
α-particle energy (MeV)

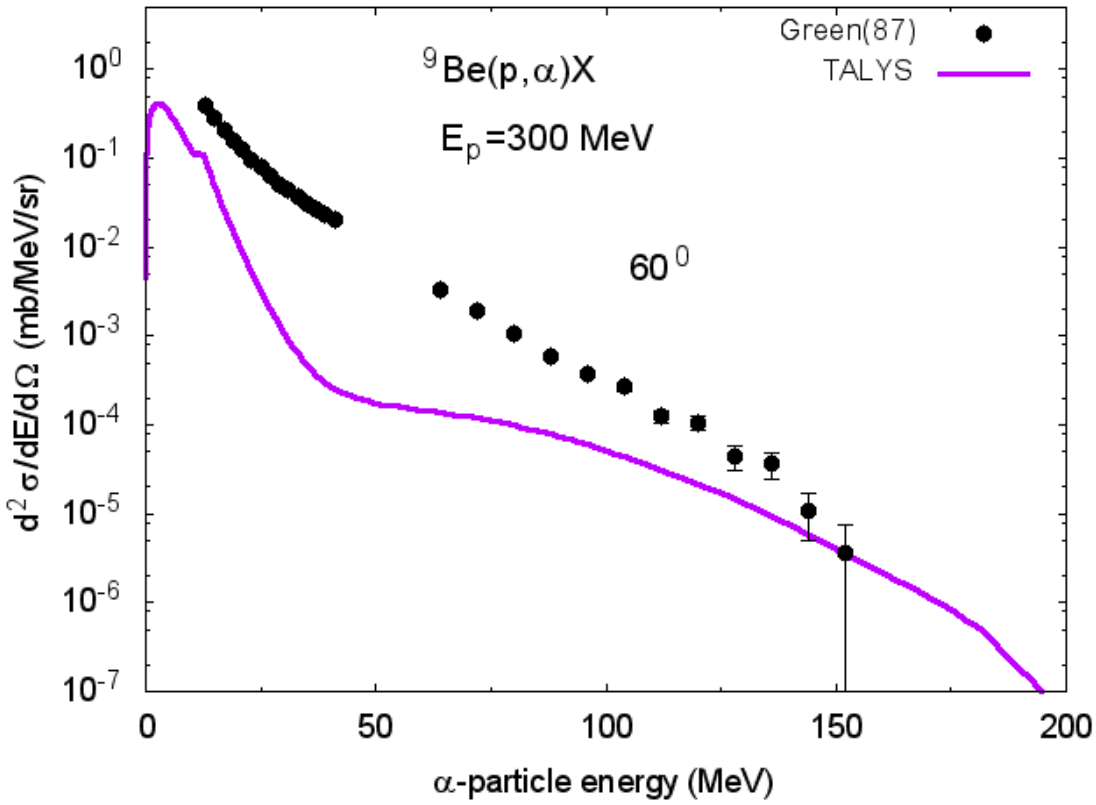
Green(87)
TALYS
^{9}Be(p,α)X
E_p=300 MeV
60^0
d^{2}σ/dE/dΩ (mb/MeV/sr)
α-particle energy (MeV)
10^0
10^{-1}
10^{-2}
10^{-3}
10^{-4}
10^{-5}
10^{-6}
10^{-7}
0
50
100
150
200

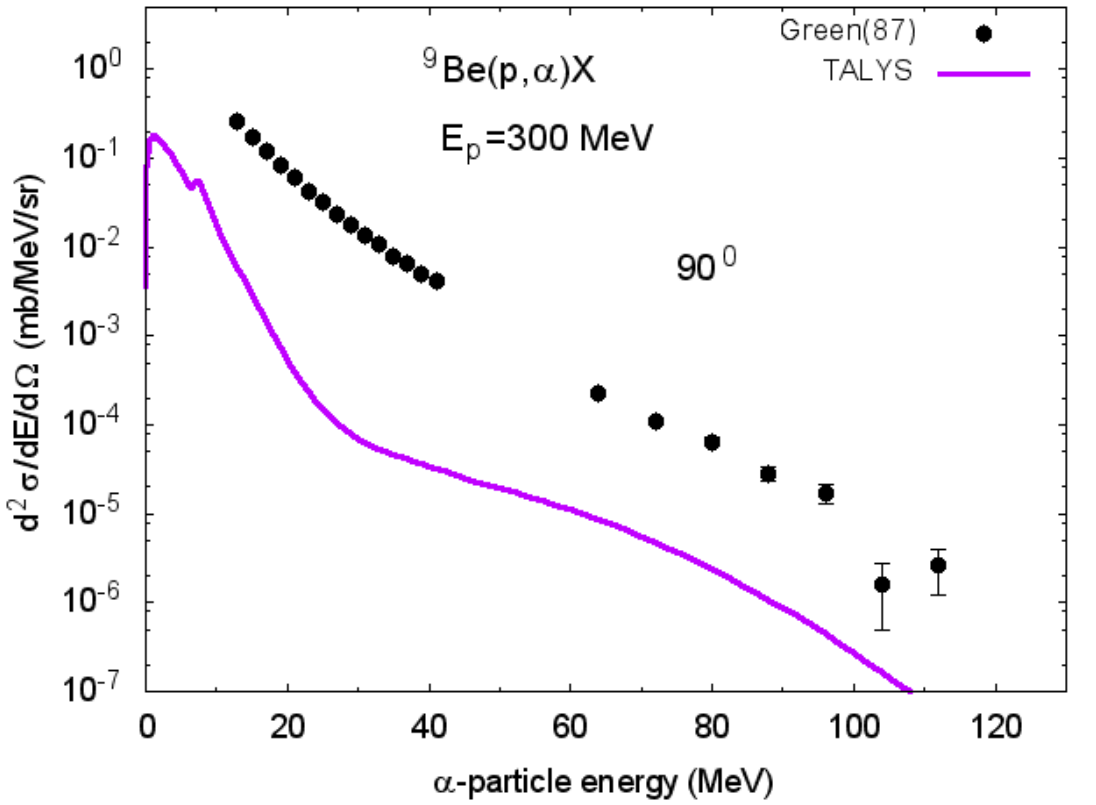
Green(87)
TALYS
^{9}Be(p,α)X
E_p=300 MeV
90^0
d^{2}σ/dE/dΩ (mb/MeV/sr)
α-particle energy (MeV)
10^0
10^{-1}
10^{-2}
10^{-3}
10^{-4}
10^{-5}
10^{-6}
10^{-7}
0
20
40
60
80
100
120

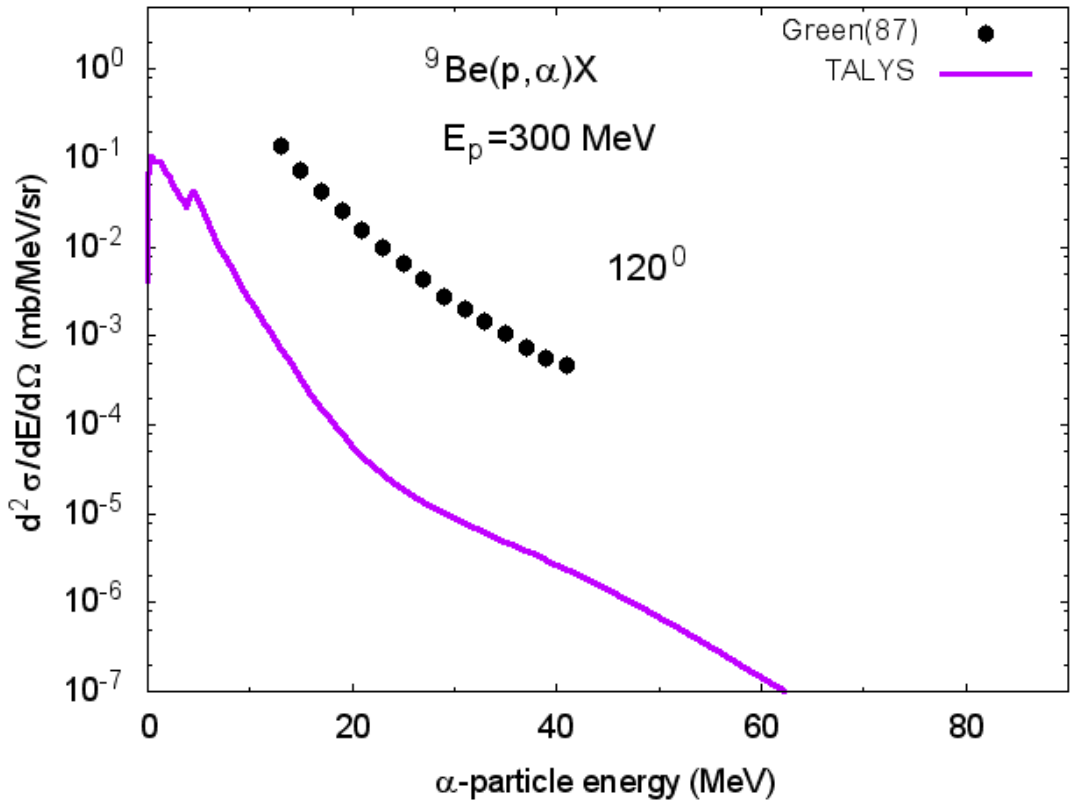
Green(87)
TALYS
^{9}Be(p,α)X
E_p=300 MeV
120^0
d^{2}σ/dE/dΩ (mb/MeV/sr)
α-particle energy (MeV)

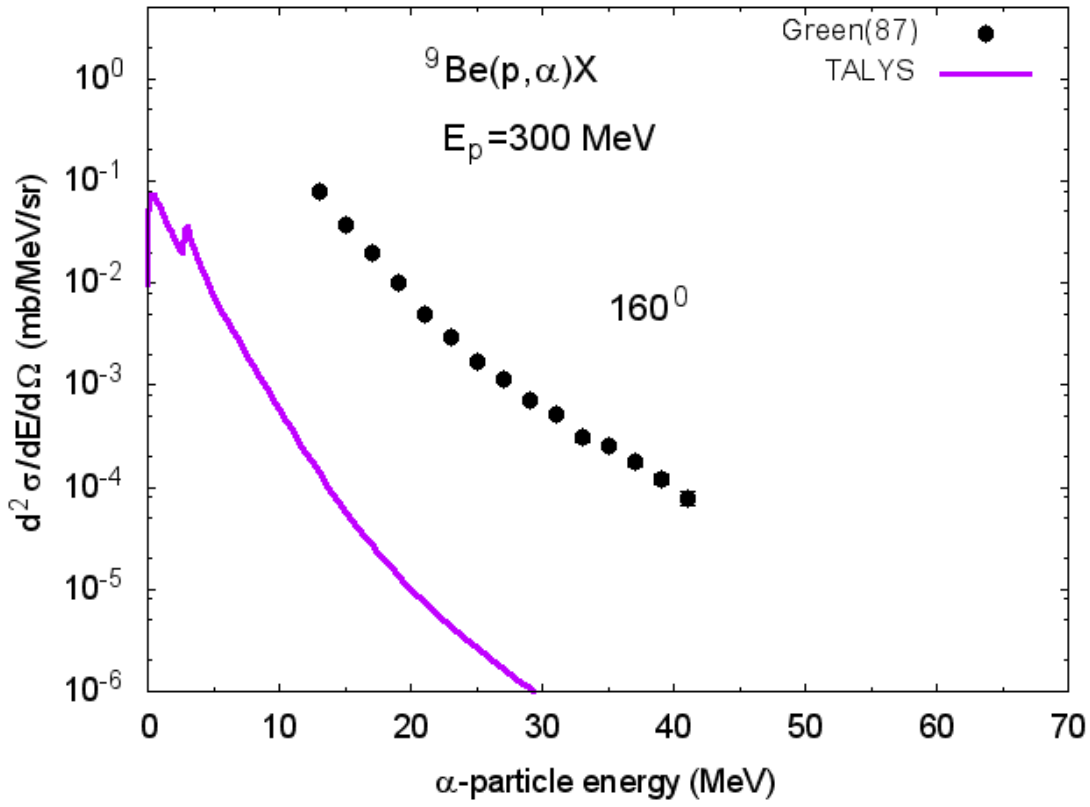
Green(87)
TALYS
^{9}Be(p,α)X
E_p=300 MeV
160^0
d^{2}σ/dE/dΩ (mb/MeV/sr)
α-particle energy (MeV)

Comparison of particle energy distributions in p+^{9}Be reactions calculated using Bertini, ISABEL, CEM03, and INCL4 models and models implemented in the TALYS code

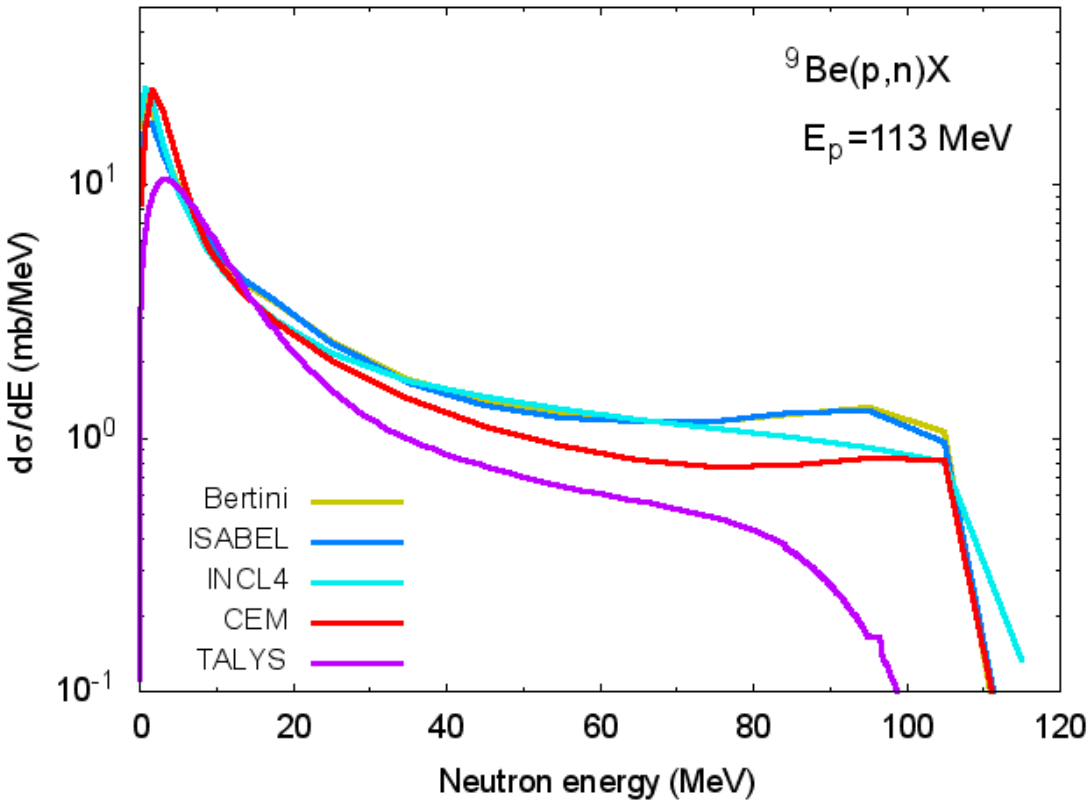
^{9}Be(p,n)X
E_p=113 MeV
dσ/dE (mb/MeV)
Neutron energy (MeV)
Bertini
ISABEL
INCL4
CEM
TALYS
10^{1}
10^{0}
10^{-1}
0
20
40
60
80
100
120

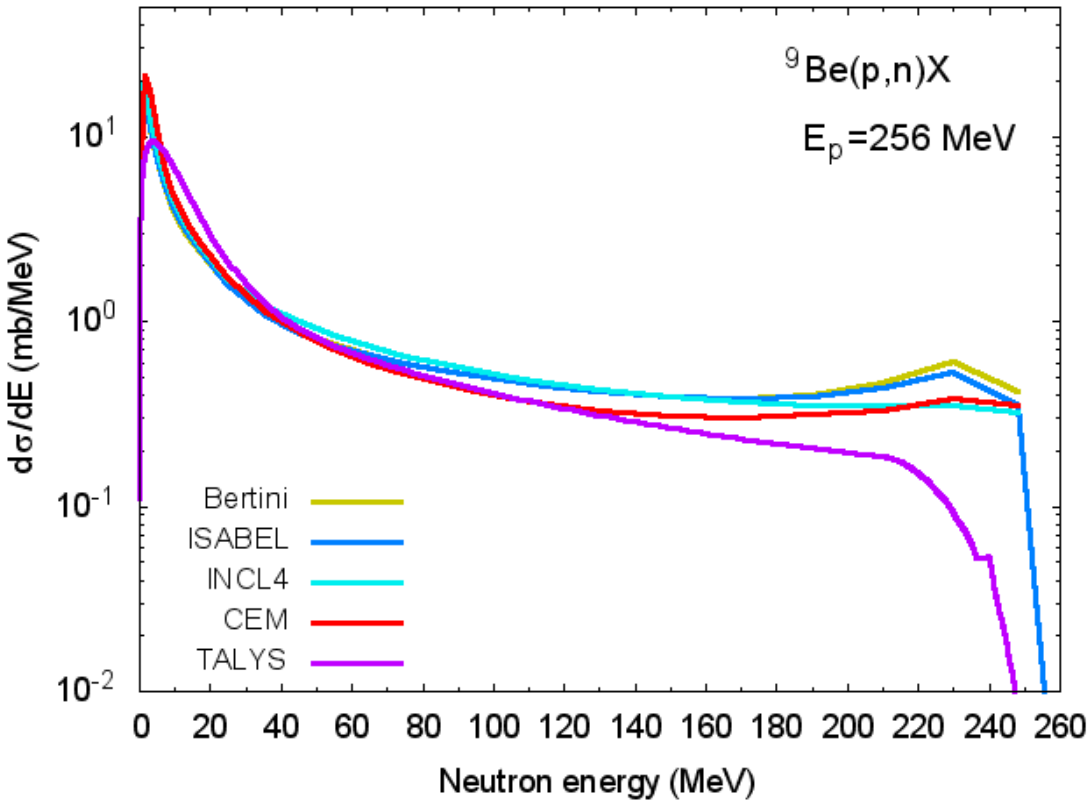
^{9}Be(p,n)X
E_p=256 MeV
dσ/dE (mb/MeV)
Neutron energy (MeV)
Bertini
ISABEL
INCL4
CEM
TALYS
10^{1}
10^{0}
10^{-1}
10^{-2}
0
20
40
60
80
100
120
140
160
180
200
220
240
260

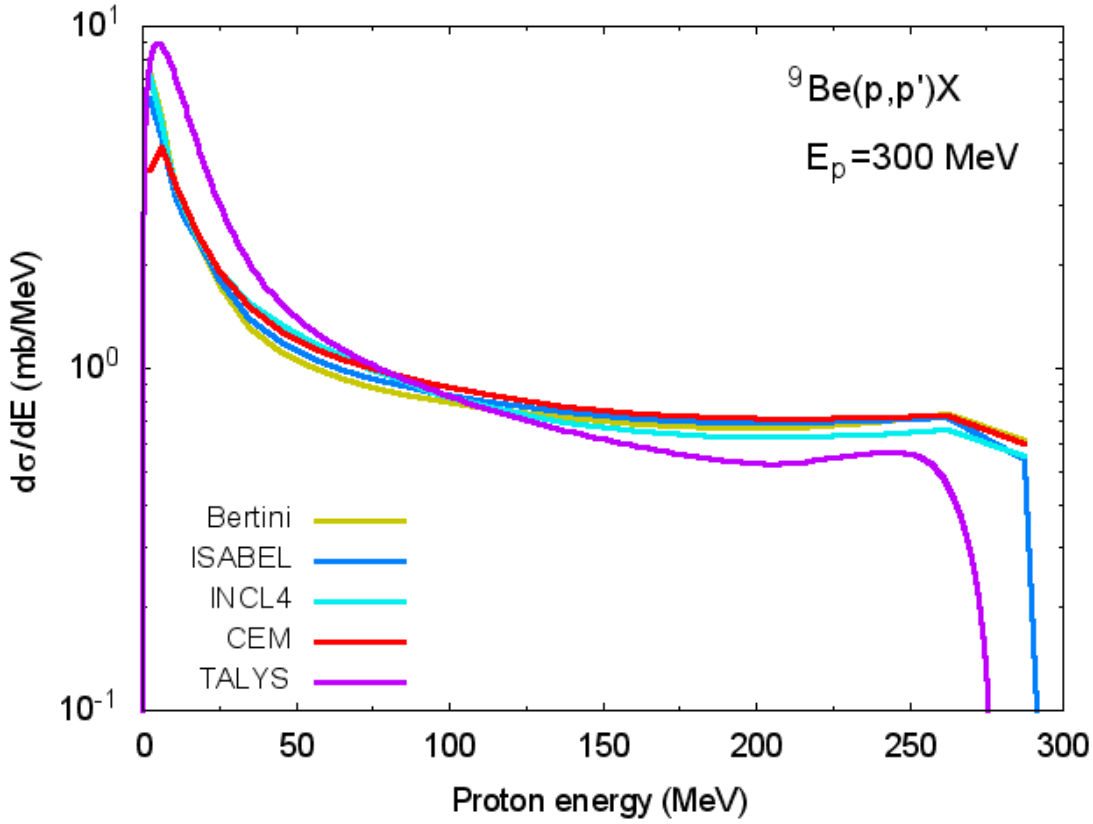
^{9}Be(p,p')X
E_p=300 MeV
Bertini
ISABEL
INCL4
CEM
TALYS
dσ/dE (mb/MeV)
Proton energy (MeV)
10^{1}
10^{0}
10^{-1}
0
50
100
150
200
250
300

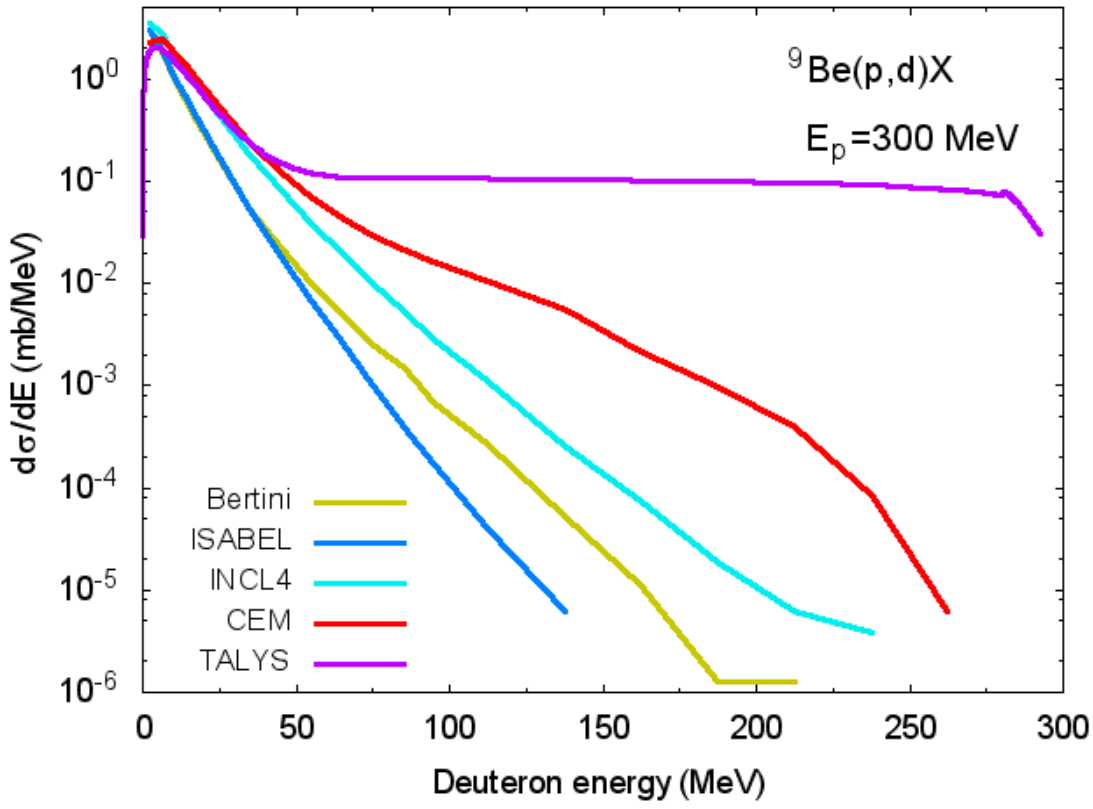
^{9}Be(p,d)X
E_p=300 MeV
Bertini
ISABEL
INCL4
CEM
TALYS
dσ/dE (mb/MeV)
Deuteron energy (MeV)
10^{0}
10^{-1}
10^{-2}
10^{-3}
10^{-4}
10^{-5}
10^{-6}
0
50
100
150
200
250
300

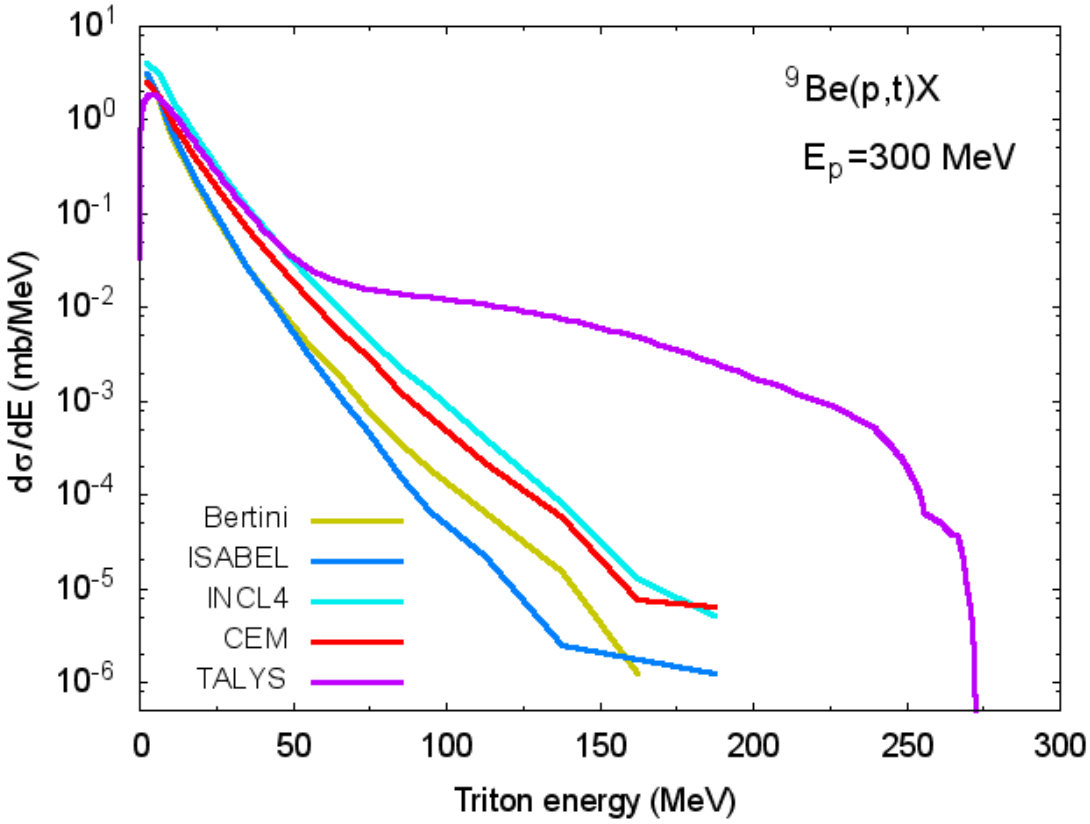
^{9}Be(p,t)X
E_p=300 MeV
Bertini
ISABEL
INCL4
CEM
TALYS
dσ/dE (mb/MeV)
Triton energy (MeV)
10^{1}
10^{0}
10^{-1}
10^{-2}
10^{-3}
10^{-4}
10^{-5}
10^{-6}
0
50
100
150
200
250
300

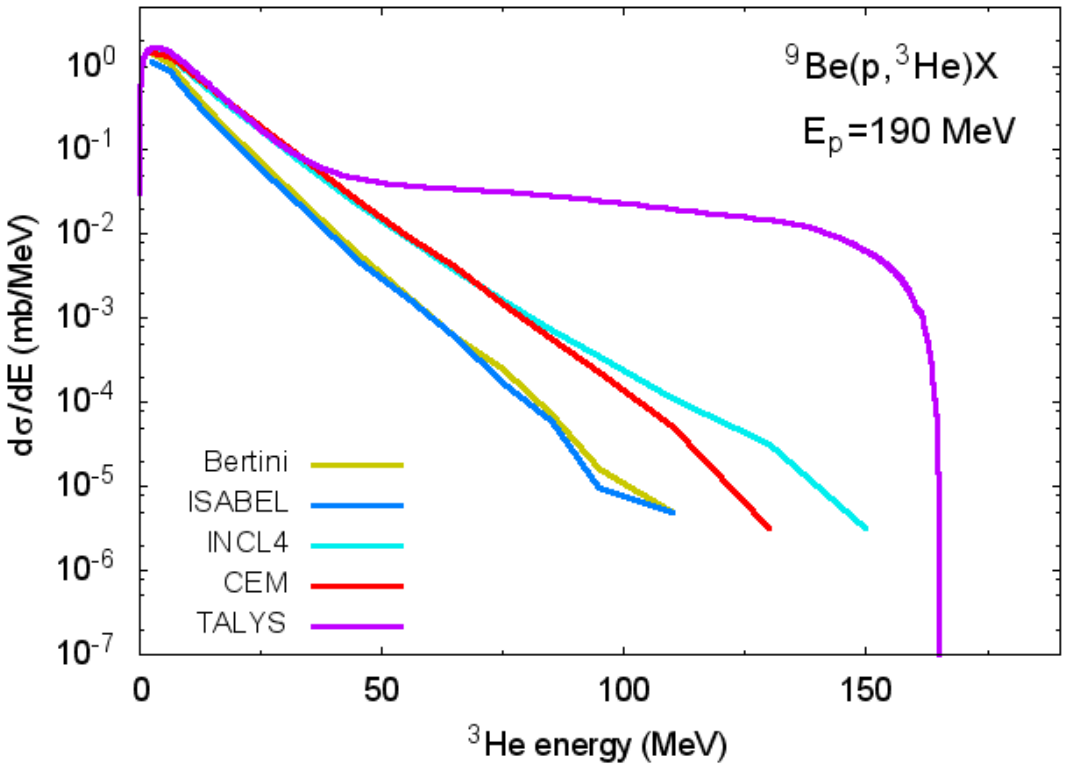
^{9}Be(p,^{3}He)X
E_p=190 MeV
Bertini
ISABEL
INCL4
CEM
TALYS
dσ/dE (mb/MeV)
^{3}He energy (MeV)
10^{0}
10^{-1}
10^{-2}
10^{-3}
10^{-4}
10^{-5}
10^{-6}
10^{-7}
0
50
100
150

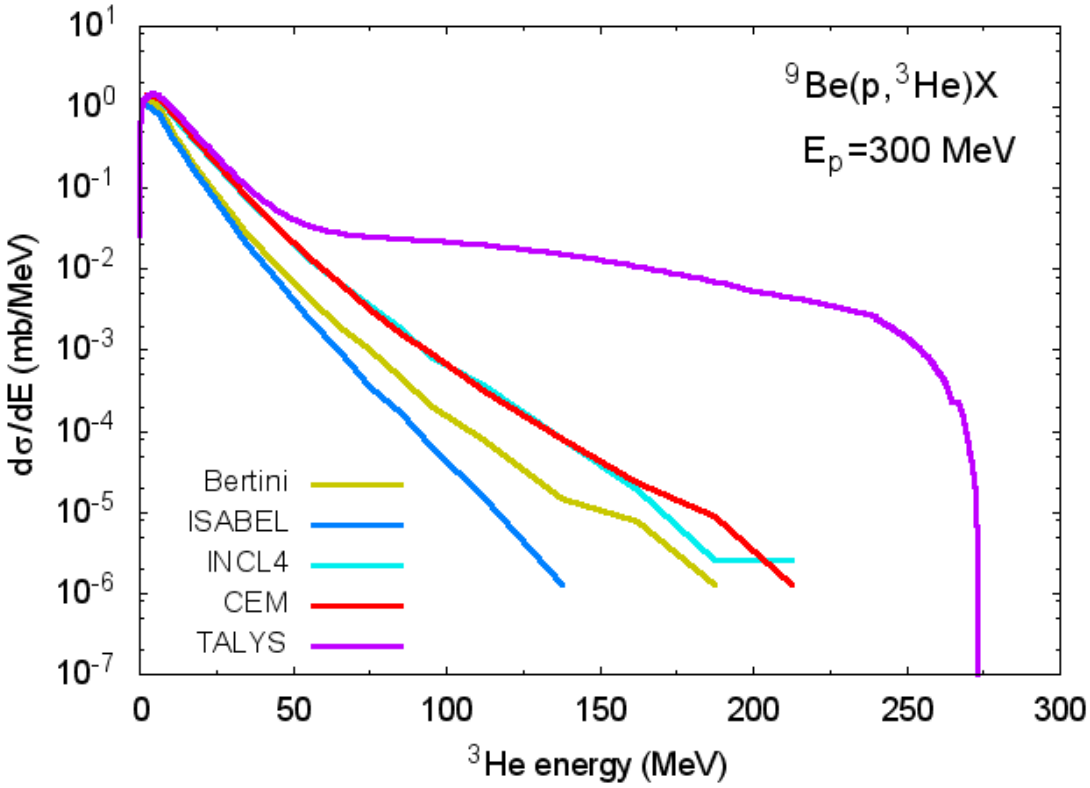
^{9}Be(p,^{3}He)X
E_p=300 MeV
Bertini
ISABEL
INCL4
CEM
TALYS
dσ/dE (mb/MeV)
^{3}He energy (MeV)

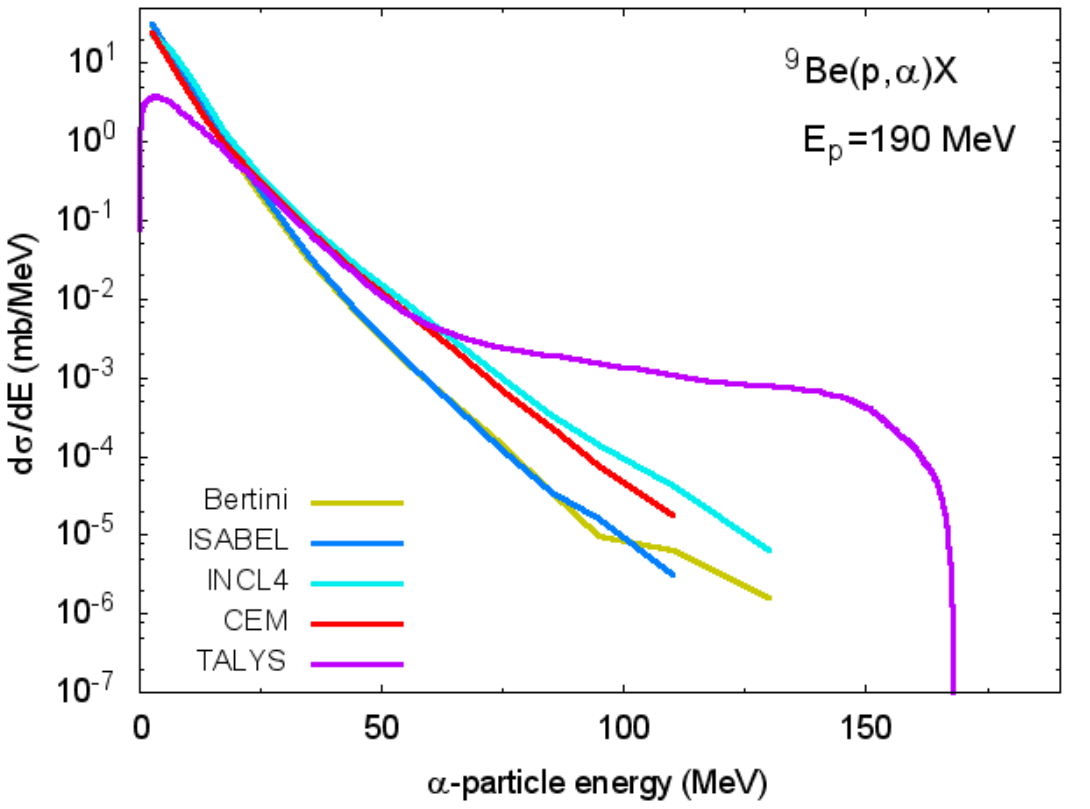
^{9}Be(p,α)X
E_p=190 MeV
Bertini
ISABEL
INCL4
CEM
TALYS
dσ/dE (mb/MeV)
α-particle energy (MeV)

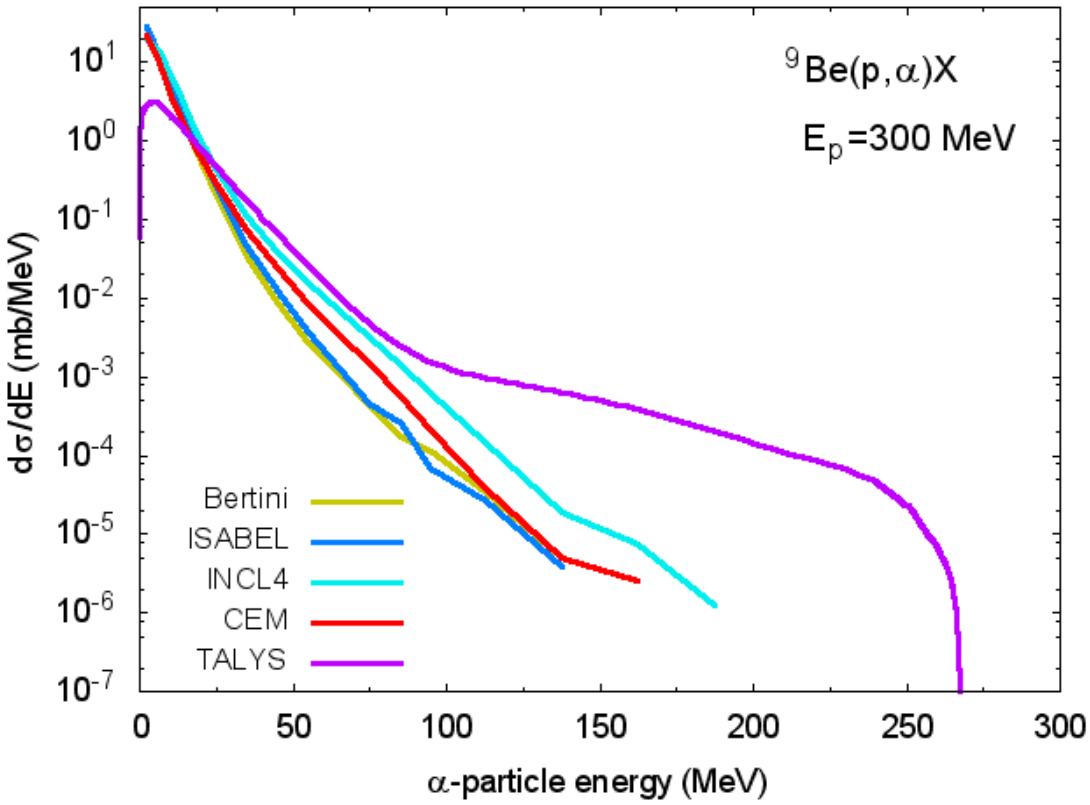
^{9}Be(p,α)X
E_p=300 MeV
dσ/dE (mb/MeV)
α-particle energy (MeV)
Bertini
ISABEL
INCL4
CEM
TALYS
10^{1}
10^{0}
10^{-1}
10^{-2}
10^{-3}
10^{-4}
10^{-5}
10^{-6}
10^{-7}
0
50
100
150
200
250
300

Comparison of recoil energy distributions in p+^{9}Be reactions calculated using Bertini, ISABEL, CEM03, and INCL4 models and models implemented in the TALYS code

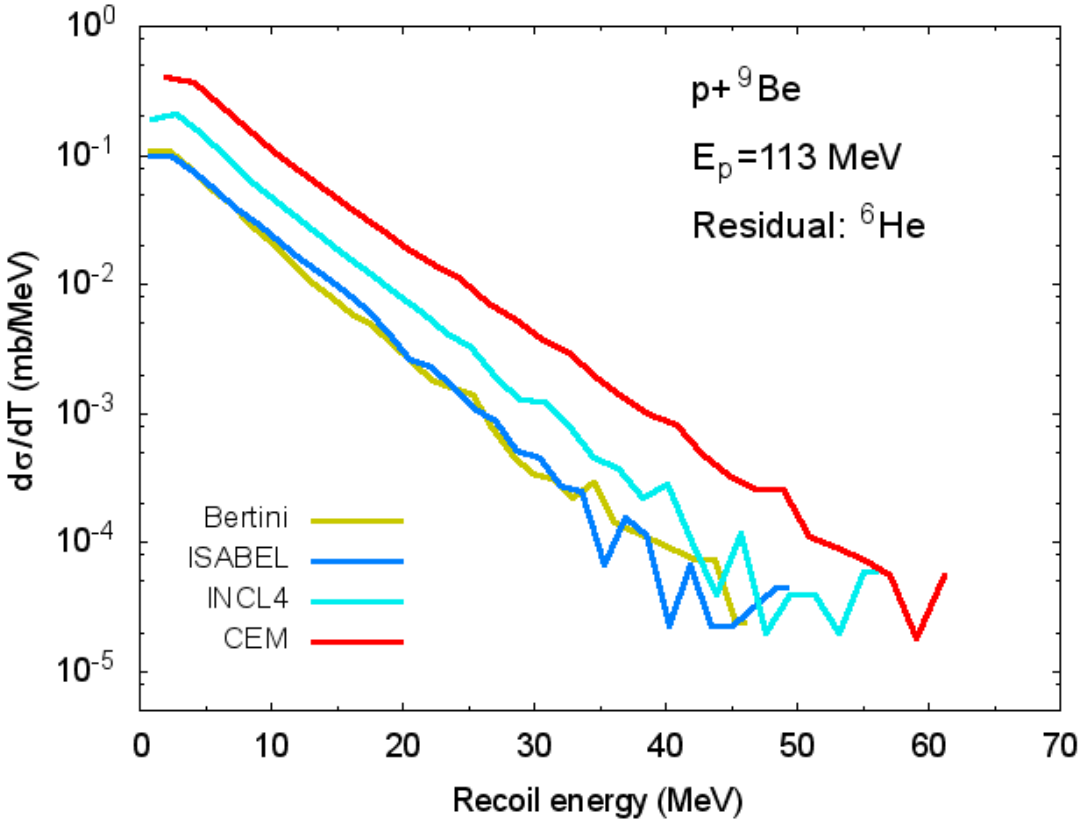
p+ 9Be
Ep=113 MeV
Residual: 6He
Bertini
ISABEL
INCL4
CEM
dσ/dT (mb/MeV)
Recoil energy (MeV)

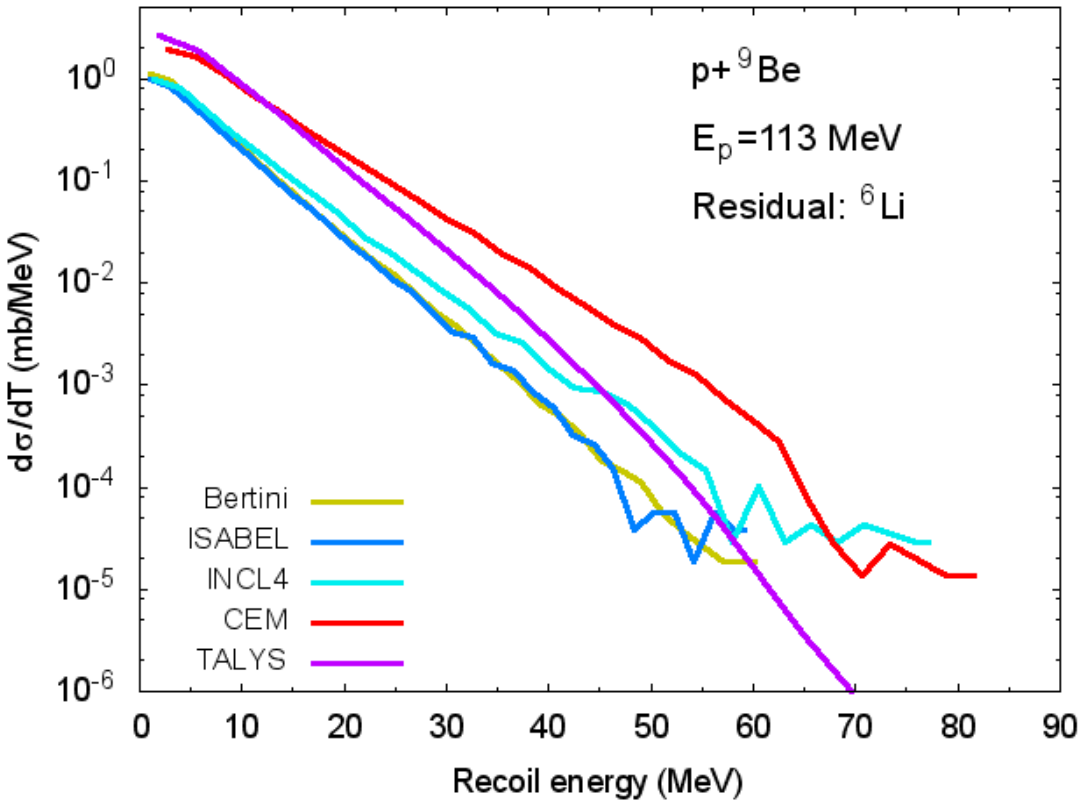
p+ 9Be
Ep=113 MeV
Residual: 6Li
Bertini
ISABEL
INCL4
CEM
TALYS
dσ/dT (mb/MeV)
Recoil energy (MeV)

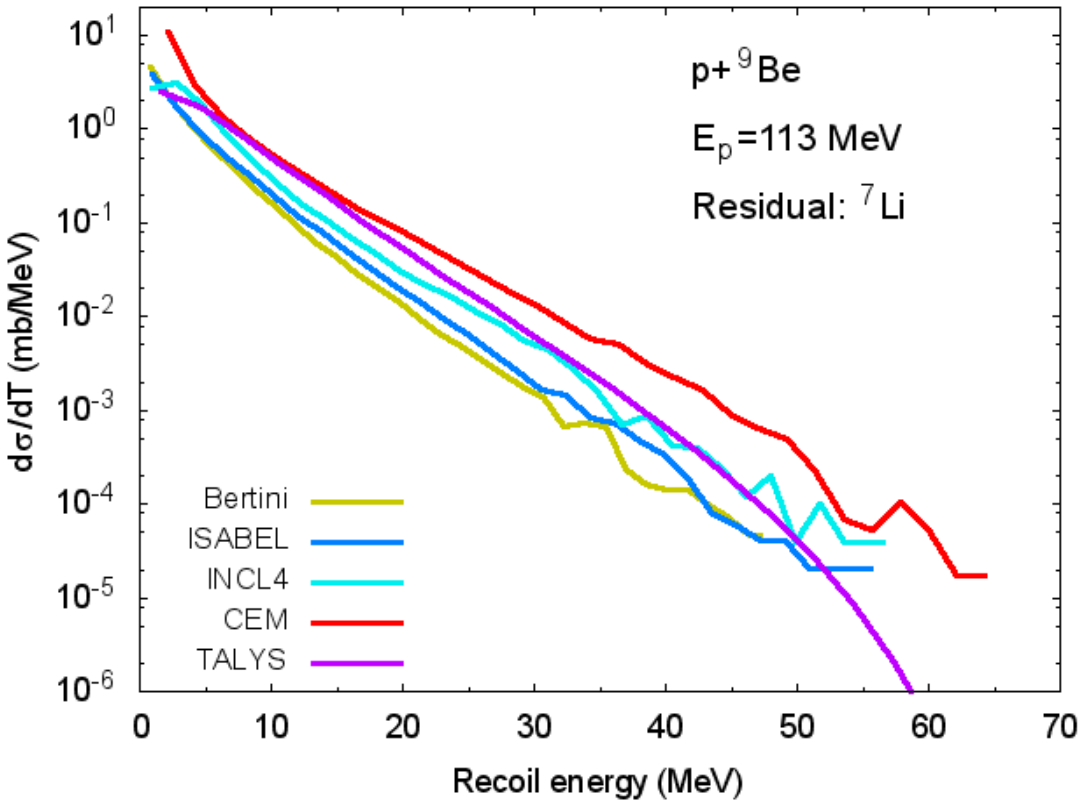
p+ 9Be
Ep=113 MeV
Residual: 7Li
Bertini
ISABEL
INCL4
CEM
TALYS
dσ/dT (mb/MeV)
Recoil energy (MeV)

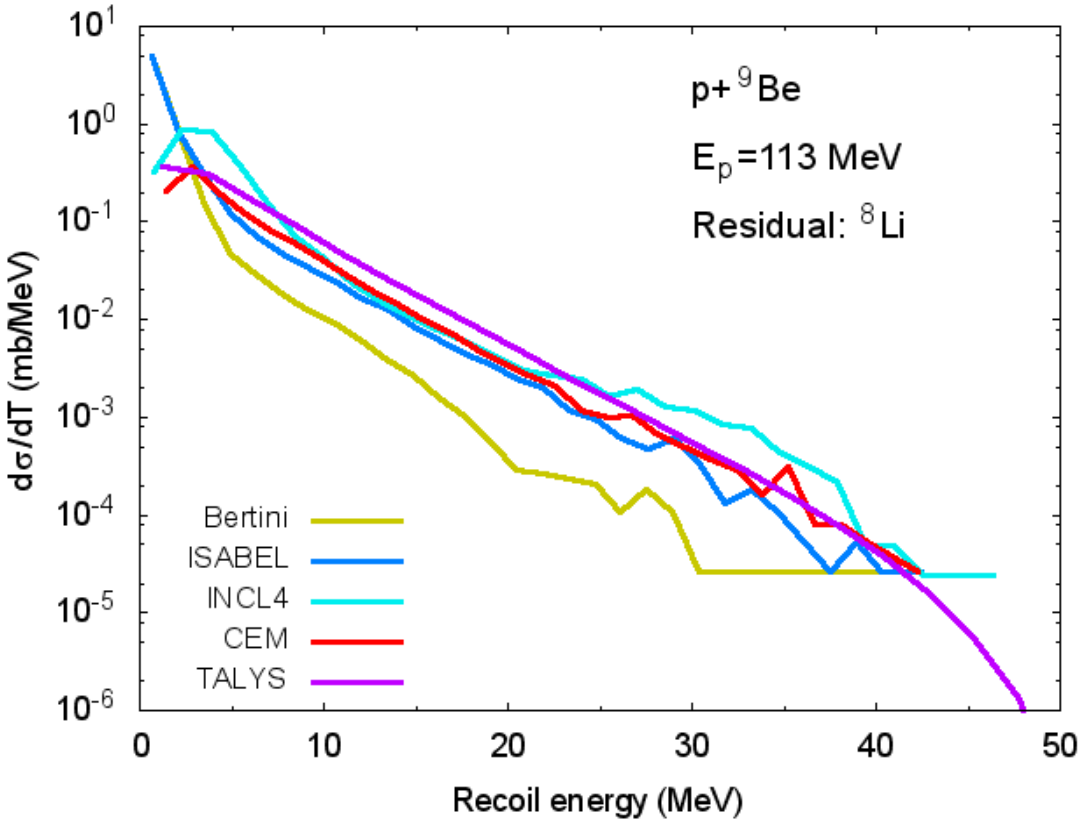
p+ 9Be
Ep=113 MeV
Residual: 8Li
Bertini
ISABEL
INCL4
CEM
TALYS
dσ/dT (mb/MeV)
Recoil energy (MeV)

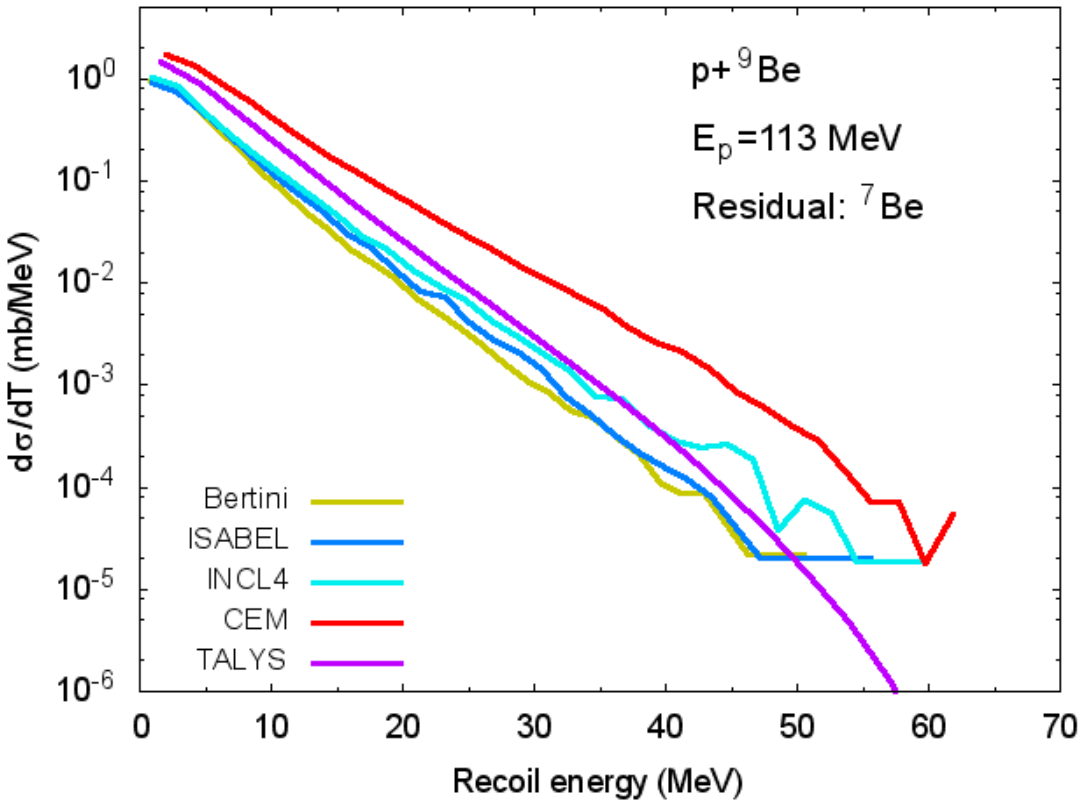
p+ 9Be
Ep=113 MeV
Residual: 7Be
Bertini
ISABEL
INCL4
CEM
TALYS
dσ/dT (mb/MeV)
Recoil energy (MeV)

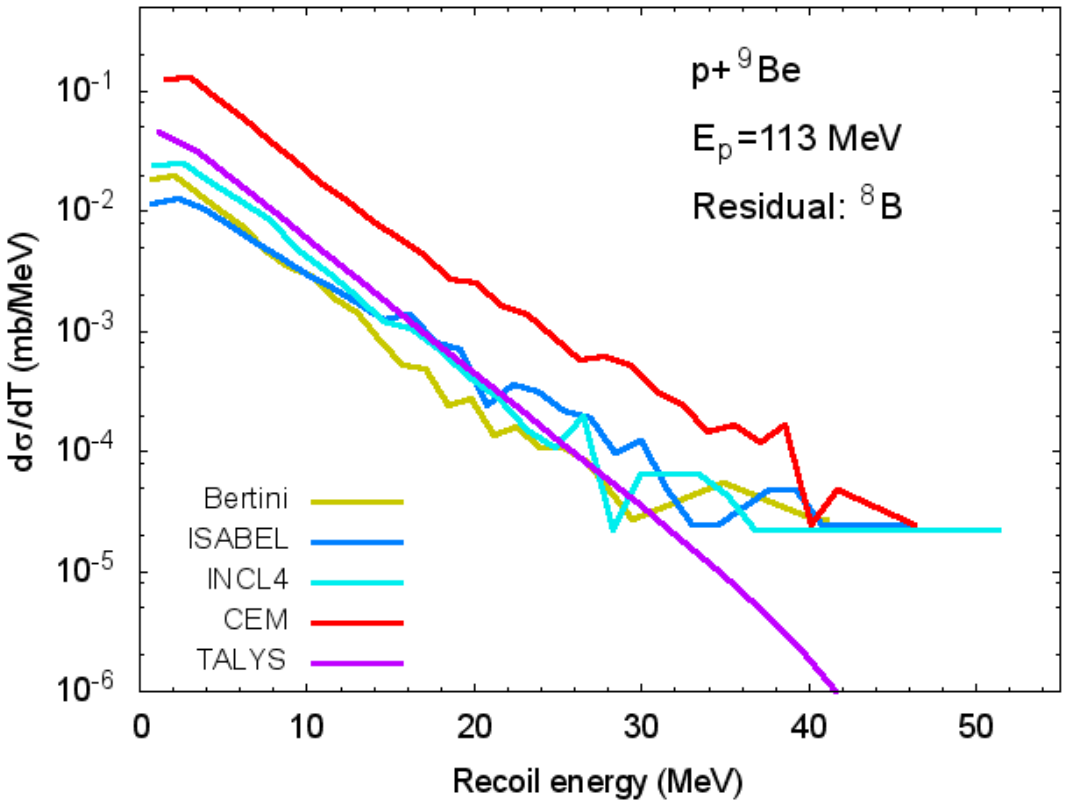
p+ 9Be
Ep=113 MeV
Residual: 8B
Bertini
ISABEL
INCL4
CEM
TALYS
dσ/dT (mb/MeV)
Recoil energy (MeV)

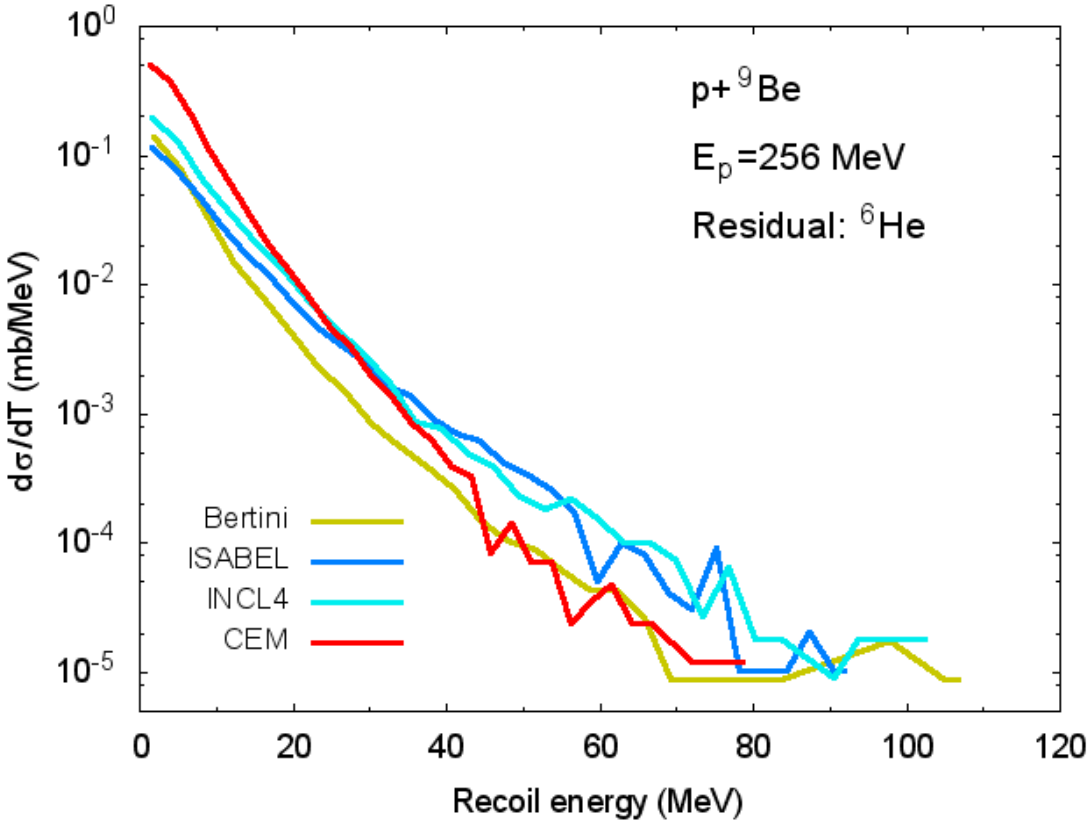
p+ 9Be
Ep=256 MeV
Residual: 6He
Bertini
ISABEL
INCL4
CEM
dσ/dT (mb/MeV)
Recoil energy (MeV)

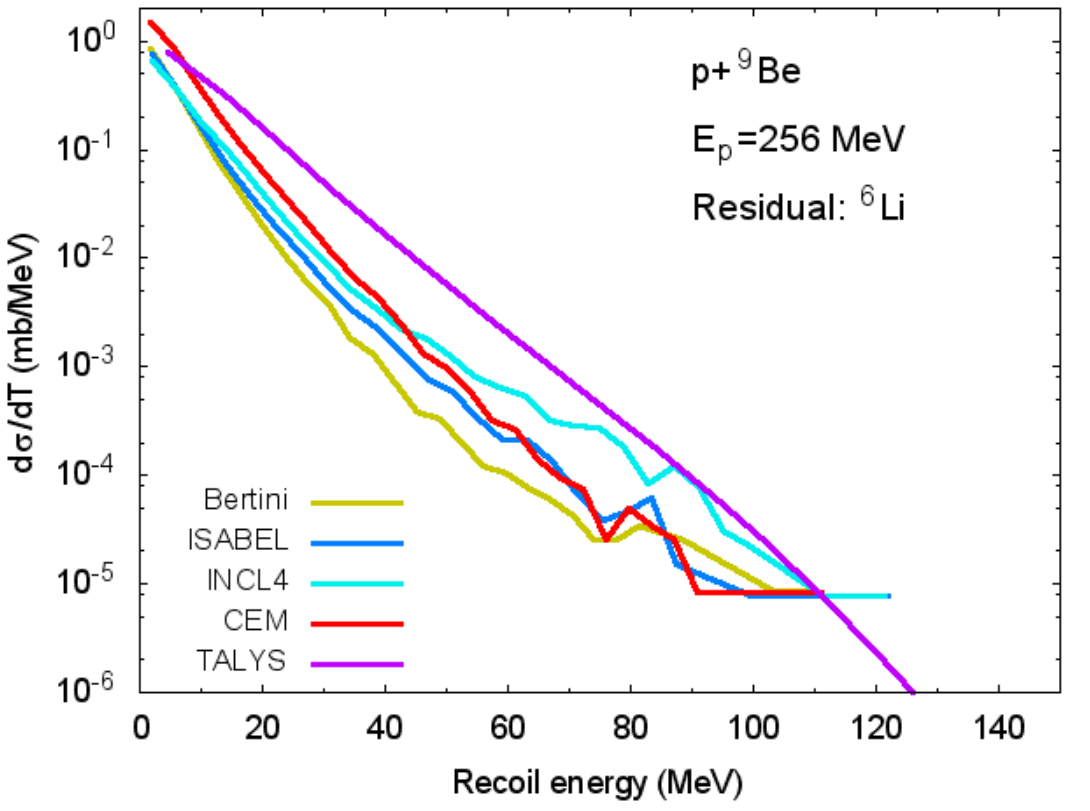
p+ 9Be
Ep=256 MeV
Residual: 6Li
Bertini
ISABEL
INCL4
CEM
TALYS
dσ/dT (mb/MeV)
Recoil energy (MeV)

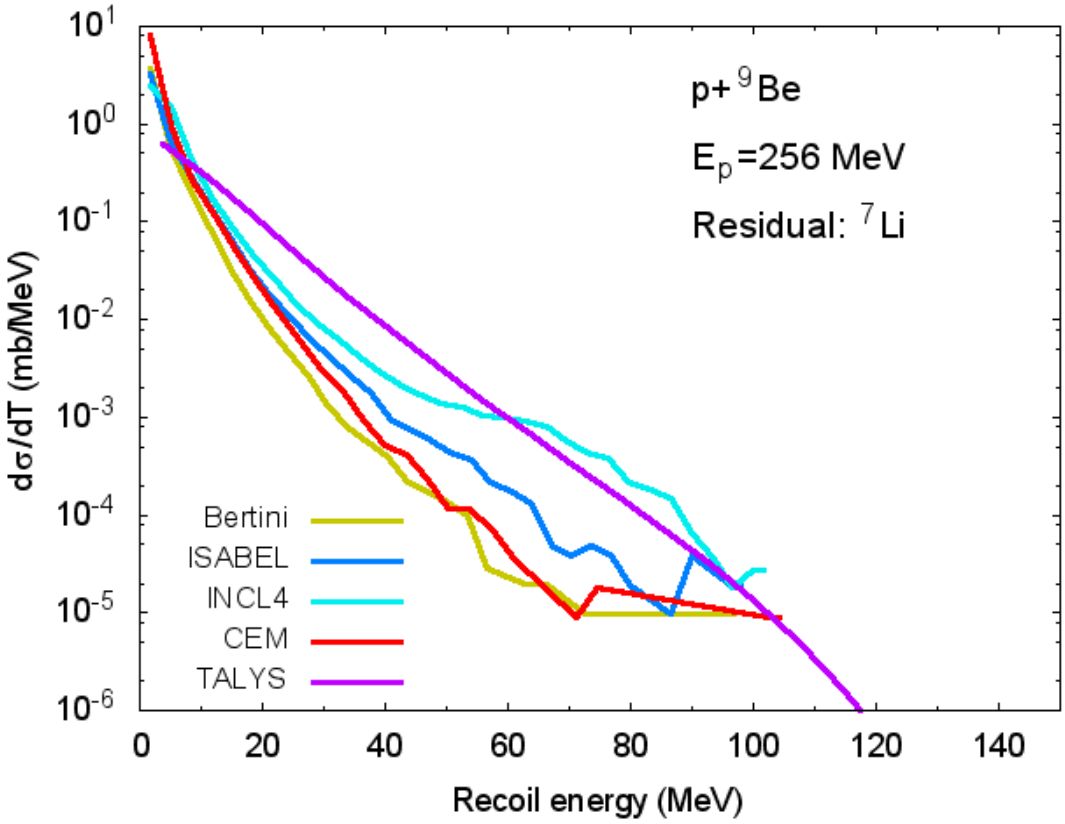
p+ 9Be
Ep=256 MeV
Residual: 7Li
Bertini
ISABEL
INCL4
CEM
TALYS
dσ/dT (mb/MeV)
Recoil energy (MeV)

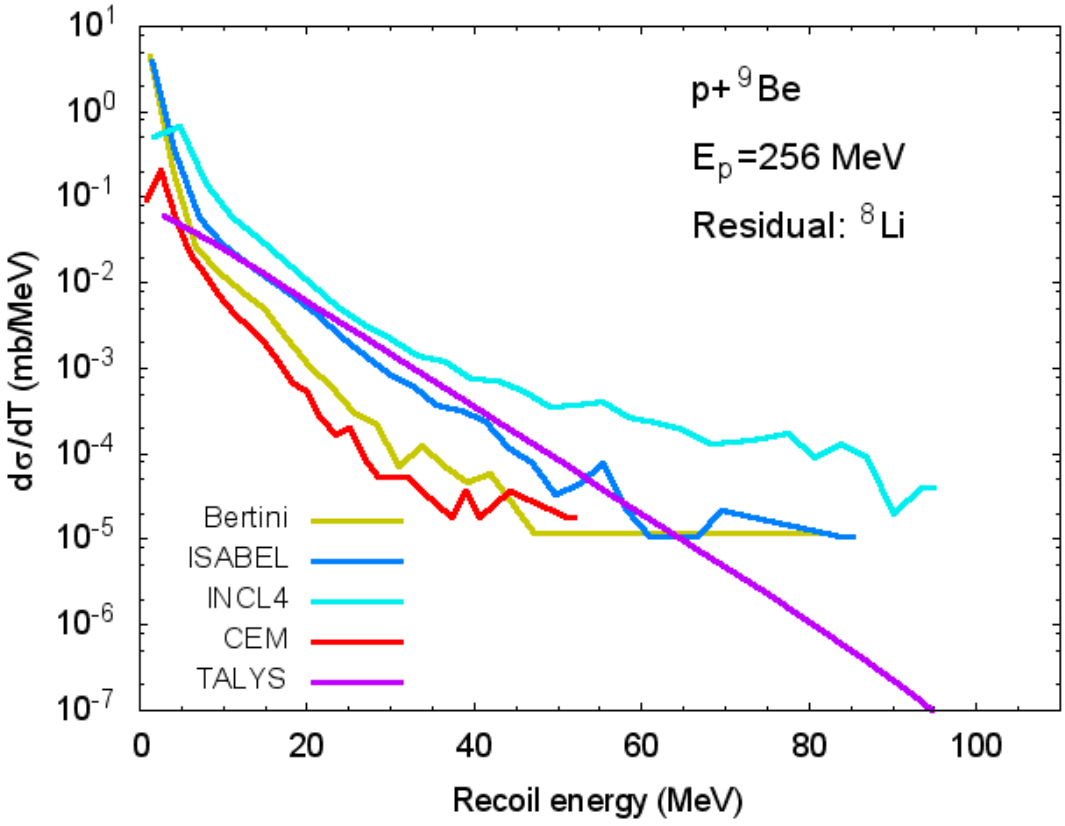
p+ 9Be
Ep=256 MeV
Residual: 8Li
Bertini
ISABEL
INCL4
CEM
TALYS
dσ/dT (mb/MeV)
Recoil energy (MeV)

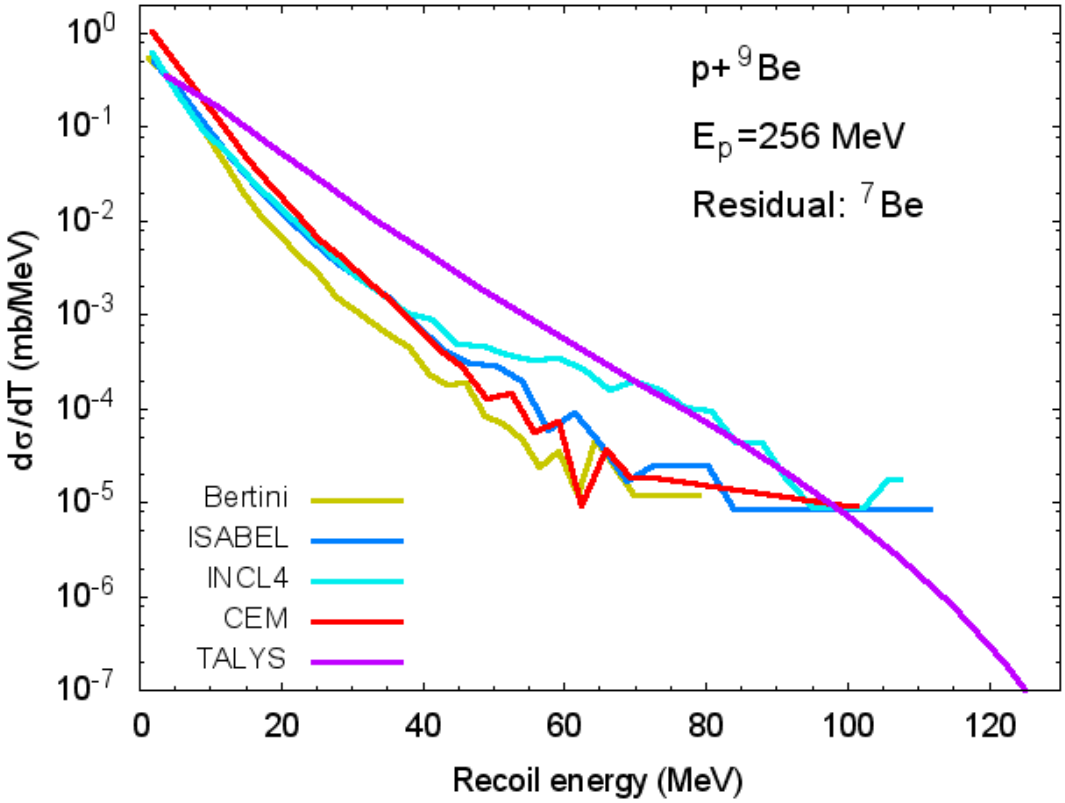
p+ 9Be
Ep=256 MeV
Residual: 7Be
Bertini
ISABEL
INCL4
CEM
TALYS
dσ/dT (mb/MeV)
Recoil energy (MeV)
10^0
10^-1
10^-2
10^-3
10^-4
10^-5
10^-6
10^-7
0
20
40
60
80
100
120

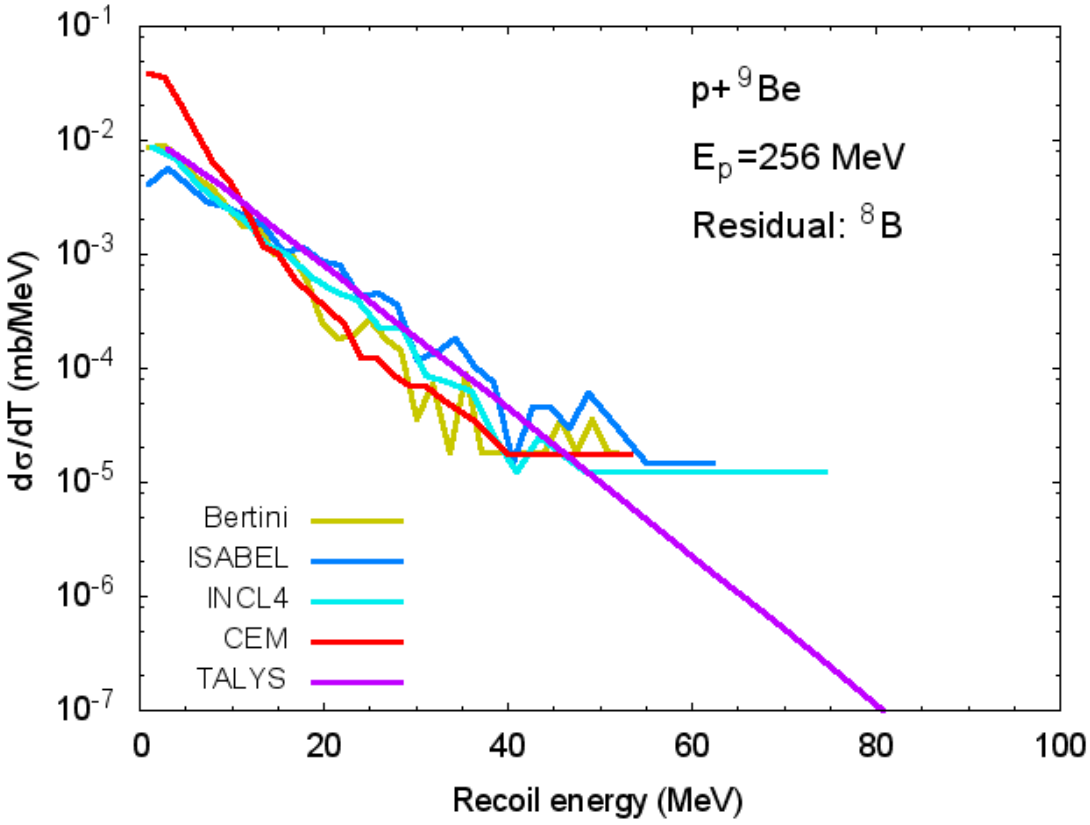
p+ 9Be
Ep=256 MeV
Residual: 8B
Bertini
ISABEL
INCL4
CEM
TALYS
dσ/dT (mb/MeV)
Recoil energy (MeV)
10^-1
10^-2
10^-3
10^-4
10^-5
10^-6
10^-7
0
20
40
60
80
100

KIT Scientific Working Papers
ISSN 2194-1629

www.kit.edu